Molecular crosstalk between apoptosis and autophagy induced by a 2-methoxyestradiol analogue (C19) in HeLa cells

by

Anne Elisabeth Theron (nee Mercier)

(02500906)

Submitted in fulfilment of part of the requirements for the degree

Master of Science (Physiology)

Faculty of Health Sciences

University of Pretoria

Supervisor: Prof AM Joubert

Department of Physiology, Faculty of Health Sciences, University of Pretoria, South Africa

Co-supervisor: Dr L Lafanechère

Université Joseph Fourier, Albert Bonniot Institute, CRI INSERM/UJF U823, Department of Cellular Differentiation and Transformation, Team# 03 –Polarity, Development and Cancer, Grenoble, France

March 2012

For my granddad

John Alistair Buchanan (04-04-1911 – 20-05-2002)

The first book was always going to be yours.

Don't think this was exactly what we had expected back then.

Summary

Cervical cancer is reported by the World Health Organisation to be the second most common type of cancer to affect women in poorer socioeconomic countries. Treatment of this pathology remains sub-optimal at advanced stages and continues to be of importance on the research agenda.

Previous studies have reported cytotoxic and antiproliferative effects of 2-methoxyestradiol (2-ME) *in vitro* on a HeLa cervical cancer cell line. These results were promising but use of 2-ME itself is limited due to pharmacodynamic constraints. In an attempt to overcome these, a sulphamoylated analogue of 2-ME, namely 2-ethyl-3-*O*-sulphamoyl-estra-1,3,5(10)16-tetraene or compound 19 (C19), was synthesised.

In this *in vitro* study, the induction of a block in mitosis with subsequent culmination of apoptosis and autophagy as types of cells death was investigated after HeLa cells were exposed for 24 hours to a 0.5 µM C19 solution. This was achieved by morphological assessment (fluorescent, Polarization-optical transmitted light differential interference contrast microscopy **(**PlasDIC) and transmission electron microscopy (TEM)) and flow cytometry (cell cycle progression, cyclin B1 analysis, phosphatidylserine (PS) flip and aggresome formation). Spectrophotometric quantification of the apoptotic initiator and executioner caspases 8 and 3 respectively was done to determine their involvement in the crosstalk between apoptosis and autophagy.

Results included the following: (i) PlasDIC microscopy illustrated the appearance of an increased number of cells blocked in metaphase, stress signaling, premature cell shrinkage, hypercondensed chromatin and the presence of apoptotic bodies after C19 exposure. The presence of ghost cells, cell debris and decreased cell density of the treated cells correlated with the autophagy control. (ii) Fluorescence microscopy employing triple staining highlighted an increased lysosomal activity and staining of C19-exposed cells when compared to the control, as well as evidence of apoptotic and metaphase-blocked cells.

This is indicative of both the autophagic and apoptotic cell death process. (iii) TEM allowed for examination of the ultrastructure of the intracellular processes, and revealed that apoptotic cells have hallmarks of both autophagy and apoptosis, confirming the results of light microscopy. (iv) Cell cycle analysis demonstrated more cells present in the sub-G_1 and G_2/M populations, indicating the induction of apoptosis (confirmed with PS fip flow cytometric quantification) and a metaphase block (corroborated by an increased cyclin B1 fluorescence). (v) The increase in autophagosome formation seen on fluorescence- and transmission electron microscopy was confirmed by flow cytometry demonstrating an upregulation of aggresome formation in C19-exposed cells. This investigation demonstrated induction of both types of cells death by this novel compound. (vi) The upregulation of caspases 8 and 3 was demonstrated in the C19-treated cells, indicating apoptosis induction via the extrinsic pathway. (vii) Confocal microscopy demonstrated complete microtubule disintegration in the C19-exposed HeLa cells.

Both apoptotic and autophagic cell death mechanisms were induced in C19-treated HeLa cells after spindle abrogation kept the cells in metaphase block. Insight gained into the molecular effect of C19 on HeLa cells may be used as a springboard for *in vivo* studies, furthering the development of this promising anticancer agent toward clinical application.

Key words: 2-methoxyestradiol, analogue, apoptosis, autophagy, caspase, cyclin B1, crosstalk, compound 19, mitotic block, spindle formation

Research Outputs

1. A manuscript was written and will be submitted to 'Cell Proliferation' for publication.
2. Conference proceedings:
    - Theron AE, Visagie M, Mqoco T, Stander A, Prudent R, Lafanechère L & Joubert AM. Molecular crosstalk between apoptosis and autophagy induced by a 2-methoxyestradiol analogue (C19) in HeLa cells. South African Journal of Science and Technology. 2012:31(1); In press.
3. Conference outputs:
    - Oral presentation at the South African Academy: Division Biological Sciences congress. 5 September 2011
        - Molecular crosstalk between apoptosis and autophagy induced by a 2-methoxyestradiol analogue (C19) in HeLa cells
        - Winner for best oral presentation in the MSc category.
    - Poster presentation at Faculty day of the Faculty of Health Sciences, University of Pretoria: Molecular crosstalk between apoptosis and autophagy induced by a 2-methoxyestradiol analogue (C19) in HeLa cells. 31 August 2011

Acknowledgements

With sincere gratitude to:

- Prof Annie Joubert, the best supervisor a girl could ask for! Thank you for your encouragement, guidance, commitment and the wonderful opportunity. Working with you has been an awesome experience.
- Dr L Lafanechère, my co-supervisor: I look forward to an ongoing collaboration.
- Professor D van Papendorp, head of the Department of Physiology. Thank you for your interest, encouragement and facilitating the logistics of this project.
- My wonderful colleagues and friends at the Department of Physiology: Dalene, Thandi, Michelle, Andre, Sumarie, Yvette, Sue and Karin. You gave your smiles, enthusiasm, support, knowledge and time freely: this would not have been possible without you.
- The lads at the Electron Microscopy Unit of Pretoria. Chris and Alan, thank you for your time, indulging my enthusiasm and sharing your knowledge and expertise.
- The Cancer Association of South Africa (CANCA), the Medical Research Council (MRC), the National Research Foundation (NRF), the Research Committee of the University of Pretoria (RESCOM) and the Struwig-Germushysen Trust: your commitment to furthering science and financial aid is acknowledged and appreciated. Appreciated also is the achievement bursary from the University of Pretoria.
- My mother, Sonja Clausen: you have always waved the pom-poms wildly and enthusiastically, especially for any academic escapade.
- To my friends, who have come to know these periods of 'Joji dropping off the planet'. Your support and encouragement means the world; as does the knowledge that you will still be there when I reappear.
- The most wonderful husband in the world! Andrè, you supported and loved me in every which way you could, and coped stoically with the neglect that comes with writing up any scientific project!
- God the Father, Son and Holy Spirit: all praise and glory go to You alone.

Table of Contents

List of Figures

List of Tables

List of Abbreviations

-	minus
˚C	Degrees centigrade
+	plus
+TIPs	Plus-end tracking proteins
2-ME	(17 beta)-2-methoxyestra-1,3,5(10)-triene-3,17-diol (2-Methoxy-17β-estradiol)
2-MEbisMATE	2-methoxyestradiol-3,17-O,O-bis-sulfamate
A2780	Ovarian carcinoma cell line
AAF	Aggresome activity factor
AIDS	Acquired immunodeficiency syndrome
AMPK	5'-AMP activated kinase
ANOVA	Analysis of variance
APAF-1	Apoptosis protease-activating factor 1
APC/C	Anaphase-promoting complex/cyclosome
ASF/SF2	Alternative splicing factor/splicing factor 2
ATCC	American Type Culture Collection
Atg	Autophagy related proteins
ATM	Ataxia-telangiectasia mutated
ATR	ATM and Rad3-related
ave	Average
BAD	BCL2 associated death promoter
BAK	BCL2 homologous antagonist/killer
BCL2	B-cell lymphoma 2
BCL2-L10	B-cell lymphoma 2 -like 10
BCL-XS	BCL-extra short
BCRP	Breast cancer resistance protein
BH3	BCL2 homology domain 3
BID	BCL2 interacting domain
BIF1	BAX interacting factor 1
BIK	BLC2 interacting killer
BIM	BCL2 interacting mediator of cell death
BMF	BCL2 modifying factor
BOK	BCL2 related ovarian killer

BOO	BCL2 homology of ovary
BRCA1	Breast cancer susceptibility protein 1
Bub3	Budding uninhibited by benzimidazoles 3
BubR1	Budding uninhibited by benzimidazoles related 1
C19	Compound 19 (2-ethyl-3-*O*-sulphamoyl-estra-1,3,5(10)16-tetraene)
CA	Carbonic anhydrase
Ca^{2+}	Calcium ions
CAD	Caspase-activated deoxyribonuclease
CAK	Cdk2-activating kinase
CAL51	Breast adenocarcinoma cell line
CB	Cytoskeletal buffer
CCD	Central coiled domain
Cdc	Cell division cycle
Cdc2L5	cell division cycle 2-like protein kinase 5
Cdh1	Cadherin-1
Cdk	Cyclin dependant kinases
CED-3	*Caehorhabditis elegans* domain 3
CENP-E	Centromere protein E plus end kinesin
cFLIP	Cellular FADD-like interleukin-1 beta-converting enzyme (FLICE)-inhibitory protein
CHD1	Chromodomain-helicase-DNA-binding protein 1
Chk	Checkpoint kinase
CIN	Carcinoma *in situ*
Cip	Cdk interacting protein
CIP	Cyclin-Dependent Kinase-Interacting Protein
CKII	Casein kinase II
CKIs	Cyclin dependent kinases inhibitors
cm^2	Square centimetre
CMA	Chaperone mediated autophagy
CO_2	Carbon dioxide
Crkrs	Cdc2-related kinase with an arginine/serine-rich (RS) domain
CTT	Cytosolic chaperonin cytosolic containing TCP-1
CYP450	Cytochrome P450
D283	Human medulloblastoma cell line

D341	Human medulloblastoma cell line
DAOY	Human medulloblastoma cell line
DAPk	p53 death associated protein kinases
dATP	Deoxyadenosine triphosphate
DD	Death domain
DED	Death effector domain
DIABLO	Direct inhibitor of apoptosis protein (IAP)-binding protein with low pI
DISC	Death-inducing signaling complex
DMEM	Dulbecco's Modified Eagle Medium
DMSO	Dimethyl sulphoxide
DNA	Deoxyribonucleic acid
dsDNA	Double stranded DNA
DTT	Dithiothreitol
ECD	Evolutionary conserved domain
EDTA	Ethylenediaminetetraacetic acid
eIF2α	Eukaryotic initiation factor 2α
Ensa	α-endosulfine
ER	Endoplasmic reticulum
ERK	Extracellular signal-regulated protein kinase
FADD	Fas-associated death domain protein
FANCD2	Fanconi anaemia, complementation group D1
FBW7	F-box and WD repeat domain containing 7
FCS	Foetal calf serum
FITC	Fluorescein isothiocyanate
FLICE	FADD-like interleukin-1 beta-converting enzyme
FoxM1	Forkhead box protein M1
G_1-phase	Gap 1 phase
G_2-phase	Gap 2 phase
Gadd45	Growth arrest and DNA damage inducible gene
GDP	Guanine diphosphate
GINS	Go, Ichi, Ni and San
GIT	Gastrointestinal tract
GTP	Guanosin-5'- triphosphate
Gwl	Greatwall

H & E	Haematoxylin and eosin
H^+	Hydrogen ions
H2A	Human histone 2A
H_2O	Water
HCO_3^-	Bicarbonate ions
HEK293	Transformed human embryonic kidney cell line
HeLa	Cervical adenocarcinoma cell line
HEPES	4-(2-hydroxyethyl)-1-piperazineethanesulfonic acid
HERs	Hypoxia response elements
HIF-1α	Hypoxia-inducible factor-1
HIV	Human immunodeficiency virus
hKIS	Human kinase interacting stathmin
HMGB-1	High mobility group box 1 protein
HPV	Human papillomavirus
HR	Homologous recombination
HRK	Harakiri
hsc70	Heat-shock protein 70
HSD	Hydroxysteroid dehydrogenase
HSIL	High grade squamous intraepithelial lesion
HUVEC	Human umbilical vein endothelial cells
IAP	Inhibitors of apoptosis proteins
IC_{50}	The half maximal inhibitory concentration
ICAD	Inhibitor of caspase-activated deoxyribonuclease
ICE	Interleukin-1β converting enzyme
IETD-*p*NA	Isoleucine–glutamic acid–threonine–aspartic acid tetrapeptide labelled with p-nitroaniline
IgG	Immunoglobulin-G
INK4	Inhibitors of the cyclin-dependent kinase 4
IP_3R	Inositol-1,4,5-triphosphate receptor
Kip	Kinase inhibitory protein
Knl1	Kinetochore nuL-1
L	litre
LAMP-2A	Lysosome-associated membrane protein type 2A
LC3	Light chain protein 3

LICE	Interleukin 1 -converting enzyme-like proteases
LLETZ	Large Loop Excision of the Transformation Zone
LNCaP	Androgen responsive prostatic adenocarcinoma cell line
LSIL	Low grade squamous intraepithelial lesion
M/A	Metaphase/anaphase
m^2	Square metre
Mad	Mitotic arrest deficiency protein
MAP	Mitogen-activated protein
MAPK	Mitogen-activated kinase
MCC	Mitotic checkpoint complex
MCF-1	Oestrogen receptor positive breast cancer cell line
MCF-12A	Non-tumorigenic breast cell line
$MCF\text{-}7_{DOX}$	Doxyorubicin resistant MCF-7 breast cancer cells
$MCF\text{-}7_{WT}$	Wild types MCF-7 breast cancer cells
MCL1	Myeloid cell leukaemia 1
Mcm	Microsome maintenance protein
MDA-MB-231	Metastatic breast cancer cell line
MDC1	Mediator of DNA-damage checkpoint-1
MDM2	Murine double minute 2
MEK	MAP/ERK kinase
mETC	Mitochondrial electron transport chain
mg	milligram (1×10^{-3} g)
Mis12	Microtubule-associated protein 12
ml	millilitre (1×10^{-3} l)
mM	millimolar (1×10^{-3} M)
MPF	Mitosis promoting factor
M-phase	Mitotic phase
mRNA	Messenger ribonucleic acid
MTA	Microtubule-targeting agents
MTOC	Microtubule organizing centre
mTOR	Mammalian target of rapamycin
Myt1	Myelin transcription factor 1
n	Sample size
N	Ploidy

NAF-1	Nutrient-deprivation autophagy factor-1
NaOH	Sodium hydroxide
NBS1	Nijmegen breakage syndrome
Ndc80	Nuclear Division Cycle 80
NEB	Nuclear envelope breakdown
Nek2	NIMA-related protein kinase 2
NES	Nuclear export signal
NHEJ	Nonhomologous end joining
NIMA	Never in mitosis A
nm	nanometre (1×10^{-9}m)
NSF	N-ethylmaleimide sensitive fusion protein
p53BP1	p53 Binding Protein 1
PARP	poly (ADP-ribose) polymerase
PAS	Pre-autophagosomal structure
PBS	Phosphate buffered saline
PC3	Androgen-independent prostatic adenocarcinoma cell line
PE	Phosphatidylethanolamine
PE-labelled	Phycoerythrin-labelled
pg	picogram (1×10^{-12} g)
PI3K	Phosphatidylinositol 3-kinase
PI3KC1	Class 1 phosphatidylinositol 3-kinase
PIDD	Cellular FADD-like interleukin-1 beta-converting enzyme (FLICE)-inhibitory protein
PIK3C3	Class III phosphatidylinositol 3-kinase
PIKKs	phosphoinositide 3-kinase-like kinases
PIPES	piperazine-N,N'-bis(2-ethanesulfonic acid)
PKA	Protein kinase-A
PKCδ	Protein kinase C delta
PlasDIC	Polarization-optical transmitted light differential interference contrast microscopy
Plks	Polo-like kinases
*p*NA	*p*-nitroaniline
PP2A	Protein phosphatase 2A
pRB	Retinoblastoma protein

Prp4	Ribonucleoprotein particle 4
PS	Phosphatidylserine
PSF	Penicillin, streptomycin, fungizone
PUMA	p53 upregulated mediator of apoptosis
QAC(R/Q)G	Glutamine, alanine, cysteine (arginine/glutamine) glycine
Rad24	Radiation 24
RBL	Retinoblastoma-like
RF	Resistance factor
RIP	Receptor-interacting protein
ROS	Reactive oxygen species
RPA	Replication protein A
RZZ	Rough Deal, ZW10 and Zwilch
SAC	Spindle assembly checkpoint
SCA-1	Spinocerebellar ataxia 1
SD	Standard deviation
SMAC	Second mitochondria-derived activator of caspases
SNAP	Soluble NSF Attachment protein
SNARE	SNAP receptor
SNO	Non-keratinizing squamous epithelial cell line
SOD2	Superoxide dismuates
S phase	Synthesis phase
Suc1	Sucrose-fermenting 1
SWI/SNF	Switch/Sucrose Non Fermentable
T98G	Human glioblastoma multiforma tumor cell line
Tao1	Thousand-and-one amino acid kinase 1
TBCs	Tubulin binding cofactors
tBID	Truncated BID
TEM	Transmission electron microscopy
TG2	Tissue transglutaminase 2
TNF	Tumour necrosis factor
TNFR	Tumour necrosis factor receptor
TNFSF10	Tumour necrosis factor superfamily member 10
Tpx2	Targeting protein for Xenopus plus end-directed kinesin-like protein 2
TRADD	TNF-R1-associated death domain

TRAIL	TNF-related apoptosis-inducing ligand
TSC	Tuberous sclerosis protein
TUNEL	Terminal deoxynucleotide transferase dUTP nick end labelling
U-87MG	Human astroglioma cell line
ULK1	Unc-51 like kinase
UVRAG	Ultraviolet resistance associated gene
VEGF	Vascular endothelial growth factor
Vps	Vacuolar protein sorting
WAF1	Wild-type p53-activated fragment 1
WHO	World Health Organization
ZW10	Zeste-White 10
γIFN	Gamma interferon
γ-TuSC	γ-tubulin small complex
µg	Microgram (1×10^{-6} g)
µl	Microlitre (1×10^{-6} l)
µM	Micromolar (1×10^{-6} M)

1. LITERATURE REVIEW

Cancer is merciful to no-one: it does not distinguish between gender, race, age, socioeconomic distinction, occupation or disposition. It is one of our major opponents in the battle for health and life. It is the nature of the enemy that differs in various forms of pathology, and perhaps the armour of education and the arsenal of treatment not issued to many that may sway the battle. (1) In the preparation for war, it is strategic to know the foe intimately, to understand the *modi operandi* in exquisite detail in order to build defences, gain insight into their strengths and weaknesses, and ultimately use the knowledge in a devastating offensive counterattack. For many years, the confrontation has been defensive: a lack of insight caused the loss of innocent life. As the many cogs in 'intelligence' are gathering more and more information, so our insight into cancer mechanisms deepens and our understanding broadens.

1.1 Cervical carcinoma

Cervical cancer is reported by the World Health Organization (WHO) to be the second most common type of cancer to affect women worldwide, with the poorer socio-economic countries bearing the brunt (85%) of this disease burden (figure 1.1). (2-4) It is the seventh overall most common cancer in the world and is responsible for over 275 000 deaths per annum (2), with an incidence ranging from 4.8 per 100 000 in the Middle East to 44.3 per 100 000 in East Africa. (5) The highest cumulative risk of developing cervical cancer is in Southern and Central Africa, South-Central Asia and South America (figure 1.1). (4) Since the implementation of Papanicolaou testing and rigorous human papillomavirus (HPV) screening of cervical smears in the 1950's, the incidence of cervical cancer has decreased by up to 80% in first world countries and this remains a life saving intervention. (2, 5-7)

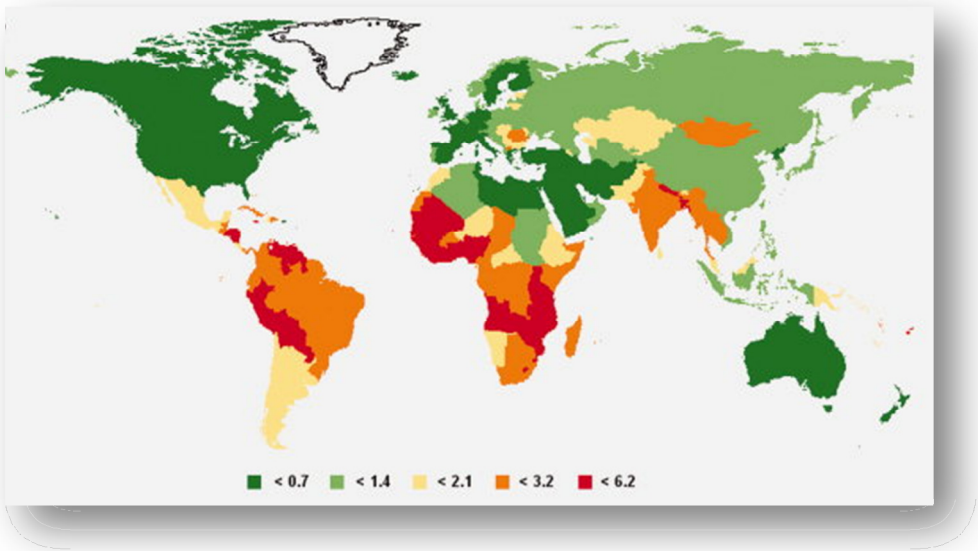

Figure 1.1: Estimated cumulative incidence risk (0–74) percent of cervical cancer. Third world developing countries show a marked elevation in the occurrence of cervical cancer when compared to developed countries. Reprinted by permission from John Wiley & Sons: [International Journal of Cancer], (4), copyright (2008).

Aetiology of cervical carcinoma has been conclusively linked to genital exposure to the human papillomavirus (HPV), in particular HPV 16 and 18. (2, 8) Expression of the HPV-specific oncoproteins E6 and E7 are reportedly necessary in maintaining the malignant properties of infected cells by inhibition of the tumour suppressor p53 and retinoblastoma (pRB) gene products. (8) Although this fact is not in question, there has been on-going debate as to whether HPV infection remains the only or sole cause of the said neoplasia. Proposals for a synergistic co-infection with herpes simplex virus type 2 to provide a 'second hit' for the neoplastic conversion to take place have been proposed in numerous studies. (8-11) Additional risk factors for developing cervical carcinoma have been extensively studied, including possible links between oral contraceptive pill usage, (9) recreational drug abuse and cervical tar exposure, (6) be it via douches, (12, 13), haematological deposition of cigarette smoke constituents, (14-16) or inhalation of burning kitchen firewood indoors. (17, 18) Associations with passive smoke inhalation have also been drawn, as has parity and age of menarche, menopause and first intercourse. (16)

Most of these hypotheses have been refuted to a greater or lesser degree, with claims that lifestyle behavioural patterns may be strong confounders. (19, 20) Patterns of a post

menopausal resurgence of cervical cancer incidences are explained by incomplete previous eradication of the HPV infections and lack of screening. (6) Important in current day sub-Saharan Africa, urban populations are identified to be at higher risk of both human immunodeficiency virus (HIV) infection and cervical carcinoma, with the latter being one of the most important acquired immunodeficiency syndrome (AIDS)-defining conditions. (21, 22) Indeed, cervical cancer may be described as the most common AIDS-related malignancy in women. (21) The hypothesis for a multifactoral component of cervical cell carcinoma induction remains, particularly against a background in which roughly 95% of the cases are definitively attributed to HPV infection, leaving about 5% aetiologically unaccounted for. (5) Moreover, many people are exposed to both HPV, as well as the above mentioned factors and do not develop cervical cancer. Nonetheless, prolonged and persistent infection with certain HPV subtypes remains the primary risk factor for anogenital, as well as certain head and neck cancers. (8)

There is large heterogeneity within the *Papillomaviridae* family, with at least 118 HPV types classified as of yet and many more still to be completely described. (23) HPV infection occurs mostly during sexual exposure via microlesions in basal layer epidermal or mucosal epithelial cells, where limited expression of 'early' viral genes (including E5, E6 and E7) induce lateral expansion of infected cells. (24) As the cells progressively differentiate through the suprabasal layers, 'late' viral genes are expressed which initiate circular viral genome replication and the translation of structural proteins. (24) Once in the superficial epidermal layers, fully assembled particles are released. For oncogenic transformation of the 'high risk' HPV subtypes to occur, the viral ring is cleaved and inserted into the host deoxyribonucleic acid (DNA). (8) Initially, this infection causes a macroscopically invisible low-grade squamous intraepithelial lesion (LSIL), most of which are cleared in 6-12 months via the immune system. Persistence of the infection in conjunction with stimuli to amplify the viral gene activity and escape from immunological control will result in the progression of LSIL to a high-grade squamous intraepithelial lesion (HSIL), followed by carcinoma *in situ* and eventual evolution to squamous- or adeno-carcinoma of the cervix (figure 1.2). (25)

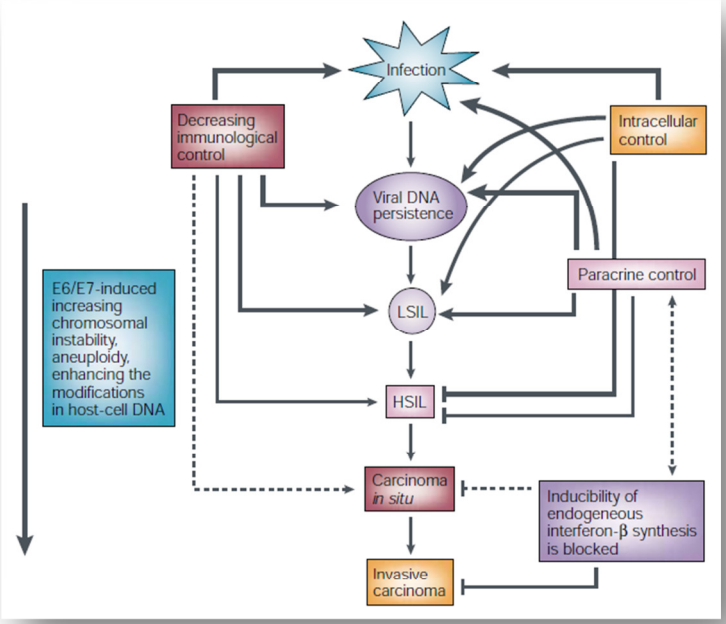

Figure 1.2: Progression of human papillomavirus infection to carcinoma. Various viral and systemic control mechanisms fail in the face of the oncogenic viral E6 and E7 expression and are shown to contribute in the transformation from low-grade squamous intraepithelial lesions (LSIL) to high-grade squamous intraepithelial lesions (HSIL), and subsequent neoplastic conversion. Paracrine control, against a background of decreased interferon-β, is excerpted by macrophages and cytokines (*e.g.* tumour necrosis factor α). Reprinted by permission from Macmillan Publishers Ltd: [Nat Rev Cancer] (8), copyright (2002)

Through rigorous cervical screening programmes, early detection of dysplastic SIL and carcinoma *in situ* (CIN) lesions may mostly be managed aggressively and easily by Large Loop Excision of the Transformation Zone (LLETZ) before the development of invasive disease. (26, 27) This pre-emptive management is highly successful, as is treatment of local infiltrative carcinoma, but the same cannot be said of metastatic and infiltrative disease. (28, 29) The overall incidence: mortality ratio remains moderately high at 52%, of which 88% of the deaths occur in developing countries, a fact which is disturbing. (4) Although the recent introduction of the HPV vaccine holds promise to decrease the incidence of cervical cancer in future, (7, 30) treatment of this pathology remains sub-optimal at advanced stages and continues to be of importance on the research agenda.

1.2 The cell cycle

It is in knowing and understanding the intrinsic mechanisms of how a normal cell grows and dies, that one may understand the pathological deregulation of it in cancer. Original studies of the cell cycle were conducted on yeast cells, *Saccharomyces cerevisiae,* where regulatory mechanisms of this tightly controlled process were described. (31, 32) Most of the intracellular aspects involving the execution and control of these mitotic phases are highly conserved and have mammalian counterparts, although there is an additional multidimensional complexity in the latter. (33)

The well accepted four phases of the traditional cell cycle comprise of the G_1 (gap 1), S (synthesis), G_2 (gap 2) and M (mitotic) phases, of which the M phase can further be divided into prophase, metaphase, anaphase and telophase (figure 1.3). (34-36) During the S phase DNA replication occurs, chromosomal condensation begins as the aurora kinases phosphorylate histones, and chromosomal and cytosolic content division follows in the M phase. (34, 36, 37) The latter occurs by chromosomal condensation in prophase, followed by equatorial alignment of the adhered sister chromatids via mitotic spindle attachment in metaphase. (38, 39) Anaphase follows, with the sister chromatids moving to opposite poles, and the process completed in telophase when the spindle disintegrates, the chromosomes unravel, the nuclear membrane reassembles and cytokinesis occurs. (39) Gap phases separate the S and M stages, allowing time in which DNA synthesis and segregation is coordinated with the microtubules, and synthesis and assembly of required cellular proteins and structures is achieved; a period of preparation for DNA synthesis during G_1, and for mitosis in G_2. (33, 35, 37) Interphase spans the period between two M phases. The rate of cell cycle completion is specie and cell line dependent. (34, 40) Cells not actively cycling are termed to be G_0, where cells have withdrawn from the division process due to high cell density, mitogen deprivation or due to terminal differentiation or entering quiescent states. (35, 40) The simplicity of this model belies the intricacy of the intracellular molecular machinery involved in the staging of these events.

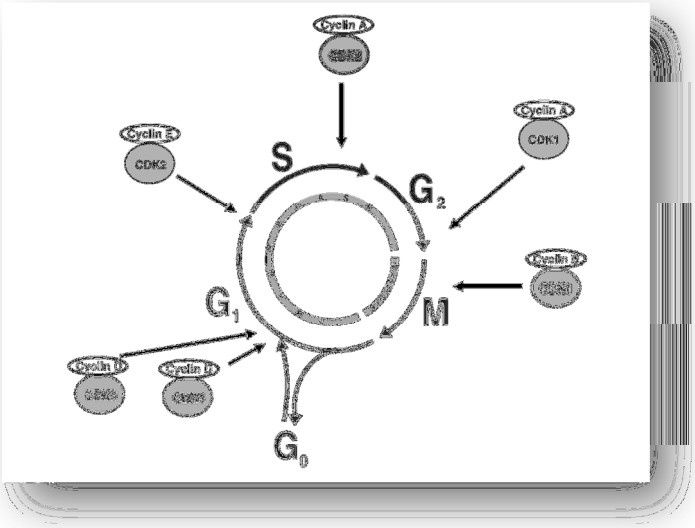

Figure 1.3: Diagram representing the stages of the cell cycle, with the appropriate Cdk-cyclin complexes which regulate the pregression though the phases. Reprinted by permission from John Wiley & Sons: [Cell Proliferation] (35), copyright (2008).

The progression of the cell through these stages is sequential and highly ordered, with failure to proceed to later phases should the preceding events not be completed correctly. (34, 35) Control mechanisms which enforce this regulation are termed 'checkpoints'. Should the sensor mechanisms detect faulty or incomplete events in any of the steps, the checkpoints will initiate cell cycle arrest until repair is completed (41) The first step in the initiation of cell division would be the activation of the transcription and translation factors, needed for the expression of the cell cycle genes. (42) These factors are mostly active in embryonic development and are subsequently repressed after terminal differentiation during organogenesis. (43) This repression is thought to be mediated by the retinoblastoma protein (pRB) and other pocket family members, transcription regulators which function via repressor complexes such as switch/sucrose non-fermentable (SWI/SNF) complexes, methylases, histone deacetylases, polycomb group proteins and the inactivation of relevant transcription factors (E2F family). (42-46)

1.2.1 Regulation of the cell cycle

1.2.1a Cyclin-dependent kinases

Cyclins and cyclin-dependent kinases (Cdks) (analogue to the cell division control (Cdc) proteins in humans) are evolutionarily conserved proteins that are essential for cell-cycle control in eukaryotes. (47) Cyclins (regulatory subunits) bind to Cdks (catalytic subunits) to form complexes that regulate the progression of the cell cycle. (47)

Phosphorylation of proteins catalyzed by relevant kinases is the mainstay of activating various factors which are responsible for the dynamic progression through the cell cycle (along with ubiquitin-mediated degradation of inhibitory factors. (48) Preventing this phosphorylation, phosphorylating active suppressors of a factor or deactivating proteins by ubiquitination serves as a method to inhibit this progression. On the appropriate mitotic signal, transcription of cyclins is induced, which activate the cyclin-dependent kinases and inactivates the pRB by phosphorylation. (49, 50) The G_1 phase is consequently entered into, and transcription of all the genes required for the following phases is up-regulated, including those that will be needed in the DNA replication complexes in the S phase. Other kinases are involved in a plethora of activities, including DNA replication (cell division control protein 7 (Cdc7)) (51) and duplication, and migration of centrosomes with spindle formation (Aurora, Polo-like kinases (Plks) and never in mitosis A-related kinases (NIMA)), amongst others. (52)

Cyclin-dependent kinases (Cdks) are catalytic subunits of mammalian heterodimeric kinases which phosphorylate their target at specific serine and threonine sites. (53) About 20 different Cdks have been indentified in mammals, which regulate the orderly progression of the cell cycle by sequential activation and destruction. Cyclins, termed so due to their cyclical expression during the cell cycle, may be seen as the regulatory subunits of the Cdks, the actual formation of a cyclin-Cdk complex being a necessary event for progression to the next stage of the cell cycle. (54) About 29 cyclins or cyclin-related proteins have been described, and are necessary for the activation of Cdks, the levels of the latter's inactive form being relatively constant within the cell cycle. (54)

Traditionally, certain cyclin-Cdk complexes are associated with specific stages of the cell cycle; Cdk2, Cdk4 and Cdk6 have functions in interphase, Cdk1 (also known as cell division control protein 2 (Cdc2) integral in mitosis, and four different classes of cyclins (A-, B, D- and E-type cyclins) composed of 10 subtypes. (33, 55, 56) As mentioned prior, under the influence of a mitogen (such growth factors), D-type cyclins (D1, D2 and D3) are expressed which bind to and activate Cdk4 and Cdk6 associated with interphase, and cause partial inactivation of the pocket proteins (pRB, Retinoblastoma-like 1 (RBL1) also known as p170) and RBL2 (p130)). (50, 55, 56) The transcription of D-cyclins, their binding to Cdk4, the stability of that interaction, as well as the holoenzyme retention in the nucleus is dependent on the receptor mediated Ras and phosphatidylinositol 3-kinase (PI3K) intracellular signaling cascades. (57) This pocket protein inactivation leads to the expression of E-types cyclins (E1 and E1) which activates Cdk2 upon binding with it, the resulting complex completing the inactivation of the pocket proteins by phosphorylation. (41, 53) The E-cyclins are strictly limited to the early phase of DNA replication and is needed to impel the G_1/S transition. (58) Cyclin A2 (or A1 in germ cells) activates Cdk2 at the later stages of DNA replication in the G_2 phase in order to drive the process towards mitosis. (53) Cdk1 is then activated by A-type cyclins, essential in initiating the M phase. As soon as nuclear membrane dissociation has occurred, the A-type cyclins are degraded by ubiquitination, a process which is responsible for the formation of the Cdk1/(Cdc2)-cyclin B complexes which are crucial to take the cell through mitosis. (55) It is to be realized that the Cdk-cyclin complexes associate with various other subunits for optimal assembly, stability and nuclear retention. (57)

Useful thus as markers of where the cell is in its cycle, one is able to detect many of the above mentioned proteins or complexes specific to certain temporal windows. For instance, D-type cyclins are high only as the cells emerge from quiescence to regulate the G_1 phase, A type cyclin activity increases gradually though S and G_2 to reach a peak before cyclin B (which has been low up to that sage) increases dramatically to allow entry onto the M phase. Many other Cdks have been identified and have specific and precise moments of activity during the cell cycle, as depicted in figure 1.4. (33, 52, 55)

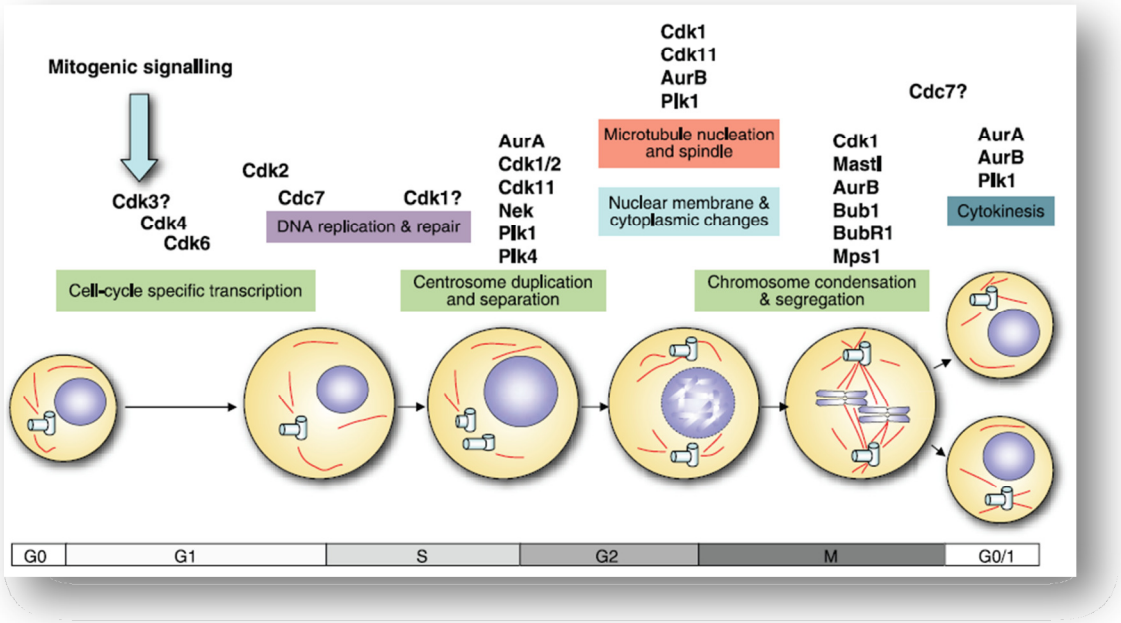

Figure 1.4: Representation of the cell cycle stages and the relevant Cdks involved in its progression and control. The cell increases in size upon entering the cycle, the chromatin is duplicated in the S phase, after which it condenses, the chromatids align themselves on the equator in metaphase, to be segregated to opposite poles via centriole and spindle action (represented with cylinders and red lines) to culminate in 2 identical daughter cells. Cdks which have unidentified function as of yet are tagged with '?'. Reprinted (no permission required for thesis/dissertation use) from The American Physiology Society Ltd: [Physiol Rev], (33), copyright (2011)

The delineation of the traditional progression though the cell cycle as described above has come into question. (59) It has been established via several knockout mouse models that not all of the Cdks are essential to the cell cycle phases. (33, 60) Cdk-2, -4 and -6 are not essential to the process, but interestingly, loss of each individually resulted in a development defect in a specific specialized tissue type. (60) Loss of more than one of these non-essential Cdks simultaneously results in more severe developmental defects, but does not interfere with the general progression of the cell cycle in most cell types *per se*. (55) The same cannot be said of Cdk1, which is indispensable to the initiation of metaphase. (59) Similarly, absence or faulty expression of all the D-type and E-Type cyclins will result in lethality. (55) Additionally, the question remains as to how the not yet fully understood Cdk family members function. Examples such as Cdk3 which interacts with cyclin C during interphase, Cdk5 which seems to function in phosphorylation of cytoskeletal proteins in post mitotic neurons, and Cdk7 which pairs with cyclin H to regulate

transcription of and activation of other Cdks, need still to be fully understood. (55, 61, 62) It has also come to light that the Cdks have additional functions above those of driving and controlling the cell cycle. (52) Cdk12 (Cdc2-related kinase with an arginine/serine-rich (RS) domain (Crkrs)) and Cdk13 (cell division cycle 2-like protein kinase 5 (Cdc2L5)) complex with L-type cyclins to regulate the mRNA alternative splicing machinery (Alternative splicing factor/splicing factor 2 (ASF/SF2)-associated protein p32). (63, 64) It has been established that Cdk 10 and Cdk 12 have a function in the G_2/M transition, and participate in regulation transcription, centrosome maturation, sister chromatid unity, microtubule formation and cytokinesis. (33, 55, 65, 66)

1.2.1b Negative control of the cyclin-dependent kinases

Cdks are both positively and negatively regulated in order to direct the induction and progression through the cell cycle. As discussed above, the cyclins are the major positive regulatory subunits of the Cdks. The transition of a quiescent cell into an active cell cycle is mediated by a mitogenic stimulus which induces D-type cyclin transcription via many of the major signaling pathways such as Ras/mitogen-activated kinase (MAPK). (50) This then sets about to abolish the inhibitory control mechanisms. These inhibitory control mechanisms are important to maintain the cell in a quiescent state, and prevent cell cycle transition via formation of inhibitory-activating component complexes.(50) For instance, persistent mitotic activation of D-cyclins leads to their nuclear accumulation, where together with E-cyclin-Cdk2 complexes, cause the phosphorylation of RB and RB-family members p107 and p130 to negate their inhibitory functions and consequently pushes the cell into S phase continuously. (57) Additionally, in the progression to the next phase of the cell cycles, some activation factors from the previous phase now become an inhibitory component. (48) Signal transduction cascades which regulate cell proliferation often use Cdk inhibitory factors as downstream targets. (50, 56)

There are a number of recognised families of Cdk and cyclin inhibitors. $p21^{Cip1}$, $p57^{Kip2}$ and $p27^{Kip1}$ are members of the Cdk interacting protein/Kinase inhibitory protein (Cip/Kip) family of Cdk inhibitors (CKIs). Both $p27^{Kip1}$ and $p21^{Cip1}$ inhibit E-cyclin when complexed with Cdk2. (67, 68) Thus in a quiescent cell, D-cyclin levels are low, D-cyclin-Cdk4 interactions do not

form, and high levels of $p27^{Kip1}$ inhibit E-cyclin-Cdk2 interaction. (57) On mitotic stimulation, the D-cylin-Cdk4 complex formation causes sequestration of $p27^{Kip1}$ from the nucleus to the cytoplasm via human kinase interacting stathmin (hKIS) phosphorylation of the position 10 serine residue, thereby allowing the nuclear formation of an active E-cyclin-Cdk2 complex. (67) On exiting the cell cycle, the above must be reversed, allowing the re-accumulation of nuclear $p27^{Kip1}$ and the inhibition of the G_1 phase Cdks which in turn allows hypophosphorylation and activation of the pRB (together with p130 and p107) to suppress the E2F family of transcription factors by deacetylation.(57) Additionally, $p27^{Kip1}$ and $p21^{Cip1}$ have been linked to extra-nuclear regulatory functions, including involvement in actin dynamics and cell migration. (67) The Cdc25 family of proteases counteract the phosphorylation-mediated inhibition of the Cdks. (69)

Further negative regulation of the above pathway may be attained by the inhibitors of the cyclin-dependent kinase 4 (INK4) family of Cdk inhibitions which block the progression of the cell cycle by binding to either Cdk4 or Cdk6, thereby eliminating the action of the D-cyclins and prevents phosphorylation of pRB. (70) Four proteins, namely $p16^{INK4a}$, $p15^{INK4b}$, $p18^{INK4c}$ and $p19^{INK4d}$, make up the INK family. (57, 71) Once again, it has been proved that individual members of the INK4 family are not essential to cell cycling, but may be more prone to neoplastic development on exposure to oncogenic stimuli. (57) $p18^{INK4c}$ and $p19^{INK4d}$ are widely expressed during mouse foetal and adult life, whereas $p16^{INK4a}$ and $p15^{INK4b}$ appear to be limited to *in utero* expression. (72) INK4 proteins have further functions beyond regulation of cell senescence, with evidence linking the specific member to various aspects of apoptosis, DNA repair and in the development of ontogenesis'. (70)

The correct cellular progression is also maintained by the appropriate intranuclear localization of phase dependent regulating proteins. (35) At the beginning of prophase, Cyclin B, which has a nuclear exclusion signal, is actively traslocated to the nucleus. (35) The CKIs kinases Wee1 (unphosphorylated active form which antagonises Cdc25) in the nucleus and myelin transcription factor 1 (Myt1) in the Golgi complexes protect the cell from early entry into mitosis. (69, 73) This intracellular trafficking of various proteins is directed by the 14-3-3 group of proteins. (74, 75) Of these 14-3-3 proteins, radiation 24 (Rad24) is specifically involved in the intracellular distribution of Cdc15 which activates the

kinases, and is banished to the cytoplasm during interphase and during a checkpoint repair process. (74) Additionally, the 14-3-3 proteins sequestrate the Cdk1-cyclin B complex to the cytoplasm should a DNA damage-mediated cell cycle arrest occur. (74)

1.2.1c The mitosis-promoting factor

The primary mechanism for a cell to establish order and precise timing of the cell cycle progression is at the transition phases, when alterations of the biochemical status of the cell division systems occur. The mitosis-promoting factor (MPF), also termed maturation promoting factor or M-phase promoting factor, is needed to activate the cellular machinery in order to allow the interphase-mitosis progression. (76) The MPF, amongst others, is needed to induce the required changes, such as condensin-mediated condensation of the chromatin, lamin phosphorylation to initiate nuclear envelope breakdown, Golgi fragmentation and promote the assembly of the mitotic spindle. (77) Additionally, MPF phosphorylates inhibitory sites on myosin in the initial phases of mitosis in order to prevent cytokinesis. (76)

The heterodimeric MPF consists of two subunits: Cdk1 which phosphorylates specific serine-threonine residues of target proteins, and cyclin B as a regulatory subunit. (76, 77) Activation of MPF requires cell cycle division control 25 (Cdc25) dependent dephosphorylation of Cdk1 at the phospoho-tyrosine^{15} residue, and phosphorylation of cyclin B. (76) On binding to cyclin B, Cdk1 must also be phosphorylated at the threonine^{161} residue by Cdk2-activating kinase (CAK), the latter consisting of a catalytic subunit Cdk7 and a regulatory subunit cyclin H. (78) A dual mode of Cdc25 activation is needed: firstly, the inhibitors of Cdc25 namely Wee1 and Myt1 must be deactivated (a process antagonised by protein phosphatase 2A (PP2A)-B55δ), and secondly, Cdc25 activation via multisite phosphorylation must occur. (78, 79) Both afore-mentioned processes are catalysed mainly by MPF itself. (78) Greatwall (Gwl) is needed for both the induction and maintenance of the cell in mitosis, primarily by inactivating PP2A-B55δ (which is highly active in interphase) by phosphorylation of α-endosulfine (Ensa). (79)

For the MPF to effect the progression into mitosis, two important biochemical kinetic features need to occur. (80) Firstly, as discussed above, activation of Cdc25 and the MPF must occur. While at low levels, the MFP is inhibited and stabilised by binding of Suc1, until such a time when MPF production exceeds stoichiometrically the amount of sucrose-fermenting 1 (Suc1). (80) This then is the second mode of inducing full autocatalytic activity of MPF, and pushing the cell into metaphase. This MPF is disassembled when the cell has completed metaphase and is ready to proceed to anaphase, by cyclin B polyubiquitination at the N-terminal 'destruction box' by the anaphase promoting complex. (48, 78)

Deregulation of cyclin B1 has been linked to oncogenic transformation of certain cells, as it is a regulatory subunit of the M-phase promoting factor essential in the initiation of mitosis. (81) Interference with microtubule dynamics and subsequent activation of the mitotic checkpoint complex (MCC) causes inhibition of cyclin B1 ubiquitination and degradation, thus resulting in an increase in cyclin B1 and Cdc2 concentration. (82) The increased cyclin B1/Cdc2 (cell division control protein 2 homolog) complex activity triggers chromosomal condensation and segregation as the progression of the G_2 phase to metaphase occurs. (83, 84) Cyclin B1 is thus part of the mitotic cyclin complex; expression is normally low in G_0/G_1, increases in S, and is maximal during G_2/M. (68, 85) Cyclin B1 is rapidly degraded at the end of mitosis, an event which is required for cells to exit from mitosis. (85)

1.2.1d The anaphase-promoting complex/cyclosome

The transition from metaphase to anaphase is an irreversible step in the cell cycle progression. Once the spindle assembly checkpoint has been satisfied (see below), the anaphase-promoting complex/cyclosome (APC/C), a ubiquitin ligase E3, promotes the degradation of cyclin B and securin to promote chromatid separation in anaphase. (86) APC/C is a very large complex consisting of many subunits, about 1500 kD in size, and degrades specific targeted proteins by the 26S proteasome. (48, 86) The site selection, and thus the activity of the cyclosome, is dependent on Cdc 20 and Cadherin-1 (Cdh1). (48) Ubiquitin chains attach to lysine residues in the targeted protein via covalent bonds, which leads to its recognition and subsequent degradation by the proteasome in a rapid and irreversible fashion. (48)

The APC/C has both positive and negative functions at various stages of the cell cycle, and is activated differently according to low Cdk levels (such as during the formation of a pre-replication complex) or high Cdk levels (during DNA unwinding and polymerase functions) via cyclical interactions with Cdc20 and Cdh1. (48) APC-Cdc20 functions when Cdk levels are high, whereas Cdh1 is directly inhibited by high Cdk concentrations. Additional control is given by active Cdk/cyclin complexes. (48) The APC/C is inhibited by the mitotic checkpoint complex (MCC), compiled of mitotic arrest deficiency protein (Mad2), Bub3 and BubR1. Mad2 inhibits Cdc20.

As an overview of the main molecules involved in mitotic progression (and their reaction to chromosomal instability), an illustration is presented in figure 1.5. (55) APC/C degrades cyclin A and Nek2 via polyubiquitination in a spindle assembly checkpoint (SAC) independent manner. (55) The SAC targets the APC/C during mitosis, the latter having important roles in regulating the protein levels or the key regulators of DNA replication and mitosis. (33, 86) Should the spindles not be attached to a centrosome, separase is kept inactive by Cdk1-cyclin B and securin. (87) In this case, the chromatids remain attached by cohesions. (55) Cdk1-cyclin B and Polo protein kinases are key in the phosphorylation of core APC/C subunits in order to confer optimal activity to APC/C prior to anaphase induction. (55) When the SAC has been satisfied by bipolar spindle attachments, the APC/C ubiquitinates cyclin B and securin, which in turn inhibits Cdk1 so that separase can be activated. (87) Separase cleaves cohesion and releases the sister chromatids for separation during anaphase. (33) Additionally, NIMA-related kinase (Nek2) which plays a role in the centromere organization and in sister chromatid cohesion, is ubiquitinated once the checkpoint has been passed, in order to allow anaphase separation to begin. (88) The APC/C-Cdh1 targets cyclin A (triggered by nuclear envelope degradation) and cyclin B, as well as Cdc20, Tpx2, forkhead box protein M1 (FoxM1), aurora kinase A and B, and Plk1 (all substrates involved in mitotic progression) during mitotic exit and in the following G_1 phase. (55, 89)

Aberrations of cell cycle regulation are the backbone of cancer pathology and thus an inviting target for therapeutic intervention. Certain cancers may display benefit from selective Cdk inhibition, as various tumours may have specific requirements for individual

Cdks. (53, 55, 90) The origin of the deregulation may be in the presence of a mitogen which causes phosphorylation of the pRB by stimulating the G_1-S Cdk activity and thus inappropriately induces the E2F transcription factors, or having mutation in the pRB suppression mechanism, thus causing a mitogen independent pathway of transcription factor overstimulation. (41, 46) One can thus postulate pRB phosphorylation is a common divergent point in most oncogenic signaling pathways, a fact which may be corroborated in that the inactivation of the RB gene is widely published. (46) Another commonly encountered root of cell cycle regulatory escape is due to inactivation of tumour suppressor genes that encode CDK inhibitors, such a p53, p16 and p27. (55) As the cell cycles unchecked from the increased initiation signals, further downstream regulatory checkpoints will lose tight control, causing the genomic instability which propels tumour evolution.

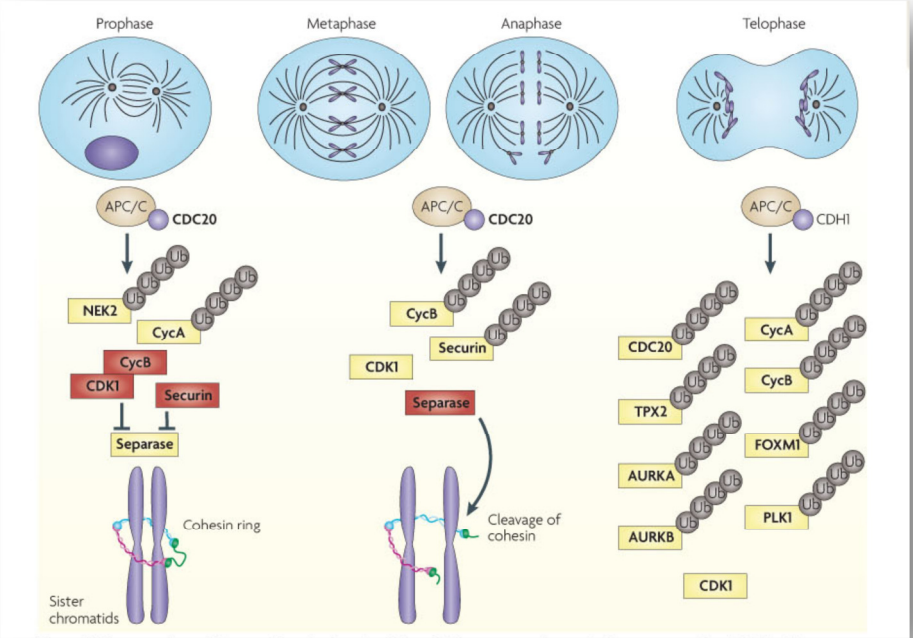

Figure 1.5: A schematic representation of key molecules involved in mitotic progression. Late in prophase, APC/C=Cdc20 ubiquitinates 2 (Nek2) and Cyclin A, while the cyclin B-Cdk1 complex and securing prevent the action of separase, thus maintaining the adhesion of the sister chromatids. The Cdk1-cyclin B complex confers optimal activity to the APC/C-Cdc20 cyclosome. At the metaphase/anaphase transition, the cyclosome targets cyclin B and securin proteolysis, thus allowing the separation of the sister chromatids by activated separase. During telophase and the following G_1 phase, the APC/Cdh1 complex ubiquitinates an array of substrates involved in mitotic

progression and DNA replication. Reprinted by permission from Macmillan Publishers Ltd: [Nat Rev Cancer](55), copyright (2009)

1.2.2 Cell cycle checkpoints

Should critical errors occur in the processing of a phase, the cell cycle will arrest at an appropriate checkpoint in order to allow for corrections to occur. Checkpoints assure fidelity in the cellular replication during strategic points, such as at the DNA damage checkpoint, DNA replication checkpoint and during segregation of chromatids (the spindle and mitotic checkpoint). (91) The function of a checkpoint is to recognise a fault, quickly halt the succession of the cell cycle and maintain the *status quo*, initiate the repair machinery, and once mended, allow re-entry into the cycle. (92) Three functional units of a checkpoint can be identified, namely a sensor (to detect genomic and functional faults and generate a signal), a signal transduction initiator (to amplify the initial signal into a cascade) and a response element (to halt the cell cycle). (36) Should the cell damage be irreparable, the checkpoints are also responsible for elimination of these aberrant cells by inducing permanent cell cycle arrest or inducing cell death. Amongst other, genetic mutation of the checkpoints may be the origin of oncotic transformation, allowing DNA changes to accumulate. (91) The elimination of the checkpoints would result in aberrations in ploidy, increased vulnerability to environmental mutagens, abnormal organelle distributions and/or cell death.

DNA may be damaged in numerous ways, and should be detected at the DNA replication checkpoint. (89) Phosphodiester bonds in the DNA may be broken by free oxygen radicals (produced by various metabolic processes or ionizing radiation) resulting in either double or single strand helical breaks. (89, 93) Purine bases may be modified by alkylating agents, changing the size of the molecule and resulting in either inter- or intra DNA strand crosslinks. (94) Additionally, inhibition of DNA topoisomerases may be enhanced with ether single or double strand breaks in the DNA helix. (95) Each type of damage must be repaired by a specific intracellular response, a challenging process which requires time to execute, which is provided for by slowing down or inducing arrest of the cell cycle. (89) To prevent the cell cycle continuing, induction of phosphatidylinositol-3-OH kinase (PI3K) and

related phosphoinositide 3-kinase-like kinases (PIKKs), ataxia telangiectasia mutated (ATM) and ATM-and radiation 3 (Rad3)-related (ATR), are initiated to activate the DNA damage checkpoint and induce the signal transduction pathways to halt the cell cycle and coordinate the relevant machinery to execute repair . (91, 93, 96) DNA nonhomologous end joining (NHEJ) (the major mechanism in G_0/G_1 and G_2) and homologous recombination (HR) (only active in G_2) are the major dsDNA repair mechanisms. (93)

Checkpoints are constitutively active, and permanently screen for mistakes, allowing cell cycle progression at the strategic points if all is well, or inducing a cellular arrest on detection of an error. (36) These tactical transitions occur upon entry of the quiescent cell into the active division pathway (G_1/S), entry into mitosis (G_2/M) and exit from mitosis (M/A).

1.2.2a The G_1 or G_1/S checkpoint

The most important checkpoint for DNA integrity is the G_1 or G_1/S checkpoint for DNA replication. This causes the initiation of the ATM(ATR)/checkpoint kinase 2 (CHK2)(CHK1)-p53/ murine double minute 2 (MDM2)-p21 pathway, which has the capacity to initiate, sustain or even cause permanent arrest in G_1. (91, 97-99) Should DNA damage be detected, ATM/ATR directly phosphorylates the transcription factor p53 while, together with CHK2/CHK1, indirectly increases p53 function by deactivating the ubiquitin ligase MDM2, which is normally responsible for the rapid degradation of p53. (99, 100) The up-regulated and stable p53 particularly increases the transcription of $p21^{Cip1}$ (also known as Cyclin-Dependent Kinase-Interacting Protein 1 (CIP1) or wild-type p53-activated fragment 1 (WAF1)), which, as previously discussed, inhibits E-cyclin-Cdk2 interaction, casing G_1 arrest by preventing the deactivation of RB/E2F transcription factors. (57, 89) In response to DNA stress, CHK1 and CHK2 levels are increased, which causes a down regulation of Cdc25A which has a resultant inhibition of E-cyclin/Cdk2 complexes. (89) This pathway of cell cycle arrest is rapidly active, but not sustainable long term without the collaboration of the p53 induction described above. p53 induction may occur due to numerous formats of DNA damage, including single ssDNA damage, insertion/deletion mismatches and free DNA ends.

(101) This transcription factor may also be induced following severe DNA damage to execute the p53-dependent apoptotic pathways.

There is a checkpoint in the S phase which responds to genotoxic insults, the details of which have not yet been fully elucidated. Apart from toxic insults, tight regulation of the replication machinery also needs to be monitored. It is essential that the DNA unwinding factors need to be intimately associated with the DNA replication units. DNA helicase comprises of two regulatory sub-units, and a structural core, the latter being made up of 6 microsome maintenance proteins 2-6 (Mcm2-7). (102, 103) Although the Mcm2-7 complex surrounds the double stranded DNA (dsDNA), it remains inactive until cell division cycle protein 45 (Cdc45) and GINS (Go, Ichi, Ni and San) bind as the activating regulatory subunits. (102, 103) This activated assembled helicase is then termed the CMG complex (Cdc45, Mcm2-7, GINS). (102) This CMG complex should theoretically be linked to the polymerase a/primase unit, (identity of this 'link' protein has not yet been defined), the uncoupling of which would lead to DNA replication aberration which would trigger the S phase checkpoint.

One of the 'red flags' in initiating the S phase checkpoint are long single strands of DNA covered in replication protein A (RPA) and unprotected telomeres. (100) ATR is induced and binds to the RPA to initiate kinase activity, causing temporary cessation of the S phase progression via the p53 pathway. (100, 103) Additional to its screening activity, ATR also serves to stabilize the replication forks which contain ssDNA, including stalled forks. (104) Stalled forks are regions of DNA with a point mutation of sorts which causes polimerase a/primase block, thus stopping the polymerization. (104) These stalled forks are thus essentially areas of ssDNA and activate ATR, which in turn phosphorylates checkpoint kinase 1 (CHK1) further downstream to protect the area during repair. (103) The precise mechanisms are still being unravelled. Once the ssDNA has been converted back into dsDNA, ATR is deactivated and the cell is released from its checkpoint. (103) Should a dsDNA break occur, either by a mutated ATR function or another factor (such as ionizing radiation of UV exposure), activation of ATM is induced, which phosphorylates the downstream checkpoint kinase 2 (CHK2) which triggers a cascade in initiating dsDNA repair. (100) Additionally, ATR activation causes p53 phosphorylation as well as phosphorylation at certain sights on the Nijmegen breakage syndrome (NBS1) and the cohesion protein

structural maintenance of chromosomes 1 (SMC1) (which is part of the cohesion complex which causes sister chromatids to stick together after replication). (38, 105) ATR/ATM is able to arrest replication via the Cdc25A degradation cascade, which inhibits Cdc45, the structural subunits of DNA helicase, to bind the chromatin. (100) Thus the two arms of the S phase checkpoint comprise of inhibition of replication-firing origin and of a replication checkpoint.

1.2.2b The G_2/M checkpoint

The G_2/M checkpoint prevents cell cycle transition into mitosis should there be any unresolved problems which escaped previous checkpoints, accumulation of the replication checkpoint, or newly occurring damage in G_2. (89) The target of this checkpoint is the cyclin B-Cdk1 complex, which may be inactivated by ATM/ATR, CHK1/CHK2, functional decrease of p38-kinase and/or inhibition of the Cdc25 kinase family (which normally activate Cdk1 during this transition). (75, 89) This cycle arrest may be p53 dependent and/or independent. (35) Cdk1 is either maintained in an inactive form, or the Cdk1-cyclin B complex (MPF) components are sequestrated to the cytoplasm. DNA damage causes ATR-dependent CHK1 and CHK2 activation in an ATM-dependent manner, which in turn inactivates Cdc15 by phosphorylation (ATM-CHK2 signalling at dsDNA breaks and ATM-ATR-CHK1 at resected dsDNA breaks). (93) This inactivation promotes Cdc25 binding with the 14-3-3 proteins resulting in cytoplasmic accumulation, thus preventing activation of the Cdk1-cyclin B complex. (74) The cell is thus declined mitotic entry. The p53 dependent pathway in the G_2/M block relies on a DNA damage induced increase of this transcription factor, which in turn up-regulates p21, growth arrest and DNA damage inducible gene (Gadd45) and 14-3-3 *sigma* (σ) transcription. (57, 75) Increased binding of 14-3-3σ to cyclin B prevents its entry into the nucleus, whereas Gadd46 causes active dissociation of the B cyclin-Cdk1 complex. (75) The p21 pathway has been discussed in previous paragraphs.

Stress detection, be it disassembly of microtubules due to drug exposure, topoisomerase II inhibition, histone deacetylases, ribotoxic insults or osmotic shock causes rapid cell cycle arrest by a p38-mediated cascade. (36) Although it has a quick onset, the block will not be sustained unless the transcription dependent p53/p21 pathway is induced. (36)

DNA damage induced mechanisms also target upstream regulators of Cdc25 and/or Cdk1-cyclin B complex formation, such as Polo-like kinases (Plk3 and Plk1) which are inhibited by DNA damage. (106) Breast cancer susceptibility protein 1 (BRCA1) and Fanconi anaemia, complementation group D1 (FANCD2), which pay a part in S phase checkpoints (their deregulation causing increased DNA frailty and susceptibility to dsDNA breaks to radiation), also may have a role at the G_2/M checkpoint. (89) The presence of mediator (adaptors or signal modifiers) proteins, such as the mammalian tumour suppressor p53 Binding Protein 1 (pp53BP1) and mediator of DNA-damage checkpoint-1 (MDC1), is needed for the amplification of the ATM signal after exposure and to maintaining the state of cellular arrest during the repair process.(93, 107)

It is important to note that throughout the literature study of this transitional period in the cell cycle, the presence of all the above mentioned factors and cascades are not essential for the described process to occur. The correct entry and progression through mitosis is critically dependent on the collaboration of many proteins, events and processes occurring in prior phases. Additionally, it is imperative that the constitutive kinases and transcription factors required for mitotic entry and correct spindle formation are switched on correctly. (36) By the end of G_2, the 4N cells starts undergoing nuclear envelope breakdown (NEB), an event which irrevocably commits the cell to mitosis. (36)

1.2.2c The spindle assembly checkpoint

The spindle assembly checkpoint (SAC) has at least 14 proteins involved in signaling mechanisms, and is highly conserved throughout eukaryotes in order to ensure fidelity in the chromosome segregation phase. (33)

Once NEB occurs, dynamic microtubular arrays generated by two separating centrosomes interact with the chromosomes to form a bipolar mitotic spindle. (36, 108, 109) Each chromosome has two sister kinetochores to which a spindle from the opposite pole must attach via K fibres formed as the NEB occurs (amphitelic attachment), in order to separate the chromatids equally between the two poles. (108, 110) Kinetochores attach the microtubules to the chromatids via a 10 subunit KMN network (kinetochore nuL-1 (Knl1),

microtubule-associated protein 12 (Mis12) and Nuclear Division Cycle 80 (Ndc80) subcomplexes) assembly. (111, 112) In vertebrates, monotelic attachment occurs, a 'search and capture' process in which kinetochores capture the elongating microtubules from the centrosome (not a simultaneous sister kinetochore attachment), resulting in chromosomal attachment to the spindle. (108) Syntelic attachments (whereby both sister kinetochores are attached to the same pole) and merotelic conditions (in which a single kinetochore is simultaneously attached to microtubules originating from both pole) are mostly efficiently and rapidly corrected via an Aurora-B kinase mechanism in the kinetochores. (109) It is also postulated that correct tension is required on the kinetochore-spindle assembly, sensed by Aurora B, for it to be stabilized. (111) In order to decrease aneuployid formations in daughter cells, a SAC is present to delay the onset of anaphase (separation of chromatids) should the presence of an unattached kinetochore be detected. (86, 111, 113)

The kinetochores also have the spindle assembly checkpoint, which work on the mitotic checkpoint complex (MCC) to prevent APC/C activation until all the chromatids have attached and have been bio-orientated. (111) At least 8 protein kinases are associated with spindle checkpoint signaling, working together with checkpoint proteins associated with the kinetochores to produce a 'wait anaphase' signal. (33) The culmination of a block at this spindle assembly checkpoint (SAC) entails Cdc20 inhibition which is needed to activate the anaphase promoting complex (APC), an E3 ubiquitin ligase which promotes metaphase to anaphase entry. (114) The checkpoint proteins involved were originally identified in yeast cells, but are conserved in higher eukaryotes. Constituents of the yeast SAC comprises of mitotic arrest deficient 1-3 proteins (MAD-1,-2 and -3), budding uninhibited by benzimidazole 3 (BUB3), Aurora B (in higher cells) and two kinases, BUB1 and monopolar spindles 1(Mps1) (Mps1 is activated in the presence of Cdc37). (114) In eukaryotes, Mad3 complexes with Bub1 related kinase domain on the C-terminus (BubR1), and is activated by the centromere protein E plus end kinesin (CENP-E) when not attached to microtubules. In addition, four protein kinases namely p38 Mitogen-activated protein (MAP)-kinase, NIMA-related protein kinase 2A (Nek2A), thousand-and-one amino acid kinase 1 (Tao1) and protein of the yeast U4/U6 small nuclear ribonucleoprotein particle 4 (Prp4) (analogous to the *Drospophila* Rough Deal, Zeste-White 10 (ZW10) and Zwilch (RZZ)) are required for this checkpoint. (39)

Checkpoint proteins are dynamically associated in a catalytic complex with unattached kinetochores, where the release of the mitotic checkpoint complex (MCC) (composed of Mad3/BubR1, Mad2, Bub3 and Cdc20) occurs, which then inhibits the APC (figure 1.6). (87, 115) The important step in this process is the Mad2-Cdc20 interaction, as due to Cdc21 sequestration the cyclosomes are prevented from recognising securin and cyclin B. (115) During prophase, Bub1 is first to localize at the assembling kinetochore, and is required for the subsequent recruitment of proteins. (33) Bub1 regulates Mad1 and Bub3 spindle attachment to the kinetochore by phosphorylation, thereby modulating Mad2 activity to inhibit APC/C-Cdc20. (33) Cdc20 is also directly inhibited by Bub1, as is centrometic cohesion via human histone 2A (H2A). (33, 116) Bub1 is important in the centrometic localization of shugoshin, a critical event as the shugoshin-PP2A complex preserves the centrometic cohesion during prophase by preventing the excessive release of cohesin. (116) Apart from the Mad/Bub based mitotic checkpoints, evidence does suggest that DNA damage can be restored by the ATM/p38 pathways described during G_2/M checkpoint. (117)

When the spindle checkpoint is not satisfied, the induced block can delay anaphase for many hours, but not indefinitely. (117) Should the cell enter anaphase without the correction of a merotelic attachment, a 'lag' chromosome can be detected: a common cause of aneuploidy. (117) Additionally, it is important to note that the checkpoint is not sensitive to incorrect kinetochore attachments, nor to the position of the chromosome on the spindle. (117) The induced cellular arrest is lifted once all the kinetochores become stably attached to the spindles and the production of the inhibitory complexes are terminated. (86) Thus the cyclosomes are allowed to function in the anaphase progression by Cdc20 regulation, by destroying securing and the B-cyclin regulatory subunit of Cdk1. (115) Cdc20 also degrades cyclin A and Nek2, independently of SAC. (55) Securin degradation causes sister chromatid disjunction, and decreasing levels of cyclin B induces the exit from mitosis. (86) Once anaphase has been completed, the functionality of SAC is maintained by chromodomain-helicase-DNA-binding protein 1 (CHD1), a co-factor in the ubiquitination of many mitotic and DNA replication proteins, in order to prevent Cdk1 activation while the cell is exiting from mitosis or in the follow-on G_1 phase. (55)

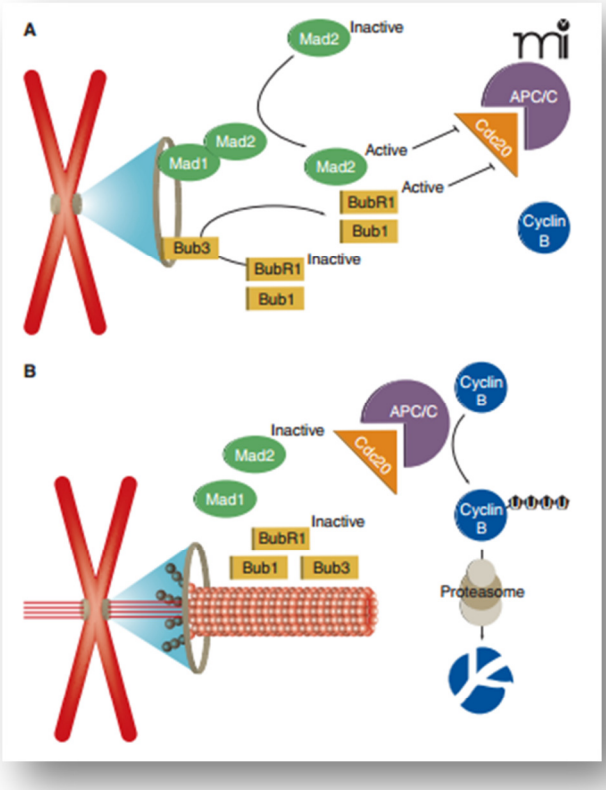

Figure 1.6: Spindle assembly checkpoint and its function in the metaphase-anaphase transition. A. Should an error occur in the spindle attachment to the kinetochore, recruitment of the checkpoint proteins Mad2, Bub3 and BubR1 to the kinetochore and will inhibit Cdc20 activation of the APC/C. This results in cellular arrest at the G_2M checkpoint. B. Once the corrections have been implemented, the kinetochores are all attached correctly to spindles and the SAC satisfied, the MCC proteins are no longer recruited to the kinetochore, the resultant available Cdc20 binds to and activates the APC/C causing cyclin B ubiquitination, the decreasing levels of which drives the cell into anaphase. Reprinted by permission from ASPET Journals: [Molecular in(ter)ventions](87), copyright (2011)

Spindle poisons (or mitotic inhibitors/anti mitotic agents) are drugs which prevent or interfere with mitosis and disrupt cell division by blocking mitosis. (117, 118) This is achieved by interrupting the microtubule dynamics and/or preventing centrosome separation, and thus not satisfying the SAC. (117, 118) A classical example is colchicine, which prevents mitotic checkpoint satisfaction and thereby blocks the cell in mitosis. (117) Cells, especially nontransformed cells, may slip out of mitotic block if it continues too long, and thus enter the next G_1 cycle as a single 4N cell. (119) At this stage, the cell may be stopped via the p53 pathway, unless as in a neoplastic cell, the functional lack of p53 allows

the progression of the cell cycle resulting in a logarithmic increase in ploidy at each cycle (a concept termed endocyclin or endoreduplication). (118, 119) There is a continued presence of kinetochore-associated check proteins such as BubR1 and Mad2 in untransformed cells, allowing the postulate that a very slow cyclosome-mediated destruction of cyclin B occurs due to less than 100% function of the mitotic checkpoint. (117)

The picture differs in transformed cells. Slippage in HeLa cells (commercially available cervical carcinoma cell line) seems to be correlated with caspase-mediated cleavage of BubR1 at the time of the metaphase block. (120) Seeing that most of mitotic spindle poison treated HeLa cells die, it remains to be determined if this is due to a gradual slippage process or suddenly as part of cell death. There is a caspase dependent and independent mechanism to induce cell death. (121) The cells are arrested in mitosis in direct proportion to the concentration of the drug, up to a certain point when they either slip into G_1 or die. (117) This indicates that the time spent in mitotic arrest is inversely proportional to the number of spindle-kinetochore interactions it can form. The duration of arrest may also show an intracellular variation, a difference between different cell lines and may vary between species. (117)

Both the slippage and mitotic arrest-induced death cascades occur via the intrinsic apoptotic pathways. (118) The upstream triggers, whether they are the same or not, that lead to this common pathway are as of yet not clearly elucidated. It does appear the spindle poison induced cell death in HeLa cells occurs via an APC/C independent mechanism, although a longer mitotic arrest causes more effective cell killing. (118)

1.3 Microtubule dynamics

Microtubules are multifunctional cytoskeletal proteins (long filamentous tube-shaped polymers about 25 nm in diameter) necessary to many essential processes in cell functioning, such as intracellular transport, cell signaling, maintenance of cell shape and as part of the spindle formed during mitosis to ensure correct chromosome segregation and cell division. (122, 123) The microtubules consist of α-tubulin and β-tubulin heterodimers,

with dimensions of 4 nm x 5 nm x 8 nm, 100 000 Da in mass, and can be many micrometers in length (figure 1.7). (124) After nucleation, the plus (+) end microtubules assembles more tubulin dimers onto a sheet-like lattice, which once sufficient growth has occurred, rolls up into a cylinder. Thus microtubule growth is not a helical process, but rather a conformation change possibly triggered by guanosine-5'-triphosphate (GTP)-tubulin hydrolysis to guanosine diphosphate (GDP)-tubulin. (124) Structural polarity is a hallmark characteristic of the microfilaments, the + end being conferred by hydrolysis of GTP associated with β-tubulin, thereby creating 'GDP-tubulin', which is stabilized by a short cap. (125) The + end grows faster than the minus (-) end, the latter which is usually anchored to the centrosome or microtubule organizing centre (MTOC). (125) On X-ray crystallography, it was demonstrated that the lateral interaction of two tubulin dimers, α1β1 and α2β2, form a curve while interacting with stathmin-like helical domain. (123) This curved configuration may serve to prevent lateral contacts between protofilaments and the N-terminal hook of the stathmin-like domain, which regulates longitudinal contacts between dimers (figure 1.8). (123) Stathmin is a cytosolic tubulin-binding protein which is phosphorylated by Cdks (under the control of PP2A) at up to 4 serine residues in response to various intra- and extracellular signaling pathways, and is essential in the spindle formation during metaphase. (126) This protein has been described as a tubulin sequestering and catastrophe factor, and requisitions tubulin dimers in a polar α1β1-α2β2 arrangement, with the NH_2-terminal of stathmin being at α-end of the tubulin dimer interaction. (125) After metaphase, stathmin is dephosphorylated. (126)

γ-Tubulin, located as either a monomer, heteromere or as a large ring complex near the MTOC which has the centromere embedded within it, is involved in the microtubule nucleation and stabilization. (123) Two γ-tubulins and two associated proteins form a tetramer (known as the γ-tubulin small complex (γ-TuSC). (123) Three or more accessory proteins associate with the γ-TuSC to form a γ-tubulin ring, proposed via two various models to initiated microtubule nucleation. (123) Microtubules grow 'outward' form the MTOC, with the + end leading. (127) Various other tubulins have been identified, which have a restricted distribution and are thought to be involved in duplication of centrioles and basal bodies. (123) A range of molecular chaperones (prefoldin at translation, cytosolic chaperonin containing TCP-1 (CCT) and later with five tubulin binding cofactors (TBCs A-E)

protect the microtubule assembly process from forming aggregations and proteasome destruction. (125, 127) Many proteins interact with microtubules including the motor proteins dynein and kinesin, plus-end tracking proteins (+TIPs) and microtubule associated proteins (MAPs).(125)

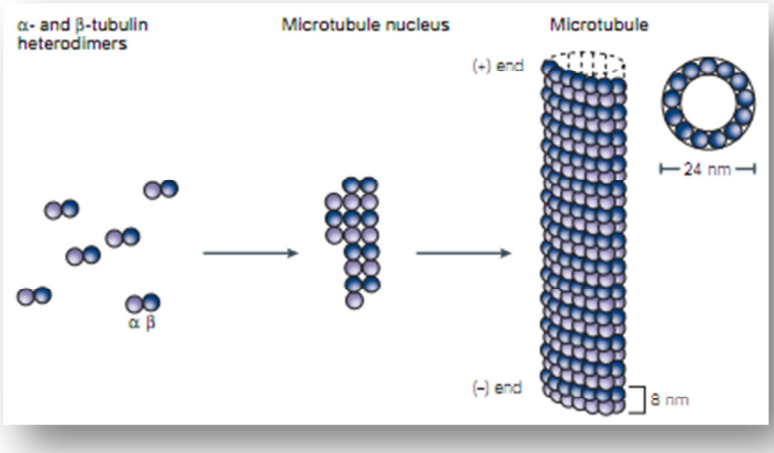

Figure 1.7: Microtubule polymerization: α-β dimers form a short microtubular nucleus, which is then followed by elongation of the microtubule at both ends (mostly the + end) to form a cylinder composed of tubulin heterodimers arranged head-to-tail in 13 protofilaments. The +ends are defined as the end at which the β-tubulin faces the solvent (as opposed to the α-tubulin at the – pole). Reprinted by permission from Nature Publishing Group: [Nat Rev Cancer] (124), copyright (2004)

These microtubules are characterised by dynamic behaviour which allows the cell to arrange them into different arrays according to the cell's specific functional need. (54) Microtubule dynamics may be regulated in several fashions: binding of regulator proteins, such as MAPs to either the soluble tubulin, to the microtubule surfaces or to the microtubule ends, by different tubulin isotope expression, and through different post-translational modifications of the tubulin. (128)

The tubulin polymers are not in equilibrium, but rather show complex polymerization dynamics which utilize energy derived from the hydrolysis of GTP. (128, 129) Dynamic instability is an essential ability of these tubules, and is characterised by the switching at the microtubule ends between phases of slow growth and rapid shortening. (128) Three main

characteristics are used to describe this dynamic instability: the rate at which the microtubules grow or shorten, the frequency between growth/pause to shortening transitions (called catastrophe) and the frequency of shortening to growth/pause (termed rescue). (125) Dynamicity describes the overall tubulin dimer exchange rate at the microtubule ends. (125) Another form of dynamic behaviour is termed 'treadmilling' and is the net growth at one microtubule end balanced with the net shortening at the opposite end (129). The phosphorylation of MAP's has a large role to play in the regulation of the tubulin dynamics, as in this state they detach from the microtubule lattice or tubulin, thereby decreasing the microtubular stability. (125) Actin cytoskeletal mechanisms have been implicated in stabilizing and guiding the microtubules in their intended journey in the cell. (125)

In interphase, microtubules are nucleated in the MTOC on the kinetochore of the chromosomes, which is rich in the γ-tubulin ring structures. (123) Additionally, during mitosis, nucleation of microtubules occur on the centrosomes at the two opposite poles. (54) This interaction, once passing the metaphase and spindle formation checkpoint, causes the alignment of the chromatids on the equator, and the sister chromatids are subsequently separated to their respective poles for cytokinesis to begin. (125)

A major anti-tumour action employed in the development of anticancer drugs is the kinetic stabilization or destabilization of spindle microtubule dynamics, resulting in mitotic arrest (124). Conventional microtubule-targeting agents (MTA) have been used in the treatment of cancer for more than 30 years. (130) The effect of these MTAs is either stabilization of the microtubules (taxanes) or prevention of polymerisation, even depolymerisation at high concentrations (vinca alkaloids) achieved by the binding to α/β heterodimers. (124) Thus, paclitaxel binds to the already formed microtubules (binds the β-tubulin in a binding pocket between two nascent tubulin dimers) (Figure 1.8) to prevent treadmilling or dynamic actions, whereas vinblastine (a vinca alkaloid) binds to the tubulin monomers preventing their association and thereby limiting tubule polymerization. (87, 123) Resulting from the abrogated tubulin network are cells which do not pass the spindle assembly checkpoint, and are arrested at the metaphase/anaphase transition. (87) Consequently, the cells blocked in metaphase will ultimately undergo cell death. (36, 131) The precise mechanisms and

affectivity of these MTAs is cell line and tissue dependent. (87) Additionally, there is a high development of resistance to these drugs. (131) This resistance is explained by drug efflux pumps or various mutations in the tubulin, amongst others. (131)

Colchicine is one of the archetypal MTAs, and it inhibits microtubule assembly by binding to tubulin stoichiometrically. (132) It binds at the β-tubulin between the α-tubulin of the same subunit, whereas vinblastine binds between different subunits as demonstrated in figure 1.8. (123) Antiproliferative effects of 2-methoxyestradiol (2-ME), the parent compound of C19 (a novel 2-ME analogue synthesized by our research team (133)), have been ascribed to, amongst others, the ability to disrupt microtubule polymerization dynamics by binding to the colchicine binding site of tubulin (a regulatory domain that interacts with endogenous substances affecting the microtubule assembly). (134)

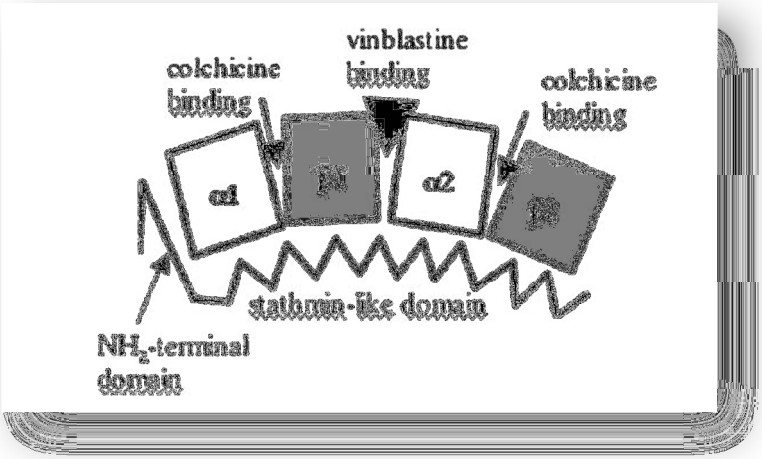

Figure 1.8: A schematic representation of two tubulin dimers in a curved formation interacting on the stathmin-like helix. Vinblastine binds between two tubulin dimers, whereas colchicine binds at the β-tubulin within the same subunit. Reprinted by permission from Springer Publishing Group: [Mol Biotechnol] (123), copyright (2009)

1.4 Types of cell death

Literature searches unfold three important and interconnected stress-response death mechanisms, namely autophagy, apoptosis and necrosis (figure 1.9). These various types of cell death differ from each other by morphological and biochemical attributes, as well as

entail differences in the mode of death. (135) Programmed cell death embraces the concept that the death mechanism is an organised and genetically controlled process, as can be seen in apoptosis and autophagy. (135) Necrosis has mostly been considered an 'accidental' type of cell death, until recently, where new evidence revealed that under exceptional circumstances, the initiation and modulation of the course of the death may have programmed mechanisms. (136)

When analysing the publications on the different types of cell death, one may get the impression of a continuum: insults at a low dose may induce a self protective autophagic response, progress to autophagic death and/or apoptosis induction, and as the insult becomes overwhelming or sustained, necrosis results. Moreover, studies have shown that autophagic and apoptotic mechanisms share common signaling pathways and are also mutually regulated. (137, 138) Depending on the mechanism of injury and cell type, one pathway of cell death may predominate, or conversely, multiple mechanisms may play a simultaneous part in the demise of a cell. (136) Understanding the crosstalk between apoptosis and autophagy has become the topic of intense investigation, and unravelling thereof will be crucial in the future development of treatment modalities for conditions such as cancer.

Other types of cell death have been identified, but the mechanisms not yet fully elucidated nor the definitions fully agreed upon. Alternate forms of cell death include: mitotic catastrophe which results from cells experiencing aberrant mitosis and are halted by the mitotic checkpoints; (139, 140) pyroptosis which encompasses a caspase 1 mediated non-apoptotic pro-inflammatory programmed cell death; paraptosis as seen in neurodegenerative diseases and is characterized by swelling of the endoplasmic reticulum and mitochondria, along with extensive vacuole formation; entosis, in which epithelial cells invade each other due to detachment from the cellular matrix; and anoikis, a classical apoptosis triggered by physical detachment of cells from either other cells or a supportive matrix. (135)

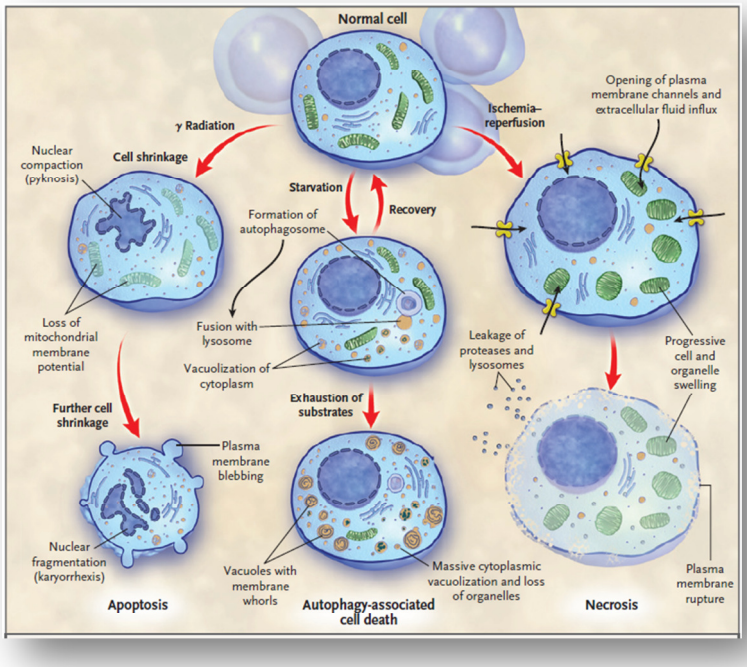

Figure 1.9: Three major types of cell death, namely apoptosis, autophagy and necrosis with their gross typical hallmarks. Not shown in the diagram are the molecular crosstalk pathways believed to exist at multiple levels. Reprinted (no permission needed for theses/dissertation) from Massachusetts Medical Society: [NEJM] (135), copyright (2009)

1.4.1 Necrosis

Cell death via necrosis, or may also be termed oncosis or oncotic necrosis, is characterized by cell and organelle swelling with consequent cell rupture and extravasation of intracellular contents. (141, 142) Necrosis is a cell death process which does not require energy, causes random DNA degradation, loses membrane integrity as an early event, and stimulates an immune inflammation response *in vivo*. (143) This type of cell death is classically caused from metabolic failure resulting in a rapid loss of ATP. Membranes are functionally compromised in this process, allowing cytosolic proteolytic enzyme leakage from the lysosomes thereby initiating the death sequence.

The onset of necrosis is mediated by a range of triggers, including the formation of reactive oxygen species (ROS), calcium ions (Ca^{2+}), poly-ADP-ribose polymerase (PARP), calcium activated non-lysosomal proteases (calpains) and cathepsin. (135, 136, 143) PARP functions

in catalyzing DNA strand break repair mechanisms in an energy intensive manner, thereby depleting the intracellular stores rapidly and inducing necrosis. (135) This response is muted early on in apoptosis, because it is an energy dependent pathway, and rapid cleavage and inactivation of PARP preserve energy stores. (135, 136) Ca^{2+} has an origin dependent effect on the cell death pathway: an influx of intracellular Ca^{2+} across the cell membrane is central to necrosis, whereas the release of Ca^{2+} stores from the endoplasmic reticulum is more inclined to induce apoptosis. (136)

Due to the loss of integrity of the cell membrane, small ionized molecules which would not normally traverse the membrane may be used to detect necrotic cells. (143) Agents such as propidium iodide have a high affinity for DNA, and increase fluorescence on binding, making them a valuable tool with which to assess the presence of necrotic cell death. (143) It is to be noted however, that cell membranes also lose their integrity late in apoptosis. (142, 143)

1.4.2 Apoptosis

In antithesis of necrosis, apoptosis is characterized by shrinkage of the dying cell and nucleus while maintaining cell membrane integrity until very late stages. (136, 143) Apoptosis is classified as type 1 programmed death. (142) Components of the subcellular infrastructure collapse due to proteolytic cleavage of cytoskeletal proteins by aspartate specific proteases. (135) Micrographic hallmarks of apoptosis include condensation of the chromatin, ordered nuclear fragmentation, membrane blebbing and the formation of apoptotic bodies. (136, 142-144) Also contrary to necrosis, death by apoptosis is highly energy dependent and immunosuppressive and thus does not cause an inflammatory response. (136) Molecules such as phosphatidylserine (PS) are flipped from an inner membrane location due to loss of membrane asymmetry, to be exposed on the external surface to facilitate annexin V recognition mediated phagocytic engulfment. (136) The latter principle may be applied in various laboratory techniques to detect and quantify cells undergoing apoptosis. (145)

In most viable eukaryotic cells, a phospholipid asymmetry exists over the inner and outer cell membrane. (145) Whereas phosphatidylcholine and sphingomyelin are predominantly

located on the outer surface, the negatively charged phospholipid phosphatidylserine (PS) is found on the cytosolic aspect of the cell membrane lipid bilayer. (145) An early event in apoptosis, occurring before any morphological changes, is the loss of this asymmetry by the translocation of the PS from the inner surface to the outer aspect of the cell membrane. (146) Conversely, during necrosis, PS only becomes accessible due to membrane disruption and loss of integrity. (145, 146) One of the triggers for macrophage recognition and phagocytosis of apoptotic cells involves the outer membrane exposure of PS on the apoptotic cells. (147) The recognition of exposed PS units occurs by Annexin V (placental anticoagulant protein 1), a 35kDa phospholipid-binding protein, which is also a major component on cell membranes of various phagocytic cells. (148, 149) In the presence of physiological concentration of calcium ions, Annexin-V has a high affinity for PS. (149)

1.4.2a The role of caspases in apoptosis

Caspases (homologous to *C. elegans* domain-3 (ced-3)) are a group of evolutionary conserved cysteine proteases, which cleave their substrate after an aspartate residue (consensus sequence is QAC(R/Q)G). (150, 151) These enzymes are essential not only in programmed cell death, but also have a role in cytokine maturation, development and haemopoietic cell line proliferation. (150, 151) Caspases are important in the orchestration of cascades which implement the mechanisms of apoptotic cell death by proteolytic cleavage of specific substrates in order to alter protein function. (152) Two subsets of caspases may be established, with the subset which cleaves specific substrates to induce the changes associated with apoptosis termed the executioner caspases (caspases 3, 6 and 7), while those which activate the afore-mentioned are termed the initiator or apical caspases (caspases 2, 8, 9, 10 and 11). (153, 154) Caspases are synthesized as zymogens, and may be activated either by oligomerization of the monomers (such as in the initiator caspases), or through cleavage of dimeric executioner caspases. (153, 154)

Apical/initiator caspases are associated with the extrinsic apoptotic pathway, in which they are activated in response to a membrane death receptor ligation, which belongs to the tumour necrosis factor receptor (TNFR) family. (151, 153) The Fas (CD95/Apo-1) death

receptor pathway has been established as a working model for caspase-8 activation. (154, 155) After the binding to Fas-ligand (on immune cells), the cytosolic tail of the Fas receptor interacts with the death domain (DD) of FADD (Fas-associated death domain protein), an adaptor molecule. (150, 153, 155) Caspase 8 is then recruited by FADD via an interaction with the homophillic death effector domain (DED) of its long prodomain, resulting in protein assemblage commonly referred to as the death-inducing signaling complex (DISC). (150, 153, 155) Once the FADD-Fas DISC receptor platform has been assembled, programmed cell death is initiated. (156) Downstream executioner caspases such as caspase 3, undergo proteolytic cleavage by an initiator caspase (such as caspase 8) to activate them. (153-155)

Caspases are key factors in the orchestration of cascades which implement the mechanisms of apoptotic cell death by proteolytic cleavage of specific substrates in order to alter protein function. (152) Two subsets of caspases may be established, with the subset which cleaves specific substrates to induce the changes associated with apoptosis termed the executioner caspases (caspases 3, 6 and 7), while those which activate the afore mentioned are termed the initiator or apical caspases (caspases 2, 8, 9, 10 and 11). (153, 154) These enzymes are important not only to programmed cell death, but also have a role in cytokine maturation, development and haemopoietic cell line proliferation. (150, 151)

Caspase 8 (also known as FLICE (FADD-like interleukin-1 beta-converting enzyme)/MACH/Mch5) is a member of the ICE (interleukin-1β converting enzyme)/*Caehorhabditis elegans* domain 3 (CED-3) family cysteine proteases. (151, 157) It is the most upstream protease in the cell death initiation signal cascade, and is thus classified as one of the initiator caspases of the extrinsic pathway. (157) Over expression of FLICE induces cell death by apoptosis. Caspase 3 (also known as cysteine protease P32 (CPP32),YAMA (after the Hindu god of death), apopain, interleukin 1-converting enzyme-like proteases (LICE), and spinocerebellar ataxia 1 (SCA-1)) is also a member of the same family of proteases, but occurs downstream together with caspase 6 and 7 in the converging pathways of apoptosis cascade and is classed as an executioner caspase. (158-160) This caspase cleaves its substrate after an aspartate residue (consensus sequence is QAC(R/Q)G). (150) Capsase 3 induces DNA fragmentation by cleaving the inhibitor of CAD (ICAD) from

the caspase-activated DNAse (CAD) which then, as an active component, causes DNA fragmentation. (160)

Apical/initiator caspases are associated with the extrinsic apoptotic pathway, in which they are activated in response to a membrane death receptor ligation, which belongs to the tumour necrosis factor receptor (TNFR) family. (153) The Fas (CD95/Apo-1) death receptor pathway has been established as a working model for caspase-8 activation. (155) After the binding to Fas-ligand (or Fas, or TNF), the cytosolic tail of the Fas (or TNF) receptor interacts with the death domain (DD) of FADD (Fas-associated death domain protein), an adaptor molecule. (150, 153, 155) Caspase 8 is then recruited by FADD via an interaction with the homophillic death effector domain (DED) of its long prodomain, resulting in protein assemblage commonly referred to as the death-inducing signaling complex (DISC). (150, 153, 155, 160) Once the FADD-Fas DISC receptor platform has been assembled, programmed cell death is initiated. (156, 160) Downstream executioner caspases such as caspase 3, undergo proteolytic cleavage by an initiator caspase (such as caspase 8) to activate them. (153, 155)

Apoptosis occurs via two main convergent cellular activation pathways: the death-receptor mediated or extrinsic pathway, and the mitochondrial or intrinsic pathway (figure 1.10). (135, 160) There are various factors which determine the pathway to be taken in order to facilitate the suicide of the cell, and may depend on the type and magnitude of the apoptotic stimuli and extent of the insult, the phase in which the cell is in the cell cycle, and the stage of cellular activation (in immune cells). (161) Numerous pathological stimuli are able to concomitantly trigger the various pathways. (161) Apoptosis is not only associated with responses to noxious stimuli, but is an essential aspect of normal organogenesis and tissue development and maintenance.

1.4.2b The extrinsic apoptotic pathway

The extrinsic pathway is activated by the death receptor pathway. (160) The TNFR death ligands, for example factor for activating ExoS (Fas), Fas ligand (FasL), tumour necrosis factor (TNF) or TNF-related apoptosis-inducing ligand (TRAIL,) form bonds with their respective transmembrane death receptors in the cellular membranes. (135, 160) On binding of the death ligand and the death receptor trimerization occurs, causing clustering of the death domains which initiates the recruitment of a cyctosolic adaptor protein, FADD (in the case of Fas mediated recruitment), or TNF-R1-associated death domain (TRADD) (when recruitment is initiated by TNF), occurs. (160) TRADD will then recruit FADD. (160) FADD not only has an analogous death domain which binds to the receptor-ligand death domains, but also a death effector which bind to the analogous domain on the zymogen caspase 8 (or 10). (135, 151, 160) This complex composed of the receptor, its ligand, caspase 8, some other regulators and co-factors is termed the DISC and allows for the autocatication and recruiting of more caspase 8 and/or 10. (160) Either inhibition or facilitation of FADD and caspase 8 binding to the activated death receptor can be mediated by the cellular FADD-like interleukin-1 beta-converting enzyme (FLICE)-inhibitory protein (c-FILP) in a concentration dependent manner. (135) Caspase 8 and 10 are upstream initiator caspases of the extrinsic pathway which will consequently cause cleavage of the downstream executioner caspases (such as caspase 3 and/or 6 and/or 7). (135, 151, 160) The executioner caspases orchestrate cellular cleavage after specific aspartase residues. (159) Irrespective of the initiating sequence, both the extrinsic and intrinsic pathway converge at the executioner caspases for the implementation of the killing mechanisms. (151, 159)

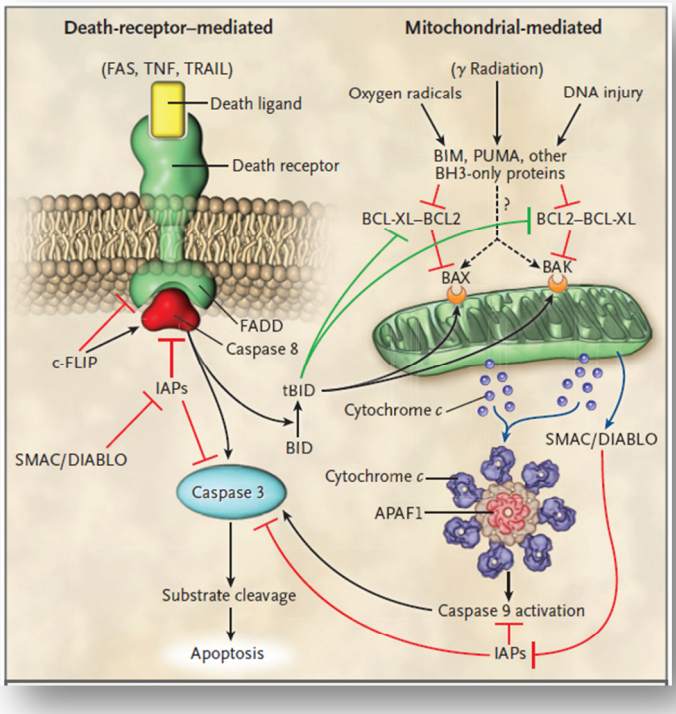

Figure 1.10: Intrinsic and extrinsic apoptotic pathways. The death-receptor mediated (extrinsic) cascade is initiated with the binding of death ligands (TNF family members) to the death receptor, which in turn sequestrates FADD followed by the initiator caspase 8 (and/or 10), which is then cleaved. This causes the cleavage of the executioner caspase 3 (and/or caspase 6 and/or7). The executioner caspases cleave cellular proteins at specific Asp residues to affect apoptosis. Interplay between pro-apoptotic and anti-apoptosis BCL2 family members controls the intrinsic pathway. Noxious stimulation induces the pro-apoptotic BH3 proteins (BIM, PUMA, other BH3 proteins), which inhibit the pro-survival BCL2 members (BCL2, BCL-XL) in order to activate BAX and BAK. The latter translocate to the mitochondrial membrane to cause increased permeability, allowing cytochrome *c* and SMAC/DIABLO to escape. Cytochrome *c* complexes with APAF-1, ADP and zymogen caspase 9, to form the apoptosome. SMAC/DIABLO inhibit IAPs, preventing caspase inhibition. Activation of caspase 9 catalysed by the apoptosome results in the downstream convergent executioner caspase (3,6,7) activation. Crosstalk between the pathways may be mediated by caspase 8 cleavage of BID, resulting in a truncated form of BID which inhibits the pro-survival BCL2 proteins. (160) A question mark still hangs over whether the BH3 proteins can also directly activate BAX and BAK when under a pro-apoptotic stimulus. Reprinted (no permission needed for theses/dissertation) from Massachusetts Medical Society: [NEJM] (135), copyright (2009)

1.4.2c The intrinsic apoptotic pathway

The mitochondria or intrinsic apoptotic pathway exhibits interplay between anti-apoptotic and pro-apoptotic members of the BCL2 family of proteins. (135, 160, 161) Should the intracellular sensors detect severe intracellular damage from an increase in reactive oxygen species (ROS), unfolded proteins, DNA damage and/or response due to deprivation of growth factors, the permeability of the mitochondria increases thereby releasing pro-apoptotic proteins (such as cytochrome c) from the inner mitochondrial space. (135, 160) These pro-apoptotic proteins act ether by causing activation of caspase 9 (by cytochrome *c*), or as in the case of Diablo homologue (second mitochondria-derived activator of caspases (SMAC)/direct inhibitor of apoptosis protein (IAP)-binding protein with low pI (DIABLO)), inhibit the activity of cytosolic apoptotic inhibitors. (161) Caspase 9 converges at the executioner caspases (3, 6 and 7) as does the death receptor caspase 8, which cleaves proteins and activates the DNAses. (160)

There are pro-apoptotic and anti-apoptotic members of the BCL2 family (see figure 1.11) which regulate the induction of the mitochondrial pathway, of which each protein must have at least one conserved BCL2 homology domain. (135, 160, 161) It is this domain which is used in the regulation of apoptosis by causing hetero- or homo-dimer formation. (160) The anti-apoptotic BCL2 members have up to 4 BCL2 homology domains. They are essential for cell survival and function, and include BCL2 , B-cell lymphoma extra large (BCL-XL), B-cell lymphoma like 2 (BCLW), myeloid cell leukaemia 1 (MCL1), A1 and BCL2 homolog of ovary (BOO)/DIVA/B-cell lymphoma 2 like 10 (BCL2-L10), with their expression varying between various tissues and disease conditions. (160-164)

The pro-apoptotic BCL2 proteins differ from pro-survival members with the number of BCL2 homology domains, as well as their function. (135, 161) Critical for the release of cytochrome *c*, are BCL2 associated X protein (BAX) and BCL2 antagonistic killer (BAK), which have three BCL2 homology domains and function to increase the permeability of the mitochondrial membranes. (160, 161) Pro-apoptotic BCL2 family members such as BCL2 interacting mediator of cell death (BIM), p53 up-regulated mediator of apoptosis (PUMA) and BID, only have the BCL2 homology 3 (BH3) domain, with which they bind to and

deactivate the pro-survival BCL2 proteins, thereby liberating BAX and BAK for increased mitochondrial membrane permeabilization. (160) Distinct apoptotic stimuli, including oncogenic activation, cause activation of one or more BH3-only proteins. (135) These stimuli include one or more of the following: DNA damage (including ionizing radiation), hypoxia, loss of growth factor stimulation and anoikis. (160, 165) There is a marked variation of cell-type dependent BH-3 protein expression. (161) Each BH3 pro-apoptotic protein is preferentially stimulated via specific death inducing stimuli. (135) Growth factor deprivation selectively stimulates BIM (166) whereas PUMA is up-regulated in response to DNA damage. (165)

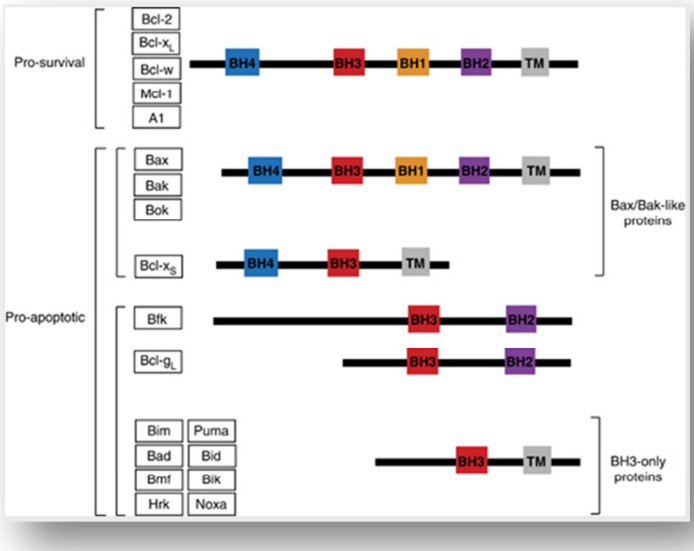

Figure 1.11: Members of the mammalian BCL2 protein family. Broad categorization divides these proteins into pro-apoptotic and pro-survival (anti-apoptotic) subgroups. These proteins show areas of homology termed BCL2 homology domains (BH), and may also have a transmembrane domain (TM) which allows for insertion into the outer mitochondrial and endoplasmic reticula membranes. The pro-survival proteins (BCL2, BCL-XL, BCLW, MCL1 and A1) all have the same 4 BH domains and a TM region. A further division of the pro-apoptotic group may be made: those with multi-BH domain proteins (BAX, BAK, BOK, BCL-XS, BCL-G_l and BFK) (with or without TM regions) and proteins which have only the BH3 domain (BAD, BIK, BID, HRK, PUMA, BIM, NOXA and BMF). Reprinted by permission from Nature Publishing Group: [Cell Death and Differentiation] (161), copyright (2011)

On the intrinsic pathway being activated by the various stress signals (ROS, γ radiation, DNA injury, withdrawal of growth factors etc), the pro-apoptotic BH3 proteins (BIM, PUMA and other BH3 proteins) are activated which bind with and deactivate the pro-survival BCL2 proteins (BCL2, BCL-XL etc). (160, 161) This frees BAX and BAK to cause a decrease in the mitochondrial membrane, allowing the escape of cytochrome *c* (or other similar functional proteins). (135, 160) A debate is still raging as to whether the BH3 proteins can directly stimulate BAX and BAK (pro-apoptotic proteins), and not just via the anti-apoptotic protein suppression route. (161, 166-168) Cytochrome *c* interacts with apoptotic protease-activating factor 1 (APAF-1) and deoxyadenosine triphosphate (dATP) to form the active apoptosome in the cytoplasm, to which pre-caspase 9 is bound. Auto-activation of caspase 9 occurs in the apoptosome, resulting in the active caspase 9, which in turn cleave the executioner caspase 3/6/7 to initiate the death sequences by activating PARP, amongst others. (160) The permeabilized mitochondria also release SMAC/DIABLO, to counteract the actions of inhibitors of apoptosis (IAPs), and to prevent them from functioning as caspase inhibitors. (135)

There seems to be crosstalk between the intrinsic and extrinsic apoptotic pathways. This interaction is mediated by the truncated form of BCL2 interacting domain (tBID), which is formed upon BID (a pro-apoptotic BH3 protein) cleavage by caspase 8 (induced by the death receptor of the extrinsic pathway). (135, 160, 161) tBID works to inhibit the BCL2/BCL2-XL suppression of apoptosis, in order to allow BAK and BAX activation and translocation to the mitochondrial membrane as part of the intrinsic cascade. (160, 161)

1.4.2d Other apoptotic pathways

Other apoptotic pathways include Ca^{2+} release from stressed endoplasmic reticula, causing caspase 12 cleavage by calpain induction. (169) Caspase 12 then activates caspase 9, which in turn cleaves the executioner caspases (3,6 and 7) to proceed with the regulated protein cleavage. (169) Another pathway involves DNA damage, which provokes the expression of p53-induced protein with a death domain (PIDD), which consequently binds to receptor-interacting protein (RIP)-associated ICH-1/CED-3 homologous protein with a death domain

(RAIDD) and caspase 2, causing the latter's activation (and later the executioner caspases) which is involved in the p53 pathway. (170)

Experimental detection of apoptotic cell death relies on satisfying 4 axes: (1) morphological detection of apoptotic hall marks (via light, various interference contrast, fluorescent and transmission electron microscopy) and cell membrane permeability by flow fluorocytometry; (2) cell surface markers specific to apoptosis (phosphatidylserine flip); (3) intracellular markers (oligonucleosomal DNA fragmentation by flow cytometer, caspase activation, BID cleavage and cytochrome *c* release by western blotting or spectrophotometrically) and (4) extracellular markers in the supernatant (caspases, high mobility group box 1 protein (HMGB-1) to detect necrosis and cytokeratin 18). (142, 143) Examples in brackets are representative of a few methods.

There are other caspase negative mechanisms of apoptosis. (171) MCF-7 breast cancer lines have been found to execute programmed cell death independently of caspase 3 executed apoptosis, indicating the existence of alternative mechanisms. (172) Kitagawa and Niikura offered an alternative to caspase mediated cell death, proposing a mechanism linkd to the failure to satisfy the spindle checkpoint. (121) On cellular treatment with spindle poisons, a caspase-independent mitotic death (CIMD) mechanism, executed via the tumour suppressor and checkpoint protein p73 (a p53 homologue) was executed. (121) This model implemented the apoptotic-inducing factor (AIF) and endonuclease G (EndoG) in this death mechanism which protects the cell from aneuploidy. (121) Terminal deoxynucleotide transferase dUTP nick end-labelling (TUNEL) analysis and other mechanisms confirm the features associated with type 1 programmed cell death. (121) Additionally, Wang *et al* published results in which inhibition of mitogen-activated protein (MAP)/extracellular signal-regulated kinase (ERK) kinase (MEK) in melanoma cells caused a caspase independent mechanism of cell death, by up-regulation of BH3 proteins PUMA and BIM while down-regulating pro-survival MCL1. (173) They proposed the release of AIF instead of caspase activation was responsible for this cascade of cell death. (173) Lastly, autophagic death (programmed death type II) may have a caspase independent death pathway, which may be useful in drug design for apoptosis resistant tumours. (174) Thus

evidence may be accumulated for caspase independent death mechanisms and must be born in mind on evaluating experimental results related to cell death mechanisms.

1.4.3 Autophagy

Initially, metabolically stressed cells will induce autophagy as a means for survival by increasing the turnover of intracellular contents in an evolutionary conserved mechanism of organelle engulfment in double membrane vesicles (termed autophagosomes or autosomes) followed by lysosomal degradation of the contents. (175) Should this environmental stress be of a prolonged duration, type II programmed cell death or macroautophagy will be induced via either caspase dependent or independent pathways. Evidence also exists that autophagy and apoptosis have signaling pathways in common and are mutually regulated. (176)

When misfolded proteins exceed a threshold level of chaperone-mediated re-folding and the ubiquitin-proteasome degradation pathway, these proteins are then actively transported along microtubules to pericentriolar inclusions. (177) These latter inclusion bodies are termed aggresomes, and are typically formed in response to a cellular insult or stressor. (178) Clearance of these proteins within the aggresomes is facilitated via autophagy. (177)

Autophagy is a catabolic state in which the cell utilizes lysosomal-dependent mechanisms of intracellular organelle degradation in order to recycle the cytosolic contents. (135) There are to date three forms of autophagy described (figure 1.12) which differ in how the cytosolic content is delivered to the lysosomes, namely microautophagy, macroautophagy and chaperone-mediated autophagy (CMA). (174, 179, 180) Macroautophagy functions by creating specialized *de novo* double membrane vesicles from a limiting membrane of non-lysosomal origin to which the cytosolic contents is sequestrated, and consequently degraded after the vesicular fusion with a lysosome. (174, 179) Within this sub-class, differentiation may be made between non-specific ‘in bulk’ cytoplasmic sequestration and degradation of heterogeneous cytosolic content, and distinctive selection of specific organelles for degradation, an autophagic process in which an extra step of cargo

recognition occurs. (179, 180) The latter lends itself to more organelle specific terms, such as mitophagy (181), pexophagy (182), reticulophagy (183) and aggrephagy (184).

Characteristic of microautophagy is the direct engulfment of cargo via invagination of the lysosomal membrane, which after it is pinched off, undergoes degradation by lysosomal hydrolases. (179) Cellular exposure to conditions causing denaturation of proteins, such as prolonged starvation and oxidative stress, CMA is the mechanism with which the misfolded proteins are escorted by heat-shock protein 70 (hsc70) and co-chaperones to the lysosomal membrane. (179, 185) On binding to the lysosome-associated membrane protein type 2A (LAMP-2A) receptor, the denatured proteins are translocated across the membrane for rapid degradation in the lysosomal lumen. (185) For this study, the focus will be on macroautophagy, which will be termed simply autophagy from now on.

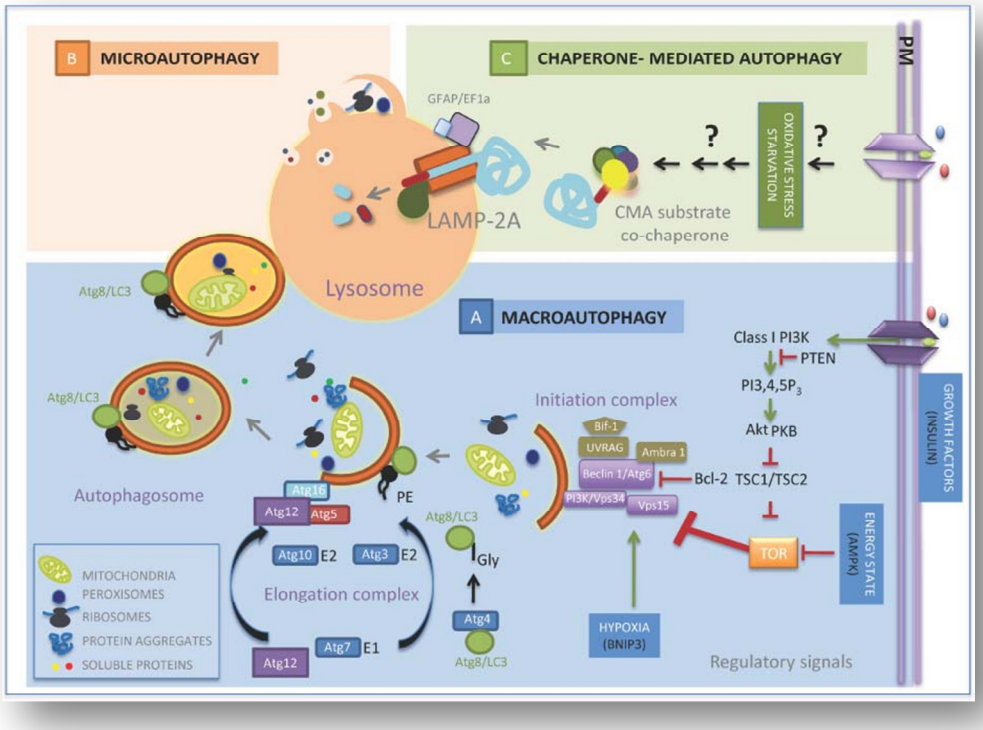

Figure 1.12: Three distinct mechanisms of autophagy. A: Macroautophagy is initiated on various intra- and extra-cellular signal induction pathways, and promotes the recruitment of the autophagy initiating complex to the desired site of autophagosomes formation. After shuttling of proteins and lipids to this sight, post-translational changes to the lipid molecules induce the formation of the limiting membrane, which subsequently elongates due to the assembly of proteins joined to

proteins or lipids while sequestering cytosolic components. The completed autophagosome then fuses with the lysosome to allow hydrolysis of the content. B: Microautophagy occurs when soluble cytosolic proteins are sequestered directly into the lysosomes by invagination of their membranes which pinch off to allow the degradation of the contents. C: Chaperone-mediated autophagy is a process whereby denatured proteins with certain targeting motifs are escorted to the lysosomes by hsc70 (and co-chaperones), which on binding to LAMP2A on the membrane initiates the translocation of the misfolded protein into the lumen for degradation. Reprinted by permission from John Wiley & Sons: [Journal of Pathology], (179), copyright (2012).

1.4.3a Functions and control of autophagy

Literature studies on autophagy lead one to a proverbial quagmire of information, in which seemingly contradictory and fragmented information is presented. Autophagy may singularly be responsible for the pathogenesis and induction of some neoplasms, the drug resistant properties of others, and a therapeutic mechanism employed to destroy yet another set of cancers. (138, 174, 186) Initially, autophagy was linked to household functions of quality control, involved in destroying damaged, degenerated or dangerous components from the cell. (137, 187) It has also been described as an adaptive mechanism, in which a metabolically distressed cell may utilize this organelle breakdown as an alternative source of energy to promote survival and suppress cell death. (138, 174) Evidence now suggests that the critical continuation of cellular deprivation or distress may then switch from pro-survival mechanisms to a form of autophagic cell death (type II programmed cell death), either together with apoptosis or in mutually exclusive applications. (137, 138) The mechanisms are still under investigation, as are the myriad of crosstalk pathways which trigger either a pro-survival or a cell death response. Autophagy has been attributed critical roles in normal development, immune response, programmed cell death, tumour suppression, removal of apoptotic cell corpses and protective functions against neurodegeneration, and thus been ascribed a fundamental pathogenic cause of many illnesses when deregulation of the pathway occurs. (174, 179)

What does seem to be clear is that there are evolutionary conserved tightly regulated autophagy related genes, the protein products of which (Atg or autophagy related proteins)

are implicated in the execution and regulation of autophagy (initially identified and classified in yeast). (187) There are several protein complexes involved in autophagy, which broadly include the Atg1-kinase complex needed in the nucleation of the vesicle (light chain protein 3 (LC3) bound to a membrane lipid with Atg5 and Atg12 between them), and two ubiquitin-like protein complexes which function in the elongation of the isolation membrane, and a retrieval system that supervises the disassembly of Atg proteins once the autophagosomes are mature. (188) Mammalian Atg 8-related proteins are incorporated in the autophagosomes and have functions in cargo recruitment and autophagosomes closure. (188) Various components such as SNAP (Soluble NSF Attachment protein) receptor proteins (SNARE)-like proteins, lipid modifying enzymes such as phosphatases and kinases, and molecular motors are involved in the fusion of lysosome and autophagosomes. (179)

One of the key pathways that control autophagy are sensors that decipher the status of cellular energy (AMP-dependent protein kinase (AMPK), the availability of nutrients and amino acids (mammalian target of rapamycin (mTOR), and the presence of growth factors such as insulin). (189, 190) mTOR is a major inhibitory signal of autophagy which antagonises autophagy in the presence of abundant nutrients and growth factors. (190) This is done mostly via activation of downstream class 1 phosphatidylinositol 3-kinase (PI3KC1)/protein kinase B (Akt) signaling molecules which link receptor kinases to mTOR activation and thereby suppress autophagy. (190) Other regulatory molecules include: 5'-AMP activated kinase (AMPK) which responds to low energy states; the eukaryotic initiation factor 2α (eIF2α) activated by starvation, dsRNA and endoplasmic reticulum (ER) stress; BH3 domain only BCL2 proteins which disrupt the BCL2/BCL-XL inhibition of the proximal step of the Beclin-1/class III PI3K (PI3KC3) complex formation; the p53 death associated protein kinases (DAPk) as a positive inducer of autophagy; Ire-1, the ER associated protein; the inositol-1,4,5-triphosphate receptor (IP_3R); GTPases; extracellular-signal-regulated kinase 1 or 2 (ERK1/2) activated by lack of growth factors in the MAPK cascade; c-JUN-N-terminal kinase which is stress activated, also part of the MAPK pathway); ceramide and calcium. (189-191)

Downstream from mTOR kinase are more than 30 genes encoding proteins needed in the execution of autophagy as demonstrated in yeast prototypes. (180, 189) The

autophagosome formation may be divided into six sequential steps namely initiation, nucleation, elongation, closure, maturation and extrusion. (192) The protein serine/threonine kinase complex Atg1p consists of Atg1, Atg13 and Atg17 (the mammalian counterpart is unc-51 like kinase (ULK1)) and responds to upstream signals (e.g. mTOR) to control the early steps in the autophagosome formation. (180, 188, 189) The production of the phosphoinositide signals, which control the assembly of the autophagosomes, are controlled by vacuolar protein sorting Vps34-Vps30p complex (mammalian counterpart PIK3C3-Beclin-1). (180, 188, 193) Sources for the building blocks of the phagophore membrane include the Golgi bodies, endosomes, the endoplasmic reticulum and the cell membrane itself. (192) Required for autophagosome maturation and cargo recruitment is a ubiquitin-like protein conjunction cascade, comprising of the E1 enzyme Atg7p, two E2 enzymes (Atg3p and Atg10p) and two ubiquitin-like proteins (Atg12p and Atg8p). (180, 188, 193) The Atg7p-Atg10p cascade joins Atg12p to a lysine residue in Atg5p, in so doing forming an oligomeric Atg12p-Atg5p-Atg16p complex which causes the joining of the carboy-terminal glycine residue of Atg8p to phosphatidylethanolamine (PE) via Atg3p. (193) The Atg8p-PE complex may be incorporated into the autophagosomes by the Atg5p complex, allowing Atg8p to operate in autophagosome cargo recruitment and closure. (188, 189, 193) Atg2p, Atg9p, Atg18p and Atg21p constitute a recycling system, in which they regulate the transfer and recycling of constituents from the source of the lipids needed in the formation of the vacuole to the growing autophagosomes. (188, 193)

The autophagy systems are far more complicated in mammals when compared to the yeast prototypes. Moreover, yeast Atg proteins may have several corresponding proteins in the mammalian cell which are involved with a parallel regulatory step. (189, 193) Bherends *et al* conducted a proteomic study on the autophagy interaction network in human cells and identified 65 autophagy related proteins and another 409 candidate proteins involved in 751 interactions involved with autosomic functioning at basal cell functioning. (193) Interestingly, the up-regulation of autophagy by inhibition of the negative regulator of autophagy mTOR did not lead to a change in the expression of the core systems, giving rise to the hypothesis that it is post-translational modification of the Atg proteins which play a part in this activation. (193) Additionally, it may also involve an increase or decrease in

interactions between the negative and positive regulators of the autophagy interaction networks. (193)

1.4.3b Autophagy and cancer

One of the first human pathologies connected to autophagy was cancer, by the discovery that Beclin-1 (Atg6/Vps30 homology) which is core in the autophagy nucleation complex was deleted in 40-75% of non-hereditary breast cancer. (194) This finding was independently confirmed when heterozygous mice (Beclin-1 +/-) had a predilection to develop various spontaneous tumours, including lung carcinoma, hepatocellular carcinoma, lymphomas and breast neoplasms. (195) Deletion of autophagy related genes such as ultraviolet resistance associated gene (UVRAG), the BAX interacting factor 1 (BIF1) and LC3, were associated with spontaneous highly proliferating tumours. (179, 196-198) To support the finding above, it has been shown that products of oncogens such as PI3KC1, TOR and BCL2 repress the induction of autophagy, whereas tumour suppressor genes such as p53, PTEN, DAPk and tuberous sclerosis protein 1 and 2 (TSC1/TSC2) induce active autophagy. (189, 198, 199) The data above lead to the theory that autophagy was anti-oncogenic, but has since been challenged with additional data indicating that under certain conditions autophagy may be pro-oncogenic as well.

Autophagy may be protective to cells against oncogenesis by quality control processes in genome maintenance early in the development. (179) Additionally autophagy could regulate entry and maintenance of cells in G_0 phase to prevent hyper-proliferation of cells. Contrary to this protective role, during late neoplastic developments, autophagy could play a role in cell survival in two ways. Firstly, it gives the cell a survival mechanism during times of metabolic stress, low pH and hypoxia, which occurs when the tumour cells outgrow their blood supply, by accommodating the acute energy demand through the citric acid cycle, β-oxidation and the Warburg effect, and conferring resistance to hypoxia in a HIF1α independent mechanism. (179, 197) It has been demonstrated that cells in which autophagy has been blocked are more sensitive to metabolic stress and die readily by necrosis, which is accompanied by the inflammation response. (179) Secondly, autophagy may confer resistance to the cells in which stress has been induced by a treatment regimen.

(174, 179, 197, 200) Much had been published on autophagic driven resistance to various therapies, including radiation therapy and chemotherapy (doxorubicin, temozolomide, etoposide, histone deacetylase inhibitors, arsenic trioxide, TNFα, γIFN, imatinib, rapamycin and tamoxifen), with an expected increase in therapeutic efficiency demonstrated if given when autophagy was suppressed (*e.g*. oxaloplatin, sorafinib, epirubicin or 5-fluorouracil). (174, 179, 201)

Autophagy may also, under certain circumstances, trigger a type of cell death (type II programmed cell death) which, like apoptosis, avoids an inflammatory immune response reaction. (135, 137, 138) This is a non-apoptotic type of death, entailing extensive autophagic degradation of intracellular content without the DNA laddering, which may be either caspase dependent or independent. (174) Shimizu *et al* demonstrated the induction of an autophagic mechanism of cell death after exposure to various cellular insults in embryonic fibroblasts from BAX/BAK double knockout mice which are resistant to apoptosis. (202) This demonstrated autophagic death was subsequently inhibited when cells were treated with inhibitors of autophagy (such as 3-methyl adenine), confirming the presence of true autophagic death induction dependent on Atg5 and Beclin-1. These finding also led to the deduction that the BCL2 family of proteins, which regulate apoptosis, are intimately involved in the induction of autophagic death as well. (202) Autophagic death was also observed in cellular systems treated with pan-caspase inhibitors such as zVAD-fmk, in which caspase-dependent apoptosis would be inhibited. (202) Identification of several compounds which induce autophagic death has occurred, and include rottlerin, cytocine arabinoside, etoposide and staurosporine. (174, 203)

1.4.3c The role of Beclin-1 in autophagy

Beclin-1 is a BCL2-homology 3 (BH3) only protein which plays a key function in the regulation of autophagy. (192, 200, 204) It is central in the localization of autophagic proteins and when in association with PI3KC3/Vps34 leads to a pre-autophagosomal structure (PAS). (180) Beclin-1 is expressed in many mammalian tissues and is localized within cytoplasmic structures such as the ER, nuclear membrane and mitochondria. (195, 205) Three structural domains have been identified on Beclin-1, namely the BH3 domain on

the N-terminal, a central coiled domain (CCD) and an evolutionary conserved domain (ECD). (205) A small leucine-rich sequence is also incorporated in the Beclin-1 structure which is needed in the efficient nuclear export signal (NES). (206) The ECD is important in Beclin-1's ability to mediate autophagy and suppress tumorigenesis. (192) The BH3 domain binds to anti-apoptotic BCL2 members, the activating molecule in Beclin-1-regulated autophagy (Ambra)/UV radiation resistance-associated gene (UVRAG)/Atg14L bind at the CCD domain and PI3KC3/Vps34 interacts with both the ECD and CCD domains. (192, 198) Beclin-1 has the capacity to self-associate via the CCD. (207)

The function of Beclin-1 in autophagy can be modified by phosphorylation and ubiquitination, modifying the Beclin-1 interaction by changing the structure of itself, altering the shape of the binding groove, altering the availability of the proteins binding together with Beclin-1, or inducing or up-regulating a transcription factor. There are also Beclin-1 independent pathways for autophagy induction. (204) Key in this signalling pathway is BCL2-interacting protein-1 (Beclin-1) which forms a complex by binding to PI3KC3 and various other proteins, and while bound, prevents cell death and activate autophagy. (200, 204, 208) Beclin-1 can be phosphorylated by the death associated protein kinase (DAPK) which is a tumour suppressor and can induce autophagy and membrane blebbing by binding to LC3. (198) The phosphorylation of Beclin-1 at position 119 at the BH3 domain prompts a dissociation of Beclin-1 from the BCL2-like proteins inducing autophagy. (189, 192, 200) c-Jun N-terminal kinase 1 (JNK1) and HMGB-1 function in a similar manner in preventing Beclin-1 association with its inhibitors. (198) Autophagy is inhibited by mTOR and RAS-cAMP-protein kinase-A (PKA) pathways. (174, 192) Phosphorylation of LC3, which is a direct substrate of PKA, prevents its recruitment to the autophagosomes. (209) Interestingly, phosphorylation of PI3KC3 occurs by Cdk1, which prevents its interaction with Beclin-1 during mitosis. (209) PI3KC3/Vps34 has also been connected to membrane trafficking processes not directly involved in autophagy. (192, 210) Fimia *et al* reported that autophagy formation was stimulated by Ambra1 release by the dynein motor complex once it has been released from there with ULK-1/Atg1 dependent mechanisms and had relocated to the ER. (210)

Should there be mutations of either the BH3 domain in Beclin-1 or the BH3 receptor domain of BCL2 or BCL-XL, the binding of the complexes would not occur, thereby inspiring autophagy. (192, 211) Although Beclin-1 is unable to neutralize the pro-survival function of BCL2, ER (but not mitochondrial) located BCL2 or BCL-XL are able to minimized the pro-autophagic function of Beclin-1. (211) Beclin-1 and ER located PI3KC3 interaction is crucial for the nucleation of autophagosomes formation. (180, 211) There are several different models as to how the association between Beclin-1 and the BCL2 regulatory proteins may be modified. (i) The Beclin-1-BCL2 interaction may be completely displaced by other members of the BCL2 protein family. (204) tBID, BAD and BCL2/adenovirus E1B 19 kDa protein-interacting protein 3 (BNIP3) inhibit the association of Beclin-1 and the anti-apoptotic proteins, but BAX and BAK do not. (192) In addition it was observed that pro-apoptotic BH3 only BCL2 members such as BAD, BNIP3, NOXA, PUMA, BIM-EL and BIK are able to induce autophagy. (204) (ii) Nutrient-deprivation autophagy factor-1 (NAF-1) dysfunction. NAF-1 functions in the IP_3R complex which facilitates the Beclin-1-BCL2 interaction in the ER. (212) The binding of NAF-1 to Beclin-1 is independent of the BH3 domain, but does depend on the redox sensitive CDGSH iron/sulphur domain. (137, 212) It is known that ROS are important in signaling the induction of autophagy but exactly how the redox state affects the cysteine-rich Beclin-1 is as yet not unknown. (192) (iii) Phosphorylation of BCL2 by the ERK pathway or phosphorylation of Beclin-1 by the DAPk pathway. (213) (iv) Beclin-1 self-interaction or homodimerization causing displacement of BCL2 or BCL-XL. (207) (v) Ubiquitination of Beclin-1 mediated by TNF receptor associated factor 6 (TRAF6). (214) (vi) Other Beclin-1 binding proteins such as HMGB, UVRAG or Atg14L/Barkor competitively displaces BLC2 in the binding of Beclin-1, causing a condition of heightened autophagy and cellular protection during times of stress. (198, 207)

1.4.3d Crosstalk between autophagy and apoptosis

The molecular inducers and regulators of both apoptosis and autophagy are similar and interconnected. The stimuli are common to both, being able to activate either one or both pathways; apoptosis and autophagy share genes needed in both of their execution. A good communication strategy must exist for these mechanisms to cohabit and co-operate. Crosstalk between autophagy and apoptosis is very complex, and at times even

contradictory, and is paramount in the development, treatment and outcome of death-related pathologies such as cancer. (138)

One of the interesting examples of crosstalk involves the HMGB-1 chromatin associated nuclear protein and extracellular damage-associated molecular pattern molecule, which binds to Beclin-1 in the maintenance of autophagy in a redox dependent way. (192, 215, 216) Oxidation of HMGB-1 determines its localisation within the cell and whether it induces autophagy or apoptosis. (215) In cancer cells treated with anti-cancer agents, the rate of apoptosis and autophagy increases as does HMGB-1 release, the latter two in a pro-survival attempt. (192) When HMGB-1 was inhibited, apoptosis predominated and autophagy was suppressed. (215) In the pro-survival state, reducible HMGB-1 binds to RAGE (receptor for advanced glycation end products), but not to toll-like receptor 4, to induce Beclin-1 mediated autophagy and thereby lending the tumour cells resistant to the various treatment agents. (215) On the opposing side, oxidized HMGB-1 makes the cells more sensitive to the anti-cancer agents as it induces a caspase mediated intrinsic apoptotic pathway. (192, 215, 216)

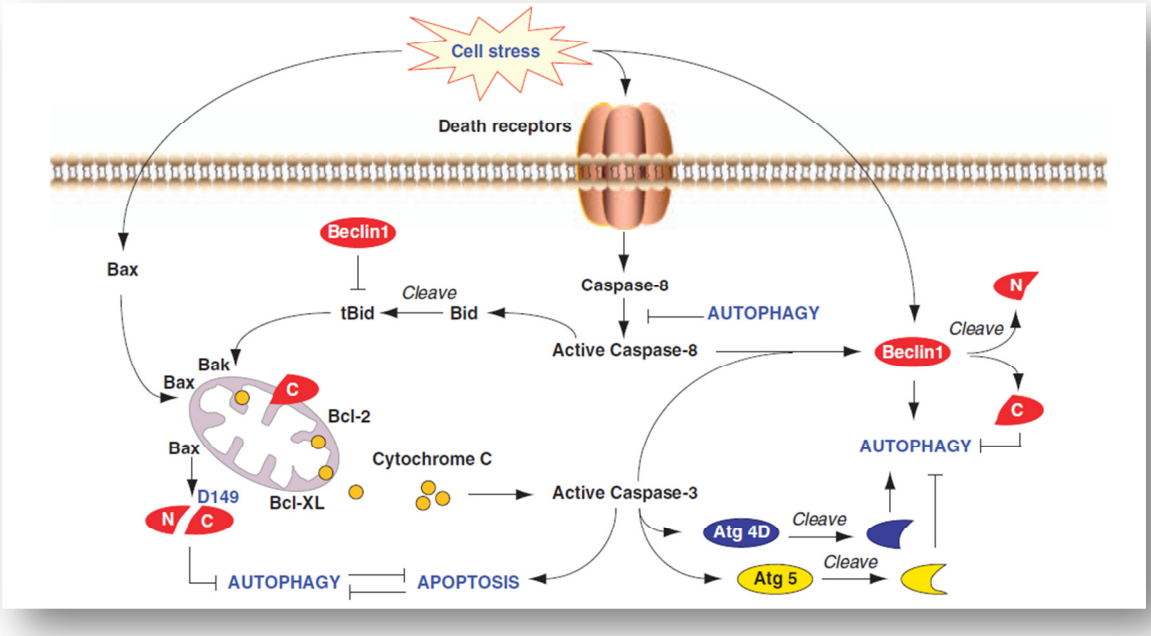

Figure 1.13: Diagram representing the proposed crosstalk mechanisms between apoptosis and autophagy. Both pathways share the same stimuli and aspects of their signaling pathways, and have some mutual inhibition. During caspase mediated apoptosis, caspase 3, 7 and 8 cleave Beclin-

1 to generate an N and a C fragment. The latter localizes to the mitochondrial to sensitize the cell to further apoptotic stimuli. Beclin-1 and Atg5 cleavage inhibits autophagy, Atg4D cleavage by caspase 3 results in a fragment which increases autophagy. A negative feedback may entail autophagic degradation of caspase 8 or Beclin-1 inactivation of BID. Reprinted by permission from Nature Publishing Group: [Cell Death and Differentiation] (192), copyright (2011).

Possibly the most well known interaction between apoptosis and autophagy is via the Beclin-1-BCL2 pathway. (204, 217) Although Beclin-1 has a BH3 only domain, it does not function as a pro-apoptotic inducer. (173, 204) Beclin-1 actually has an anti-apoptotic function in various setting such as chemotherapy, radiation therapy, nutrient depletion, angiogenesis inhibition and hypoxia. (192) The precise mechanism behind this inhibition is unclear. It has been found that caspases may be the functional link between apoptosis and autophagy. (217) In caspase dependent induction of apoptosis, caspase 3, 7 and 8 cleave the Beclin-1/PI3KC3 complex to yield fragments unable to induce autophagy (figure 1.13). (208, 217) The C-terminal of Beclin-1 then localizes primarily to the mitochondria and sensitizes them to pro-apoptotic factors. (208, 217) The death receptor ligand TRAIL has been shown to trigger caspase mediated cleavage of Beclin-1 in HeLa cells. (218) In apparent contradiction, Hou *et al* demonstrated that caspase 8 may be inactivated by autophagy. (219) This indicates that Beclin-1 may have a role in the molecular crosstalk, being the convergence point between autophagy and apoptotic cell death. (217) Caspase independent mechanisms of autophagy are also described, in which calpains may be responsible for the Beclin-1 complex cleavage. (220) Other areas of possible crosstalk between autophagy and apoptosis may include the interaction between Atg5 and BCL2/BCL-XL, regulation of Ca^{2+} signals by BCL2, Beclin-1-BCL2 or BCL2-BIK interaction switch mediated by NAF-1 at the ER and the dual role of JNK1 mediated phosphorylation of BCL2. (197, 204, 221)

Detection of autophagic hallmarks is achieved by various techniques and described in detail by Agostinis *et al* in their manuscript entitled “Guidelines for the use and interpretation of assays for monitoring autophagy in higher eukaryotes”. (222) The gold standard remains the observation of the typical whorls in the autophagic vacuoles which are the remnants of membranes via transmission electron microscopy. (135)

1.5 Antiproliferative and anti-angiogenic properties of 2-methoxyestradiol

2-Methoxyestradiol (2-ME) (figure 1.14 and table 1.1), is an endogenous metabolite of 17β-estradiol resulting from sequential hepatic hydroxylation and methylation by cytochrome P450s (CYP450's) and catechol-O-methyltransferase (COMT) respectively, has undergone phase II clinical trials registered as Panzem® by Entremed, Inc (Rockville, MD) due to published literature on its pre-clinical anti-angiogenic and antimitotic effects on both *in vitro* cell lines and *in vivo* studies. (223-226) Many cell lines and cancer types have demonstrated cellular susceptibility to the toxic effects of 2-ME over the years (table 1.2). This anti-cancer agent has multiple mechanisms of action which include abrogation of microtubule dynamics, direct and indirect angiogenesis inhibition, suppression of translation, induction of programmed cell death (apoptosis and autophagy) and induction of G_2/M block of the cell cycle. (224) An added advantage was the observation that 2-ME preferentially targeted rapidly dividing tumorigenic cells over normal cells. (227-229) The antiproliferative effects of therapeutic concentrations of 2-ME, as well as its disruptive effects on microtubule dynamics, are not dependent on the presence of an oestrogen receptor in exposed cancer cell lines. (230) 2-ME does not demonstrate any oestrogenic activity, and transported highly bound to sex hormone binding globulin. (231) Human serum levels have been determined at less than 10 pg/ml for men, 18-138 pg/ml for women (menstrual phase dependent) and up to 1678 pg/ml in pregnant women, which are much lower than concentrations needed to disrupt tubulin function. (232-234)

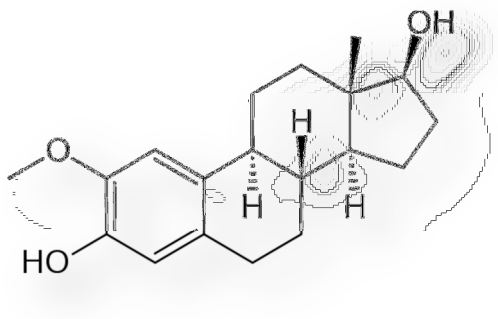

Figure 1.14: Structure of (17 beta)-2-methoxyestra-1,3,5(10)-triene-3,17-diol. (235)

2-ME has both direct and indirect anti-angiogenic characteristics. (224, 236) As a direct angiogenesis inhibitor 2-ME targets proliferating endothelial cells by inducing apoptosis

(224). Indirect angiogenic inhibitors target tumour-produced angiogenic factors, which in the case of 2-ME, can be seen by the down-regulation of the expression, nuclear accumulation and transcriptional activity of the hypoxia-inducible factor-1 (HIF-1α) at a post-translation level within the tumour and endothelial cells (236). HIF-1 is a transcription factor which interacts with hypoxia response elements (HREs) and consequently causes the transcription of pro-angiogenic proteins, the most prominent being vascular endothelial growth factor (VEGF). (237) Additionally, HIF-1-targeted genes are implicated in cell proliferation, survival, drug resistance, glucose metabolism and metastasis. (237) Increased expression of HIF-1α is associated with increased patient mortality in certain cancer types. (237)

Hypoxia-inducible factor-1α is the regulated subunit of the transcription factor HIF-1 which is induced in hypoxic (or other stress) conditions to up-regulate the transcription and translation of numerous genes involved in mechanisms to adjust to this hostile condition. (238) The stress signals stabilize HIF-1α and aid in its nuclear translocation and subsequent binding to HIF-1β. (238) The process facilitates angiogenesis (to provide a better blood supply), oxygen transport, glucose metabolism, growth factor signaling, apoptosis, as well as having a role in tumour invasion and metastasis. (239) There is a mechanistic link between 2-ME damaged microtubules and the inhibition of angiogenesis. 2-ME down regulates HIF-1 at a post-transcriptional level downstream from the 2-ME-tubulin interaction by HIF-1α down regulation, and inhibits HIF-1 transcription of VEGF. (236)

Table 1.1: Molecular characteristics of 2-methoxyestradiol. Chemical Abstracts Service (CAS), International Union of Pure and Applied Chemistry (IUPAC). (235)

2-methoxyestradiol	
Systemic or IUPAC name	(8R,9S,13S,14S,17S)-2-methoxy-13methyl-6,7,8,9,11,12,14,15,16,17-decahydrocyclopental[a]phenanthrene-3,17-diol
CAS number	362-07-2
CAS name	(17 beta)-2-methoxyestra-1,3,5(10)-triene-3,17-diol
Formula	$C_{19}H_{26}O_3$
Molecular mass	302.408 g/mol

The functional link between microtubule disruption and the anti-angiogenic effects of 2-ME lies in the ability of the compound to inhibit HIF-1α. (234, 236, 238) 2-ME disrupts tubulin dynamics by binding β-tubulin near the colchicine-binding site, and either causes stabilization of microtubule dynamics (at low concentration) or inhibition of tubulin polymerisation (at high concentrations). (134, 240-242) This binding causes cell cycle arrest at the G_2/M transition spindle checkpoint. As disruption of interphase microtubules is necessary for HIF-1α down regulation, it stands to reason that inhibition of HIF-1 occurs downstream of the 2-ME/tubulin interaction. (236) Advantages of 2-ME over the traditional microtubule targeting agents encompass a better tolerated side effect profile, no induction of neurotoxicity or myelosuppression, and it is not the substrate of multidrug resistant pumps. (224, 241, 243-245)

2-ME induces apoptosis in the endothelial cells, as well as cancer cells, by the intrinsic and extrinsic pathways, by caspase dependent and independent pathways. (229, 246) Characteristic of the extrinsic apoptotic pathway, initiation is induced by up-regulation of the cell surface death receptor DR5, making the cell more sensitive to the cytotoxic actions of the DR5 ligand TRAIL which leads to the sequential activation of caspase 8 (an initiator caspase), caspase 9 and caspase 3 (an executioner caspase). (236, 247) Demonstrating the induction of the intrinsic apoptotic pathway, multiple myeloma cells on exposure to 2-ME causes phosphorylation of c-*jun* NH_2-terminal kinase (JNK) followed by JNK translocation to the mitochondria where it causes a decreased mitochondrial membrane potential with subsequent release of cytochrome *c* and SMAC, which in turn induces the caspase cascade. (248) 2-ME may also act directly on the mitochondria to stimulate caspase 3, an executioner of apoptosis. (246)

At the core of the intrinsic pathway is generation of reactive oxygen species (ROS), giving the mitochondria a significant role in this pathway. Initially it was reported that 2-ME stimulated the production of ROS by inhibiting superoxide dismutases (SOD2) and copper, zinc-oxide dismutase (SOD1), which are essential in the elimination of the superoxide radical. (249) However a report by Hagen *et al* challenged this finding by publishing that 2-ME can inhibit mitochondrial respiration leading to ROS production by inhibiting mitochondrial electron transport chain (mETC) complex 1. (250) p53 is traditionally held

responsible for the induction of the mitochondrial pathway, but studies have proven that 2-ME can induce apoptosis with a p53-dependent and -independent mechanism. (251, 252)

Table 1.2: Malignant cell and cancer types reported to show antiproliferative effects after 2-ME exposure

Cells/cancer types	References
Breast cancer	Kimbro *et al* (238)
MCF-7	Seegers *et al* (234), Lottering *et al* (253, 254), Stander *et al* (82), Joubert *et al* (255), Klauber *et al* (245), Zoubine *et al* (256), Lippert *et al* (257), Liu *et al* (258), Han *et al* (259), Lewis *et al* (260),Cushman *et al* (242)
MDA-MB-435	Liu *et al* (258)
T-47D	Liu *et al* (258)
MDA-MB-435 /231	Han *et al* (259)
Colorectal cancer	
HCT116 & SW613-B3	Parks *et al* (228)
Leukaemia	Haung *et al* (249)
Glioma	Kirches & Warich-Kirches (261)
Erwing sarcoma	Lorin *et al* (262)
Prostate cancer	Sweeney *et al* (241), Davoodpour *et al* (263), Qadan *et al* (264), Kimbro *et al* (238)
Multiple myeloma	Rajkumar *et al* (243)
Cervix cancer	Li *et al* (265, 266), Joubert *et al* (267)
Pancreatic cancer	Schumacher *et al* (268)
Eye	Fotsis *et al* (269)
Melanoma	Dobos *et al* (270)
Lung cancer	Amorino *et al* (271), Mukhopadhyay *et al* (272)
Ovarian cancer	Matei *et al* (273), Kato *et al* (229)
Musculature	Fotsis *et al* (269)
Angiosarcoma	Reise *et al* (274)
Oesophageal	Joubert *et al* (275)
Stomach	Lin *et al* (276)

In theory, pro-apoptotic members of the B-cell lymphoma-2 (BCL2) protein family (BAX, BAK, p38-kinase and (ERK1/2) are transcriptionally induced, while the anti-apoptotic members of the BCL2 family (BCL-XL and BCL2) are suppressed by phosphorylation during the intrinsic apoptotic pathway. (275, 277, 278) Joubert *et al* demonstrated an altered BAX/BCL2 ratio in squamous epithelial carcinoma and cervix adenocarcinoma cell lines due to the decreased BCL2 expression and unaltered BAX expression levels, which is postulated to be one of the causes of apoptosis induction. (267, 275) Evidently, the precise signal transduction mechanisms are cell line and exposure agent dependent. An increase in reactive oxygen species may also be mediated by an increased expression of relevant genes by p53 induction. (248)

Previous dose-dependent studies of 2-ME exposure of oesophageal cancer cells revealed characteristic hallmarks of apoptosis with microscopy studies; namely a decrease in cell density, shrinkage of the cells, membrane blebbing, hypercondensation of the chromatin and nuclear fragmentation after 24 hours of exposure. (275) In more recent studies, tumorigenic breast cell lines which were exposed to 2-ME confirmed the apoptotic morphological changes via microscopy, and increased levels of cyclin B protein and cytochrome *c* levels, as well as increased hydrogen peroxide levels. (82) Additionally, evidence suggested the presence of a second form of programmed cell death, namely autophagy, which occurred concurrently with apoptosis. (82) This was seen in the acidic vesicle formation when stained with acridine orange during light microscopy, and increased number of vacuoles was observed in the transmission electron microscopy images. (82) Literature cites many more references to the induction of autophagy in various cell lines (including HeLa cells) by 2-ME. (82, 261, 262, 279) Gene expression microarrays revealed that many genes involved in both autophagy and apoptosis were affected, confirming the morphological data. (82)

According to Stander *et al*, sufficient evidence exists to premise the co-occurrence of tubulin disruption, apoptosis and autophagy as mechanisms of cell death in cancerous cell lines when exposed to 2-ME. (82) This is then a promising anti-cancer agent, especially in the light of findings that normal cell lines were less affected than the cancerous cell lines by exposure to the compound. (280) Not only has 2-ME proven effective in primary treatment

settings, but many reports have been published on the capability of 2-ME to sensitize conventional therapy resistant cancer strains to mainline treatment modalities, including radiation therapy. (259, 271) The pharmacodynamics appeared to be desirable in the treatment of neoplasms, but when looking at the pharmacokinetics, the picture looked different. 2-ME has a short half-life and a poor bioavailability, being a target for 17β-hydroxysteroid dehydrogenase-mediated metabolism into inactive 2-methoxyestrone. (241, 281, 282) These obstacles needed to be circumvented for the compound to be used at its full potential as anti-neoplastic agent. Methods to overcome the rapid biodegradation and improve bioavailability include designing nanocrystal dispersion techniques (started in clinical trials as Panzem NCD^{TM}) (283), finding new methods of delivery (such as encapsulation) (284) and the design of 2-ME analogues.(130, 242, 244, 285-288)

1.6 2-Methoxyestradiol analogues

The creation of 2-ME analogues has the aim of enhancing the already present anti-mitotic and anti-angiogenic properties of the compound, while modifying the undesirable or suboptimal characteristics. One of the largest obstacles to overcome in the clinical application of 2-ME as an anti-cancer agent was to decrease its rapid 17β–hydroxysteroid dehydrogenase-mediated metabolism, thereby increasing the bioavailability of the drug. 2-ME is metabolized with conjunction at the 3- and 17- positions, together with oxidation at the 17-position, and in so doing, forms inactive metabolite 2-methoxyestrone which has 10-100 fold loss of cytotoxic activity *in vitro.* (269)

1.6.1 Structural modifications of 2-methoxyestradiol

In the quest to make a 2-ME analogue with more potent anti-mitotic and spindle disruption properties, various substitutions at different side groups, and/or combinations thereof, have been produced and tested. Cushman *et al* discovered that maximal anti-tubulin activity of 2-ME was achieved by substituting unbranched chains at the 2-position. (242) They produced 2-ethoxyestradiol and 2-((E)-1-propenyl)-estradiol which demonstrated substantially higher tubulin polymerization inhibition (by binding to the colchicine binding site) and cytotoxicity than 2-ME in the MDA-MB-435 breast cancer cell line. (242) In

another study, the estrone derivative 2-methozyestron-3-*O*-sulphamate and 2-ethylestrone-3-*O*-sulphamate demonstrated a 10-fold cytotoxicity comparative to 2-ME in MCF-7 and CAL51 cells. (289) These sulphamoylated estrone derivatives induced apoptosis via BCL2 and BCL-XL phosphorylation and an increased p53 expression, and prevented tubulin assembly with a resultant inhibition of microtubule dynamics. (289) By substituting a methylsulphanyl group at the 2-position, Leese *et al* achieved an enhanced 2-ME antiproliferative activity, whereas a 2-ethyl substitution caused greater augmentation of anti-mitotic capabilities of the compound. (290) From these publications, it may be deduced that specific substitutions within the A ring are able to confer superior cytotoxic properties to 2-ME.

Tinely *et al* synthesised a range of 2-ME analogues, focusing on D ring modifications. (244) When tested in a range of tumour cell types (cervical, breast prostate and ovarian), they reported an increased antiproliferative action with the 14-dehydro-2-ME analogue, with evident microtubule disruption, decreased tumour proliferation and inhibition of angiogenesis. (244) The authors noted that the position of desaturation was important, as the 15- 7- and 2-dehyro-2-ME analogues did not show any advantage in cytotoxic capabilities over 2-ME, and some were even less so. (244) In a series of novel analogues, Edsall *et al* designed compounds to decrease the metabolic inactivation of 2-ME responsible for its poor bioavailability, by modifying the 2 and 17 positions of the compound. These compounds, including 2-ethoxy-17-(1'-methylene)estra-1,3,5(10)-triene-3-ol, were tested in cell lines and found to be as cytotoxic and poisonous to tubules as 2-ME (if not more), and were expected to inhibit the deactivation process.

Staying with the D ring, dehydration at the metabolically active 17 position indicated retention of cytotoxic and anti-tubulin characteristic together with a decreased metabolic breakdown. (291) When combined with a substitution at the 3-position to increase potency, 3-carboxyamide-2-methoxyestra-1,3,5(10)16-tetraene demonstrated suitable anti-mitotic (G_2/M arrest followed by apoptosis), anti-tubule (via colchicine site binding) and decreased HIF-1α activities, with an improved pharmacokinetic profile *in vitro* and *in vivo*. (291) This substance, ENMD-1198, is currently undergoing clinical trials and a clinical effect

has been documented, but a dose-limiting side effect of myelosuppression has been documented, although no neurotoxicity has been reported. (291)

Sulphamate substitutions on oestrogen molecule analogues increase the oestrogenic bioavailability due to avoidance of the hepatic first-pass metabolism. (292) This phenomenon is attributed to the sulpha moieties' ability to reversibly bind to carbonic anhydrase II (CAII) in red blood cells, followed by a slow release into the plasma. (292) Carbonic anhydrases (CAs) are a family of enzymes which reversibly catalyze the reaction in which water and carbon dioxide are converted into hydrogen and bicarbonate ions ($H_2O + CO_2 \leftrightarrow H^+ + HCO_3^-$). (293, 294) Eleven different subtypes of CA have been identified, of which some are located intracellularly (of which CAII is an example), and others have extracellular distributions (such as CAIX and CAXII). (294) CAIX is over-expressed in the immediate tumour environment giving neoplastic cells a growth advantage in their acidic and hypoxic extracellular milieu. (295, 296) This allows for increased intracellular bicarbonate ions (via membrane transporters) required for pyrimadine synthesis and acidic activation of the metalloproteinases thereby enhancing its invasiveness. (297) Under hypoxic conditions, CAIX and CAXII expression is increased under the control of HIF-1α. (295) The CAIX gene, which is over-expressed in a variety of tumours and causes extracellular acidification, contains a HRE which binds with activated HIF-1α to induce CAIX transcription and translation. (295) Thus selective inhibition of CAIX would provide a useful mechanism in which to manipulate the extracellular tumour milieu and curtail metastatic tendencies.

1.6.2 2-Methoxyestradiol-3,17-O,O-bis-sulfamate

In an effort to utilize the improved pharmacokinetic profile sulphamoylation imparts, 2-ME side groups were substituted accordingly. 2-Methoxyestradiol-3,17-O,O-bis-sulfamate (2-MEbisMATE) is a 2-ME analogue, which by adding a sulpha moiety at position 3 fulfils 2 objectives; increasing the anti-mitotic and spindle disruption capacities (position 3 modification) and decreasing the bioavailability with the sulpha group (by binding to CAs and eliminating the fist-pass liver metabolism). (281, 298, 299), (300, 301) Publications demonstrate a more potent anti-mitotic (10 fold), anti-spindle and anti-angiogenic (60 fold)

effect of 2-MEbisMATE when compared to 2-ME *in vitro* and *in vivo*. (281, 298, 301) The IC_{50} value (inhibition constant: concentration of substance at which 50% of the cell growth is inhibited when compared to the control) of 2-MEbisMATE has been shown to be about 10-fold less that 2-ME, indicating a great improvement in potency of the analogue. (302) The effect of this 2-ME analogue showed dose, cell line/tissue type (inhibiting both oestrogen receptor positive and negative breath cancer cells) and exposure duration dependent reports of the anti-mitotic and anti-angiogenic effects. (303, 304) Exact cellular mechanisms also seem to be cell type dependent. Results published are positive on the improved pharmacokinetics, with Newman *et al* correlating the poor oral bioavailability of 2-ME with high amounts of 17β-hydroxysteroid dehydrogenase type 2 in the gut mucosa, against which the sulphamoylation offers protection. (281) In fact, oral bioavailability of the analogue was 85%, with no active metabolites being produced by metabolism.

Modeling studies done by Leese *et al* indicated that 2-MEbisMATE bound to tubulin at the colchicine site, in the same manner as 2-ME does, accounting for the microtubule abrogative effects of the compound. (298) Additionally, they demonstrated 2-MEbisMATE binding to CAII. 2-MEbisMATE causes cells to arrest in G_2/M, followed by the induction of apoptosis (increased sub-G_1 fraction). (253, 274, 300, 304) Apoptotic induction has been linked to BCL2 phosphorylation and p53 expression in human umbilical vein endothelial cells, with other possible molecular targets including HIF-1α and mTOR. (300, 302) Wood *et al* reported a predominance of the caspase-dependent intrinsic apoptotic pathway activation in MCF-7 cells exposed to 2-MEbisMATE, with a corroborating increase in caspases 9 and 3, but not caspase 8. (303) This intrinsic pathway activation was corroborated by Visagie & Joubert by demonstrating an increased ROS production, although no change could be detected in the mitochondrial membrane potential. (285) Additionally, their data demonstrated the induction of autophagy, possibly as a response to ROS regulation of Atg4. (285, 304) Reports on tumour cell versus normal cell selective toxicity are varied. Reiser *et al* reported no differentiation of the cytotoxic effects between neoplastic and untransformed cells. (274)

1.6.3 Compound 19

Although 2-MEbisMATE has a positive profile for anticancer and anti-angiogenic activities, potency and specificity in CAIX binding was sought to be improved. Stander *et al*. designed a range of 3' sulphamoylated 2-ME analogues *in silico* by modifying the 2' and 17' positions with moieties known to improve the anti-mitotic activity and increase their half-life. (133) The panel of designed compounds was analysed using AutoDockTools4 with the prepare_ligand4py script to determine which of them bound best with the tubulin colchicines binding site and with CAIX. (133) It was demonstrated that an ethyl group on the 2 position yielded the highest binding with the colchicine site on the tubulin, which correlated with the findings of Leese *et al*. (133, 298) One of the compounds, namely 2-ethyl-3-*O*-sulphamoyl-estra-1,3,5(10)16-tetraene (C19) demonstrated a significantly stronger association with CAIX than with CAII. (133) These compounds were also modified at position 17 by dehydration in order to decrease 17β-hydroxysteroid dehydrogenase activity. After docking analysis, two of these compounds were synthesised (compound 9 and compound 19 (described by Stander *et al* in their article as C12 not as C19) and exhibited properties of microtubule interference with a resulting mitotic block and an increase in the sub-G_1 fraction of the cell cycle indicating the induction of apoptosis and/or other forms of cell death in MFC-7 breast cancer cells. (133)

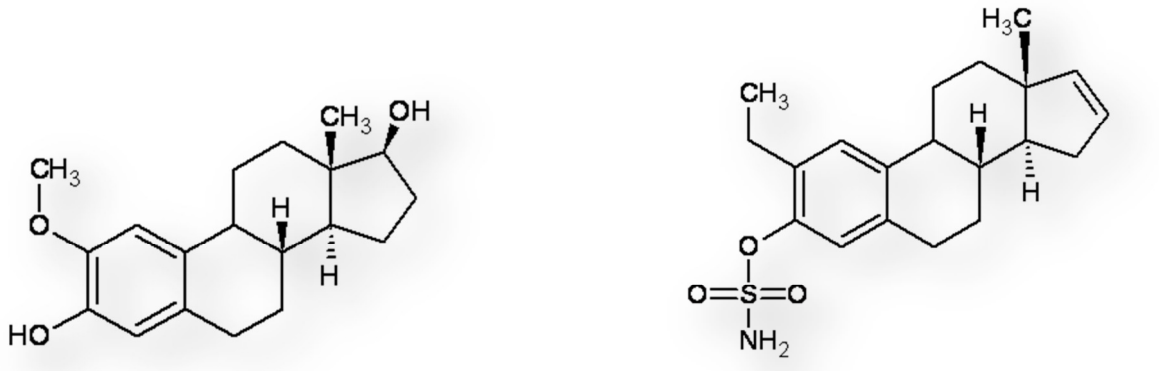

A **B**

Figure 1.15: Structure of 2-ME and C19. **A** shows the parent compound, (17 beta)-2-methoxyestra-1,3,5(10)-triene-3,17-diol (2-methoxyestradiol). **B** indicates the substitutions at position 2', 3' and 17' (position 16' dehydration) of 2-ethyl-3-*O*-sulphamoyl-estra-1,3,5(10)16-tetraene (C19), a sulphamoylated 2-ME analogue. (133)

Compound 19 (C19), 2-ethyl-3-*O*-sulphamoyl-estra-1,3,5(10)16-tetraene (figure 1.15), is one of the novel *in silico*-designed sulphamoylated 2-ME analogues which is still to be fully investigated. C19 is not currently commercially available. It possesses alterations at the 3' and 17' position to decrease its metabolism, a sulphamoylation at the 3' position which binds to CAs to assist limiting the first-pass liver metabolism, and an ethyl group on the 2' position to enhance the anti-cancer potency. Additionally, *in silico* modeling analysis has indicated a significant preference of CAIX over CAII binding, presenting a method to deliver the drug more specifically to acidic tumour environments. Unpublished data demonstrates anticancer properties of this compound in estrogen receptor-negative cervical cancer HeLa cells, with data suggesting the induction of autophagy and apoptosis as programmed cell death. (288) Additionally, exposure of HeLa cells to 0.5 µM C19 has resulted in statistically significant reduction in cell viability, and increase in cells with a reduced mitochondrial membrane potential and an up-regulation of caspase 6 and 8 activity. (287) The exact molecular mechanisms of the crosstalk between autophagy and apoptosis at an intracellular level caused by C19 have to be fully elucidated.

1.7 Relevance and specific aims of this study

Pilot studies in our laboratory have indicated that the novel *in silico*-designed 2-ME sulphamoylated analogue C19 does reduce the numbers of HeLa cells when they are exposed to the compound *in vitro.* (287) Furthermore, there has been evidence that this compound generates a statistically significant increase in the number of cells with reduced mitochondrial potential and increased levels of lactate dehydrogenase, indicating the possible induction of apoptosis and/or other forms of cell death. (287, 288) Not yet elucidated are the precise modes of cell death and the details of the molecular crosstalk between apoptosis and autophagy, as well as the effect on spindle assembly, as induced by this compound.

The objective of this study was to investigate molecular crosstalk between apoptosis and autophagy induced by a 2-methoxyestradiol analogue C19 on HeLa cells, and to examine the *in vitro* effect that this compound exerts on microtubule dynamics.

i. Evaluation of the *in vitro* effect of C19 exposure on HeLa cell morphology via:

a. polarization-optical transmitted light differential interference contrast microscopy (PlasDIC)
b. fluorescent microscopy employing a triple staining technique
c. transmission electron microscopy

ii. Determination the effect that C19 has on the cell cycle progression and induction of apoptosis by means of:
    a. flow cytometric analysis of cell cycle progression
    b. flow cytometric analysis of cyclin B1
    c. Phosphatidylserine flip detection using annexin-V-fluorocein isocyanate antibody labelling in the flow cytometric detection of apoptosis

iii. Evaluation of induction of autophagic cell death by quantifying autophagosome formation via:
    a. Flow cytometric determination of aggresome formation

iv. Evaluation of the signal transduction pathways involved in the induction of apoptosis by C19 via:
    a. spectrophotometric quantification of caspase 8 and 3

v. Establishment of a link between cell cycle progression, influence on α-tubulin and microtubule dynamics and induction of the two types of cell death via:
    a. confocal microscopy to determine α-tubulin assembly

Investigating the induction of both autophagy and apoptosis as modes of cell death, as well as dysregulated spindle formation, will contribute to the further development of this novel sulphamoylated 2-ME analogue in the struggle against cervical cancer. Further more, knowledge gained will aid in understanding of the molecular mechanisms of C19-induced cell death, as well as the possible insights into the crosstalk between autophagy and apoptosis. This information may be used in assessing the efficacy of C19-induced cell death and mitotic arrest in other cancer cell lines, and thus have a broader impact on cancer treatment.

2. Materials and Methods

All experiments were conducted in the cell culture laboratory in the Department of Physiology, Faculty of Health Sciences, University of Pretoria. Flow cytometric analysis was performed at the Department of Pharmacology (University of Pretoria). Transmission electron and confocal microscopy was done at the Electron Microscopy Unit of the University of Pretoria.

2.1 Cell cultures

The commercially available tumorigenic human epithelial cervical cell line, namely the Hela cell line, acquired from Highveld Biological (Pty) Ltd (Sandringham, Johannesburg, South Africa) was used for *in vitro* studies to determine the effect of C19 exposure. As catalogued by the American Type Culture Collection (ATCC), this cell line consists of epithelial cells collected from a human cervix having undergone neoplastic transformation into adenocarcinoma. (305) HeLa cells have been reported to contain human papilloma virus 18 (HPV-18) sequences and P53 expression has been reported as low.

Ethics approval for the proposed study on the HeLa cell line was obtained during 2011 from the Faculty of Health Sciences Research Ethics of the University of Pretoria (ethics approval number: 208/2011).

Only human cervical adenocarcinoma cells were used in this study. In order to evaluate the therapeutic and/or prognostic value of the results, it was assumed that *in vitro* results are representative of *in vivo* conditions. Although there cannot be a direct extrapolation to *in vivo* conditions, the *in vitro* results are necessary in order to form a base of knowledge and to gain understanding of the molecular mechanics exerted by C19 on the cells. The results obtained from this study have provided a solid point of departure for future *in vivo* studies yet to be conducted.

2.2 General laboratory procedures

2.2.1 Materials

The non-commercially available C19, a sulphamoylated analogue of 2-methoxyestradiol (2-ME) was synthesised by IThemba (PTY) Ltd. Pharmaceuticals (Modderfontein, Gauteng, South Africa), and a 10 µM working stock was prepared. Aliquots were stored frozen, and were defrosted at room temperature before use. The optimum concentration of C19 was established as 0.5 µM via a crystal violet staining technique in a dose-dependent study to determine the IC_{50} (inhibition constant: concentration of substance at which 50% of the cell growth is inhibited when compared to the control) of C19 in HeLa cells. (288) This IC_{50} was confirmed with a second set of experiments conducted by Vissagie *et al.* (287)

Actinomycin D is an anti-neoplastic agent that inhibits cell proliferation and is a cytotoxic inducer of apoptosis in neoplastic cells. (306) The proliferation of cells are inhibited in a non-specific manner by forming a stable complex with double-stranded DNA via deoxyguanosine residues, and in this way inhibiting DNA-primed RNA synthesis. (306) The compound also causes single-strand breaks in the DNA. Actinomycin D (Sigma Chemical Co. (St Louis, MO, USA)) at a final concentration of 0.1 µg/ml was used as a positive control for apoptosis in the experiments conducted. Aliquots were stored at 4˚C, protected from light.

Tamoxifen is an anti-oestrogen agent which induces autophagy and cell death by increasing the intracellular ceramide (a sphingolipid involved in cellular stress response) concentration and abolishing the inhibitory effect of the class-I phosphoinositide 3-kinase (PI3KC1) pathway of autophagy (307-309). 20µM tamoxifen (purchased from Sigma-Aldrich (St Louis, Missouri, United States of America)) was used as a positive control for autophagy in the experiments conducted. Aliquots were kept frozen, and were thawed at room temperature before use.

2-Methoxyestradiol (2-ME) is an endogenous metabolite of 17β-estradiol, and sufficient scientific publication has reported the induction of a metaphase block with cellular exposure

to a 1 µM concentration. (82, 224, 310) A statistically significant increase in the G_2/M phase of MCF-7 breast cancer cells when compared to the vehicle control was reported by Stander *et al.* (82), and evidence suggested that the cells entered the sub-G_1 stages of apoptosis thereafter instead of completing mitosis. 2-ME has also demonstrated a role in causing disruption of microtubule dynamics, contributing to the cell to arrest in G_2/M. (310) Thus 2-ME was used as a positive control in detecting metaphase block and microtubule abrogation. The compound was acquired from Sigma-Aldrich (St Louis, Missouri, United States of America), and stored at room temperature protected from light.

Dulbecco's Modified Eagle Medium (DMEM) was purchased from Separations (Johannesburg, South Africa). European grade heat-inactivated foetal calf serum (FCS) was obtained from BIOCOM biotech (Pty) Ltd. (Clubview, South Africa). 0.22 µm syringe filters, sterile cell culture flasks and plates were obtained through Sterilab Services (Kempton Park, Johannesburg, South Africa). Penicillin, streptomycin and fungizone were purchased from Highveld Biological (Pty) Ltd. (Sandringham, South Africa), as was the trypsin/versene. All additional chemicals were of analytical grade, and were purchased from Sigma-Aldrich (St Louis, Missouri, United States of America), as was the 0.2 mM trypan blue.

2.2.2 Methods

2.2.2.1 General cell culture procedures

Cells were propagated and maintained in 25 cm^2 or 75 cm^2 tissue culture flasks in a humidified atmosphere at 37°C, 5% CO_2 in a Forma Scientific water-jacketed incubator (Ohio, United States of America). HeLa cells were cultured in Dulbecco's Modified Eagle Medium (DMEM) and supplemented with 10% heat-inactivated FCS (56°C, 30 min) for optimal cell growth. 100 U/ml penicillin G, 100 µg/ml streptomycin and fungizone (250 µg/L) were added to the medium for infection control. Eagle published optimal growth nutrient requirements of HeLa cells (311, 312), and the original Eagle's medium formula has been further modified into the most commonly used DMEM. DMEM contains a high

glucose concentration (4500 mg/L), sodium pyruvate, the essential L-glutamine and pyridoxine (a modification to the original pyridoxal for improved stability). (313)

A one times working solution of phosphate buffered saline (PBS) was made up from a 10 times concentrated stock solution (80 g/L NaCl, 2 g/L KH_2PO_4 and 11.5 g/L $Na_2HPO_4.H_2O$), by diluting the latter ten times and adjusting the pH adjusted to 7.4 with 1M NaOH. The buffer was autoclaved before use.

When confluent (every 2 to 3 days), the HeLa cells were trypsinized, and the medium was replaced. This was achieved by removing the old DMEM and rinsing each flask twice with 1x PBS. Cells were then incubated with trypsin/versene for approximately 4 minutes at 37˚C. Trypsin was then removed, and the cells were detached by firmly tapping the flask against the hypothenar aspect of the hand. The loose cells were resuspended in fresh medium, and divided into subcultures, used for experiments, or frozen to preserve the stock of cells. Fresh DMEM was also added to the remaining attached cells in the mother flasks.

Cells were frozen in cryotubes, after being suspended in freeze medium (10% DMEM, 10% DMSO and 80% FCS), at a rate of about -1˚C/minute to -70˚C. Thereafter, the tubes were transferred into the liquid nitrogen freezer. When the frozen stock needed to be utilized, the cryotube was removed from the liquid nitrogen, and was allowed to defrost slowly at room temperature. The 1ml sample was then suspended in 3 ml DMEM after which the cells were centrifuged in order to remove the toxic DMSO, and seeded into the appropriate flask with the appropriate amount of pre-warmed DMEM. The medium was changed daily, until healthy confluent cells were obtained.

All the above procedures were carried out as sterile and aseptic techniques: cell culture work was done in the laminar flow cabinet (Labotec, Midrand, South Africa), all solutions were autoclaved and filter-sterilised (0.22 µm pore size), and all glassware and non-sterile equipment were autoclaved (120˚C with 15 psi for 20 minutes) and sprayed with 70% ethanol before placing in the cabinet.

2.2.2.2 General methods for experiments

Experiments were performed in either 6-well plates or 25 cm^2 cell culture flasks. For six-well plates, exponentially growing cells were seeded at 250 000 cells per well in 3 ml maintenance medium. After a 24 hour incubation period at 37°C to allow for cell adherence, the cells were exposed to 0.5 µM C19, equivalent concentration of dimethyl sulphoxide (DMSO) vehicle as a negative control, 20 µM tamoxifen as the autophagy positive control, 1 µM 2-ME as a positive control for G_2/M arrest, and 0.1 µg/ml (final concentration) actinomycin D as the apoptosis positive control. Cells were incubated for 24 hours at 37°C. For 25 cm^2 cell culture flasks, exponentially growing HeLa cells were seeded at 1×10^6 cells per flask to a final volume of 5 ml of maintenance medium. After 24 hours, allowing for cell attachment, the medium was discarded and cells were exposed to 0.5 µM C19 (in 5 ml fresh medium) as well as the relevant controls, and incubated for a further 24 hours.

In order to seed the cells at the required numbers, the mother flask was trypsinized as described in 2.2.2.1, the cells were collected, centrifuged and resuspended in 3 ml medium. Cells in a representative aliquot were counted using a haemocytometer (Improved Neubauer RS 748, depth 0.1mm, 1/400 mm^2 from Weber, England), in a ratio of 80 µl PBS, 20 µl of the cell sample and 100 µl of 0.2 mM trypan blue. Viable cells do not take up the dye, and are seen as clear cells which are counted. The number of cells per millilitre of the harvested cells was calculated via the equation shown in figure 2.1. The cell suspension was then diluted with DMEM in order to achieve the required cell number, and was seeded into the required tissue culture plates.

Cells/ml = average of count per 4 quadrants of the haemocytometer x dilution factor x 10^4

Figure 2.1: Calculation to determine the number of cells per millilitre.

A stock solution of 10 mM C19 dissolved in DMSO was prepared and diluted with medium to the desired concentration (0.5µM) when required for the exposure of the cells. The medium of the control cell samples were all supplemented with an equal concentration of DMSO (vehicle). The DMSO content of the final dilutions never exceeded 0.1% (v/v).

All the following techniques were carried out on cells exposed to 0.5 µM C19, in parallel with cells propagated in medium only as a negative control, a DMSO vehicle control, and as required, a positive control for autophagy (20 µM tamoxifen), a positive control for mitosis block (1 µM 2-ME) and a positive control for apoptosis (final concentration of 0.1 µg/ml actinomycin D).

2.3 Analytical experimental protocols

2.3.1 Morphology studies: Microscopy

To assess the effect that C19 exposure has on the morphology of the HeLa cells, microscopic techniques were employed.

2.3.1.1 Polarization-optical transmitted light differential interference contrast microscopy (PlasDIC)

To visualize and assess the morphological changes to the cellular structures and cell density caused by exposure to C19 as compared to both positive and negative controls, a PlasDIC microscopy technique was employed.

a) Materials

All materials were mentioned in section 2.2.1 above.

b) Method

Viable cells (2.5 x 10^5), as determined by trypan blue exclusion, were seeded in 6 well plates and allowed to attach for 24 hours. PlasDIC images were obtained using the Zeiss Axiovert-

40 microscope (Göttingen, Germany) before and after 24 hours of exposure to vehicle controls, positive controls or C19 respectively.

2.3.1.2 Fluorescent microscopy: Triple staining technique

Fluorescent staining techniques were employed in combination with microscopy in order to detect and differentiate certain morphological changes associated specifically with both apoptosis and autophagy, which enabled semi-quantitative comparisons between the treated cells and the relevant control cells.

a) Materials

The fluorophors Hoechst 33342 (3.5 µg/ml in PBS), acridine orange (15 µg/ml in PBS) and propidium iodide (40 µg/ml in PBS), were acquired from Sigma-Aldrich (St Louis, Missouri, United States of America).

b) Method

After a 24 hour allowance for cell attachment and a further 24 hours for exposure of the cells to 0.5 µM C19 and the relative controls in six-well plates, 0.5 ml of Hoechst 33342 solution was added to the medium (to provide a final concentration of 0.9 µM) and incubated for 30 min at 37°C in a CO_2 incubator. After 25 min, 0.5 ml of acridine orange solution (to give a final concentration of 3.77 µg/M) and 0.5 ml propidium iodide (to give a final concentration on the cells of 12 µM) were added to the medium and incubated for 5 min at 37°C. Thereafter, the medium was removed, and the cells were washed twice with 2 ml PBS. The stained cells were then covered with 1 ml PBS to prevent drying out during viewing. The cells were examined with a Zeiss inverted Axiovert CFL40 microscope and Zeiss Axiovert MR monochrome camera using Zeiss Filter 2 for Hoechst 33342-stained cells (blue emission: excites light at 365 nm and emits at 420 nm) and Zeiss Filter 9 for acridine orange-stained cells (green emission: excites between 450 – 490 nm and allows emission at 515 nm). (314) Zeiss Filter 15 was used to detect the red fluorescence emitted from the necrotic cells stained with propidium iodide (excitation at 538 nm and emission at 617 nm). (314) In order to prevent fluorescent dye quenching, all procedures were performed in a dark room.

2.3.1.3 Transmission electron microscopy

In order to visualize the microstructure of the HeLa cells exposed to C19, as compared to the relevant positive and negative controls, transmission electron microscopy was used.

a) Materials

Components of diluted Karnovsky's fixative (2.5% glutaraldehyde and 2.5% formaldehyde in 0.075 M phosphate buffer at pH 7.4–7.6), 0.5% aqueous osmium, quetol epoxy resin, 4% aqueous uranyl acetate and Reynolds' lead citrate were obtained from Merck (Darmstadt, Germany). 100% ethanol as well as all other chemicals were purchased from Sigma-Aldrich (St. Louis, Missouri, United Sates of America)

b) Method

In this protocol, due to the proposed loss of cells during the fixation procedure, 2 x 10^6 cells were seeded per 25 cm^2 cell culture flask. After 24 hours of exposure to C19 and the relative controls (Actinomycin D, Tamoxifen, DMSO vehicle control and medium only exposed cells), cells were collected via trypsinization, and then fixed in 1 ml diluted Karnovsky's fixative for 45 minutes at room temperature. The cells were then washed with 1 ml 0.075 M phosphate buffer (repeated twice). Thereafter the cells were fixed in 0.5% aqueous osmium for 2 hours, followed by a rinsing step with distilled water (three washes). Dehydration steps followed, which entailed 10 minute suspension of the cells in increasing concentrations of ethanol (30%, 50%, 70%, 90%, 100%, 100%, 100%). Following this, the cells were infiltrated with a series of increasing percentage of quetol epoxy resin (30% for 30 minutes, 60% for 30 minutes and 100% quetol for 4 hours). Embedding of the samples followed and polymerisation of the specimens was allowed for 36 hours at 60˚C. Ultra-thin sections were then prepared with a microtome and mounted on a copper grid. Samples were contrasted with 4% aqueous uranyl acetate (10 minutes) and Reynolds' lead citrate (2 minutes), followed by a rinsing step using water. Samples were viewed with a JEM-2100F field emission transmission electron microscope (JEOL, Tokyo, Japan) at the Electron Microscopy Unit of the University of Pretoria (Pretoria, South Africa). Semi-quantitative analysis of the cells was performed visually.

2.3.2 Cell cycle progression and apoptosis studies via flow cytometry

2.3.2.1 Cell cycle analysis

Flow cytometry measures fluorescence per cell or particle (0.5-40 µm diameter), distinguishing this method form spectrophotometry. Using principles of hydrodynamic focusing, one cell is presented at a time to the argon laser beam, which causes light scatter. (315) Additionally, it excites the fluorochrome with which the cell has been stained and releases photons with specific spectral properties to each fluorochrome. (315) Various morphologies of normal and apoptotic cells can be detected by analysing their light scattering properties. Side scatter is used to determine the cell size (which can differentiate between apoptotic cells and apoptotic bodies), whereas side scatter correlates with the granularity of the cell. (142) Propidium iodide fluorescence may be detected using the FL3 channel (far red fluorescence) on the flow cytometer. Thus specific multi-parameter data is generated from particles, cells and the introduced fluorophors, implementing the principles of light scattering, light excitation and fluorochrome emission.

Flow fluorocytometry is a reliable, reproducible and efficient method which is able to identify the cell distribution during the various phases of the cell cycle. Three phases, namely the G_0/G_1 phase (quiescent cells/the initiation of interphase), the S phase (DNA synthesis stage) and the G_2/M (end of interphase/mitosis), can be distinctly recognised utilizing this method. (316)

Apoptosis is defined as type 1 programmed cell death. (142) As part of this process, there are several delineated and well defined changes which occur to the cell undergoing this process. Hallmarks include chromatin condensation with chromatin margination to the nuclear membrane, nuclear fragmentation (karyorhexis) and the formation of apoptotic bodies. (144, 317) Resultant low molecular weight DNA fragments, consisting of 180 base pairs or multiples of 180, are lost from the cell, leaving the non-degraded DNA in the hypodiploid nucleus. (318)

After exposing the cell line to an apoptotic inducting agent, the cells can be stained with propidium iodide and analysed on a flow cytometer, where a wide sub-G_1 peak should be evident. (316) This represents the hypodipoid cell fraction, which should be distinguishable from the narrow normal diploid G_0/G_1 peak, indicating the presence of apoptotic cells. Important in the protocol was to exclude low level staining, cell debris and cell aggregates by standardizing the flow cytometer beforehand, gating relevant scatter sections, setting the correct acquisition parameters (volume of particle/forward scatter), and including appropriate negative and positive control samples. (318)

To be taken into account with the flow cytometic cell cycle determination is that the sub-G_1 distribution may also contain necrotic cells which sometimes have some nuclear degradation, nuclear fragments, chromosomal clumps, micronuclei and normal nuclei with different chromatin conformation. (319) Thus along with the various controls, the results of this method were validated via both morphological and other biochemical evidence and methods.

Ethanol was used as an organic solvent fixative, and is advantageous in that it inactivates the cellular processes but does not form DNA, RNA, protein or carbohydrate epitopes by covalent modification. It also causes permeabilization of the cells, but has the disadvantage of potentially causing cell aggregation. Ethanol was used preferentially to formaldehyde fixation in this case, as paraformaldehyde has been shown to broaden DNA histogram peaks when using propidium iodide as an intracellular staining method. (320)

Propidium iodide (PI) is an intercalating agent with a molecular mass of 668.4 Da which may be used to analyse cell viability, apoptosis and cell cycle progression by flow cytometry. PI fluoresces when excited by a 488 nm lazer and can be detected with a 562-588 nm band pass filter. As PI binds to the nucleotide pair cytosine and guanine, it stains both DNA and RNA and therefore the fixed permeabilized cells were first treated with RNase A to eliminate the dual origin of signal. (321) Due to the ability of this fluorogenic compound to bind stoichiometrically to nucleic acids, the fluorescence emission is directly proportional to the DNA content of the cell, making it available to be used in quantitative processes. (318) PI is unable to permeate intact cell membranes, making it useful for the differentiation of live

healthy cells and necrotic cells. Thus should this substance be utilised in applications for viable cell analysis such as flow cytometric application, the cells must first be permeablized to allow PI entry. This was achieved by using Triton X-100, a detergent used to promote rapid permeabilization of fixed cell membranes. This compound however does hold the possible complication of increasing cell fragility and incurring the loss of cytoplasmic cell content. (320)

Flow fluorocytometry was used in order to identify the cell distribution during the various phases of the cell cycle and the possibility of the presence of a sub-G_1 phase as a result of C19 exposure.

a) Materials

Triton X-100, 100% ethanol, and propidium iodide were purchased from Sigma-Aldrich (St. Louis, Missouri, United States of America). RNase A was obtained from BIOCOM biotech (Pty) Ltd. (Clubview, South Africa). European grade foetal calf serum was acquired from Separations (Johannesburg, South Africa).

b) Method

HeLa cells (1 x 10^6) were seeded in 25 cm^2 flasks in 5 ml complete DMEM (supplemented with 10% heat inactivated foetal calf serum, 100 U/ml penicillin G, 100 µg/ml streptomycin and 250 µg/ml fungizone) and cells were incubated in a humidified environment at 37˚C and 5% CO_2 in a Forma Scientific water-jacket incubator (Ohio, United Sates of America) to allow for cell attachment. 24 hours later, the cells were exposed to 0.5 µM C19 along with the relevant controls for a further 24 hours. Cells were trypsinized, and the entire contents of the flasks were collected for analysis. A washing step followed, in which pelleted cells were resuspended in 1ml ice-cold phosphate buffered saline solution (PBS). Cells were centrifuged for 2 minutes at 1 X 10g, after which the cells were resuspended in 200ul ice-cold PBS containing 0.1% FCS. In order to fix the cells, ice-cold 70% ethanol was added in a drop-wise manner while simultaneously vortexing the sample gently to prevent clumping of cells. Samples were incubated at 4˚C for a minimum of 12 hours, after which the cells were centrifuged at 1 X 10*g* for 5 minutes. The supernatant was discarded and cells were resuspended in PBS containing propidium iodide (40 µg/ml), RNase A (100 µg/ml) and Triton

X-100 (0.1%). Cells were incubated and protected from light at 37˚C for 40 minutes. Analysis entailed measurement of propidium iodide fluorescence (FL3) on a FC500 system flow cytometer (Beckman Coulter, South Africa (PTY) Ltd.) equipped with an air-cooled argon laser excited at 488 nm. Anueploid and aggregated cells, as well as cell debris were gated out by visual inspection. Data from at least 10 000 cells were captured. This experimental procedure was repeated three times in order to attain statistically relevant data for analysis.

Data collected from the sample readings were analysed by creating histograms using Cyflogic version 1.2.1 software (Pertu Therho, Turko, Finland), and evaluated using the analysis of variance (ANOVA)-single factor model and a two-tailed Student's *t*-test. Cell cycle distributions from generated histograms were expressed as percentage of cells in each phase.

2.3.2.2 Cyclin B1 detection (metaphase block)

In order to detect and confirm morphological evidence of a C19-induced G_2/M mitotic block in HeLa cells, a flow cytometric quantification of cyclin B1-phycoerythrin-conjugated antibody binding in the above mentioned cells was done.

a) Materials

Milli-Mark™ Anti-Cyclin B1-PE, clone GNS3 (8A5D12)) was ordered from Millipore Corporation (Temecula, California, United States of America) and stored at 2-8˚C in a light protected environment. 100% ethanol and Triton X-100 were purchased from Sigma-Aldrich (St. Louis, Missouri, United States of America). FCS was purchased from Separations (Johannesburg, South Africa).

b) Method

1 x 10^6 HeLa cells were seeded in 25 cm^2 flasks and were allowed to attach during a 24 hour incubation period. After a further 24 hours of C19 exposure (in parallel with the relevant negative and positive metaphase block (2-ME) controls), cells were trypsinized, collected, centrifuged and washed with 1 ml ice-cold PBS. Cells were centrifuged, the supernatant

was discarded and resuspended in 200 µl ice-cold PBS containing 0.1% FCS (the latter to prevent non-specific antibody binding in subsequent steps). Cells were fixed with 10 ml ice-cold 70% ethanol added drop-wise while vortexing the sample in order to avoid clumping of the cells, and stored at 4°C for 24 hours. Cells were centrifuged at 1 x 10*g* and washed twice with 500 µl PBS to remove the ethanol. A working antibody solution was prepared by diluting the primary antibody with PBS in a 1:5 ratio. 10 µl of the working antibody solution was added per 1×10^6 cell sample to provide a final volume of 100 µl with 90 µl PBS (with 0.1% Triton X-100). Cells were incubated in the conjugated cyclin B1 antibody solution for 40 minutes at 37˚C while protected from light. Cells were washed twice with 1 ml PBS and resuspended in 0.6 ml PBS. All procedures after the incubation with the antibody were carried out in a light protected environment. PE (FL3) fluorescence was measured with a FC500 System flow cytometer (Beckman Coulter South Africa (Pty) Ltd.) equipped with an air-cooled argon laser excited at 488 nm. Aggregated and aneuploid cells were removed from the analysis. 10 000 cells were analysed per sample, and the experiment done in triplicate.

Measurement of PE-conjugated cyclin B1 fluorescence of control and exposed HeLa cells was measured utilizing the normalized area of the dot-plot. Data were analysed using Cyflogic version 1.2.1 software (Pertu Therho, Turko, Finland), and evaluated using the analysis of variance (ANOVA)-single factor model and a two-tailed Student's *t*-test.

2.3.2.3 Phosphatidylserine flip detection (apoptosis)

In order to detect and discriminate between the induction of apoptosis, necrosis and viable cells, flow cytometric analysis based on the translocation of the phosphatidylserine from the inner surface to the outer aspect of the cell membrane during the induction of apoptosis was used. This experiment was conducted to quantify the induction of apoptosis in C19 cells, compared to control samples.

a) Materials

Analysis was performed using the BioVision Annexin V-FITC reagent kit acquired from BioVision Research Products (Mountain view, California, United States of America). The

binding buffer was included in the kit, and a 1x dilution was prepared with sterile double distilled water and stored at 4˚C before use. Propidium iodide was purchased from Sigma-Aldrich (St. Louis, Missouri, United Sates of America).

b) Method

According to manufacturer's protocol, 1 x 10^6 cells were seeded in 25 cm^2 flasks and after 24 hours of attachment, exposed to 0.5 µM of C19 along with the appropriate controls (medium only exposed cells, DMSO vehicle control and actinomycin D). Thereafter, the cells were trypsinized and 500 000 cells from each flask were counted out and utilised further. Cells were washed in PBS and after being centrifuged at 1 x 10*g* and the supernatant discarded, were resuspended in 500 µl 1 x binding buffer. Double staining was done by adding 1 µl Annexin V-FITC and 1.2 µl 40 µg/ml propidium iodide stock solution to the cells which were incubated for 5 minutes at room temperature in the dark. Annexin V (FL1) and propidium iodide (FL3) fluorescence were measured with a FACS FC500 System flow cytometer (Beckman Coulter South Africa (Pty) Ltd.) equipped with an air-cooled argon laser excited at 488 nm. This experiment was conducted thrice in order to achieve statistical significance. Data from at least 20 000 cells were analysed using Cyflogic version 1.2.1 software (Pertu Therho, Turko, Finland), and evaluated using the analysis of variance (ANOVA)-single factor model and a two-tailed Student's *t*-test. Results were expressed in percentage of cells in three categories namely; viable cells, apoptotic cells and necrotic cells.

2.3.3 Aggresome detection (autophagy)

The ability of C19 to induce autophagy, programmed cell death type II, in HeLa cells was assessed by the quantification of aggresomes within the cells via a flow cytometic assay.

a) Materials

The Enzo Life Sciences' ProteoStat® Aggresome Detection Kit was purchased from Enzo Life Sciences Inc. (New York, United Sates of America). The kit provided the ProteoStat® Aggresome Detection Reagent and the 10 X assay buffer. Ethylenediaminetetraacetic acid (EDTA), formaldehyde, NaOH, and Triton X-100 were acquired from Sigma-Aldrich (St. Louis, Missouri, United States of America)

Reagents were prepared according to the manufacturers protocol (322), which included the preparation of a 1 x assay buffer (from 10 x stock assay buffer) warmed to room temperature, a 4% formaldehyde solution and a permeabilizing solution consisting of 0.5% Triton X-100 in 3 mM EDTA at a pH 8 mixed to a final solution with 1 x assay buffer. The ProteoStat® Aggresome Detection Reagent was diluted 5 000 fold with 1 x assay buffer.

Formaldehyde (paraformaldehyde) is utilised for fixation of cells for surface or intracellular staining when followed by lipid solvents. (320) It is a mild fixative, and cell membrane integrity is preserved. It is however, not indicated when staining with propidium iodide simultaneously to cell surface staining as it broadens the histogram peaks in flow cytometric analysis. (320)

b) Method

The attachment of one million cells per 25 cm^2 flask was allowed for 24 hours, after which the cells (in the log phase of growth) were exposed to 0.5 µM C19 parallel to the appropriate controls. The positive control for autophagy entailed exposure of cells to 20 µM tamoxifen. Negative controls include cells grown in medium only and cells treated with vehicle DMSO for an equal length of time under the same conditions. Subsequent to the 24 hours of exposure, cells were harvested via trypsinization, and the pellet washed in 2 ml PBS after centrifugation for 2 minutes at 100 x *g*. Cells were centrifuged again and resuspended in 200 µl PBS prior to adding 2 ml of the 4% formaldehyde in a drop wise manner while vortexing the tube continuously. This suspension was left at room temperature for 30 minutes. Samples were centrifuged at 350 x *g* for 10 minutes in order to collect the cells. The supernatant was discarded and the cells washed in 2 ml PBS and then centrifuged as in the previous step. The supernatant was removed, and cells were resuspended in the small amount of fluid remaining. While vortexing, 2 ml of permeabilizing solution was added in a drop-wise fashion, after which the sample was incubated for 30 minutes on ice. The cells were collected by centrifugation at 350 X *g* for 10 minutes, after which they were washed in 2 ml PBS. The cells were pelleted by centrifugation, the supernatant poured out, and resuspended in 500 µl diluted ProteoStat® Aggresome detection reagent with repeated

pipetting to ensure a monocellular suspension. Tubes were covered in foil, and allowed to incubate at room temperature for half an hour.

Fluorescence within 10 000 cells of each sample was analysed in the FL3 channel of the FACS FC500 System flow cytometer (Beckman Coulter South Africa (Pty) Ltd.) equipped with an air-cooled argon laser excited at 488 nm. After obtaining the mean fluorescence intensity (MFI) for the samples (cells propagated in medium only as the negative control, C19-treated cells and positive autophagy control), the aggresome activity factor (AAF) was calculated (figure 2.2). An AAF of more than 25 was indicative of a positive result and a significant increase in aggresome formation. Statistical analysis was conducted using the ANOVA-single factor model and a two-tailed Student's *t*-test, with a *P*-value of less than 0.05 being considered statistically significant. This experiment was repeated 3 times for statistical significance.

$$AAF = 100 \times (MFI_{Rx} - MFI_{cont}) / MFI_{Rx}$$

Where
AAF = aggresome activity factor
MFI_{Rx} = mean fluorescence intensity of the treated sample
MFI_{cont} = mean fluorescence intensity of control sample

Figure 2.2: Formula to determine the aggresome activity factor (AAF)

2.3.4 Signal transduction: quantification of caspases 8 and 3

Quantification of both caspase 8 (an initiator caspase) and 3 (an executioner caspase) was done using spectrophotometric principles, the up-regulation of which would indicate the induction of the extrinsic apoptotic cell signalling pathway in response to C19 exposure of HeLa cells. In this way, information about the cross signalling between the apoptotic and autophagic pathways would be gained.

Both the caspase-8 and caspase-3 assay procedures were done according to manufacturer protocol. In both cases a sample number (n) of 3 was used, and the assays were repeated 3 times in order to complete statistical analysis and achieve significance. Thus for each assay, 1 x 10^6 HeLa cells were seeded in to 25cm^2 flasks in 5ml DMEM. For each of the three replicates, there were 3 flasks as medium only controls, 3 flasks of DMSO as vehicle controls, 3 flasks of actinomycin D positive apoptosis controls and 3 flasks of 0.5uM C19-exposed cells.

Statistical analysis comprised of the mean ±SD of the 3 repeats per experiment, as well as the 3 replicates, and significance using the ANOVA-single factor model followed by a two-tailed student's *t*-test was ascertained. *P*-values of less than 0.05 were regarded as statistically significant. An increase in caspase activity was expressed as a fold increase when compared to the value measured for the vehicle-treated exposed cells.

2.3.4.1 Caspase 8 activation assay

Investigation of possible caspase 8 activation and/or amplification was quantified via a calorimetric method utilizing spectrophotometric principals.

a) Materials

The FLICE/Caspase 8 colorimetric kit from BioVision Research Products (Mountain View, California, United States of America) was used to run this assay. Included in this kit was the cell lysis buffer, 2 x reaction buffer, 4 mM IETD-*p*NA (isoleucine–glutamic acid–threonine–aspartic acid tetrapeptide labelled with p-nitroaniline), 1 M dithiothreitol (DTT) and the dilution buffer, all of which were delivered and stored frozen. Before starting the experiment, sufficient 2 X reaction buffer and dilution buffer were thawed, aliquotted, and left at 4˚C. DDT was added to the 2 x reaction buffer immediately prior to use to provide a final concentration of 10 mM. IETD-*p*NA was protected from light.

The Pierce® BCA protein assay kit was purchased from Thermo Fisher Scientific Inc. (Rockford, Illinois, United States of America) in order to determine the protein concentration of the samples. This assay utilizes the biuret reaction in which Cu^{2+} is

reduced to Cu^{1+} by protein in an alkaline medium, using bicinchoninic acid (BCA) as a reagent, after which the cuprous cation can be sensitively and selectively quantified via spectrophotometric analysis of the purple-colour reaction. This kit supplies BCA Reagent A (containing sodium carbonates, sodium bicarbonate, bicinchoninic acid and sodium tartrate in 0.1 M sodium hydroxide) and BCA Reagent B (containing 4% cupric sulphate). Prior to use, a working solution was prepared by mixing 50 parts BCA Reagent A with 1 part BCA Reagent B (50:1, Reagent A:B), which is stable for 3 days when stored at room temperature.

b) Method

A 24 hour attachment protocol was implemented, in which one million cells were seeded into 25 cm^2 flasks, and incubated at 37˚C. Following exposure to 0.5 µM C19 concurrently with relevant controls, namely medium only-exposed cells, DMSO vehicle control and actinomycin D, for a further 24 hours, cells were detached and harvested via trypsinization. Cells were counted, and between 1-5 $x10^6$ cells were pelleted by centrifugation at 130 x *g* for 2 minutes. After the cells were resuspended in 50 chilled cell lysis buffer, they were incubated for 10 minutes on ice. The cytosolic extract in the form of the supernatant was collected in new eppendorf tubes and left on ice after centrifugation at 100 x *g* for one minute. The protein concentration was determined by incubating 5 µl of the cytosolic extract with 100 µl of the premixed reagent A and B (50:1) from the Pierce® BCA protein assay kit in a 96-well microtiter plate. Spectrophotometric readings using the BioTek Epoch multi-volume spectrophotometer system (BioTek Instruments Inc., Analytical Diagnostic Products, Weltevreden Park, South Africa) were acquired at 570nm, from which protein concentration values were calculated using a pre-determined standard curve. 100 µg protein was diluted to 50 µl cell lysis buffer for each assay in a 96 well plate, to which an equal volume (50 µl) of 2X reaction buffer containing 10 mM DTT was added. After adding 5ul of the 4mM IETA-*p*NA (p-nitroaniline) substrate (final concentration of 200 µM), the plate was incubated in the dark at 37˚C for 2 hours. Absorbances were determined at 405 nm on the BioTek Epoch multi-volume spectrophotometer system (BioTek Instruments Inc., Analytical Diagnostic Products, Weltevreden Park, South Africa), after which a fold-increase of caspase-8 activity was calculated by comparing the medium only control sample absorbance with that of the positive apoptotic control and the C19-treated samples.

Background readings from buffers were first subtracted from all the readings before the calculations were done.

2.3.1.2 Caspase 3 activation assay

Investigation of possible caspase-3 activation and/or amplification was done via a calorimetric method and quantified with the use of spectrophotometry.

a) Materials

The BioVision Caspase-3/CPP32 Colorimetric Assay Kit was purchased from BioVision Research Products (Mountain View, California, United States of America). The kit contained the cell lysis buffer, 2X reaction buffer, 4 mM DEVD-*p*NA, 1 M DTT and a dilution buffer. Enough 2X reaction buffer was aliquoted and thawed for the number of assays. DTT was added to the 2X reaction buffer immediately before use to make a 10 mM final concentration. DEVD-*p*NA was protected from the light during all the steps.

In order to determine the protein concentration of the samples the Pierce® BCA protein assay kit was purchased from Thermo Fisher Scientific Inc. (Rockford, Illinois, United States of America). This kit supplies BCA Reagent A (containing sodium carbonates, sodium bicarbonate, bicinchoninic acid and sodium tartrate in 0.1 M sodium hydroxide) and BCA Reagent B (containing 4% cupric sulphate). Prior to use, a working solution was prepared by mixing 50 parts BCA Reagent A with 1 part BCA Reagent B (50:1, Reagent A:B), which is stable for 3 days when stored at room temperature.

b) Method

After a 24 hour attachment period, 1 x 10^6 HeLa cells seeded into 25 cm^2 flasks were exposed to 0.5 µM C19. Appropriate controls for the same mentioned time frame were included. 1-5 x 10^6 cells were pelleted (by centrifugation at 100 x *g* for 2 minutes) after trypsinization, and resuspended in 50 µl ice-cold cell lysis buffer and incubated on ice for 10 minutes. Following a 1 minute centrifugation at 1 x 10*g*, the supernatant was transferred to fresh eppendorf tubes and placed on ice. Protein concentration was determined as in the caspase-8 experiment described in 2.3.4.1, utilizing the Pierce® BCA protein assay and a

standard curve. 50 ug protein of each assay was diluted in 50 µg cell lysis buffer and placed in a 96 well plate, to which an equal volume of 2X reaction buffer (containing 10 mM DTT) was added. The reaction was initiated by adding the colorimetric substrate, namely 5 µl DEVD-*p*NA, to make a final concentration of 200 µM. The plate was incubated for 120 minutes at 37˚C, protected from light and the absorbance was read at 405 mn on the BioTek Epoch multi-volume spectrophotometer system (BioTek Instruments Inc., Analytical Diagnostic Products, Weltevreden Park, South Africa). Background readings from the buffers were first subtracted from the total readings, after which the fold increase of caspase 3 activity was determined by using the medium only control as the base-line reading.

2.3.5 Microtubule dynamics: Confocal microscopy to determine α-tubulin assembly

Laser scanning confocal microscopy is a technique which enables visualization deep within both living and fixed cells and tissues, allowing the collection of sharply defined optical sections from which three-dimensional images can be created. This form of microscopy may be used in conjunction with fluorescent labelling, and has advantages over conventional optical microscopy. (323) These advantages include being able to control the depth of field, to eliminate degrading out-of-focus information, and to collect serial optical sections from thick specimens. The key element to the confocal technique is the use of spatial filtering to eliminate out-of-focus light or flare in specimens that are thicker than the plane of focus. (323)

In order to observe the effects of C19 on the HeLa cell cytoskeletal microtubule architecture, cells were stained with anti-alpha-tubulin antibodies, which were visualised by an Alexa-488 fluorescent probe utilizing confocal microscopy.

a) Materials

The following buffers and reagents were prepared beforehand:

- Cytoskeletal buffer (CB) consisting of 60 mM PIPES (piperazine-N,N'-bis(2-ethanesulfonic acid), a buffer with a pKa value near physiological pH that is not

absorbed through cell membranes), 27 mM HEPES (4-(2-hydroxyethyl)-1-piperazineethanesulfonic acid), 10 mM EGTA (ethylene glycol tetraacetic acid) as a chelating agent with a high affinity for calcium ions, and 4 mM magnesium sulphate with the pH adjusted to 7.0 with NaOH.

- 0.3% gluteraldehyde fixative consisting of 0.6 ml of 50% gluteraldehyde in 100 ml CB.
- Permeabilization buffer, consisting of 1% Triton X-100 in CB.
- Reducing agent, made by dissolving 5 mg sodium borohydrite in 5 ml PBS immediately before use of the solution.
- 10% normal host serum blocking buffer consisting of 10% foetal calf serum (FCS) in PBS containing 0.05% Triton X-100.
- PBS-Triton wash buffer, consisting of PBS with 0.05 % Triton X-100
- PBS-Triton wash buffer with blocking serum, containing PBS, 0.05% Triton X-100 and 1% FCS.

All the chemicals in the above mentioned solutions were obtained from Sigma-Aldrich (St. Louis, Missouri, United States of America), unless otherwise stated. European grade FCS was purchased from BIOCOM biotech (Pty) Ltd. (Clubview, South Africa).

Monoclonal Antibody to Tubulin-alpha (clone DM1A), purchased from Imgenex (San Diego, California, United States of America) was selected to be the primary mouse anti-tubulin alpha antibody. A primary antibody cocktail was prepared for use by diluting the antibody in PBS-Triton wash buffer diluted with 50% blocking buffer, at a 1:100 ratio.

The Alexa Fluor®488 donkey anti-mouse IgG secondary antibody (raised in donkeys) was obtained from Invetrogen (Paisley, United Kingdom). A working cocktail was made by adding the antibody at a 1:125 ratio to blocking buffer diluted 50% with PBS-Triton wash buffer.

Lab Star 1000 glass 76 mm x 26 mm microscope slides (1.0 – 1.2 mm thickness), parafilm and Imittel Glaser 22 x 50 mm cover slips were purchased from Merck (Darmstadt, Germany). The 4',6-diamidino-2-phenylindole fluorescent stain (DAPI) was purchased from Thermo Fisher Scientific Inc. (Rockford, Illinois, United States of America).

b) Method

Exponentially growing HeLa cells were seeded at 350 000 cells per well in 6-well plates on flame sterilized cover slips. After a 24 hour incubation period at 37°C, cells were exposed to 0.5 µM C19 for a further 24 hours. Appropriate controls were included as previously described. Cover slides were washed three times for 2 minutes each with pre-warmed cytoskeletal buffer (CB). Fixation of the cells in the following step was achieved with 1.5ml of pre-warmed 0.3% gluteraldehyde for 10 minutes at 37°C. This was followed by a wash step, in which 1.5ml warmed cytoskeletal buffer was added to the wells while being placed on an orbital shaker for 2 minutes (repeat 2 times). The cell membranes were permeablized using the premade permeabilization buffer and incubating the samples on an orbital shaker for 15 minutes.

Following permeabilization, cells were washed once with CB buffer, and then washed twice with PBS. Unreacted aldehydes were removed by treating samples three times with the reducing agent, prepared within a minute prior to application. Cells were washed twice with PBS.

Non-specific secondary antibody binding sites were blocked by incubation of the cover slips in the 10% normal host serum blocking buffer for 60 minutes. Thereafter, primary antibody binding was carried out by incubating the cover slides in a primary mouse anti-tubulin alpha antibody (monoclonal Antibody to Tubulin-alpha (clone DM1A), Imgenex) cocktail for 90 minutes at 37°C in a humidity chamber. This was done by covering 2 x 3 inch glass microscope slides with parafilm, and placing two 100 µl drops of the primary antibody cocktail per slide on the smooth upper surface. Cover slips were carefully removed from the 6-well plates with fine pincets, and placed with the cells down on the prepared droplet. Slides were placed inside a humidity chamber for incubation. Cover slips were subsequently returned to the 6-well plates, and washed 3 times at room temperature for 10 minutes each with PBS-Triton wash buffer mixed with FCS in order to remove unbound antibodies.

Samples were incubated while protected from light for 90 minutes at 37°C in a humidity chamber after adding a secondary fluorescent labelled (alexa Fluor® 488 dye) anti-mouse

antibodies (raised in donkeys) cocktail of final concentration 2 mg/ml in the same manner as described above. Following secondary antibody binding, samples were washed three times with PBS-Triton wash buffer with FCS to remove unbound antibodies.

Nuclear staining was achieved by incubating the cover slips in 50% DAPI to equal volumes of PBS for 5-10 minutes while protected from light. Counterstained cover slips were then washed thrice with distilled water, mounted with a glycerol-based mounting fluid and cells were examined with a Zeiss LSM 510 Meta Confocal Microscope (Zeiss, Jena, Germany) at the Electron Microscopy Unit of the University of Pretoria (Pretoria, South Africa).

2.4 Statistical analysis of data

Statistical support was procured and granted from Dr Olorunjo from the Biostatistics unit of the South African Medical Research Council after discussion of the protocol and planned analysis methods.

a) Statistical planning

Variation in experimental results can be due to variation between subjects in a random sample, variation within the subjects (biological variation) or variation in analytical procedure. Since there was minimal biological variation within the cell line, the variation in the experimental set-up was the only statistical parameter that could be determined.

b) Quantitative studies: Enzymatic activity and flow cytometry

Data obtained from three independent experiments (each conducted in 3 replicates) are shown as the mean ± standard deviation (SD) and were statistically analysed for significance using the analysis of variance (ANOVA)-single factor model followed by a two-tailed Student's *t*-test. Means are presented in bar charts, with T-bars referring to standard deviations. *P*-values of less than 0.05 were regarded as statistically significant and are indicated by an asterisk (*). Flow cytometric measurement of cell cycle progression and

protocols involving FITC-labels and the aggresome kit are expressed as relative fluorescence (a percentage of the value measured for vehicle-treated negative control cells). For flow cytometry, data from at least 10 000 cells were analyzed employing Cyflogic version 1.2.1 software (Pertu Therho, Turko, Finland).

c) Qualitative studies: Microscopy

Morphological studies by means of microscopy were conducted, and a minimum of three representative images were captured from each sample. Semi-qualitative data was obtained from PlasDIC, TEM, light- and fluorescent microscopy.

3. Results

3.1 Morphology studies

Optical or light microscopy involves passing visible light transmitted through, or reflected from the sample, through a single or system of multiple lenses to allow a magnified view of the required sample. Microscopy was employed to visualise the morphological changes occurring in HeLa cells after exposure to C19. Typical cellular changes associated with apoptosis (hypercondensed chromatin, decrease in cell density, apoptotic bodies) and autophagy (increase in autophagosomes, compromised cell density) were compared to the relevant positive control, as well as the negative controls in a semi-quantitative manner.

3.1.1 Polarization-optical transmitted light differential interference contrast microscopy (PlasDIC)

Living cells are difficult to observe under traditional brightfield illumination using the full aperture and resolution of the microscope objective and condenser system. (324) Differential interference contrast (DIC) microscopy involves a beam of light which, after being split in two, are polarized at 90˚ to each other and take different pathways through the sample. Interference of these two beams is caused by the optical density of the sample before their recombination. (325) Images obtained with DIC microscopy display in a visible relief, manifested through a shadow-cast effect that gives a realistic three-dimensional image of the objects viewed. (324) These shadow cast images have large optical gradients that thus do not obscure smaller specimen features. (324) This, together with the sensitivity of imaging small features in combination with larger structures, is an advantage to studying intracellular and subcellular changes and is an improvement on previous forms of phase contrast microscopy. (324)

Polarization-optical transmitted light differential interference contrast microscopy (PlasDIC) is an improved method for polarization-optical transmitted light differential interference contrast where linear polarized light is only generated after the objective. (255, 324, 325)

In order to determine whether C19 has antiproliferative effects similar to the parental compound 2-ME on HeLa cells, PlasDIC microscopy was used. 2.5×10^5 HeLa cells were seeded in six well plates, and allowed to attach for 24 hours. Figure 3.1 is a representative PlasDIC image of HeLa cells as they appear at the end of this attachment stage, demonstrating clearly defined cell membranes at various stages of cell division and with more than 70% confluence. Cells were subsequently exposed for 24 hours to C19, in parallel with the required negative controls (cells propagated in medium only and exposed to DMSO vehicle control) and positive controls (tamoxifen for autophagy, actinomycin D for apoptosis and 2-ME to show metaphase block).

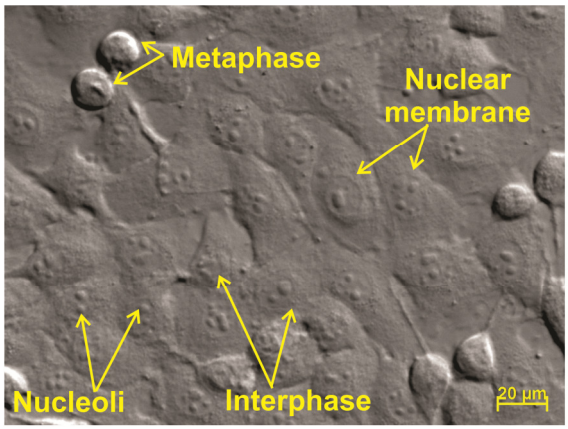

Figure 3.1: PlasDIC microscopy of HeLa cells after a 24 hour attachment period prior to exposure to the various agents. Various stages of mitosis, demarcated cell membranes and confluency in cell density were observed.

Unexposed cells grown in medium only (figure 3.2.a) continued to grow in a logarithmic manner, resulting in confluent healthy cell appearance. DMSO added as a vehicle control (v/v%), had no apparent effect on cell growth or morphology, rendering images (figure 3.2.b) identical to the cells grown in medium only. In both the representative were present in various stages of mitosis, with most being in interphase. Cellular structures such cell membranes, nuclear membranes and nucleoli are clearly identifiable.

As part of the positive control panel, HeLa cells were exposed to 1 µM 2-ME as exhibition of metaphase block, 1 µg/ml actinomycin D as an apoptosis inducer, and 20 µM tamoxifen to demonstrate characteristics of autophagy. Figure 3.2.c shows rounded cells in metaphase block on a background of a slightly compromise cell density, as reported by previous literature in HeLa and other cell lines, of cells in metaphase block. (82, 240, 255, 326) Cells treated with tamoxifen revealed the presence of autophagy, compromised cell density and cells in distress (cell protrusions) (figure 3.2.d). Cells exposed to actinomycin D revealed apoptotic bodies, multiple shrunken cells, ghost cells, scattered cell debris and a decreased cell density indicated(figure 3.2.d).

With the PlasDIC characteristics of autophagy and apoptosis highlighted in the representative micrographs of the positive control panel, the images obtained from the C19-treated HeLa cells were analysed accordingly. A marked decreased in cell density, shrunken and round cells in metaphase block, the formation of apoptotic bodies as well as evidence of cell debris in the background were visible.

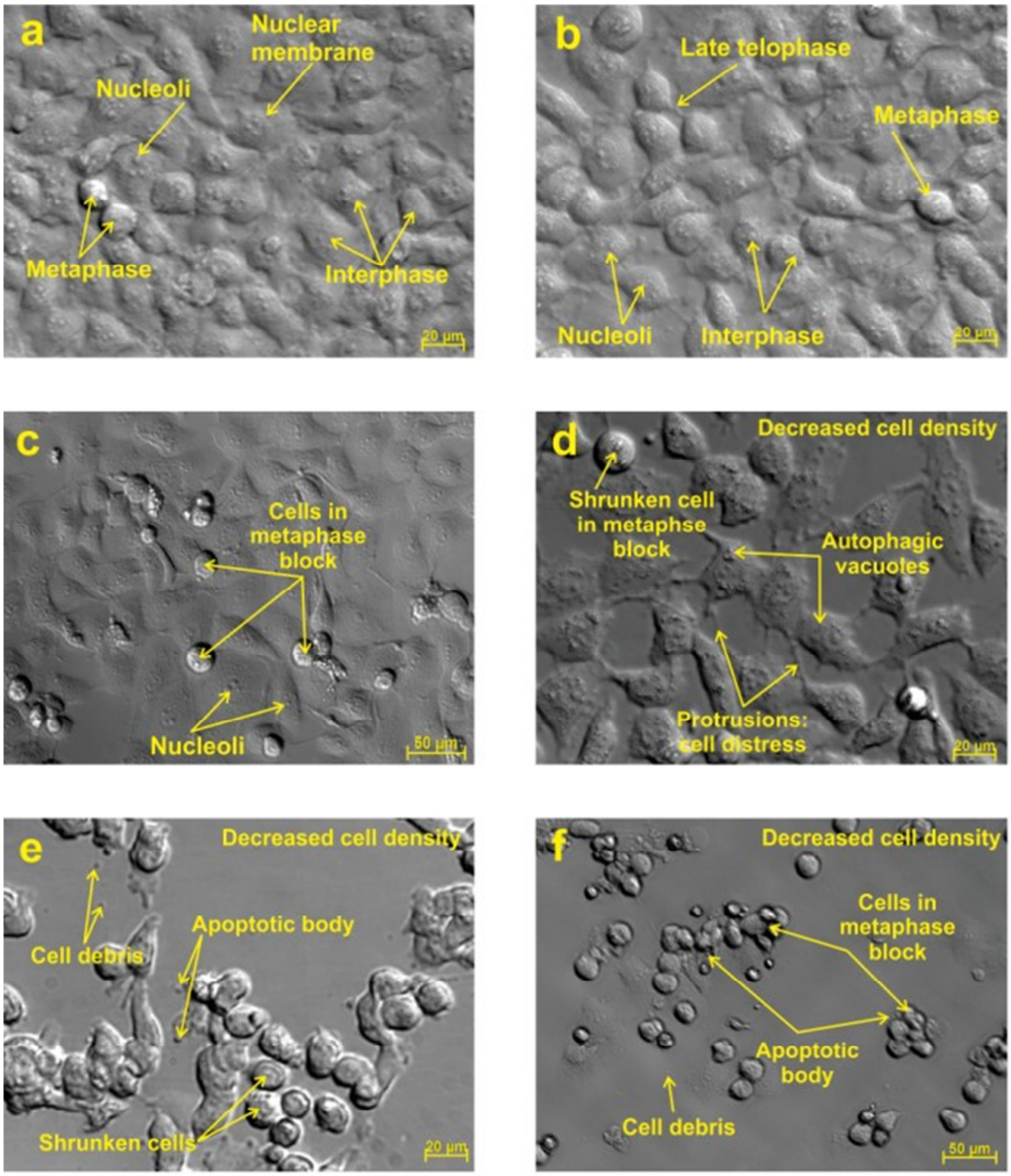

Figure 3.2: PlasDIC micrographs of HeLa cells. (a) Confluent growth of the HeLa cells cultivated in growth medium for 24 hours was illustrated. (b) HeLa cells after exposure to DMSO for a 24 hour period as a vehicle control demonstrated a similar pattern of growth when compared to (a). Round cells in metaphase are known (c) after exposure to 0.5 µM C19 and positive control for metaphase blocks (d) displays a reduction in cell density, autophagic vesicles and cell protrusions representing cell distress after 20 µM tamoxifen treatment as a positive control for autophagy; and 0.1 µg/ml actinomycin D exposure (e) as a positive control for apoptosis resulted in a reduction in cell density, apoptotic bodies, shrunken cells, ghost cells and cellular debris. (f) HeLa cells exposed to 0.5 µM C19 demonstrated the hallmarks of metaphase block and apoptosis.

3.1.2 Fluorescent microscopy: triple staining technique

In order to substantiate the morphological changes observed in the PlasDIC images, a fluorescent microscopic technique was employed. A triple fluorescent dye staining method was utilized to determine the effect that C19 has on acidic vesicular organelle formation and cellular changes associated with apoptosis. Acridine orange is a lysosomotropic fluorescent compound that serves to stain acidic vesicular organelles, including autophagic vacuoles and lysosomes, green when utilizing the Zeiss Filter 9. (133, 314, 327). Cells undergoing autophagy have an increased tendency for acridine orange staining representing the formation of the autophagosomes, when compared to viable cells. (327) Hoechst 33342 is a fluorescent dye that has the ability to penetrate intact cell membranes of viable cells and as well those of cells undergoing apoptosis, to stain the nucleus blue when using the Zeiss Filter 2. The third stain used was propidium iodide (PI), in order to distinguish necrotic cells. PI has the ability to intercalate with the DNA of cells which have lost their membrane integrity, resulting in a red fluorescence when light is filtered with the Zeiss Filter 15.

Previous studies on the *in vitro* effects of 2-methoxyestradiol (the parent compound of C19) and its bis-sulphamate analogue on MCF-7 breast cancer cell lines have shown this triple staining method successfully implemented, and researchers were able to demonstrate the increase of acidic vesicle formation as part of the autophagic process, as well as the various hallmarks of apoptosis. (82, 300, 328) Additionally, increased acridine orange staining has been demonstrated in HeLa cells when exposed to an autophagy inducing agent. (329)

After seeding 2.5 x 10^5 viable HeLa cells in six well plates and allowing 24 hours for attachment, the cells were exposed to 0.5 µM C19 for a further 24 hours, along with the relevant negative and positive controls. Figure 3.3.a and 3.3.b are HeLa cells exposed to growth medium only and DMSO vehicle control respectively, both of which display confluent growth, cells in various stages of mitosis (mostly in interphase) and pale residual acridine orange staining.

The positive control panel, consists of cells exposed to 2-ME (figure 3.3.c), tamoxifen (figure 3.3.d) and actinomycin D (figure 3.3.e). All of the micrographs exhibit a decrease in cell

population. Cells were demonstrated to be blocked at metaphase after 2-ME treatment, but show no increase in acridine orange staining. The later is evident in the autophagy control slide (figure 3.3.d), showing cells with intense acridine orange staining, along with cell protrusions indicating cellular distress, and DNA margination. Figure 3.3.e depicts the typical hallmarks of apoptosis, which include round shrunken cells, hypercondensed chromatin and apoptotic body formation.

Confirming the findings in the PlasDIC images, C19-treated cells revealed a marked decrease in cell density, with aspects of both metaphase block and apoptosis evident. Additionally, intense acridine orange staining indicates an increase in acidic vesicle or aggresome formation, alluding to the induction of autophagy as well in the C19-exposed HeLa cells. Figure 3.3.f shows the various aspects mentioned above, including margination of DNA, rounded, shrunken cells in metaphase, hypercondensed chromatin, intense acridine orange staining and apoptotic bodies.

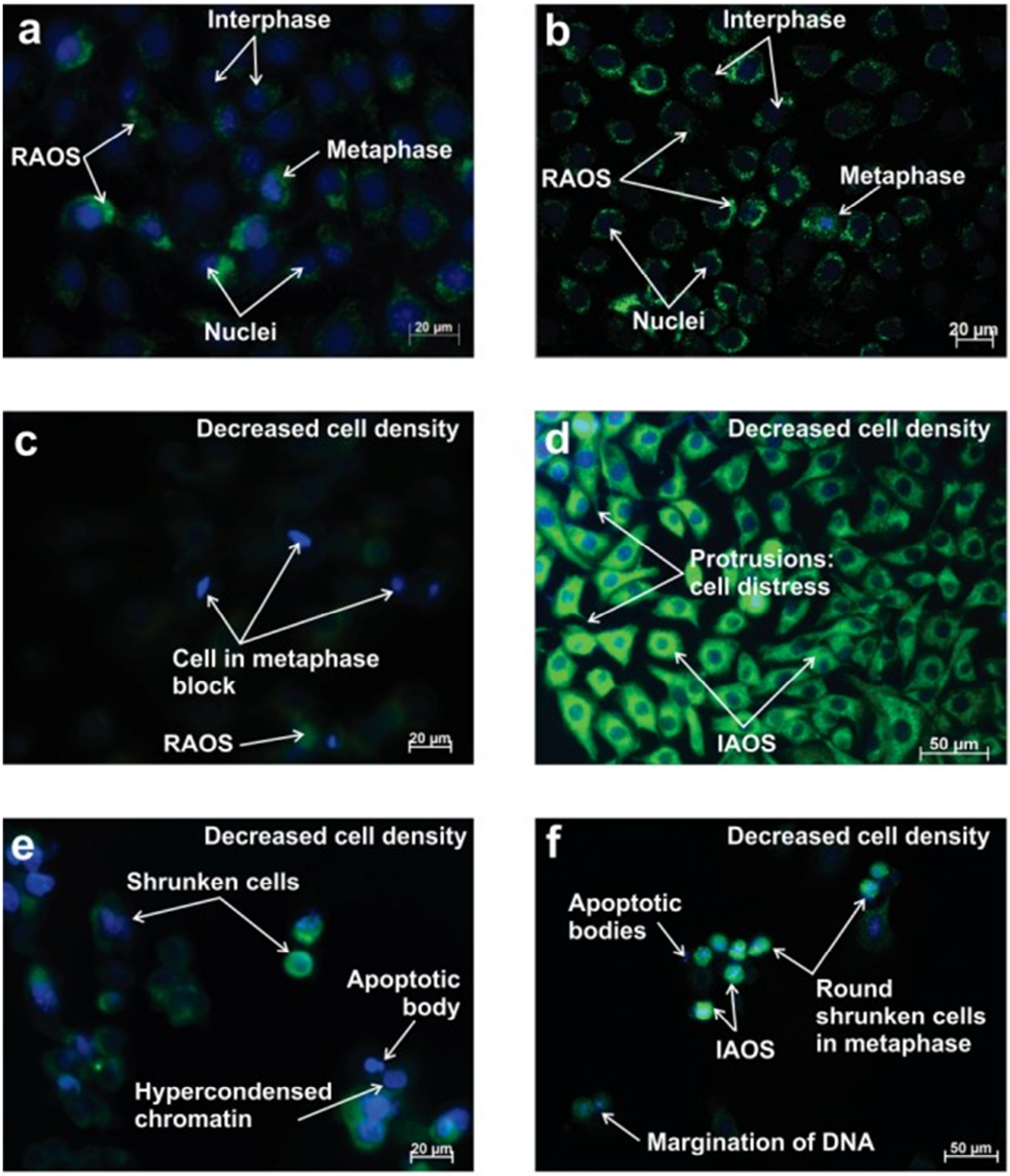

Figure 3.3: Triple staining fluorescence microscopy using Hoechst 33342 as a nuclear stain (blue), acridine orange to detect acidic vacuoles (green) and propidium iodide to exclude necrotic cells (red). Microscopic images representative of the HeLa cells cultivated in medium only (a) showed dividing cells with satisfactory confluency and residual acridine orange staining (RAOS), as was also seen in the DMSO vehicle control (b). All cells exposed to a positive control agent showed a compromise in cell density, with a significant metaphase block in the 2-ME-exposed cells (c), an intense and marked increase in acridine orange staining (intense acridine orange staining (IAOS)) in the [illegible] cells indicating autophagic processes (d) and apoptotic bodies, shrunken cells and hypercondensed chromatin in the second positive control (actinomycin D-exposed cells) (e). C9-exposed cells (f) demonstrated compromised cell density and a combination of the characteristics observed in the positive control panels including the formation of apoptotic bodies, cells in metaphase block and intense acridine orange staining (IAOS). This may be indicative of autophagic and apoptotic cell death processes. Few necrotic cells were evident, and thus were not included in the representative images.

3.1.3 Transmission electron microscopy

Transmission electron microscopy (TEM) was used to determine the ultrastructure of intracellular components of exposed and control cells. TEM is able to produce images at a significantly higher resolution than light microscopes (due to the small de Broglie wavelengths of electrons), and applies the use of an electron beam projected through ultra-thin sections of fixed and embedded material (324). This imaging modality was used to analyse detailed intracellular and membrane properties of the HeLa cells exposed to C19 in order to examine evidence of autophagosomes, nuclear membrane disruption, hypercondensation and fragmentation of chromatids, apoptotic bodies and membrane blebbing: signs of autophagic and apoptotic cell death, both of which were hypothesised to be caused by C19.

2 million HeLa cells were seeded into the various 25 cm^2 cell culture flasks, and after 24 hour exposure to the test compound and the relative controls, the cells were collected via trypsinization and fixed in gluteraldehyde and aqueous osmium, underwent sequential ethanol dehydration and were embedded in Quetol resin. Ultra-thin sections were prepared using a microtome, which were contrasted with 4% uranyl acetate and Reynold's lead citrate after being mounted on copper grids.

Images captured from the electron microscope displayed detailed images of the cellular microstructure. Figure 3.4.1a demonstrates the smooth cell membrane with normal cell protrusions (higher magnification in figure 3.4.1b) of the cells grown only in growth medium. A nuclear membrane is distinguishable, as are mitochondria. Comparative morphology was seen in the DMSO-exposed cells (figure 3.4.2a) and the higher magnification of the membrane (figure 3.4.2b) indicating that the vehicle had no influence on the cellular structures. Intracellular organelles, including mitochondria and nucleoli are clearly identifiable, with no obvious or excessive vesicle formation. The impression of ordered and healthy cellular mechanisms is gleaned from the images.

In contrast to the above-mentioned healthy cells, cells exposed to the positive control agents, tamoxifen and actinomycin D, displayed characteristics of cellular distress and

processes of autophagy and apoptosis respectively. Figure 3.4.3a shows the marked increase of autophagic vacuoles. Cells are smaller in size, and the nuclear membrane, nucleolus and cell membrane are still intact. Figure 3.4.3b is a high magnification of an autophagosome found within the previous cell, demonstrating the engulfed cellular contents and organelles within a double membrane. Actinomycin D treatment had a dramatic effect on the cell membrane structure, with a notable increase in the number of protrusions, as is represented in micrograph 3.4.4a and 3.4.4b. Additionally, signs of apoptosis are evident, and include hypercondensation of chromatin, karyorhexis and the presence of apoptotic bodies.

Figure 3.4.5 demonstrates the dramatic effect that C19 exposure has on HeLa cells. Pictured in figure 3.4.5a is a significantly distressed cell (representative of all the imaged cells treated with C19), in the process of undergoing both apoptosis and autophagy. The combination of cell death type I and II are represented by the characteristic apoptotic body formation, chromatin hypercondensation and an increased number of cell membrane protrusions of the former, and the presence of numerous autophagosomes as part of the latter. The nuclear membrane is absent. Figure 3.4.5b is a higher magnification of the previous cell, in which the autophagosomes and organelles such as Golgi bodies were identified.

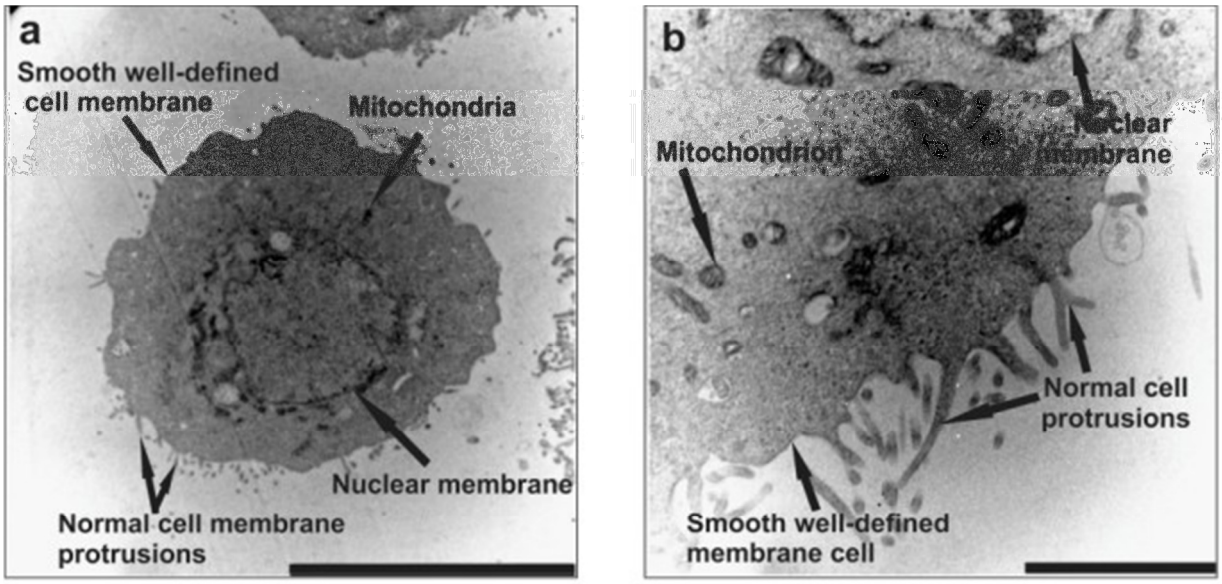

Figure 3.4.1: Transmission electron microscopy of HeLa cells propagated in medium only. (a) A HeLa cell demonstrating characteristics of cells unexposed to any agents, namely a smooth well defined cell membrane with normal cell protrusions as well as an intact nuclear membrane. Some organelles such as mitochondria are identifiable. (Scale bar represents 10 µm). (b) A higher magnification of the cell membrane showed normal cellular protrusions. (Scale bar represents 2 µm)

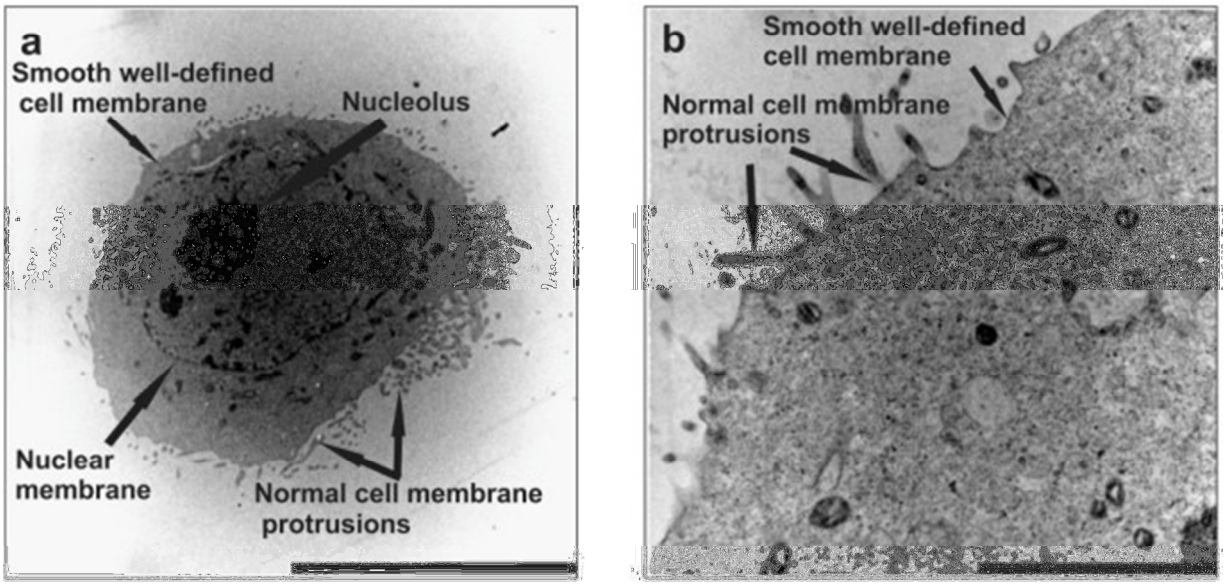

Figure 3.4.2: Transmission electron microscopy of HeLa cells after exposure to DMSO as the vehicle control. The images show no noteworthy differences when compared to the cells propagated in medium only (Figure 2.4.1). A smooth well-defined cell membrane with normal protrusions was demonstrated in (a), which was verified with a higher magnification of the cell membrane in (b). (Scale bars represent 10 µm in (a) and 2 µm in (b))

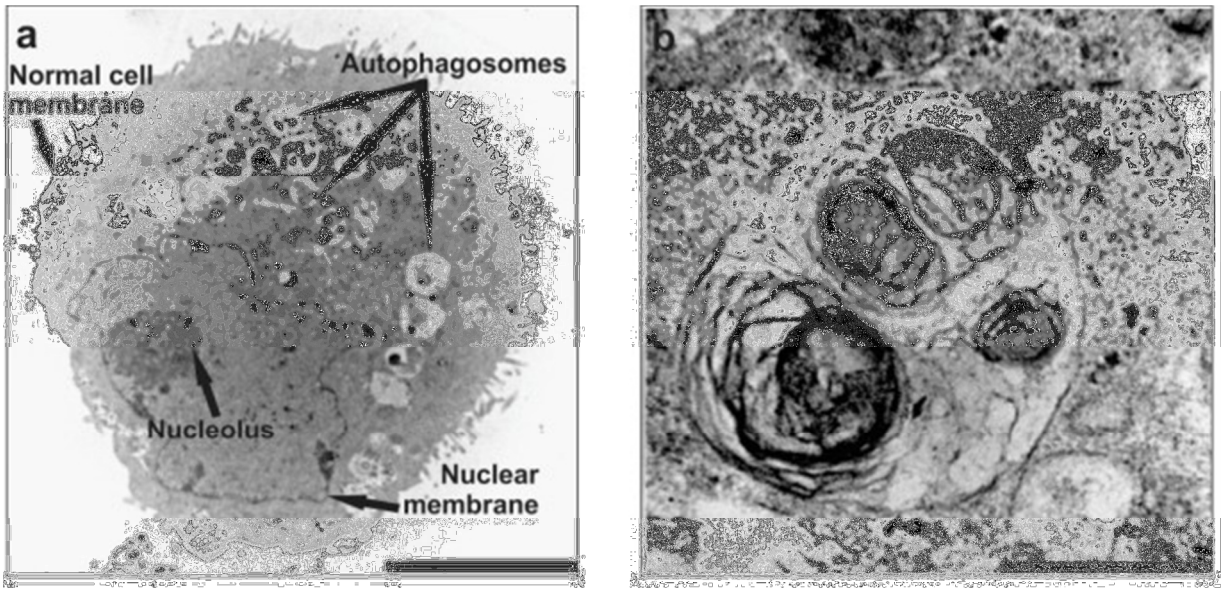

Figure 3.4.3: Transmission electron microscopic images showing the ultra structure of the HeLa cells after exposure to tamoxifen as a positive autophagy control. HeLa cells exposed to tamoxifen (a) were smaller, and displayed numerous autophagosomes with whorls (ingested organelles), but the cell membrane, nucleolus and nuclear membrane remained intact. (b) represents a higher magnification of an autophagosome, with ingested membranous organelles clearly visible. (Scale bars represent 5 µm in (a) and 0.5 µm in (b))

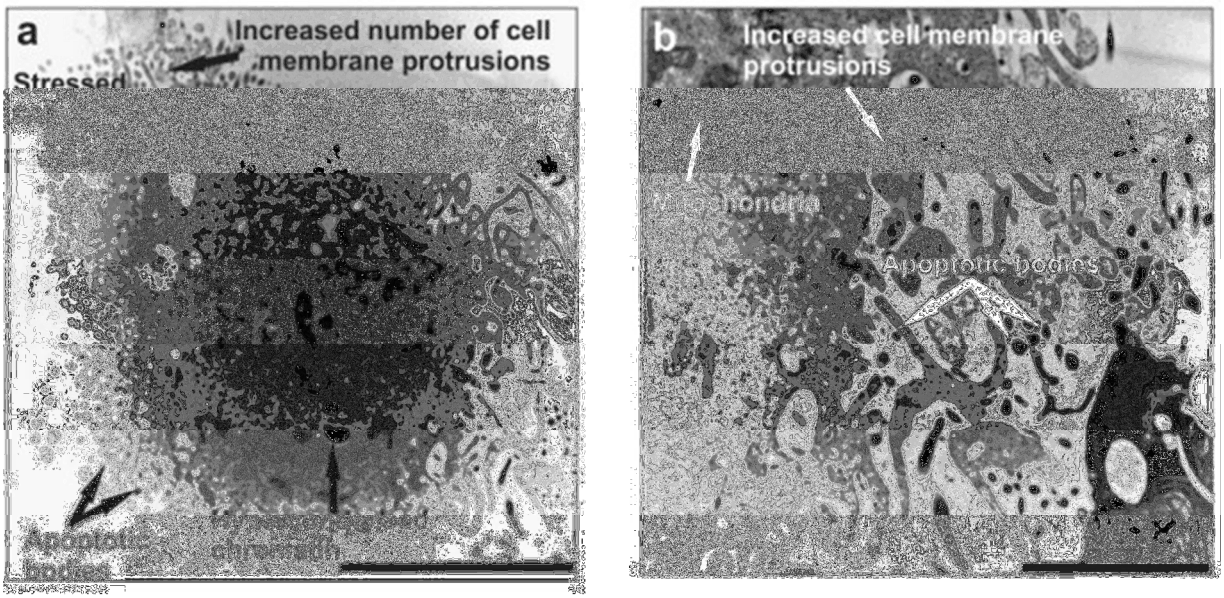

Figure 3.4.4: Transmission electron microscopy of HeLa cells and their intracellular components as seen after exposure to actinomycin D as a positive apoptosis control. Figure (a) and higher magnification of the cell membrane (b) are representative images, and evidence of apoptosis was detected by identifying apoptotic bodies, hypercondensed chromatin and a distinct increase in the amount of cellular membrane protrusions. The nuclear membrane is absent and the cells are smaller in size. (Scale bars represent 5 µm in (a) and 2 µm in (b))

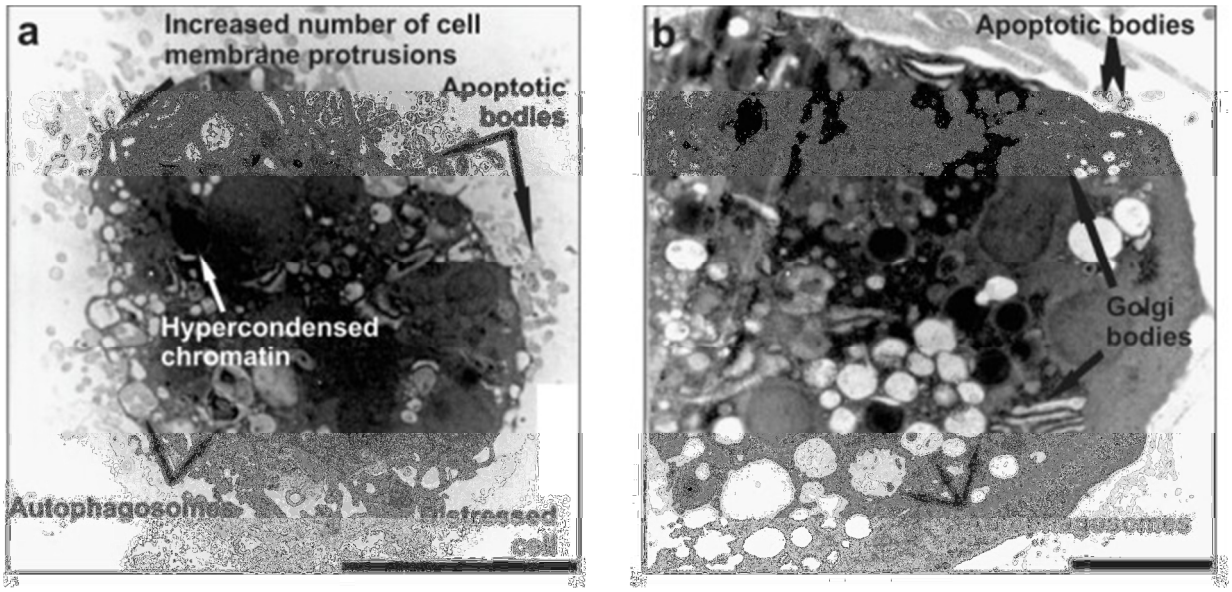

Figure 3.4.5 Transmission electron microscopy of HeLa cells in response to 24 hours C19-exposure. Images (a) and higher magnification (b) of C19-treated cells showed a combination of the characteristics from Figures 3.4.3 and 3.4.4 above. The presence of autophagosomes, apoptotic bodies, hypercondensed chromatin, increased membrane protrusions and absence of the nuclear membrane gave the impression of a shrunken cell in clear distress. (Scale bars represent 5 µm (a) and 2 µm (b) respectively)

3.2 Cell cycle progression and apoptosis studies via flow cytometry

In order to confirm and quantify the morphological changes observed in the microscopy studies of the HeLa cells exposed to C19, biochemical and quantitative techniques were employed to identify stages in the cell progression and induction of apoptosis.

3.2.1 Cell cycle analysis

Flow cytometric analysis was performed on the C19-exposed HeLa cells in conjunction with the relevant controls, after ethanol fixation and nuclear staining with PI in order to determine the fraction of cells in each stage of the cell cycle. A minimum of 10 000 events were captured per run and the data plotted as FL3 Lin (indicating cell complexity) along the X-axis against the number of cells on the Y-axis using Cyflogic version 1.2.1 software (Pertu Therho, Turko, Finland). Statistical evaluation of data accumulated from the 3 run repeats comprised the application of the analysis of variance (ANOVA)-single factor model and a two-tailed Student's *t*-test.

The histograms generated are displayed in figure 3.4.1. The distribution of the cells in the cell cycle in the medium only exposed cells and the DMSO vehicle control were comparable, with an average of 50.82 % and 54.12 % of the cells in G_1 respectively. An average of 21.41 % growth medium exposed cells were in the S phase, and 21.73 % in G_2/M phase. Only an average of 0.55 % of the cells were in sub-G_1. This distribution is representative of a healthy cell population in logarithmic growth. The DMSO vehicle control demonstrated a very similar distribution within the cell cycle, with 22.82 % in S, 22.20 in G_2/M and 0.63 % in sub-G_1. There was no statistically significance between the values obtained from the growth medium and vehicle control samples when analysed with the two-tailed Student's *t*-test., with a *P*-value of > 0.05. Average percentage of cells per cell cycle stage (of 3 experimental repeats), the standard deviation and the *P* values are displayed in table 2.

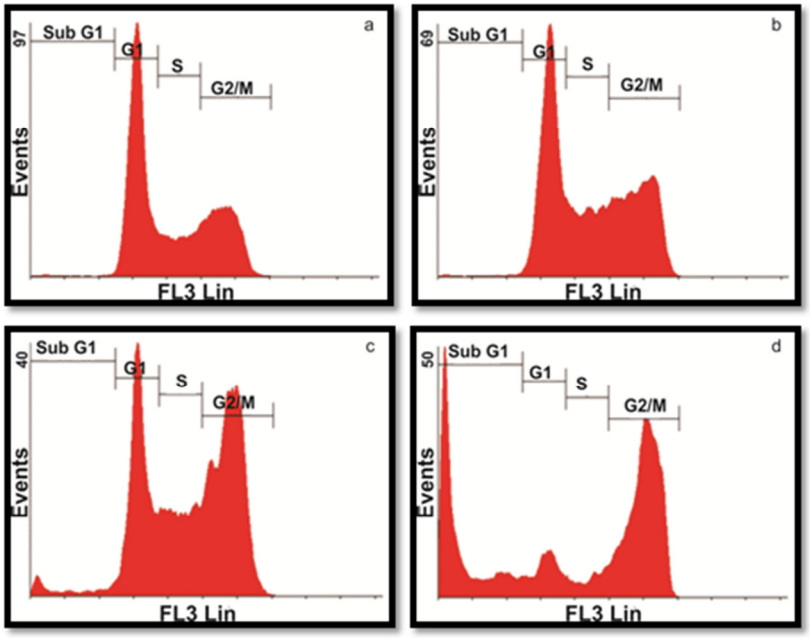

Figure 3.5.1: Histograms created from flow cytometric events captured in order to assess cell cycle progression, plotting FL3 Lin (PI) against number of fluorescent events. Cycle distribution of cells grown in medium only as a negative control is shown in (a), and the DMSO exposed cells are shown in (b) as a vehicle control. Both of these samples have similar distributions, with most of the cells in the G_1 phase and very few detected in the sub-G_1 stage. (c) and (d), representing the actinomycin D control and C19-exposed cells respectively, both demonstrate a significant portion of the cells in apoptosis (represented by the sub-G_1 phase).

Table 3: Cell cycle flow cytometric analysis. Statistical data calculated were generated via Cyflogic version 1.2.1 software (Pertu Therho, Turko, Finland) and analyzed using of the analysis of variance (ANOVA)-single factor model and a two-tailed Student's *t*-test. Displayed is the average percentage (of three repeats) of cells in each phase of the cell cycle, the standard deviation (STD), and the *P* value calculated to determine a statistical significant difference when compared to the DMSO vehicle control.

	Stage of cell cycle											
	Sub G1			G1			S			G2/M		
	ave %	STD	P value	ave %	STD	P value	ave %	STD	P value	ave %	STD	P value
MO	0.55	0.19	0.65	50.82	2.36	0.48	21.41	1.85	0.53	21.73	2.61	0.86
DMSO	0.64	0.24		54.12	7		22.82	2.99		22.2	3.85	
Act D	4.93	2.7	0.048	37.29	5.08	0.028	23.62	1.61	0.71	33.35	3.1	0.017
C19	27.93	3.86	0.0002	10.16	3.79	0.0007	9.42	2.3	0.0036	51.28	7.09	0.0034

The cell cycle distribution changed significantly with actinomycin D and C19 exposure. A statistically significant increase of cells in sub-G_1 was demonstrated in the apoptosis control sample (4.93 %), with a dramatic spike in the C19-treated cells (27.93 %). G_1 populations were significantly decreased, with 37.29 % and 10.16 % of the cell population in actinomycin D- and C19-treated cells respectively. C19 had a pronounced effect on the cell cycle distribution, with a marked decrease of viable cells (G_1 and S), and a distinct increase of cells in G_2/M (51.28 %), all being statistically significant with a *P* value < 0.05 (values given in table 2).

Figure 3.5.2 represents the calculations and values obtained for the cell cycle analysis graphically. These results demonstrated that C19 is toxic to the HeLa cells, decreasing the viability as represented by a decreased percentage of cells in G_1 and S, inducing apoptosis visualized by the sub-G_1 spike, and causing a metaphase block as seen in the amplified G_2/M peak.

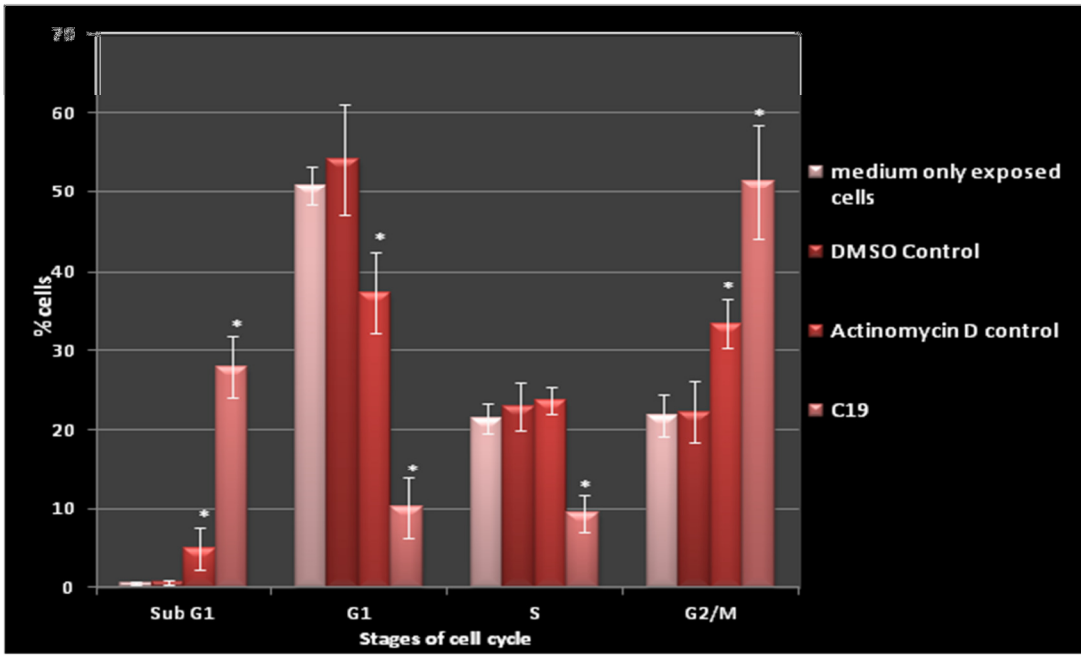

Figure 3.5.2: Histogram comparing the stages of the cell cycle between the control samples and the C19 treated cells. (* indicates a statistically significant difference when compared to DMSO samples, with a *P* value of < 0.05). Standard deviation is indicated by the T-bars.

3.2.2 Cyclin B1 detection

A cyclin B1-phycoerythrin conjugated antibody (Milli-Mark™ Anti-Cyclin B1-PE, clone GNS3 (8A5D12)) was used to quantify cyclin B1 protein up-regulation in C19-treated HeLa cells by employing flow cytometric analyses, as a determinant of the compound's ability to induce a metaphase block. One million HeLa cells were seeded in 25 cm^2 culture flasks, exposed to C19 in parallel to the negative (medium only and DMSO-exposed cells) and positive control (2-ME), harvested via trypsinization and stained with the anti-cyclin B1 antibody. Flow cytometric analysis was done to determine an increase in fluorescence (Fl3), in conjunction with a variation of cell size (forward scatter) and complexity (side scatter).

Figure 3.6.1 displays representative scatter plots, with the fluorescent intensity of the PE-conjugated cyclin B1 antibody plotted against forward scatter as a determinant of cells size (a and b), and side scatter indicative of cell complexity. No statistically significant difference was detected between the negative controls cells propagated in medium only and the DMSO vehicle control (results not shown). No statistically significant difference was observed between the negative controls and the positive metaphase block control induced by 2-ME. Visual microscopic inspection of 2-ME exposed cells exhibited a significant metaphase block (24 and 48 hours of exposure) and different concentrations (1 and 1.5 µM). No statistically significant increase of cyclin B1 expression was observed.

Scatter plots in figure 3.6.1 displayed a higher fluorescent signal in more complex and smaller sized cells, which are representative of cells in metaphase. (330, 331) Upregulation of cyclin B1 expression corroborates the finding of the cell cycle analysis in section 3.2.1 above, in which there was a significant increase in the cells in metaphase after C19 exposure.

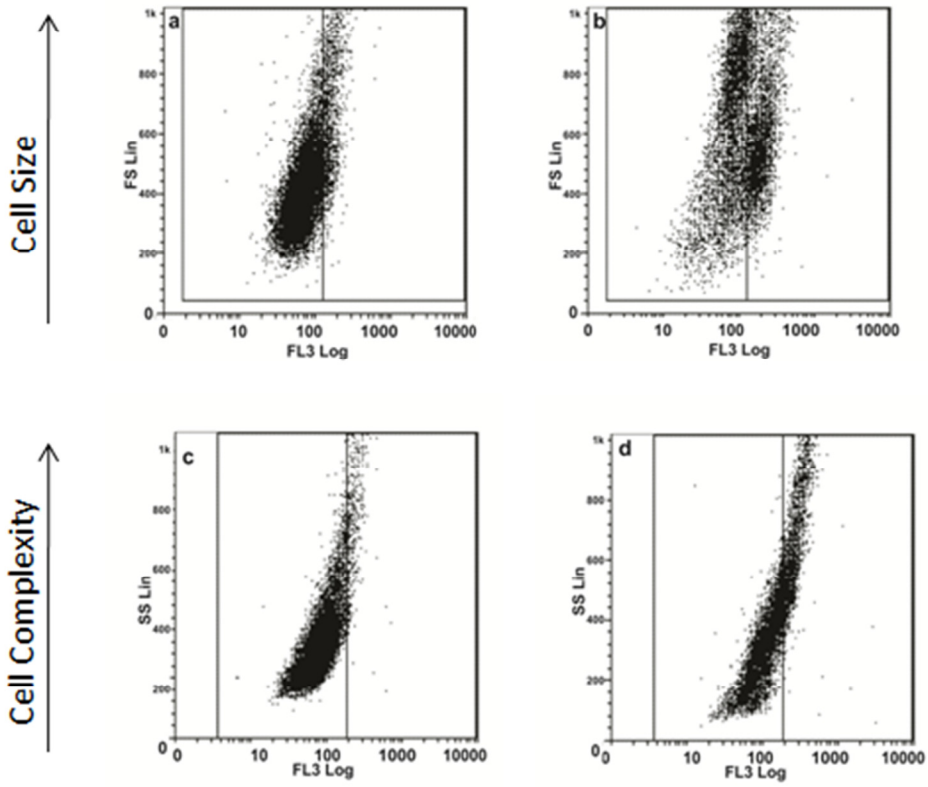

Figure 3.6.1: Flow cytometric evaluation of cyclin B1 up-regulation in HeLa cells (b and d) compared to the DMSO vehicle control (a and c). FL3 log fluoresce intensity (phycoerythrin) was plotted against cell size determined by forward scatter (a and b) and cell complexity as established with side scatter (c and d). An increase in expression of cyclin B1 in the C19-treated cells was observed, more so in the smaller (b) and more complex (d) cells

An increase in cyclin B1 expression in the C19-treated cells was observed. A 2.47-fold increase of cyclin B1 expression ($P < 0.05$) in the C19-exposed cells was revealed when compared to the DMSO vehicle controls (figure 3.6.2). An overlay histogram (figure 3.6.3), demonstrates a right shift in the C19-treated cells. Formation of tetrapoidic cells after mitotic spindle inhibition may have caused forced overexpression of cyclin B1, as well a showing a role of this molecule in cell size determination. (330, 332)

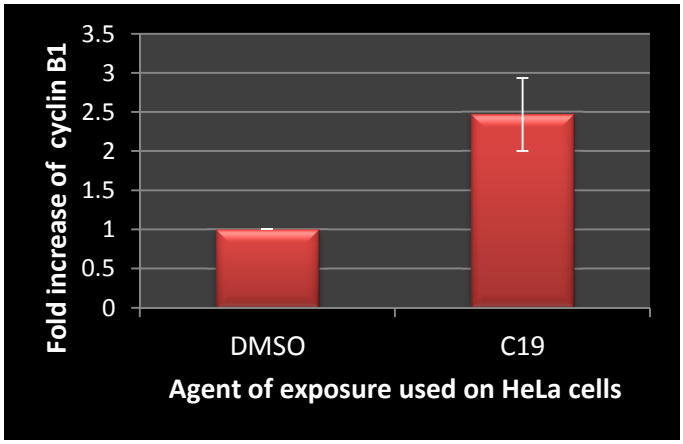

Figure 3.6.2: Fold increase of cyclin B1 expression in HeLa cells when comparing C19-exposed cells to DMSO controls (taken as 1). A 2.47-fold increase in cyclin B1 expression was observed in cells treated with C19. Standard deviation is displayed by T-bars.

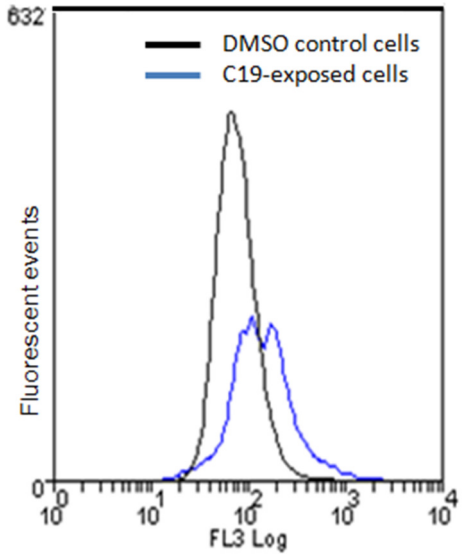

Figure 3.6.3: Overlay histogram of cyclin B1 fluorescence demonstrating a right shift when C19-exposed cells (blue) are compared to DMSO-exposed negative controls (black).

3.2.3 Phosphatidylserine flip detection

In order to detect and discriminate between the induction of apoptosis, necrosis and viable cells, flow cytometric analysis of the C19-exposed cells in parallel to the relevant controls, was used. Recombinant Annexin V labelled with fluorescein isothiocyanate (FITC), a derivative of fluorescein (an organic synthesized fluorophor), was used to measure the

translocation of PS (BioVision Annexin V-FITC reagent kit from BioVision Research Products). When excited by an argon laser at 488nm, apoptotic cells were stained with Annexin V-FITC (FL1), but not propidium iodide (PI) (FL3). Viable cells were stained by neither Annexin V-FITC nor PI whereas dead cells were stained positively by both as seen in the scatter plots (figure 3.7.1). Utilization of labelled annexin-V in the flow cytometric determination of apoptosis has been reported as a sensitive qualitative and robust assay which renders highly reproducible results. (148)

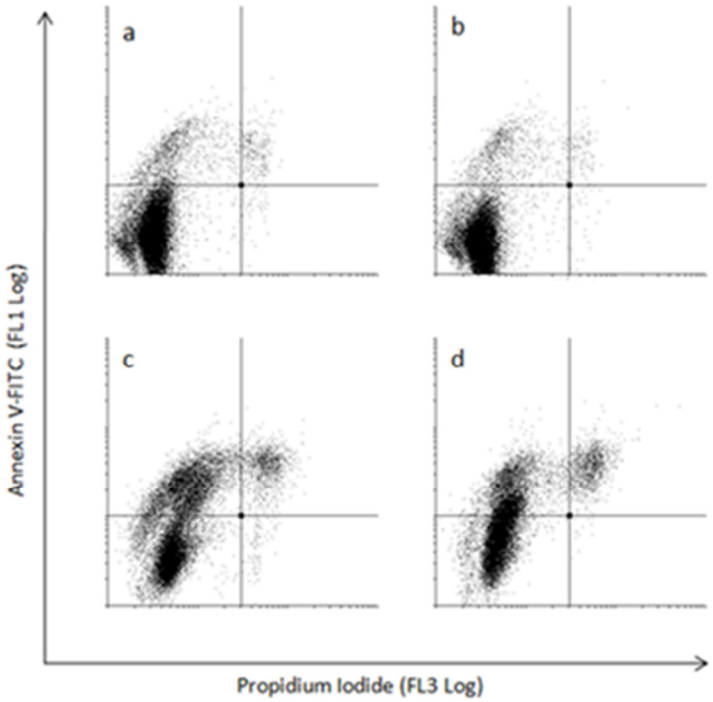

Figure 3.7.1: Flow cytometric scatter dot plots of propidium iodide (FL3 Log) versus annexin-V (FL1 Log) in the determination of apoptosis induction of HeLa cells exposed to (a) medium only, (b) DMSO, (c) actinomycin D and (d) C19. The bottom left quadrant represents the viable cells, the upper two quadrants apoptotic cells, and the lower right shows necrotic cells.

Analysis of the data generated from the dot plots via Cyflogic version 1.2.1 software revealed that in a healthy cell population (DMSO as a vehicle control), 92.8 % of the cells were viable, with 7.02 % undergoing apoptosis and an insignificant 0.16 % in necrosis (table 4). There were insignificant differences between the medium only exposed cells and the DSMO negative controls. Actinomycin D induced apoptosis (21.28 %), with a significant

decrease of viable cells (77.68 %). A decrease in cell viability was demonstrated in the C19-exposed cells (64.22 % viability), and a corresponding rise in apoptotic numbers (27.32 % of the cell population). There was no significant difference in the proportion of necrotic cells between the samples. Data (10 000 cells per run repeated thrice) were interpreted using the analysis of variance (ANOVA)-single factor model and a two-tailed Student's *t*-test. A *P*-value < 0.05 was considered as statistically significant (indicated with *) and results are represented in a histogram (figure 3.7.2)

Table 4: Average percentage (ave %) and the standard deviation (STD) of cells which were viable, in apoptosis, or nectrotic in the various controls (MO, DMSO and Act D as a potitive apotosis control) and the C19-treated HeLa cells as determined with PS-flip flow cytometric quantification. Statistically significant differences ($P < 0.05$) were calculated with the DMSO as a baseline using the analysis of variance (ANOVA)-single factor model and a two-tailed Student's *t*-test.

	Cell viability										
	MO			DMSO		Act D			C19		
	ave %	STD	P value	ave %	STD	ave %	STD	P value	ave %	STD	P value
Viable cells	92.25	2.27	0.76	92.8	1.84	77.61	1.89	0.00057	64.22	4.68	0.00069
Apoptosis	6.82	2.77	0.77	7.02	1.83	21.28	1.76	0.000629	27.32	2.67	0.031
Necrosis	0.51	0.74	0.455	0.16	0.02	1.09	1.56	0.36	7.44	4.46	0.08

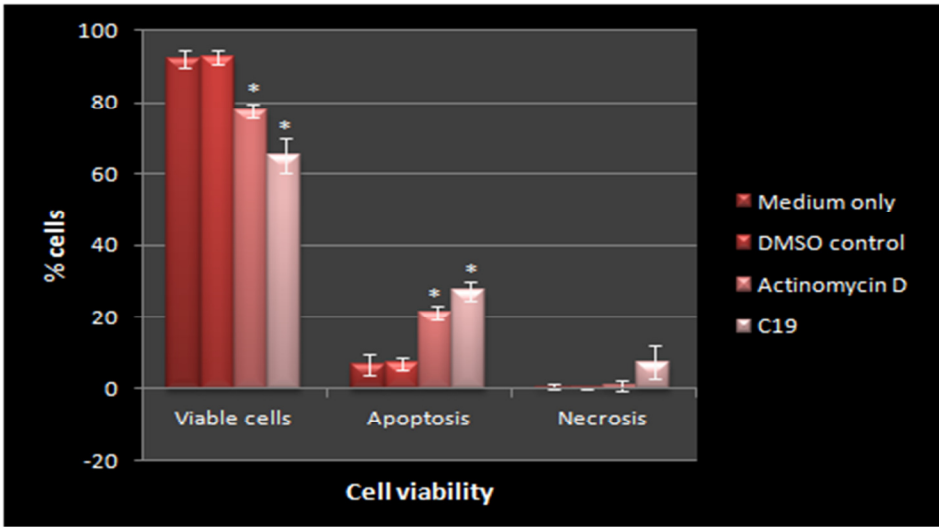

Figure 3.7.2: Comparative histogram of HeLa cell viability as determined by flow cytometric quantification of phosphatidylserine-flip post C19 exposure. A statistically significant decrease of

viable cells was seen in actinomycin D- and C19-exposed cells, with a concurrent increase of apoptotic cells. There were no statistically significant differences between the cells propagated in growth medium only and the DMSO vehicle controls in any of the cell cycle categories. Neither was a significant difference calculated in the necrotic cells of all samples. (* $P < 0.05$, standard deviation represented by T-bars).

3.3 Aggresome detection

In order to confirm the morphological results obtained via the triple staining fluorescent microscopy and to evaluate the induction of autophagy in the C19-treated cells, the Enzo Life Sciences' ProteoStat® Aggresome Detection Kit was used. This kit contained a novel 488 nm excitable red fluorescent molecular rotor dye to specifically detect denatured protein inclusions within aggresomes in fixed and permeablised cells. The detection reagent supplied in the ProteoStat® Aggresome Detection Kit become brightly fluorescent upon binding to aggregated proteins within vesicles produced during aggresome formation, allowing quantification statistical analysis of the induction of autophagy.

Table 5: Data generated from flow cytometric readings of the aggresome kit using Cyflogic version 1.2.1 software, showing the MFI (mean fluorescent intensity) and standard deviations (STD) of three experimental repeats, of both negative controls (MO and DMSO), the tamoxifen positive autophagy control and C19-treated HeLa cells. The AFF was calculated as given in figure 2.2, using the DMSO sample as the baseline reading.

	MFI			Aggresome Activity Factor (AAF)	
	Average	STDEV	P-value	Average	STDEV
MO	4.85	0.509117	0.390625329		
DMSO	5.295	0.275772		1	0
Tamoxifen	9.54	0.59397	0.011691	44.29890615	6.35869248
C19	8.925	0.544472	0.013841794	40.65608987	0.53041413

Table 5 summarizes the data gained from the flow cytometric reading of the 3 experimental repeats. Cyflogic version 1.2.1 software was used and the mean fluorescent intensity was calculated for the various cell samples, including the medium only exposed cells, the DMSO

vehicle control, the positive autophagy control (induced by tamoxifen) and the C19-exposed HeLa cells. There was no statistical difference between cells propagated in growth medium only and DMSO control samples, caluclated by the analysis of variance (ANOVA)-single factor model and a two-tailed Student's *t*-test (*P*-value < 0.05 being statistically significant). Using the formula described in section 2.3.3 (figure 2.2), the aggresome activity factor (AFF) was calculated. According to the the manafacture's protocol, an AFF of more than 25 is indicative of a statistically significant increase in aggresome formation. Thus,
if an increase in aggresomes formation is demonstrated in the C19-treated cells, one can almost synonymously see that as an increase in autophagy.

Figure 3.8 is a histographic representation of the AFF of the tamoxifen and the C19-treated cells, being 44.3 (standard deviation of 6.36) and 40.7 (standard deviation of 0.53) repectively. These data indicate that C19 induces autophagy, confriming conclusions drawn from the triple staining flourescence microscopy results.

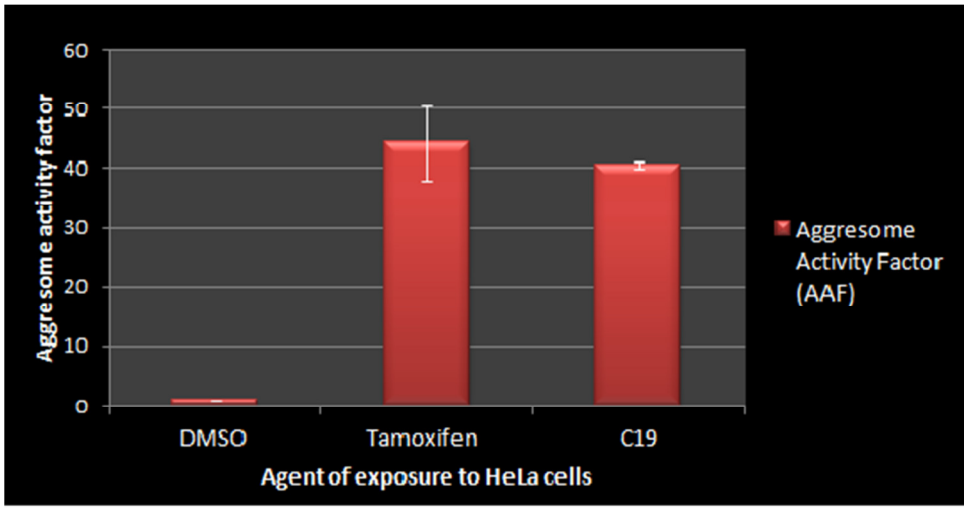

Figure 3.8: Histogram of the aggresome activity factor in HeLa cells, treated with tamoxifen and C19 and compared to the DMSO vehicle negative control. Standard deviations are annotated with T-bars. An AFF > 25 is suggestive of an increased intracellular aggresome formation and thus a positive indicator for autophagy. (Standard deviation represented by T-bars)

3.4 Signal transduction: quantification of caspases 8 and 3

Quantification of both caspases 8 and 3 were done using spectrophotometric principles. In the quantification of caspase 3, an amino acid sequence homologous to that within PARP1 (polyADP-ribose polymerase 1) which is cleaved by caspase 3 during apoptosis is used as the base of this colorimetric reaction. The aspartate-glutamate-valine-aspartate (DEVD) sequence is conjugated to the chromophore *p*-nitroanilide (*p*NA), which emits light at 405 nm following cleave by caspase 3. Caspase 8 activity is assayed when the *p*NA-labelled recognition tetra-peptide sequence isoleucine–glutamic acid–threonine–aspartic acid (IETD) (amino acids 172-175) is cleaved by the protease, the emission being detectable using a spectrophotometer at 405 nm. In both cases, the absorbance of *p*NA from the C19-exposed samples was compared to the un-induced HeLa cells to obtain a fold increase in the relevant caspase activity.

3.4.1 Caspase 8 activation assay

The FLICE/Caspase 8 colorimetric kit was used to determine caspase 8 activation in the cell lysates of the C19 HeLa cells as compared to that of the relevant controls (the medium only exposed cells, the DMSO vehicle treated and the actinomycin D positive apoptotic control). Statistical analysis was completed using the analysis of variance (ANOVA)-single factor model and a two-tailed Student's *t*-test, with $P < 0.05$ being statistically significant.

Table 6 lists the averages (ave) and standard deviations (STD) of the fold increase of caspase 8 activity (using the medium only exposed cells as the baseline) calculated from three experimental runs, comprising of three samples of each sample group, in order to give statistical significance to the enzymatic based reactions. There was no statistically significant difference noted between readings of the medium only, DMSO and actinomycin controls. Caspase 8 was not shown to be significantly up-regulated in the actinomycin control due to alternative activators such as caspase 2 and/or 9. There was a 1.9-fold increase in caspase 8 induction in the C19-exposed HeLa cells when compared to the

baseline (*P*-value 0.04) (figure 3.9). C19 induces apoptosis in HeLa cells via the extrinsic pathway, with the up-regulation of the initiator caspase 8.

Table 6: Spectrographic determination of caspase 8 activity. Cells propagated in medium only were taken as a baseline of and readings of the DMSO-exposed cells, actinomycin D positive control and C19-treated cells were normalized according to the baseline. DMSO-exposed cells showed the same ratio the MO-exposed cells and actinomycin controls were not significantly increased. C19-treated cells demonstrated a statistically significant 1.9-fold increase in caspase 8 activity.

	fold increase		
	ave	STD	P value
MO			
DMSO	1.04	0.007	0.06
Act D	1.11	0.24	0.4
C19	1.9	0.49	0.04

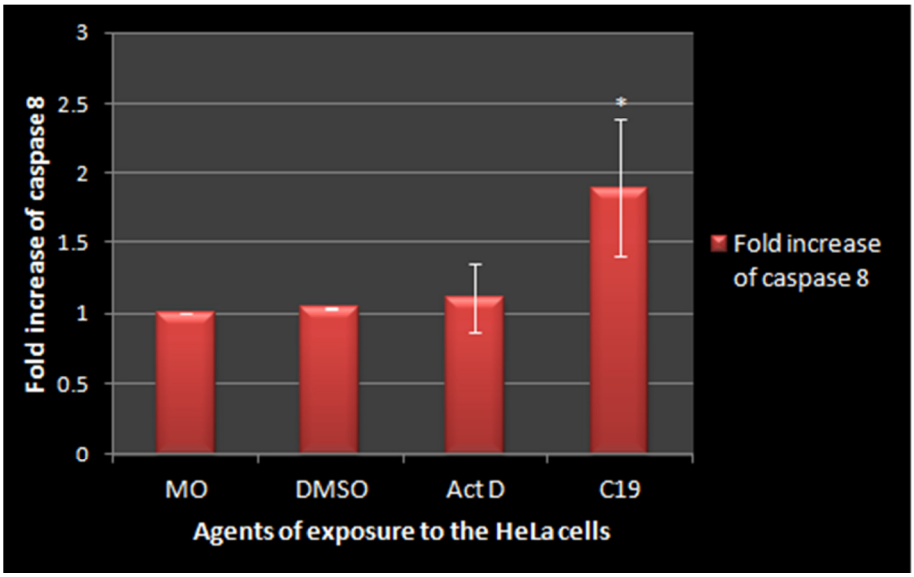

Figure 3.9: Fold increase in caspase 8 activity in C19-treated cells, when compared to cells propagated in growth medium (MO), the DMSO vehicle and actinomycin D controls. (* $P < 0.05$, standard deviation represented by T-bars).

3.4.2 Caspase 3 activation assay

Caspase 3 activity in cell lysates was measured using the BioVision Caspase-3/CPP32 Colorimetric Assay Kit (Table 3.7). Medium only exposed cells and DMSO vehicle controls showed a near identical picture. Figure 3.10 graphically represents the fold increase in caspase 3 activity, showing a statistically significant up-regulation of the mentioned caspase in the actinomycin D positive control (3.75-fold increase) and a pronounced increase in the C19-treated cells (8.03-fold increase) ($P < 0.05$).

Table 7: Spectrophotometric analysis of caspase 3 induction. As the medium only exposed cells not differ at all from the DMSO vehicle control, the latter was used as the baseline when calculating the fold increase, which showed a statistically significant 3.75-fold increase in actinomycin D exposed cells and 8.03-fold increase in C19-treated cells when normalized to the DMSO control.

	fold increase		
	ave	STD	P value
MO	0.999	0.022	0.99
DMSO	1		
Act D	3.75	0.205	0.011
C19	8.03	0.208	0.008

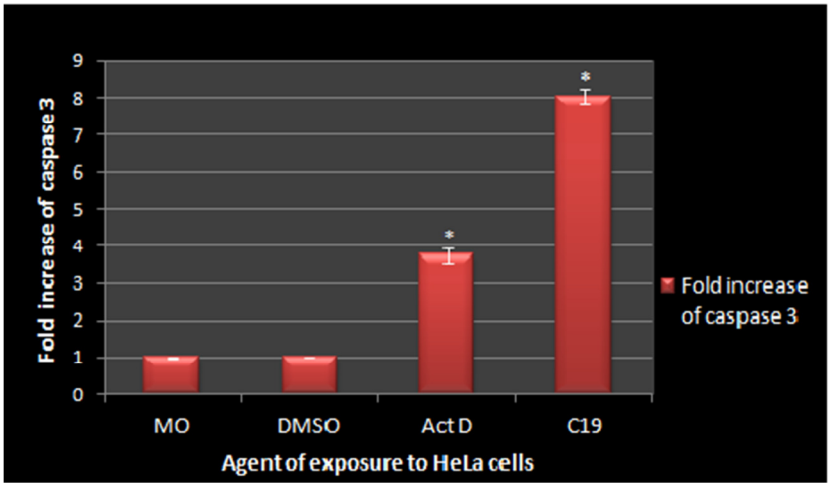

Figure 3.9: Histogram representing the fold increase of caspase 3 activity in C19-treated HeLa cells when compared to the negative controls. (* indicates $P < 0.05$. Standard deviations are represented by T-bars)

This increase in caspase 8 and 3 activity as an initiator and downstream executioner caspase of apoptosis respectively corroborates the theory that C19 induces apoptosis via the extrinsic pathway. Increase of caspase 3 activity is not an exclusive finding to the extrinsic pathway however, as caspase 3 is part of the common convergence of both the extrinsic and intrinsic pathways.

3.5 Microtubule dynamics: confocal microscopy to determine α-tubulin assembly

In order to observe the effects of C19 on the HeLa cell cytoskeletal microtubule architecture, cells were stained green with anti-alpha-tubulin antibodies, which were visualised by an Alexa-488 fluorescent probe. The nucleus was counterstained using 4',6-diamidino-2-phenylindole (DAPI) before viewing the samples via confocal microscopy. (333) DAPI may be used as a blue nuclear counter stain in fixed cells, with specific binding to A-T rich double stranded DNA regions, which increases its fluorescent intensity. (334) DAPI has an excitation wavelength of around 360 nm and an emission spectrum of between 456 and 460 nm when bound to double stranded DNA. (334) This method was used to establish a possible link between the effect of C19 on cell cycle progression, influence on α-tubulin function and the induction of the two forms of cell death.

Figure 3.11.1 are representative images of a HeLa cells propagated in medium only. Confluency of cell growth, showing various stages of mitosis (mostly interphase) was demonstrated, with clear organized spindle formation visible within the cells. Figure 3.11.1b is a higher magnification of one of the cells undergoing metaphase, demonstrating chromatid alignment on the equator and organised spindle formation present. Similar morphology was seen in representative images from the DMSO-exposed cells, with an appropriate cell density, intact, organised microtubule structures, and cells mostly in interphase. This indicates that the DMSO vehicle is not toxic to the cells at the exposed concentration. A cell undergoing telophase is shown in figure 3.11.2b at higher magnification, with the chromatids being separated by a well-defined and functional spindle formation.

As part of the positive control panel, cells were exposed to a metaphase block inducing agent (2-ME), a compound which causes autophagy (tamoxifen) and a pro-apoptotic compound (actinomycin D). Confocal micrographic evidence of these effects on the cells is shown in figure 3.11.3, 3.11.4 and 3.11.5 respectively, all of which present with compromised cell density. Figure 3.11.3.a and the higher resolution 3.11.3.b demonstrate cells in metaphase block and a disorganised tubulin structure after 2-ME exposure. Tamoxifen also disrupts the cytoskeletal network (figure 3.11.4a and b) and additionally causes 'dark rounded spaces' between the green stained tubulin. When compared to the transmission electron microscope images of cells undergoing autophagy (figure 3.4.3), it was postulated that these 'spaces' may be the autophagosomes or acidic vacuoles, because they have a similar intracellular distribution pattern. 'Frayed' microtubule networks within the apoptotic control cells are evident in figure 3.11.5a and 3.11.5b, demonstrating that the tubulin structure is compromised as the cells progress through this type of cell death. Additional hallmarks of apoptosis, such as hypercondensation of the chromatin, margination of DNA, round shrunken cellular morphology and the formation of apoptotic bodies are clearly evident in these representative slides.

Figure 4.6 depicts the effect that C19 exposure has on the HeLa cell microskeleton. Total disintegration of the tubulin network is visible in figure 3.11.6a, 3.11.6b and 3.11.6c. Additional evidence of apoptosis may also be identified, and include margination of DNA, a dramatic decrease in cell density and apoptotic body formation.

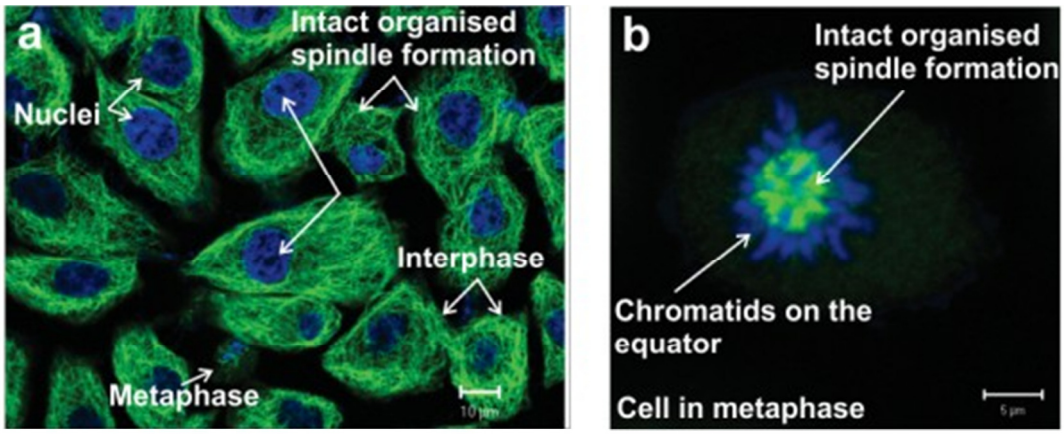

Figure 3.11.1: Confocal microscopic immunofluorescent images of the microtubule structure of HeLa cells propagated in medium only as a negative control. Alexa-488 fluorescent labelled tubulin-α antibodies fluoresce green allowing visualisation of the tubulin network, while counter staining with DAPI results in blue stained nuclear material. Image (a) demonstrates no compromise in cell density, various stages of cell division and intact organised tubulin networks. Figure (b), taken at a higher magnification, allows detailed examination of a cell undergoing metaphase, with the chromatids arranged on the equator and a distinctly organised tubulin network.

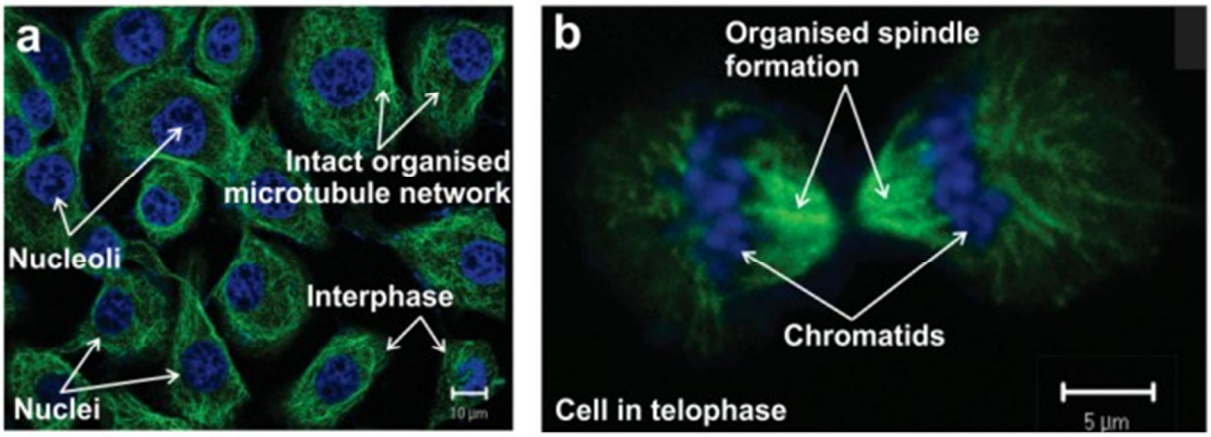

Figure 3.11.2: Confocal microscopy of HeLa cells exposed to DMSO, employing alexa-488 fluorescent labelled tubulin-α antibodies resulting in green fluoresce of the tubulin network, and blue nuclear counter staining with DAPI. Image (a) showed no difference when compared to the cells propagated in medium only (3.10.1). Higher magnification (b) showed a cell in telophase demonstrating intact microskeletal structure of the dividing cell.

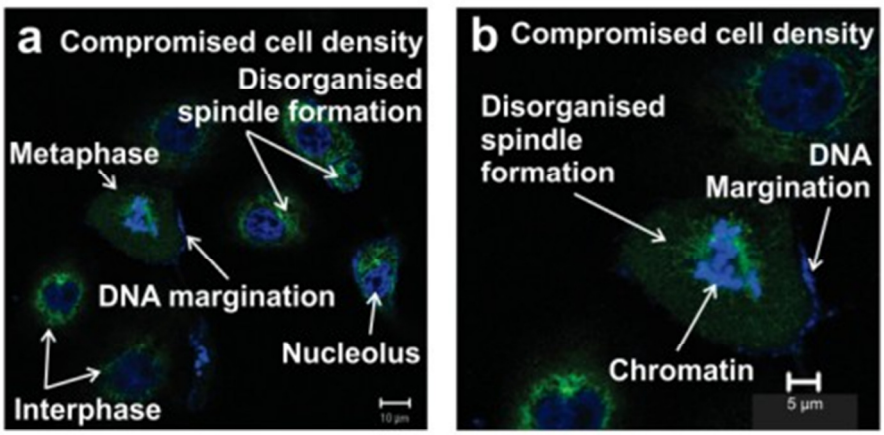

Figure 3.11.3: Confocal microscopy of HeLa cells exposed to 2-ME as an agent inducing metaphase block using an alexa-488 fluorescent labeled tubulin-α antibody resulted in green fluoresce of the tubulin network, and blue nuclear counterstaining with DAPI. Figure (a) and (b) demonstrated a compromised cell density and cells in metaphase block with disorganised tubulin structures after the treatment with 2-ME.

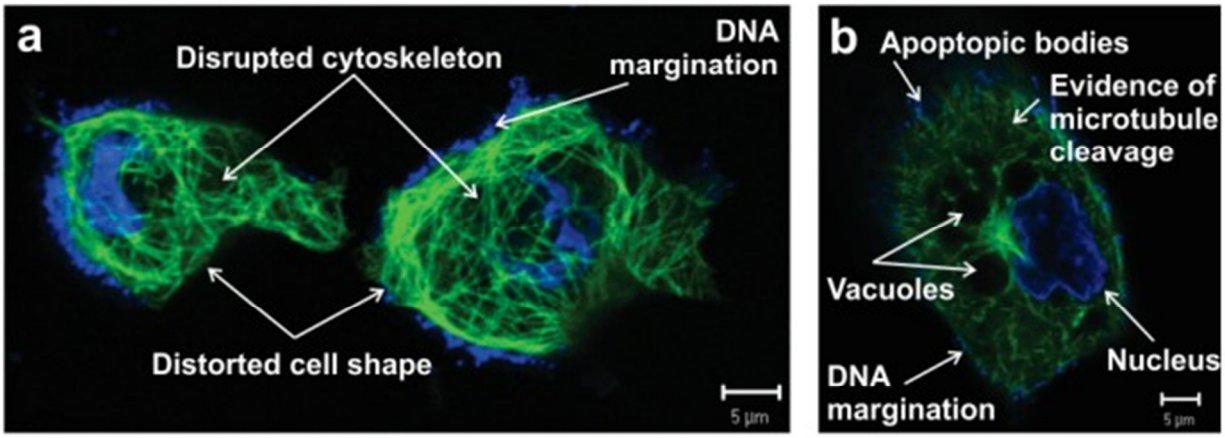

Figure 3.11.4: Confocal microscopic images of HeLa cells treated with tamoxifen with the tubulin network fluorescing green due to binding of alexa-488 fluorescent labelled tubulin-α antibodies and blue nuclear material due to DAPI counterstaining. Tamoxifen-treated cells present evidence of decreased cell density, as well as microtubule cleavage, DNA margination and large vacuole formation (expressed in apoptosis) as seen in (a) and (b).

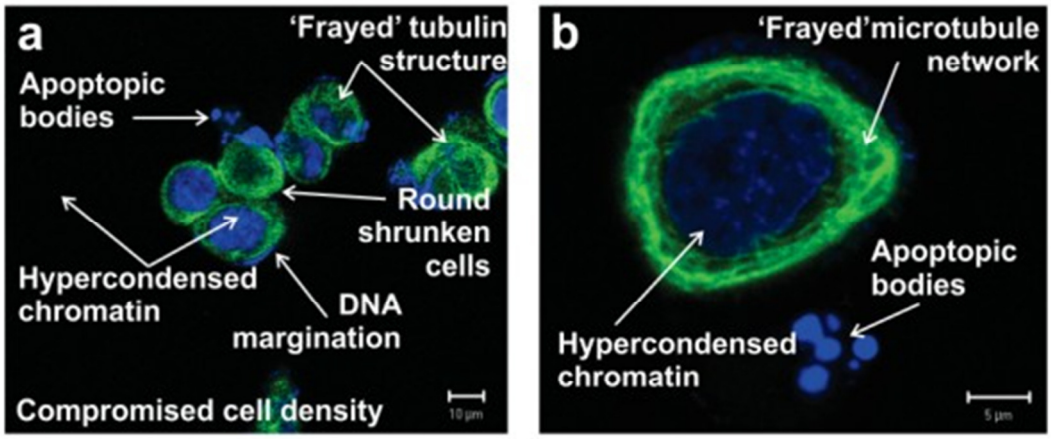

Figure 3.11.5: Confocal immunofluorescent images of HeLa cells treated with actinomycine D, using alexa-488 fluorescent labelled tubulin-α antibodies resulting in green fluoresce of the microtubule network. DAPI was used to stain the nuclear material blue. Figures (a) and the higher magnification (b) demonstrate the hallmarks of apoptosis namely a compromised cell density, round shrunken cells, hypercondensed chromatin, apoptotic body formation, margination of DNA and 'frayed' microtubule structure.

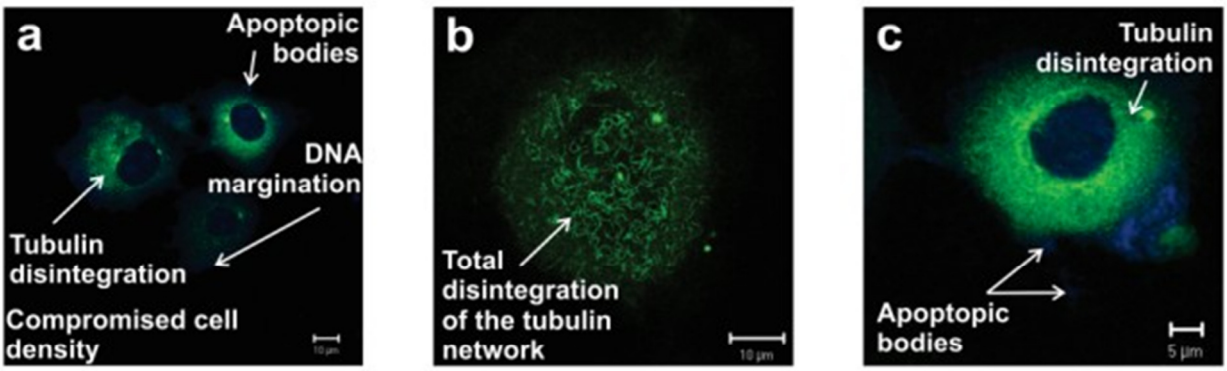

Figure 3.11.6: Confocal microscopic images, in which the effect of C19 on the microtubule structure of HeLa cells was seen. The C19-treated cells in (a), (b) and (c) revealed the effect of the compound on the microskeletal structure with complete tubulin disintegration, along with apoptotic body formation and compromise in cell density.

4. Discussion

For over 3 decades, spindle poisons have been a mainstay in cancer treatment. (130) Their mode of action relies on disrupting tubulin dynamics, either by stabilizing the microtubules as the taxanes do, preventing polymerization or causing depolymerisation of the microtubules as the vinca alkaloids do. (87, 124) Either way, the resultant loss of the dynamic nature of the spindles prevents the cell passing the spindle assembly checkpoint (SAC), charged with assuring accurate segregation of chromatids, causing the cells to arrest at the G_2/M interphase. (87) One unattached kinetochore (to a spindle) can generate a signal to block the cell cycle progression. (36) Should the cell remain in metaphase block too long, they may either escape from this state into a faulty second cell cycle, or be killed via apoptosis. (36) Two major issues with the spindle poisons have prompted scientists to press on in finding alternatives to this treatment modality, namely the unfortunate development of cellular resistance to these drugs before tumour eradication is complete (attributed to P-glycoprotein drug efflux pumps or tubulin mutation), and the unacceptable side effect profile, including neurotoxicity and myelosuppression. (131)

2-ME has shown promise as a spindle poison, binding to the colchicine binding sites of the tubules and in so doing, abrogating their function resulting in a G_2/M block. (134, 224) 2-ME is a natural metabolite produced from 17-β estradiol by sequential hepatic hydroxylation and methylation, and has demonstrated substantial anti-tumourigenic properties *in vitro* and *in vivo* (although lower anti-tumour activity is exhibited in the latter). (224, 266) What makes this drug particularly appealing is the low side effect profile that it carries (no neurotoxicity nor myelosuppresive effects), as well as the relative sparing of non-neoplastic tissue. (283) Additionally, there has been no demonstration of tumour cell resistance occurring after prolonged exposure. (283) Furthermore, this drug does not only induce tumour cell apoptosis, but also has an anti-angiogenesis action, which has the potential to work synergistically with cancer cell toxicity by decreasing new blood vessel supply to the advancing tumour cells. The lack of gaseous exchange and nutrient provision

then cause a relatively toxic environment for the cells, including hypoxia, nutrient deprivation and build-up of metabolic waste products.

Normally, hypoxia and other stress conditions would cause the up-regulation of HIF-1α, which is responsible for the transcription and translation of numerous cellular proteins in order to adapt to and survive the hostile conditions. (238) Additionally, HIF-1α is associated with increased activity of extracellular matrix metalloproteinases which enables local tumour invasion and increased metastatic spread. (239) By inhibiting microtubule dynamics, 2-ME down regulates HIF-1α at the post-transcriptional level inhibiting the cascades which allow for cellular adaptation and preventing HIF-1α transcription of VEGF. (236) This then explains the indirect anti-angiogenic effect of 2-ME, also resulting in the cells being more susceptible to the stress signals and permitting a more rapid onset of apoptosis. 2-ME is also directly toxic to the newly proliferating endothelial cells, inducing apoptosis. Recent evidence also shows the process of autophagy as a possible second mechanism of cell death in MCF-7 breast cancer cells. (82)

2-ME holds much potential as an anti-cancer agent in its pharmacodynamic profile and mechanisms of action, and is currently in phase I and phase II clinical trials by Entremed registered as Panzem®. (224, 226, 283, 335) However, 2-ME has a fundamental drawback in its pharmacokinetic behaviour. Poor oral bioavailability and rapid metabolism resulting in a short half-life affords this drug a poor tissue availability and inability to provide sustained concentrations of the drug at cellular level *in vivo*. (241, 282)

In order to circumnavigate the shortfall in its pharmacokinetic profile, and to expound the positive anti-cancer effect of 2-ME, analogues of this drug have been synthesized. Substitutions at the 2 position increased the potency of 2-ME cytotoxicity, where as alteration of the 3 and 17 positions made the molecule less available for 17β-hydroxysteroid dehydrogenase (HSD)-mediated metabolism and thereby extending its half-life. (242, 244, 290) Additionally, sulphamoylation of estradiol compounds prevented first-pass metabolism by the liver, facilitated by its binding to CAII in erythrocytes. (292) This has lead to an new generation of 2-ME-like compounds, which have demonstrated both a greater toxicity and better bioavailability than the parent drug.

One of the analogues, 2-methoxyestradiol-3,17-O,O-bissulfamate (2-MEbisMATE, also known as STX140) was proven to be a potent inhibitor of cell proliferation in many different tumour cell types in a dose-dependent manner. (336) 2-MEbisMATE was found to bind in a 2-ME-likewise manner to the colchicine binding site of tubulin filaments, causing metaphase block and apoptosis induction. (298) In addition, this analogue crystallized together with CAII, indicating an increased binding affinity to this enzyme. (298) As with 2-ME, the analogue demonstrated an anti-angiogenic action. Potent inhibition of human umbilical vein endothelial cells (HUVEC) was demonstrated by Newman *et al*, with an IC_{50} of 0.05 µM over 4 days, signifying a 60-fold increase over 2-ME. (302) The same paper reported an IC_{50} of 0.25 µM in the inhibition of MCF-1 breast cancer cells over 4 days, with significant correlation in the compound's ability to inhibit HUVEC and MCF-1 cells. (302) *In vivo* studies have substantiated the anti-cancer properties of 2-MEbisMATE. Nude mice bearing MCF-7 derived tumours were assessed for 2-MEbisMATE efficacy on tumour growth. (337) Oral administration of the compound (50 mg/kg) reduced angiogenesis to below the control levels after 7 days, and 5 mg/kg *per os* caused a 52% reduction in tumour growth after 21 days. (337)

With the idea of combining the positive anti-cancer effects of 2-ME, together with the advantages gained by strategic modification as seen in the analogues, a novel 2-ME compound was designed with an added advantage of possible superior tumour-specific localization *in vivo*. The 2 position of C19 had been ethylated, conferring increased cytotoxic potency, together with a 3 position sulphamoylation and dehydration at position 16, allowing an increased gastrointestinal tract (GIT) absorption and decreased 17 HSD metabolism. (133) Additionally, *in silico* modeling has demonstrated a preferential CAIX binding of the complex, the former being selectively over-expressed in the tumour microenvironment creating an acidic milieu. (133) Thus C19 would possible be more selectively delivered to the tumour, decreasing side effects in other proliferating cells. The exact cellular mechanisms of this novel compound, as well as proving the maintenance or any enhancement of the anti-angiogenic and anti-tumour properties of 2-ME still need full elucidation, as does *in vivo* evidence of preferential tumour localization of the drug.

2-ME is known to cause spindle fibre abrogation by binding to the colchicine sites, thereby causing the cell to arrest in G_2/M due to dissatisfaction of the SAC. (224) Confocal microscopy has been used to visualize the effects of 2-ME on the kinetics of spindle polymerization, by incubating the treated cells with anti-tubulin antibodies which are labelled with a fluorescent dye. Perturbations of spindle formation were observed via this method in oocytes after 5-7.5 µM 2-ME exposure for 20 hours. (338) Microtubule structure disruptions were also observed in HK-1 nasopharangeal carcinoma cells incubated in 20 µM 2-ME for 48 hours and stained with anti-tubulin β labelled antibodies, and also exhibited endoreduplication of the cells after metaphase arrest. (339) This process was linked to MAPK signaling pathway upregulation. The technique was also employed to visualize endothelial cells exposed to the traditional spindle poison Paclitaxel, which at low concentrations (between 0.1 – 100 pM) had an anti-angiogenic effect without tubule disruption, and associated metaphase block induced at higher concentrations (1 – 10 nM). (340) Stander *et al* visualized the interference of C19 with spindle formation in MDA-MB-231 cells via confocal microscopy of cells stained with labelled anti-tubulin α antibodies, indicating that the novel synthesised compound did retain the colchicine binding activity and spindle disruption abilities of the parent compound 2-ME *in vitro*. (133)

The confocal images obtained in this study in which HeLa cells were exposed to 0.5 µM C19 for 24 hours and stained with anti-tubulin α antibodies confirmed the previous report of microtubule abrogation in MDA-MB-231 cells. Visualized in the HeLa cells was disintegration of tubulin structure, in a more pronounced manner than in the 2-ME control cells. These results confirmed the high potency of C19 as a spindle poison, this action resulting in the G_2/M block as can be seen in the rounded shrunken cell morphology.

After synthesis of C19, Stander *et al* screened the compound for antiproliferative activity via the DNA crystal violet staining technique, and demonstrated a dose-dependent reduction in proliferation of MCF-7 (oestrogen receptor positive breast cancer cells), metastatic MDA-MB-231 breast cancer cells, non-tumourigenic MCF-12A breast cells, non-keratinizing squamous epithelial SNO cells and HeLA cervical adenocarcinoma cells. (133) When compared to the concentration range with which the parent compound inhibits cell proliferation (between 1-2 µM 2-ME) in HeLa, SNO, MCF-7 and MCF-12A cells *in vitro*, C19

was shown to be more potent by needing nanomolar IC_{50} (also known as GI_{50}) concentrations to inhibit 50% of cellular proliferation. (133) Dose-dependent studies over a 24 hour time period conducted by Mqoco *et al* revealed an IC_{50} of 0.5 µM on HeLa cervical adenocarcinoma cells using crystal violet staining. (288)

To assess morphological changes that 0.5 µM C19 caused during a 24 hour exposure to HeLa cells, microscopic analysis was conducted. Demonstrated in the PlasDIC images of the C19-exposed HeLa cells was a marked decrease in cell density, with the remaining cells being mostly shrunken and rounded. Cellular debris was evident, as well as the presence of apoptotic bodies. This overview gave the impression of apoptotic cellular demise, the images being similar to the actinomycin D apoptotic control plate. Although an increased peri-nuclear vesicular presence was visualized in the tamoxifen autophagy control, this was not clearly seen in the PlasDIC images of the C19 micrographs.

Similar results have been obtained utilising the PlasDIC technique in which MCF-7 cells were exposed to 1 µM 2-ME for 24 hours. (255) A decrease in cell density, as well as rounded cells suggestive of metaphase block were visualized, which, together with evidence of apoptotic bodies, allowed the deduction of 2-ME provoked mitotic block with subsequent apoptotic cell death. Demonstration of apoptotic hallmarks and metaphase block via light microscopy implementing the haematoxylin and eosin (H & E) cell staining techniques corroborated these findings in 2-ME exposed MCF-7 cells. (341) These findings appear to be more evident in cancerous cell lines, with a higher concentration of 2-ME required to inhibit less growth in the non-tumourigenic MCF-12A cell line. (341) Kumar *et al* reported 2-ME induced growth inhibition in medulloblastoma and astrocytoma/glioblastoma cell lines, which was accompanied by the induction of apoptosis which was demonstratable via morphological changes and DNA fragmentation analysis. (252)

Treatment of MCF-7 cells with 0.4 µM 2-MEbisMATE for 24 hours (determined by time- and dose-dependent proliferation studies) demonstrated a clear decrease in cell population density, altered cell morphology and cell debris littering on differential interference contrast microscopy. (300) In a different study, PlasDIC staining after a 48 hour exposure of MCF-7 cells to 0.4 µM 2-MEbisMATE displayed a similar picture, with rounded shrunken cells, a

decrease in cell density as compared with the negative control, and the formation of apoptotic bodies. (304) H & E staining of the same cells revealed hypercondensed chromatin, apoptotic bodies and a compromise in cell density. (304) Light microscopic evaluation of prostate cancer cell lines (LNCaP (androgen responsive) and PC3 (androgen-independent)) as well as the ovarian carcinoma cell line A2780 and its adriamycin and cisplatin resistant derivatives, revealed cells with the characteristics of undergoing apoptosis after 48 hour exposure to 2-MEbisMATE, in a more pronounced picture than the parent compound 2-ME. (342)

In order to attain slightly more information about the morphological changes seen in the PlasDIC images, a triple staining fluoresence microscopic technique was employed. Hoechst 33342, visualized through Zeiss filter 2, stained the nuclei blue which allowed the detection of hypercondensed chromatin in a representative amount of the C19-exposed cells, as well as identification of apoptotic bodies. A striking decrease in cell density was once again confirmed, with morphologically round and shrunken cells being predominant. These images, together with the PlasDIC micrographs, indicated the presence of a metaphase block, with subsequent induction of apoptosis. Necrosis was ruled out by propidium iodide staining, which had cellular membrane integrity been lost would have stained the DNA bright red viewed through a Zeiss number 15 filter. Additionally in the C19-treated cells, there was intense acridine orange staining under the Zeiss 9 filter when compared to the negative control samples. This correlated well with the tamoxifen autophagy control micrographs and gave an indication of a potential second form of cell death, namely autophagy. The thought process generated by these microscope images was that of concurrence of two forms of cell death, apoptosis and autophagy, induced due to a spindle poison resulting in metaphase block. This lead to speculation over the molecular crosstalk which must exist within the cells to regulate their fate and to decide between either one, or both, of the types of cell death.

Both light microscopy techniques carried out in this protocol, demonstrated the effect of 0.5 µM C19 on the HeLa cells being far more devastating than the 1 µM 2-ME on the same cells incubated for an equivalent time period. This could be ascribed to a greater potency of the

analogue, or a greater susceptibility of HeLa cells to C19. Either conclusion would need confirmation in follow-up studies.

After exposure of HeLa cells to 5 µM 2-ME for 20 hours, an increased number of cells were demonstrated in metaphase, along with many cells containing hypercondensed chromatin in fluoresce microscopy studies. (265) Reports were published by Stander *et al* on MCF-7 cells exposed to 1 µM 2-ME for 24 hours, in which the Heochst 33342 stain assisted visualization of cells in normal metaphase block or in tripolar metaphase, together with normally cycling cells. (82) Acridine orange staining was shown to be increased in the 2-ME treated cells, when compared to the negative and actinomycin D apoptosis controls, indicating the presence of an autophagic process. (82) The 2-ME analogue, 2-MEbisMATE also displayed a reduction in cell density, a metaphase block and intense acridine orange staining using this triple staining fluorescent microscopic protocol after a 24 hour exposure to MCF-7 cells in two separate and independent studies. (300, 304) The authors speculated the up-regulation of autophagy together with apoptosis after a metaphase block due to spindle abrogation which correlates well with the findings in this study.

The use of acidotropic dyes such as acridine orange is a frequently employed technique to assess autophagic processes with *in vitro* fluorescent microscopic analysis. (222) Results should be interpreted with care as these dyes are not specific for early autophagic vacuoles, but rather represent a later stage in the degradation process, once the lysosome has fused with the vesicle to form the autolysosome. (222) Acridine orange is not in itself sufficient to prove autophagic functions, as lysosmes may be stained positively by the dye as well. Confirmatory methods must be employed to substantiate the data. (222)

Since light microscopic analysis revealed characteristics of a metaphase block, apoptosis and autophagy, transmission electron microscopy was employed to observe the intracellular infrastructure response to C19. Previous electron microscopic analysis of MCF-7 cells after incubation for 24 hours with 1 µM 2-ME demonstrated an increase formation of vacuoles, tying in with the increased acridine orange staining with fluorescent microscopy. (82) A more dramatic effect was seen in MCF-7 cells incubated in 0.4 µM 2-MEbisMATE, where TEM images displayed fragmentation and condensation of the nuclei, apoptotic body

formation and an increase in autophagosomes or vesicles. (285) Similar findings reported, a 24 hour (300) and 48 hour (304) exposure of MCF-7 to the same concentration of 2-MEbisMATE, including apoptotic body and vacuolar formation together with chromatin hypercondensation, this again led to the observation of both autophagic and apoptotic processes occurring simultaneously in the distressed cells. TEM is a valid and important technique in assessing the overall autophagy status of cells, and for visualization of autophagic structures such as the phagophore, autophagosomes, amphisome and autolysosome. (222) As autophagy is a dynamic process, TEM images cannot specify where in the process the vacuoles may be: i.e. if they have been completely formed, contain only the organelles for breakdown, if they have fused already with the lysosomes or if the contents are at an advance stage of degradation. (222)

After a 24 hour exposure of HeLa cells to the novel 2-ME analogue C19, transmission electron micrographs exhibited a dramatic display of both autophagy and apoptosis concurrently in severely distressed and morphologically deformed cells. Negative controls of HeLa cells grown in medium only and with vehicle only exposure provided the baseline images of healthy cellular morphology: smooth intact cell membranes with a normal amount of protrusions, no obvious vacuoles visible, normal sized organelles and a traceable nuclear membrane. Tamoxifen, used as an autophagy control, demonstrated a significant increase in autophagosomes/autophagolysosomes, with hallmark membrane whorls identifiable within the structures representing the degrading organelles. (307-309) The actinomycin D-exposed HeLa cells (as an apoptotic control) demonstrated the findings expected in that process: hypercondensed chromatin, fragmentation of the nuclear membrane, abnormal cellular protrusions and apoptotic bodies. (306) On examining the micrographs of the HeLa cell exposed to C19, characteristics of both the positive controls could be identified within the cell. Hallmarks of both autophagy, as well as apoptosis were clearly noticeable. (135, 142, 143, 222) This, along with a dramatic decrease in cell numbers, gave a distinct impression of the toxicity of compound 19 on the cells.

It is well published that exposure of cells to spindle poisons induces metaphase block. (87) Studies have shown that apoptosis can be induced during a mitotic block induced by the traditional spindle poisons, with the extent of cellular death being directly proportional to

the length of the block. (131) 2-ME and its synthesised analogues have been proven to induce metaphase block by binding to the colchicine sites on the microtubules and may therefore be classified as spindle poisons. (82, 224, 310, 335) The cells may subsequently die via apoptosis. Bhati *et al* exposed MDA-MB-435 breast cancer cells to 2 µM 2-ME before conducting RNA genomic profiling, and were able to demonstrate enrichment in genes involved in spindle assembly checkpoints and apoptosis. (310) The authors demonstrated a resultant anaphase-promoting complex (APC) inhibition by the SAC, by showing an increase in securin and cyclin B1 (targets of the APC/C). These experiments were done in parallel in a MDA-MB-435 cell line with two β-tubulin mutations, in which 2-ME treatment did not induce APC/C inhibition. (310) Collectively, the data was interoperated as proving that 2-ME induces cell cycle arrest with a tubulin dependent mechanism thereby regulating the genes involved in SAC which cause inhibition of the APC, and the consequent induction of apoptosis.

The induction of mitotic block followed by apoptosis (and autophagy) was confirmed by Stander *et al* in MCF-7 cells exposed to 1 µM 2-ME for 24 hours. (82) Cell cycle histograms displayed a significant increase in the percentage of cells in G_2/M, which simultaneously showed an increase in cyclin B1 expression when compared to the negative controls. (82) There was also a decreased number of 2-ME treated cells in the S phase. (82) Additionally, an increase in cells in the sub-G_1 fraction was demonstrated, indicating that the 2-ME exposed cells enter apoptosis instead of completing mitosis. Corroboration of this data was attained via gene expression microarrays, which showed differential expression of genes mapped to a variety of processes involved in managing the cell in metaphase block and subsequent death induction (including genes involved in microtubule dynamics, cell cycle checkpoints, cyclin B1 degradation, autophagy and apoptotic regulation). (82)

2-ME analogues such as 2-MEbisMATE have not demonstrated deviations from the results obtained when mechanisms in which the parent compound induced metaphase block and subsequent cell death were analysed. Calculation of mitotic indices indicated a disproportional amount of cells in metaphase block and apoptosis, with almost no cells progressing to stages beyond mitosis after 0.4 µM 2-MEbisMATE exposure of MCF-7 cells for 24 hours. (300) These results were substantiated with flow cytometric analysis of the cell

cycle, which demonstrated an increased number of cells in G_2/M block and sub-G_1 fractions. (300) Induction of a G_2/M block was demonstrated via flow cytometry within the first 24 hours of 1 µM 2-MEbisMATE exposure of prostate and ovarian cancer cell lines (including adriomycin and cisplatin resistant variants of the ovarian A2780 line). (342) This metaphase block was demonstrated along with an increasing sub-G_1 apoptotic population as exposure time progressed. (342) Visagie and Joubert published data after 48 hours exposure of MCF-7 cells to 0.4 µM 2-MEbisMATE, analysing the cell cycle progression with the aid of flow cytometry (suing propidium iodide to stain the nuclei), in which sub-G_1 apoptotic cells were significantly increased, but no G_2/M block was demonstrated. (285) This then representing the effect of 2-MEbisMATE on cells further down the time-line. These two reports on the effects of 2-MEbis MATE correlate with studies done by Day *et al*, in which a 24 hour exposure of the compound to 2-MEbisMATE resistant cells derived from a human ovarian carcinoma cell line (A2780.140) resulted in G_2/M arrest, whereas a further 24 hour incubation shifted the distribution to a predominantly sub-G_1 peak with no mitotic block identifiable. (343) CAL51 breast adenocarcinoma cells were proven to undergo caspase mediated apoptosis on 2-MEbisMATE exposure. (303)

On this background of evidence suggesting a metaphase block and consequent apoptotic death in a variety of cell lines exposed to 2-ME and its analogue 2-MEbisMATE, cell cycle progression analysis by flow cytometry of C19-exposed HeLa cells did not hold surprises. A clear decrease in the S population was demonstrated, with a concurrent increase of the cells in G_2/M (51.28%) indicating a metaphase block when comparing the treated cells to the medium only exposed cells. Actinomycin D caused a similar distribution, but effects were more pronounced in the C19-treated cells, with 4.93% of the cells being in apoptosis in the actinomycin D control and 27.93% in the C19-treated cells. Data correlated well with the observations of a metaphase block and apoptosis induction of the C19-exposed HeLa cells made from the earlier mentioned microscopic morphological studies. Additionally, the results confirmed prior data from our laboratory that (200 nM) C19-exposed MDA-MB-231 cells showed a G_2/M block after 24 hours, as well as an increase in the sub-G_1 fraction, whereas after 48 hours nearly all the cells were seen to be in the sub-G_1 fraction. (133)

Under normal circumstances, the SAC is only active very briefly as it halts the cell cycle progression while it assures that all kinetochores are correctly attached to spindles. (36) The driving force behind the cell entering mitosis is Cdk-1 activation by cyclin B, the degradation of which signals the dissolution of cohesion between the sister chromatids and the progression into anaphase. (55) This transition is policed by the anaphase promoting complex or cyclosome (APC/C) which ubiquitinates cyclin B and securin causing Cdk1 inhibition, allowing activation of separase which consequently cleaves cohesion to release the sister chromatids for polar segregation. (53, 55, 86) Should the checkpoint not be satisfied, the SAC actively inhibits the APC/C, thereby increasing cyclin B levels and protecting Cdk1 and cohesin activity, the process resulting in a metaphase block. (33)

Exposure of cells to spindle poisons induces metaphase block. (87) In this situation, due to spindles not attaching to all the kinetochores, the SAC proteins Mad2 and BubR1 (assisted by Bub1) bind to the APC/C-Cdc20, preventing its ubiquitinase action. (86, 115) Once all the kinetochores have attached to spindle correctly, the SAC deactivates, Cdc20 is free to activate the cyclosome which degrades the Cyclin B rapidly and promotes anaphase onset. (33, 116) To be noted, despite an active SAC, should the cell remain in a mitotic block too long, the cyclin B will start to degrade slowly, allowing the cell to 'slip' out of the control and to exit mitosis. (33, 87, 120)

There are numerous inconsistencies and question marks hanging over the exact cellular pathways induced in cells in response to the traditional spindle poisons. Observations were made that incubation in spindle poisons induced a metaphase block, but the exact pathway the cells then followed to determine their fate remained unclear. (87, 117) Initially, the explanation seemed simple, namely that these cell died via apoptosis following the prolonged mitotic block. However this failed to explain numerous observations: many substances are able to cause a mitotic block, but are not useful as treatment modalities as they are unable to induce this block for a sufficient amount of time to induce apoptosis; some cancers are highly sensitive to paclitaxel, whereas others are almost completely unresponsive to the compound; and lastly, there is a large variation within cells of a monoclonal population as to what percentage of cells die via apoptosis after exposure to anti-mitotic agents, representing a heterogeneous response. (87, 119)

Newman *et al* conducted a set of experiments to demonstrate direct efficacy of 2-ME, 2-MEbisMATE, and taxol (a traditional spindle poison) at the same dose (500 nM) on MCF-7_{WT} and MCF-7_{DOX} (doxorubicin resistant) cell lines. (344) Both 2-MEbisMATE and taxol caused a significant G_2/M block at 48 hours (45% and 72% respectively) and had corresponding rates of apoptosis induction (2-fold and 3-fold compared to control respectively) after 72 hours in the wild type cells, whereas 2-ME caused no significant metaphase block in the cell line, with only a small increase (1.7-fold versus control) in apoptosis noted. (344) Although both 2-MEbisMATE and taxol induced a metaphase arrest in the MCF-7_{DOX} resistant cells (68% and 23% respectively), there was no corresponding increase in apoptosis in the taxol-treated cells. (344) Only 2-MEbisMATE increased apoptosis in the resistant MCF-7_{DOX} cell line after 72 hours, demonstrating the ability of the cells to 'slip' out of the G_2/M block induced by traditional spindle poison treatment. 2-ME caused a small percentage of the cells to stop cycling at metaphase, alluding to its weaker activity. (344)

Only 37% of HeLa cells died after treatment with a microtubule depolymerising agent (nocodazle), with the surviving cells being either in the following interphase cycle or undergoing rapid duplication of their genome via endocycling. (119) HeLa cells were proposed to have various possible routs of death, with only 6% demonstrating apoptosis due to prolonged metaphase. (119) As opposed to this 73% of HeLa cells treated with a different spindle poison, namely paclitaxel, died after exiting the mitotic arrest in the subsequent interphase. (119) By blocking the function of caspases, death during mitotic arrest was completely inhibited, leading to the hypothesis that apoptotic induction and mitotic exit are controlled through two separate pathways. (87, 119)

Flow cytometric cell cycle studies have confirmed the induction of a metaphase block by 2-ME and its analogues 2-MEbisMATE and C19, with a subsequent increase in the sub-G_1 peak representing cells in apoptosis. These studies required confirmation, as they are only indicative of early apoptotic induction, and more information regarding cell fate needed to be established. The existing results were substantiated by flow cytometric analysis based on the principal of loss of cell membrane asymmetry occurring with the translocation of phosphatidylserine to the outside of the cell during apoptosis induction (PS-flip). This event occurs already early in apoptosis, before morphological changes become apparent, and may

be detected using a FITC-labelled phospholipid binding protein, annexin V. Analysis of the C19-exposed HeLa cells demonstrated a decrease in cell viability to 64.22%, with a concomitant increase if the number of cells in apoptosis (27.32% of the population). These differences were statistically significant when compared to the negative control samples, and confirm the cell cycle results on apoptosis induction (27.93% of cells) seen with the sub-G_1 spike.

Flow cytometry was similarly employed to demonstrate apoptosis induction (36% of the cells) with a 24 hour exposure of MCF-7 cells to 0.4 µM 2-MEbisMATE. (304). In a panel consisting of MCF_{DOX} cells exposed to 500 nM 2-ME, 2-MEbisMATE and taxol, only the 2-ME analogue demonstrated an increase in apoptotic cells after 72 hours using this method. (344) 1 µM 2-ME treated MCF-7 cells (24 hours) also reported an increase in apoptosis (about 15% of the cells) utilizing this protocol when compared to the vehicle treated cells. (82) Foster *et al* used this PS filp technique to analyse the induction of apoptosis in A2780 ovarian cancer (280 nM), LNCaP prostate carcinoma (260 nM) and MCF-7 breast cancer (250 nM) cells. (336) Exposure of these cell lines to 1 µM 2-MEbisMATE induced apoptosis in all the cells at different times of exposure: maximal apoptosis was induced in A2780 cells after 48 hours, in LNCaP after 72 hours and MCF-7 cells after 168 hours. (336)

Studies have shown that apoptosis (usually via the intrinsic pathway) can be induced during a mitotic block induced by the traditional spindle poisons, with the extent of cellular death being directly proportional to the length of the block. (118, 131) MCL1 is one of the pro-survival members of the BCL2 family of proteins, binding to BAX and BAK to inhibit their pore forming action on the mitochondrial membrane. (160, 161, 345) MCL1 expression seems to peak during critical checkpoint periods, including when the dissatisfaction of the SAC causes metaphase arrest. (345, 346) It has been proposed that this increased expression of MCL1 allows the cell time to repair, staving off the induction of apoptosis in response to the damage. (347) The expression of this protein is tightly regulated, with FBW7 (the substrate binding subunit of an ubiquitin ligase complex) targeting MCL1 degradation by the 26S proteasome (deubiquitinase Usp9X) . (345, 347) Should the cell remain in metaphase block, JNK (Jun N-terminal kinase), p38 and casein kinase II (CKII) are activated, causing phosphorylation of MCL1, promoting its interaction with F-box and WD

repeat domain containing 7 (FBW7, a tumour suppressor), resulting in the ubiquitination of MCL1 and a gradual decrement in its concentration. (347) If, however, the cell corrects the issues resulting in the block, JNK, p38 and CKII activity cease rapidly, allowing PP2 to dephophorylate MCL1, apprehending its interaction with FBW1 and maintaining high levels of the pro-survival actions of MCL1. (347)

The fate of a cell in unmitigated mitotic arrest seems to depend on the interplay between cyclin B and MCL1 levels. (87) Both MCL1 and cyclin B are at peak concentrations just after spindle poisons have induced the mitotic block: the former to apprehend the onset of apoptosis while cellular restoration is being attempted, and the latter due to the SAC induced arrest of cell cycle progression due to unattached kinetochores. (347) In the process of slippage, cyclin B levels drop slowly despite an active SAC. (120) Concurrently, as the time period of the block lengthens, MCL1 levels fall due to ubiquitination. (347) Should the SAC be satisfied by the correct attachment of kinetochores to spindles, the correct sequence to relieve the block would entail stabilization of MCL1 to stop the apoptotic onset, and the activation of the cyclosome causing a rapid cyclin B degradation to promote the onset of anaphase. (345, 347) In the presence of spindle poisons, this process is disallowed, and the cell either progresses into apoptosis should the MCL1 levels deteriorate faster than the cyclin B levels. (347) MCL1 may also be rapidly cleaved by caspases during apoptosis. (345) Conversely, should cyclin B levels fall below the threshold for mitotic exit, the cell will be allowed to progress into anaphase or slip into the successive interphase. (87, 347) Thus strategies for enhancing spindle poison action may be to prolong the metaphase block by either preventing cyclin B degradation, or stimulating the ubiquitination of MCL1 to induce apoptosis more rapidly. (87)

A rapid up-regulation of cyclin B1 was demonstrated by Newman *et al* in MCF-7_{WT} cells on exposure to 500 nM taxol, 2-ME and 2-MEbisMATE after 24 hours. (344) The increase in cyclin B blocks the progression of the cell through the cycle and apoptosis, until it is degraded, when the cell is able to resume its cycle or undergo apoptosis. After 48 hours, the levels of cyclin B had deteriorated in all of the exposed MCF-7 cells, allowing the cells to undergo apoptosis via p53 induction demonstrated with immunoblotting techniques (2-ME did not induce p53 at that concentration). (344) Additionally, the anti-apoptotic BCL2

protein had been deactivated by phosphorylation in the 2-MEbisMATE and taxol treated MCF-7 cells after 24 hours of exposure. (344) In contrast, only 2-MEbisMATE exposure to MCF-7_{DOX} resistant cells caused a significant increase of cyclin B after 24 hours, and phosphorylation of BCL2 when analysed in a series consisting of 500 nM 2-ME, 2-MEbisMATE and taxol exposure to these cells. (344) BCL2 was weakly phosphorylated in the taxol sample while p53 was constitutively over expressed in all the samples, including the control sample. (344) These results once again demonstrated the advantage of the 2-ME analogues in treatment of traditional spindle poison resistant cells.

In the light of the mitotic block demonstrated in HeLa cells exposed to 0.5 µM C19 for 24 hours by morphological studies and flow cytometric analysis, the levels of cyclin B1 were determined using flow cytometry to quantify a cyclin B1-phycoerythrin conjugated antibody. An overall 2.47-fold increase of cyclin B1 was determined when compared to the vehicle control, with a higher fluorescent signal being emitted from the smaller more complex cells (representing cells in metaphase block) when plotting fluorescence against side and forward scatter. Scatter plots indicated the possibility of either multi-ploidic cells or perhaps presence of HeLa cells in the cell cycle. (330, 332) Cyclin B1 levels were not raised significantly in comparison to the negative controls in the 2-ME treated positive control HeLa cells, although microscopic visualization indicted the presence of a metaphase block. This may have multiple possible causes. The cyclin B levels are tightly regulated in a temporal fashion differing in dose of toxin, cell line type and time of exposure. Kamar *et al* previously published the occurrence of a G_2/M block in medulloblastoma cell lines (DAOY, D341 and D283) and high-grade anaplastic astrocytoma/glioblastoma cell lines (U-87MG and T98G) after exposed to 3 µM 2-ME for 24 hours. (252) This cycle block, as well as the induction of apoptosis occurred without increased cyclin B1 or p34/Cdc2 expression, but did demonstrate decreased 14-3-3 proteins. The apoptotic induction was attributed to NF-kappa B signaling disruption, and does not involve altered expression of p53 and BAX. (252) The non-consensual reports demonstrate different possible mechanisms of 2-ME action on various cell lines.

C19 clearly causes a disrupted spindle assembly, and in doing so, may activate the spindle assembly checkpoint (SAC) resulting in mitotic block and inducing apoptosis. (118)

Increased cyclin B1 levels result, but may also be due to C19 blocking the mitotic escape routes downstream of the checkpoint, which prevents the premature exit of cells from the induced apoptosis pathways, thereby preventing resistance to the compound's effects and increasing its anti-tumorigenic properties. The latter serves to slow down proteolytic breakdown of cyclin B1, allowing an increase opportunity for death initiation. (118) Death initiated in this manner usually is routed via the intrinsic pathway. Further research needs to be executed to determine the feasibility of this hypothesis, by amongst others, determining decreased Cdc20 activity levels as well as establishing the possibility of intrinsic apoptotic pathway activation. The reason for cell survival (64.22% viable cells) after C19 treatment must also be established, as must the fate of these cells.

Van Zyl *et al* demonstrated a G_2/M block in MCF-7 cells (preferentially over non-carcinogenic MCF-12A cells) after exposure to 1 µM 2-ME for 20 hours, and on analysis found a significant increase in Cdc2 kinase activity after microtubule disruption, causing the persistence of the SAC resulting in the cells entering apoptosis. (341) Cdc2 regulates the activity of the APC/C complex via phosphorylation, preventing its association with cadherin 1, thereby averting its degradation of securin and consequent release of separase which in turn would need to cleave cohesion to allow sister chromatid separation. (35) Stander *et al* demonstrated an increase in cyclin B1 levels in 2-ME treated MCF-7 cells in metaphase block, correlating with the previously reported increased Cdc2 kinase activity. (82) They also reported an increase in cytochrome *c* release from the mitochondria for the exposed cells, suggesting a possible intrinsic apoptotic induction. (82) Metaphase block induced by 2-MEbisMATE exposure to MCF-7 cells also revealed an increase in cyclin B1 levels after 24 hours. (300)

It is a well established fact that 2-ME induces apoptosis in cells exposed to the agent. One of the most common mechanisms whereby this process functions is via JNK signaling, induced by an increase of ROS, with resultant phosphorylation and inactivation of the pro-survival BCL2 proteins and cytochrome *c* release from the mitochondria. (248) Evidence of this intrinsic apoptotic pathway may be gathered in literature, as Stander *et al* reported a cytochrome *c* and hydrogen peroxide (H_2O_2) increase in MCF-7 cells exposed to 1 µM 2-ME. (82) Formation of H_2O_2 was reported in Ewing sarcoma cells treated with 2-ME, initiating a

rapid activation of the JNK pathway resulting in a decreased mitochondrial transmembrane potential, release of cytochrome *c* and activation of the caspases. (348) Although there have been previous reports that 2-ME causes an increased superoxide production (4 µM 2-ME in U937 leukaemia cells after 6 hours (349); 2 µM 2-ME treated human myeloid leukaemia HL-60 and U937 cells (350); 0.1 mM in transformed HEK293, U87 and HeLa cells (279)), at lower concentration such as 1 µM 2-ME exposure on MCF-7 cells, this phenomenon was not demonstrated. (82)

Visagie and Joubert published a statistically significant reduction in mitochondrial transmembrane potential in MCF-7 cells exposed to 0.4 µM 2-MEbisMATE, indicating that induction of apoptosis via the intrinsic pathway due to loss of the mitochondrial electrochemical gradient is not the most important mechanism. (285) The authors also reported an increase in H_2O_2 (but not superoxide) in the treated cells, without being able to state the source of these ROS. (285) Literature has proposed an inhibition of superoxide dismutase causing the increased ROS in 2-ME treated leukaemia cells. (349), or alternatively (perhaps simultaneously) an increase in mitochondrial matrix calcium causes ROS production. (351) The causal link between ROS production and the reduction of the mitochondrial transmembrane potential has been established, with the subsequent induction of the intrinsic apoptotic pathway by cytochrome *c* release and caspase activation. (160)

Mqoco *et al* established a reduction in the mitochondrial transmembrane potential in a significant amount of the HeLa cells exposed to 0.5 µM C19 for 24 hours, indicating the induction of apoptosis. In this panel, C19-treated HeLa cells resulted in 68.43% of the cells having affected mitochondrial membranes compared with 22.51% of the 2-MEbisMATE control exposed cells, perhaps hinting at an increased potency of the C19 apoptotic induction. (288)

The intrinsic apoptotic pathway is linked to the deactivation of pro-survival BCL2 proteins and the activation of the pro-apoptotic members. (160) Anti-apoptotic BLC2 members such as BCL2 and BCL-XL are inactivated by pro-apoptotic BH3 proteins such as BIM and PUMA in response to a stress signal such as increased ROS, thereby releasing BAX and BAK to be

activated, causing a decrease in mitochondrial transmembrane potential thereby allowing the release of cytochrome *c*. (160, 161) Previous experiments with 1 µM 2-ME exposure indicated that the ratio of pro-apoptotic BAX to anti-apoptotic BCL2 played an important role in apoptosis observed in HeLa and oesophageal carcinoma cells. (275) A decrease in MCL1 was also observed in the 2-ME treated leukaemia cells. (349) Pro-survival BCL2 inactivation by phosphorylation has been demonstrated in K562 leukaemia cells exposed to 2-ME (352), and in MCF-7 cells exposed to a 2-ME sulphamoylated analogue. (289) Day *et al* proved BCL2 deactivation by phosphorylation caused by microtubule damage in a panel of A2780 cells exposed to taxol, 2-ME and 2-MEbisMATE, indicating a similar mode of drug action between them. (342)

Induction of the intrinsic apoptotic pathway, with the release of cytochrome *c* causes the formation of the active apoptosome, resulting in the activation of caspase 9, which in turn cleaves the downstream executioner caspases 3, 6 and /or 7 which activate PARP to initiate DNA cleavage and other activities involved in the mechanics. (160) Foster *et al* established that an increase in the amount of caspase 3/7 was preceded by mitochondrial collapse in 1 µM 2-MEbisMATE treated LNCaP, A2780 and MCF-7 cells in a time dependent manner. (336) The LNCaP and A2780 cell lines showed a decrease in survivin and XIAP expression after 2-MEbisMATE treatment, but not so in the MCF-7 cells. (336) Despite MCF-7 cells being deficient in caspase 3, apoptosis was still induced after 2-MEbisMATE and STX641 exposure, and a significant increase in caspase 7 was demonstrated after 48 hours. (336) Caspase 7 upregulation correlates well with PS exposure on the outer membrane, both being a part of classical apoptotic activation. (336) The authors could not rule out the possibility of a caspase-independent cell death in the treated MCF-7 cells. In a different study, 2-MEbisMATE caused caspase dependent induction of apoptosis in CAL51 breast cancer cells, and demonstrated an upregulation of caspase 9 and 3 (but not caspase 8 as determined by BID cleavage). (303) These authors also proved that there was no concurrent increased expression of the DR5 TRAIL receptor in these cells.

2-ME has also been implicated in induction of the extrinsic apoptotic pathway. LaVallee *et al* demonstrated an upregulation of tumour necrosis factor superfamily member 10 (TNFSF10/TRAIL) which could partially explain the increase of DR5 expression *in vitro* and *in*

vivo. (247) Additionally, they substantiated this finding by demonstrating a sequential increase of caspases 8, 9 and 3, and blocking DR5 signaling severely attenuated the apoptotic response in HeLa, MDA-MB-231, MDA-MB-435, U-87MG glioma cells and PC3 prostate cells. (247) Thus evidence exists that both intrinsic and extrinsic apoptotic pathways are induced by 2-ME treatment of cells. (335) It may be summarized that 2-ME inhibits the pro-angiogenic HIF-1α transcription factor, induction of JNK signaling and generation of ROS, in a time, dose and cell type dependent manner. (335)

The fact that the mitochondrial membrane potential is affected in HeLa C19-exposed cells gives an indication of the intrinsic apoptotic pathway, a fact which may be substantiated by the demonstration of caspase 6 upregulation. (288) Additionally, caspase 8 was found to be increased, indicating a possible extrinsic apoptotic pathway involvement in the cell death. (288) This study confirmed these findings, as both caspase 8 and 3 were up-regulated after a 24 hour exposure of HeLa cells to 0.5 µM C19. As caspase 3 is an executioner caspase common to both intrinsic and extrinsic pathways, the deduction that it is a caspase-dependent mode of cell death can be made.

The increase in caspase 8 indicates the possibility of an extrinsic pathway concomitantly with the intrinsic pathway alluded to by Mqoco *et al*. (288) The exact signaling pathway involved in the extrinsic pathway induction still needs to be elucidated. As does making certain that another concomitant caspase-independent pathway co-exists in this process. Also to be determined is the possibility of crosstalk between the two pathways in the C19-treated cells, in which the truncated BID is cleaved by caspase 8, which then in turn suppresses BCL2/BCL2-XL inactivation of BAK and BAX. (160, 161) The possible role of calcium^{2+} concentration in the mitochondria and ER, and the subsequent induction of caspase 12 and 9 also needs to be investigated.

Caspase 8 is the most upstream protease in the cell death initiation signal, and thus is classified as one of the initiator caspases. (157) Over expression of FLICE induces cell death by apoptosis. Caspase 3 (also known as CPP32,YAMA, apopain, LICE, and SCA-1) is also a member of the same family of proteases, but occurs downstream in the apoptosis cascade and is classed as an executioner caspase. (158) Thus, by demonstrating the up-regulation

or activation of these caspases in the HeLa cells exposed to C19, an indication of the extrinsic apoptotic cell signaling pathway was gained.

The actinomycin D-exposed HeLa apoptotic control cells did not show a significant increase in caspase 8, indicating the most likely induction of the intrinsic pathway as expected in DNA damaged cells. It has been demonstrated that actinomycin D exposure to lymphocytes induced a PUMA-mediated mitochondrial apoptosis, involving BCL2 destabilization and p53 upregulation. (353) Convergence of the pathways involves activation of the executioner caspase 3, which was seen in both the actinomycin D and C19-exposed HeLa cells.

An increase of H_2O_2 and other ROS in cells has also been linked to the induction of autophagy. (354) This process is regulated by inactivation of mTOR, and Atg4, with activation of Beclin-1. (354) An increase of ROS in U937 leukaemia cells treated with 4 µM 2-ME caused a gradual decrease of mTOR and phospho-mTOR protein levels over a time period. (349) It was shown that an increase of H_2O_2 can induce autophagy in HEK293 transformed cells, U-MG87 and HeLa cancer cells when treated with 2-ME, and if the autophagic process was blocked, the cells underwent cell death. (279) However, inhibition of caspase mediated apoptosis did not lead to the inhibition to autophagy. Stander *et al* demonstrated an increase in acridine orange staining in MCF-7 cells exposed to 1 µM 2-ME for 24 hours, indicating an increase in acidic vesicle/autophagic vesicle formation. (82) They also demonstrated an increase in H_2O_2 in the cells, TEM images of increased vacuole formation and gene analysis showing the down regulation of eukaryote translation initiation factors (EIFs) involved in translation and control of downstream mTOR activity. (82)

As mentioned earlier, 2-MEbisMATE causes an increase of ROS in various exposed cells. MCF-7 cells exposed to 0.4 µM 2-MEbisMATE caused a significant increase in ROS, and demonstrated the induction of autophagic processes along with apoptosis. (285, 304) Analysis of flow cytometric data collected from binding of a conjugated anti-LC3B antibody in the 2-MEbisMATE-exposed cells indicated an increase of autophagy in 20% of the cells when compared to the control. (304) Additionally, TEM images revealed an increase in vacuoles in the treated cells and triple fluorescent staining indicated increased acridine orange staining, corroborating the finding of autophagy up-regulation. (304) Vorster *et al*

also presented the co-occurrence of apoptotic and autophagic processes in 0.4 µM 2-MEbisMATE exposed MCF-7 cells (24 hours), with intense acridine orange staining in fluoresce microscopy and increased autophagic vesicle formation on TEM evaluation. (300)

In this study, evidence of autophagy occurring simultaneously to apoptosis in HeLa cells exposed to 0.5 µM C19 had been collected. Intense acridine orange staining in the triple straining fluorescent microscopy indicated an increase in acid vacuole formation, indicating an autophagic process. Additionally, autophagosomes/autophagolysosomes were clearly pictured via TEM analysis. In order to support these findings, the aggresome activity factor (AAF) was calculated in a flow cytometric assay based on the principle that misfolded proteins are relegated to aggresomes, which are cleared by autophagy. Results demonstrated an increase in the AFF in C19-treated cells, similar to the value obtained in the tamoxifen autophagy control cells, thus confirming that autophagy is also present in the C19-treated cells, along with apoptosis.

It has been proposed that ROS generation is able to induce autophagy via Atg4 oxidation, catalase and the mitochondrial electron transport chain, and may lead to either cell survival or death. (192) There is an indication that caspases and Beclin-1 may mediate the cross talk between apoptosis and autophagy. (217) When Beclin-1, a BH3 family member of BCL2, is bound to BCL2 or BCL-XL its interaction with PI3KC3 along with other proteins which are core to the autophagy-inducing complex is inhibited, thereby preventing autophagy. (137, 180) However, the Beclin-1 and PI3KC3 are direct substrates of caspases (3, 7 and 8), a process which may be observed during induction of both the intrinsic and extrinsic apoptotic pathway. (208) BAX over expression, which induced the intrinsic apoptotic pathway, has been shown to cause caspase cleavage of Beclin-1, as does activation of TRAIL (a death receptor part of the extrinsic signaling pathway). (355, 356)

Once cleaved, the C-terminal acquires a new apoptotic-promoting function, and is localized to the mitochondrial membranes where it amplifies apoptosis, in a manner not yet fully understood. (208) Apart from Beclin-1, Atg5 (which has a role in autophagosomes membrane elongation) and Atg4D (which is responsible for proteolytic maturation of Atg8) are autophagic proteins which are cleaved during apoptosis. (180) Atg5 is cleaved via a

calpain-mediated action, producing a truncated product which interacts with BCL2 proteins at the mitochondria. (357) Contrary to this, Atg4D cleavage by caspase 3 induces autophagy activity, but has a cytotoxic effect which will amplify apoptosis via the intrinsic mitochondrial pathway. (358) Additionally, Flip (Flice inhibitory protein) suppresses both caspase 8 and receptor mediated apoptosis, and can also suppress autophagy. (359) Thus it can be proposed that caspase cleavage of Beclin-1, Atg5 and Atg4D can prevent protective autophagic induction, and the C-fragment of Beclin-1 can sensitise cells to pro-apoptotic signals. (217)

There is controversy in the literature regarding autophagy as a form of cell death. The question remains as to whether autophagy is indeed a form of death, or signs of a distressed cell trying to facilitate the cell's survival up to a point where sacrificing essential organelles no longer is able to compensate. Even though evidence may be accrued as to the coexistence of apoptosis and autophagy in the same cell induced by a spindle poison or stressor, the question does remain as to whether autophagy actually confers a protective effect on the cell against the stressor. Thus experiments would have to be designed to determine whether the cells die more rapidly should the autophagic mechanisms be suppressed. Akar *et al* demonstrated that silencing of BCL2 expression causes an increase in autophagic, but not apoptotic, death. (360) Additionally, Dalby *et al* showed that autophagy and cell death caused by BCL2 silencing was prevented for up to 7 days in a knockdown models of autophagic genes. (174) This, in conjunction with the fact that many tumour cells such as MCF-7 breast cancer cells are caspase 3 deplete, lead the authors to conclude that the presence of autophagy was in the role of a cell death mechanism. (174)

It is however crucial to clarify the functions and mechanisms of the autophagic processes seen in the toxin treated cells. The observation of increased autophagic components may be indicative of either an increased formation, a decreased ability for clearance, or perhaps even both. Accumulation of the vacuoles may interfere with intracellular trafficking, preventing the recycling of essential nutrients, causing 'congestion' and resulting in toxic leakage out of them. (179) Thus autophagy and apoptosis seem to be in a balance, share common molecular components and have an intricate crosstalk mechanism between them. Thus the exact mechanisms of autophagy induction and its precise function must still be

elucidated in HeLa cell exposure to C19. With the inhibition of autophagy and apoptosis, at which rate would the cells die? Would they be more susceptible to the C19 if autophagy was inhibited? Would they still die if only apoptosis was inhibited? These questions remain to be answered in future research.

Publications have shown that Ambra1 an upstream regulator of autophagy, is released from dynein motor complexes when autophagosome nucleation occurs. (210) Thus Ambra1 is bound to the motor complexes under normal conditions, and mutations of the protein enhances autophagosome formation. (210) As 2-ME and its analogues are spindle poisons, the dynein motor functions are also affected in their functions. (125) It remains necessary to explore the causal route between spindle fibre and dynein deregulation, and the increase of autophagy as seen in response to 2-ME and its analogues.

The traditional spindle toxins are diverse on their affectivity in killing cells. (87) Although they all excerpt their toxicity via SAC activation and inducing a metaphase block, some drugs, such as the taxanes and vinca alkaloids are more effective than the tubule depolymerising nocodazole. (87) This could be due to different death inducing mechanisms, or the fact that the latter binds to spindles reversibly and may be washed out of the cells by the time they get to metaphase. (87) Thus, any effective anti-mitotic agent would need to bind irreversibly to the spindles and have a good bioavailability.

In a comparative study between 2-MEbisMATE and traditional therapeutic spindle poisons which are substrates for the P-glycoprotein pump causing tumour cell resistance, taxol and doxorubicin (both at 500 nmol/l) still allowed the cells to divide and reach confluence over 96 hours in resistant MCF-7_{DOX} cells (although the wild type MCF-7 cells were still susceptible). (344) In contrast both the MCF-7_{WT} and MCF-7_{DOX} cells were inhibited to a similar extent by 2-MEbisMATE (STX140). These finding correlated with the calculated resistance factor, which numerically depicts the fold increase in drug-resistance of a cell line when compared to the wild type. The resistance factor in MCF-7_{DOX} cells was very low for 2-MEbisMATE (RF of 1.5), whereas the cells displayed significant resistance to doxorubicin (RF of 150) and taxol (RF of 1000) *in vitro*. (344) Cells treated with 2-MEbisMATE induced cell cycle arrest, an increase in cyclin B1 and subsequent apoptosis in both the cell lines, and

was effective in both tumour type reduction *in vivo*, unlike taxol which was only active on the wild type. (344) Additionally, Day *et al* demonstrated superior tumour inhibition efficacy by 1µM 2-MEbisMATE in cisplatin and adriamycin resistant ovarian cancer cell lines (A2780-derived lines) when compared to taxol and colchicine treatment. (342) Prostate cell lines were more sensitive to the 2-ethoxyestradiol analogues. (342) Wild type cells were equally sensitive to the orthodox spindle poisons and 2-ME analogues. (342) Adriamycin (DOX) resistant derivative line of the ovarian cancer line A2780 (A2780adr) also has an over expression of P-glycoprotein whereas the cysplatin resistant A2780cis has many proposed mechanisms of acquired drug resistance. (342) The latter cell line proved more resistant to all the treatment modalities.

In vivo studies encompassing 20 mg/kg 2-MEbisMATE oral administration of female MF-1 nu/nu mice injected with MCF-7wt and MCF-7.MR lines subcutaneously demonstrated a significant tumour regression of both the wild type and BCRP expressing resistant types. (343) Untreated tumours grew to 400% of their starting value over 35 days, whereas 2-MEbisMATE treated tumours were completely inhibited, demonstrating 78% tumour regression by day 35. (343) These *in vitro* and *in vivo* results indicated that the sulphamoylated 2-ME analogues may overcome the multiple forms of cellular resistance that tumour cells develop toward traditional spindle poisons. Breast cancer resistance protein (BCRP) expressing tumours are notorious for conventional drug resistance and a poorer prognosis, and is prevalent in tumours of the digestive tract and haematological malignancies such as lymphoblastic leukaemia and acute myeloid leukaemia. (361) The sensitivity of BCRP expressing tumours, as well as the spindle poison resistant P-glycoprotein expressing cancer cells, to 2-MEbisMATE (proven *in vitro* and *in vivo*), along with its excellent bioavailability, good side effect profile and anti-angiogenic properties, make this a promising drug in future cancer therapy.

5. CONCLUSION

In summary, a novel 2-ME analogue (C19) was *in silico* designed and synthesised by our laboratory. It was designed to encapsulate the advantages of the parent drug, namely its anti-angiogenic properties, microtubule abrogation capabilities causing a metaphase block and thereby inducing apoptosis. C19 has been shown effective in tumours resistant to traditional spindle poisons, without the consequences of the side effects. C19 also harnessed the advantages shown by 2-ME analogues, designed to increase its potency in anti-tumorigenesis and increase the bioavailability and half life, which was poor in the original oestrogen analogue. In a series of *in vitro* experiments, the intracellular mechanisms of C19 action on HeLa cells was investigated by exposing the cells to a 0.5 µM concentration for 24 hours. Confocal microscopy of the treated cells incubated in anti-tubulin α labelled antibodies displayed the devastating effect that the compound had on the HeLa cell spindle formation, attributed to its ability to bind to the colchicine site and deregulate microtubule dynamics. Evidence that there is a consequential G_2/M block was gained by visualization via light and fluoresce microscopic techniques, and demonstration of an up-regulation of cyclin B1 and an increased G_2/M fraction of the cell cycle determined flow cytometrically. The mitotic block resulted in apoptotic cell death, as seen on light, fluorescent and transmission microscopy, corroborated with flow cytometic determination of loss of membrane PS asymmetry representing cells undergoing apoptosis. Additionally, cell cycle analysis displayed an increase in the sub-G_1 fraction, which is indicative of apoptosis. To provide an insight into the cellular signaling mechanisms, caspase analysis revealed an increase in caspase 8 and 3, which taken together with evidence of decreased mitochondrial transmembrane potentials obtained by Mqoco *et al*, indicates the induction of apoptosis via both the intrinsic and extrinsic pathways by C19. Transmission electron and fluorescence microscopy exhibited the presence of autophagy in the treated cells, giving the possibility of a second form of cell death. Crosstalk between these two modes of death may be mediated by caspase cleavage of Beclin-1.

In answering a few questions, many more have been generated. It remains to be established whether autophagy is actually a form of cell death in these cells, or if it conveys resistance to the compound until overwhelmed. Additional, it must be established if it is indeed Beclin-1 which mediates the crosstalk between the two processes. The presence of other non-caspase dependent mechanisms of apoptosis and autophagy must be established. The pathways which lead to the extrinsic pathway activation must be determined, as does the autophagy induction, whether it be JNK or p53 or another, or perhaps combinations of a few. The connection, if any, between the spindle block and autophagy induction must be elucidated. Demonstration of C19's retention of 2-ME anti-angiogenic properties must also be demonstrated. Preference of C19 to tumourigenic cells above normal dividing cells needs confirmation. Moving onto the next platform, the effects of C19 *in vivo* need to be determined. Altogether, the data collected thus far gives the picture of a highly efficient anti-cancer drug, with possible minimal side effects with a good oral bioavailability which will probably be active in cells with traditional spindle poison resistance. Future studies will not only further this drug as a possible anti-neoplastic agent, but molecular experiments will also contribute to the global effort in unravelling and understanding crosstalk mechanisms between apoptosis and autophagy.

5. ACKNOWLEDGEMENT OF FUNDING

This study was financially supported by The Cancer Association of South Africa (CANCA) (AOS201), the Medical Research Council (MRC) (AOS536), the National Research Foundation (NRF) (AOT060), the Research Committee of the University of Pretoria (RESCOM) (AOR984) and the Struwig-Germushysen Trust, granted towards the project under Professor A Joubert. An academic achievement bursary was awarded by the University of Pretoria.

6. REFERENCES

1. Siegel R, Ward E, Brawley O, Jemal A. Cancer statistics, 2011. CA Cancer J Clin. 2011;61(4):212-36.

2. World Health Organization [homepage on the internet]. Geneva: World Health Organization; [updated 2011; cited 2011 Sept 30]; Cancer of the cervix [1 screen]. Available from: http://www.who.int/reproductivehealth/topics/cancers/en/.

3. Pisani P, Bray F, Parkin DM. Estimates of the world-wide prevalence of cancer for 25 sites in the adult population. Int J Cancer. 2002;97(1):72-81.

4. Ferlay J, Shin H-R, Bray F, Forman D, Mathers C, Parkin DM. Estimates of worldwide burden of cancer in 2008: GLOBOCAN 2008. Int J Cancer. 2010;127(12):2893-917.

5. Haverkos HW. Multifactorial etiology of cervical cancer: a hypothesis. MedGenMed. 2005;7(4):57.

6. Syrjanen K. New concepts on risk factors of HPV and novel screening strategies for cervical cancer precursors. Eur J Gynaecol Oncol. 2008;29(3):205-21.

7. Adams M, Jasani B, Fiander A. Human papilloma virus (HPV) prophylactic vaccination: Challenges for public health and implications for screening. Vaccine. 2007;25(16):3007-13.

8. zur Hausen H. Papillomaviruses and cancer: from basic studies to clinical application. Nat Rev Cancer. 2002;2(5):342-50.

9. Daling JR, Madeleine MM, McKnight B, Carter JJ, Wipf GC, Ashley R, et al. The relationship of human papillomavirus-related cervical tumors to cigarette smoking, oral contraceptive use, and prior herpes simplex virus type 2 infection. Cancer Epidemiol Biomarkers Prev. 1996;5(7):541-8.

10. Hildesheim A, Mann V, Brinton LA, Szklo M, Reeves WC, Rawls WE. Herpes simplex virus type 2: a possible interaction with human papillomavirus types 16/18 in the development of invasive cervical cancer. Int J Cancer. 1991;49(3):335-40.

11. Smith JS, Herrero R, Bosetti C, Munoz N, Bosch FX, Eluf-Neto J, et al. Herpes simplex virus-2 as a human papillomavirus cofactor in the etiology of invasive cervical cancer. J Natl Cancer Inst. 2002;94(21):1604-13.

12. Zackheim HS. Should coal tar products carry cancer warnings? Cutis. 2004;73(5):333-4.

13. Zhang J, Thomas AG, Leybovich E. Vaginal douching and adverse health effects: a meta-analysis. Am J Public Health. 1997;87(7):1207-11.

14. Levitz JS, Bradley TP, Golden AL. Overview of smoking and all cancers. Med Clin North Am. 2004;88(6):1655-75.

15. Prokopczyk B, Cox JE, Hoffmann D, Waggoner SE. Identification of tobacco-specific carcinogen in the cervical mucus of smokers and nonsmokers. J Natl Cancer Inst. 1997;89(12):868-73.

16. Trimble CL, Genkinger JM, Burke AE, Hoffman SC, Helzlsouer KJ, Diener-West M, et al. Active and passive cigarette smoking and the risk of cervical neoplasia. Obstet Gynecol. 2005;105(1):174-81.

17. Ferrera A, Velema JP, Figueroa M, Bulnes R, Toro LA, Claros JM, et al. Co-factors related to the causal relationship between human papillomavirus and invasive cervical cancer in Honduras. Int J Epidemiol. 2000;29(5):817-25.

18. Velema JP, Ferrera A, Figueroa M, Bulnes R, Toro LA, de Barahona O, et al. Burning wood in the kitchen increases the risk of cervical neoplasia in HPV-infected women in Honduras. Int J Cancer. 2002;97(4):536-41.

19. Tran-Thanh D, Provencher D, Koushik A, Duarte-Franco E, Kessous A, Drouin P, et al. Herpes simplex virus type II is not a cofactor to human papillomavirus in cancer of the uterine cervix. Am J Obstet Gynecol. 2003;188(1):129-34.

20. Syrjanen K, Shabalova I, Petrovichev N, Kozachenko V, Zakharova T, Pajanidi J, et al. Oral contraceptives are not an independent risk factor for cervical intraepithelial neoplasia or high-risk human papillomavirus infections. Anticancer Res. 2006;26(6C):4729-40.

21. Maiman M, Fruchter RG, Clark M, Arrastia CD, Matthews R, Gates EJ. Cervical cancer as an AIDS-defining illness. Obstet Gynecol. 1997;89(1):76-80.

22. Leitao MM, Jr., White P, Cracchiolo B. Cervical cancer in patients infected with the human immunodeficiency virus. Cancer. 2008;112(12):2683-9.

23. de Villiers EM, Fauquet C, Broker TR, Bernard HU, zur Hausen H. Classification of papillomaviruses. Virology. 2004;324(1):17-27.

24. zur Hausen H. Papillomavirus infections--a major cause of human cancers. Biochim Biophys Acta. 1996;1288(2):F55-78.

25. zur Hausen H. Papillomaviruses causing cancer: evasion from host-cell control in early events in carcinogenesis. J Natl Cancer Inst. 2000;92(9):690-8.

26. Prendiville W, Cullimore J, Norman SUE. Large loop excision of the transformation zone (LLETZ). A new method of management for women with cervical intraepithelial neoplasia. BJOG. 1989;96(9):1054-60.

27. Alvarez RD, Helm CW, Edwards RP, Naumann RW, Partridge EE, Shingleton HM, et al. Prospective Randomized Trial of LLETZ versus Laser Ablation in Patients with Cervical Intraepithelial Neoplasia. Gynecol Oncol. 1994;52(2):175-9.

28. González González D, Ketting BW, van Bunningen B, Van Dijk JDP. Carcinoma of the uterine cervix stage IB and IIA: Results of postoperative irradiation in patients with microscopic infiltration in the parametrium and/or lymph node metastasis. Int J Radiat Oncol. 1989;16(2):389-95.

29. Ishikawa H, Nakanishi T, Inoue T, Kuzuya K. Prognostic Factors of Adenocarcinoma of the Uterine Cervix. Gynecol Oncol. 1999;73(1):42-6.

30. Westra TA, Rozenbaum MH, Rogoza RM, Nijman HW, Daemen T, Postma MJ, et al. Until which age should women be vaccinated against HPV infection? Recommendation based on cost-effectiveness analyses. J Infect Dis. 2011;204(3):377-84.

31. Spellman PT, Sherlock G, Zhang MQ, Iyer VR, Anders K, Eisen MB, et al. Comprehensive Identification of Cell Cycle–regulated Genes of the Yeast Saccharomyces cerevisiae by Microarray Hybridization. Mol Biol Cell. 1998;9(12):3273-97.

32. Nurse P. Genetic control of cell size at cell division in yeast. Nature. 1975;256(5518):547-51.

33. Malumbres M. Physiological Relevance of Cell Cycle Kinases. Physiol Rev. 2011;91(3):973-1007.

34. Hartwell LH, Weinert TA. Checkpoints: controls that ensure the order of cell cycle events. Science. 1989;246(4930):629-34.

35. Vermeulen K, Van Bockstaele DR, Berneman ZN. The cell cycle: a review of regulation, deregulation and therapeutic targets in cancer. Cell Prolif. 2003;36(3):131-49.

36. Riedl SJ, Salvesen GS. The apoptosome: signalling platform of cell death. Nature Rev Mol Cell Biol. 2007;8:405-13.

37. Schafer KA. The cell cycle: a review. Vet Pathol. 1998;35(6):461-78.

38. Hirano T. The ABCs of SMC proteins: two-armed ATPases for chromosome condensation, cohesion, and repair. Genes Dev. 2002;16(4):399-414.

39. Salaun P, Rannou Y, Prigent C. Cdk1, Plks, Auroras, and Neks: the mitotic bodyguards. Adv Exp Med Biol. 2008;617:41-56.

40. Zetterberg A, Larsson O. Kinetic analysis of regulatory events in G1 leading to proliferation or quiescence of Swiss 3T3 cells. Proc Natl Acad Sci U S A. 1985;82(16):5365-9.

41. Williams GH, Stoeber K. The cell cycle and cancer. J Pathol. 2012;226(2):352-64.

42. Macaluso M, Montanari M, Giordano A. Rb family proteins as modulators of gene expression and new aspects regarding the interaction with chromatin remodeling enzymes. Oncogene. 2000;25(38):5263-7.

43. Classon M, Harlow E. The retinoblastoma tumour suppressor in development and cancer. Nat Rev Cancer. 2002;2(12):910-7.

44. Ryan MP, Jones R, Morse RH. SWI-SNF complex participation in transcriptional activation at a step subsequent to activator binding. Mol Cell Biol. 1998;18(4):1774-82.

45. Muller H, Helin K. The E2F transcription factors: key regulators of cell proliferation. Biochim Biophys Acta. 2000;1470(1):1-12.

46. Nevins JR. The Rb/E2F pathway and cancer. Hum Mol Genet. 2001;10(7):699-703.

47. Norbury C, Nurse P. Animal cell cycles and their control. Annu Rev Biochem. 1992;61:441-70.

48. Harper JW, Burton JL, Solomon MJ. The anaphase-promoting complex: it's not just for mitosis any more. Genes Dev. 2002;16(17):2179-206.

49. Grana X, Reddy EP. Cell cycle control in mammalian cells: role of cyclins, cyclin dependent kinases (CDKs), growth suppressor genes and cyclin-dependent kinase inhibitors (CKIs). Oncogene. 1995;11(2):211-9.

50. Malumbres M, Barbacid M. To cycle or not to cycle: a critical decision in cancer. Nat Rev Cancer. 2001;1(3):222-31.

51. Hollingsworth-Jr. RE, Ostroff RM, Klein MB, Niswander LA, Sclafani RA. Molecular Genetic Studies of the Cdc7 Protein Kinase and Induced Mutagenesis in Yeast. Genetics. 1992;132(1):53-62.

52. Lowery DM, Lim D, Yaffe MB. Structure and function of Polo-like kinases. Oncogene. 2005;24(2):248-59.

53. Malumbres M, Barbacid M. Mammalian cyclin-dependent kinases. Trends Biochem Sci. 2005;30(11):630-41.

54. Nigg EA. Mitotic kinases as regulators of cell division and its checkpoints. Nat Rev Mol Cell Biol. 2001;2(1):21-32.

55. Malumbres M, Barbacid M. Cell cycle, CDKs and cancer: a changing paradigm. Nat Rev Cancer. 2009;9(3):153-66.

56. Harbour JW, Luo RX, Dei Santi A, Postigo AA, Dean DC. Cdk phosphorylation triggers sequential intramolecular interactions that progressively block Rb functions as cells move through G1. Cell. 1999;98(6):859-69.

57. Sherr CJ, McCormick F. The RB and p53 pathways in cancer. Cancer Cell. 2002;2(2):103-12.

58. Gladden AB, Diehl JA. Cell cycle progression without cyclin E/CDK2: Breaking down the walls of dogma. Cancer Cell. 2003;4(3):160-2.

59. Santamaria D, Barriere C, Cerqueira A, Hunt S, Tardy C, Newton K, et al. Cdk1 is sufficient to drive the mammalian cell cycle. Nature. 2007;448(7155):811-5.

60. Malumbres M, Sotillo R, Santamaria D, Galan J, Cerezo A, Ortega S, et al. Mammalian cells cycle without the D-type cyclin-dependent kinases Cdk4 and Cdk6. Cell. 2004;118(4):493-504.

61. Fujii W, Nishimura T, Kano K, Sugiura K, Naito K. CDK7 and CCNH are Components of CDK-Activating Kinase and Are Required for Meiotic Progression of Pig Oocytes. Biol Reprod. 2011;85(6):1124-32.

62. Hofmann F, Livingston DM. Differential effects of cdk2 and cdk3 on the control of pRb and E2F function during G1 exit. Genes Dev. 1996;10(7):851-61.

63. Ko TK, Kelly E, Pines J. CrkRS: a novel conserved Cdc2-related protein kinase that colocalises with SC35 speckles. J Cell Sci. 2001;114(14):2591-603.

64. Even Y, Durieux S, Escande M-L, Lozano JC, Peaucellier G, Weil D, et al. CDC2L5, a Cdk-like kinase with RS domain, interacts with the ASF/SF2-associated protein p32 and affects splicing in vivo. J Cell Biochem. 2006;99(3):890-904.

65. Kasten M, Giordano A. Cdk10, a Cdc2-related kinase, associates with the Ets2 transcription factor and modulates its transactivation activity. Oncogene. 2001;20(15):1832-8.

66. Bartkowiak B, Liu P, Phatnani HP, Fuda NJ, Cooper JJ, Price DH, et al. CDK12 is a transcription elongation-associated CTD kinase, the metazoan ortholog of yeast Ctk1. Genes Dev. 2010;24(20):2303-16.

67. Denicourt C, Dowdy SF. Cip/Kip proteins: more than just CDKs inhibitors. Genes Dev. 2004;18(8):851-5.

68. Sherr CJ. Mammalian G1 cyclins. Cell. 1993;73(6):1059-65.

69. Wroble BN, Finkielstein CV, Sible JC. Wee1 kinase alters cyclin E/Cdk2 and promotes apoptosis during the early embryonic development of Xenopus laevis. BMC Dev Biol. 2007;7:119.

70. Canepa ET, Scassa ME, Ceruti JM, Marazita MC, Carcagno AL, Sirkin PF, et al. INK4 proteins, a family of mammalian CDK inhibitors with novel biological functions. IUBMB Life. 2007;59(7):419-26.

71. Chim CS, Fung TK, Wong KF, Lau JS, Law M, Liang R. Methylation of INK4 and CIP/KIP families of cyclin-dependent kinase inhibitor in chronic lymphocytic leukaemia in Chinese patients. J Clin Path. 2006;59(9):921-6.

72. Zindy F, Quelle DE, Roussel MF, Sherr CJ. Expression of the p16INK4a tumor suppressor versus other INK4 family members during mouse development and aging. Oncogene. 1997;15(2):203-11.

73. Mueller PR, Coleman TR, Dunphy WG. Cell cycle regulation of a Xenopus Wee1-like kinase. Mol Biol Cell. 1995;6(1):119-34.

74. Lopez-Girona A, Furnari B, Mondesert O, Russell P. Nuclear localization of Cdc25 is regulated by DNA damage and a 14-3-3 protein. Nature. 1999;397(6715):172-5.

75. Taylor WR, Stark GR. Regulation of the G2/M transition by p53. Oncogene. 2001;20(15):1803-15.

76. Borgne A, Ostvold AC, Flament S, Meijer L. Intra-M Phase-promoting Factor Phosphorylation of Cyclin B at the Prophase/Metaphase Transition. J Biol Chem. 1999;274(17):11977-86.

77. Ford CC. Maturation promoting factor and cell cycle regulation. J Embryol exp Morph. 1985;89(Supplement):271-84.

78. King RW, Jackson PK, Kirschner MW. Mitosis in transition. Cell. 1994;79(4):563-71.

79. Mochida S, Maslen SL, Skehel M, Hunt T. Greatwall phosphorylates an inhibitor of protein phosphatase 2A that is essential for mitosis. Science. 2010;330(6011):1670-3.

80. Thron CD. A model for a bistable biochemical trigger of mitosis. Biophys Chem. 1996;57(2-3):239-51.

81. Yuan J, Yan R, Kramer A, Eckerdt F, Roller M, Kaufmann M, et al. Cyclin B1 depletion inhibits proliferation and induces apoptosis in human tumor cells. Oncogene. 2004;23(34):5843-52.

82. Stander BA, Marais S, Vorster CJ, Joubert AM. In vitro effects of 2-methoxyestradiol on morphology, cell cycle progression, cell death and gene expression changes in the tumorigenic MCF-7 breast epithelial cell line. J Steroid Biochem Mol Biol. 2010;119(3-5):149-60.

83. Blajeski AL, Phan VA, Kottke TJ, Kaufmann SH. G(1) and G(2) cell-cycle arrest following microtubule depolymerization in human breast cancer cells. J Clin Invest. 2002;110(1):91-9.

84. Choi HJ, Fukui M, Zhu BT. Role of Cyclin B1/Cdc2 Up-Regulation in the Development of Mitotic Prometaphase Arrest in Human Breast Cancer Cells Treated with Nocodazole. PLoS ONE. 2011;6(8):1-13.

85. Hwang A, Maity A, McKenna WG, Muschel RJ. Cell cycle-dependent regulation of the cyclin B1 promoter. J Biol Chem. 1995;270(47):28419-24.

86. Manchado E, Eguren M, Malumbres M. The anaphase-promoting complex/cyclosome (APC/C): cell-cycle-dependent and -independent functions. Biochem Soc Trans. 2010;38(1):65-71.

87. Matson DR, Stukenberg PT. Spindle poisons and cell fate: a tale of two pathways. Mol Interv. 2011;11(2):141-50.

88. Hames RS, Crookes RE, Straatman KR, Merdes A, Hayes MJ, Faragher AJ, et al. Dynamic Recruitment of Nek2 Kinase to the Centrosome Involves Microtubules, PCM-1, and Localized Proteasomal Degradation. Mol Biol Cell. 2005;16(4):1711-24.

89. Kastan MB, Bartek J. Cell-cycle checkpoints and cancer. Nature. 2004;432(7015):316-23.

90. Iorns E, Turner NC, Elliott R, Syed N, Garrone O, Gasco M, et al. Identification of CDK10 as an Important Determinant of Resistance to Endocrine Therapy for Breast Cancer. Cancer Cell. 2008;13(2):91-104.

91. Bentley NJ, Carr AM. DNA structure-dependent checkpoints in model systems. Biol Chem. 1997;378(11):1267-74.

92. van Vugt MATM, Yaffe MB. Cell cycle re-entry mechanisms after DNA damage checkpoints: Giving it some gas to shut off the breaks! Cell Cycle. 2010;9(11):2097-101.

93. Shibata A, Barton O, Noon AT, Dahm K, Deckbar D, Goodarzi AA, et al. Role of ATM and the Damage Response Mediator Proteins 53BP1 and MDC1 in the Maintenance of G2/M Checkpoint Arrest. Mol Cell Biol. 2010;30(13):3371-83.

94. Moschel RC, McDougall MG, Dolan ME, Stine L, Pegg AE. Structural features of substituted purine derivatives compatible with depletion of human O6-alkylguanine-DNA alkyltransferase. J Med Chem. 1992;35(23):4486-91.

95. Froelich-Ammon SJ, Osheroff N. Topoisomerase Poisons: Harnessing the Dark Side of Enzyme Mechanism. J Biol Chem. 1995;270(37):21429-32.

96. Friesner JD, Liu B, Culligan K, Britt AB. Ionizing Radiation–dependent γ-H2AX Focus Formation Requires Ataxia Telangiectasia Mutated and Ataxia Telangiectasia Mutated and Rad3-related. Mol Biol Cell. 2005;16(5):2566-76.

97. Bartek J, Lukas J. Chk1 and Chk2 kinases in checkpoint control and cancer. Cancer Cell. 2003;3(5):421-9.

98. Honda R, Tanaka H, Yasuda H. Oncoprotein MDM2 is a ubiquitin ligase E3 for tumor suppressor p53. FEBS Lett. 1997;420(1):25-7.

99. Iwakuma T, Lozano G. MDM2, An Introduction. Mol Cancer Res. 2003;1(14):993-1000.

100. Cimprich KA, Cortez D. ATR: an essential regulator of genome integrity. Nat Rev Mol Cell Biol. 2008;9(8):616-27.

101. Luch A. Cell cycle control and cell division: implications for chemically induced carcinogenesis. Chembiochem. 2002;3(6):506-16.

102. Bochman ML, Schwacha A. The Mcm Complex: Unwinding the Mechanism of a Replicative Helicase. Microbiol Mol Biol Rev. 2009;73(4):652-83.

103. Cortez D, Glick G, Elledge SJ. Minichromosome maintenance proteins are direct targets of the ATM and ATR checkpoint kinases. Proc Natl Acad Sci U S A. 2004;101(27):10078-83.

104. Katou Y, Kanoh Y, Bando M, Noguchi H, Tanaka H, Ashikari T, et al. S-phase checkpoint proteins Tof1 and Mrc1 form a stable replication-pausing complex. Nature. 2003;424(6952):1078-83.

105. Stiff T, Reis C, Alderton GK, Woodbine L, O'Driscoll M, Jeggo PA. Nbs1 is required for ATR-dependent phosphorylation events. EMBO J. 2005;24(1):199-208.

106. Smits VAJ, Klompmaker R, Arnaud L, Rijksen G, Nigg EA, Medema RH. Polo-like kinase-1 is a target of the DNA damage checkpoint. Nat Cell Biol. 2000;2(9):672-6.

107. Bartek J, Lukas C, Lukas J. Checking on DNA damage in S phase. Nature Rev Mol Cell Biol. 2004;5(10):792-804.

108. Rieder CL. Formation of the astral mitotic spindle: ultrastructural basis for the centrosome-kinetochore interaction. Electron Microsc Rev. 1990;3(2):269-300.

109. Cimini D. Detection and correction of merotelic kinetochore orientation by Aurora B and its partners. Cell Cycle. 2007;6(13):1558-64.

110. Yang Z, Tulu US, Wadsworth P, Rieder CL. Kinetochore Dynein Is Required for Chromosome Motion and Congression Independent of the Spindle Checkpoint. Curr Biol. 2007;17(11):973-80.

111. Santaguida S, Vernieri C, Villa F, Ciliberto A, Musacchio A. Evidence that Aurora B is implicated in spindle checkpoint signalling independently of error correction. EMBO J. 2011;30(8):1508-19.

112. Carmena M, Earnshaw WC, Ruchaud S. Chromosomal passengers: conducting cell division. Nat Rev Mol Cell Biol. 2007;8(10):798-812.

113. Cleveland DW, Mao Y, Sullivan KF. Centromeres and Kinetochores: From Epigenetics to Mitotic Checkpoint Signaling. Cell. 2003;112(4):407-21.

114. Abrieu A, Magnaghi-Jaulin L, Kahana JA, Peter M, Castro A, Vigneron S, et al. Mps1 Is a Kinetochore-Associated Kinase Essential for the Vertebrate Mitotic Checkpoint. Cell. 2001;106(1):83-93.

115. Burke DJ, Stukenberg PT. Linking Kinetochore-Microtubule Binding to the Spindle Checkpoint. Dev Cell. 2008;14(4):474-9.

116. Kawashima SA, Yamagishi Y, Honda T, Ishiguro K, Watanabe Y. Phosphorylation of H2A by Bub1 prevents chromosomal instability through localizing shugoshin. Science. 2010;327(5962):172-7.

117. Rieder C. Mitosis in vertebrates: the G2/M and M/A transitions and their associated checkpoints. Chromosome Res. 2011;19(3):291-306.

118. Huang H-C, Shi J, Orth JD, Mitchison TJ. Evidence that Mitotic Exit Is a Better Cancer Therapeutic Target Than Spindle Assembly. Cancer Cell. 2009;16(4):347-58.

119. Gascoigne KE, Taylor SS. Cancer cells display profound intra- and interline variation following prolonged exposure to antimitotic drugs. Cancer Cell. 2008;14(2):111-22.

120. Kim M, Murphy K, Liu F, Parker SE, Dowling ML, Baff W, et al. Caspase-mediated specific cleavage of BubR1 is a determinant of mitotic progression. Mol Cell Biol. 2005;25(21):9232-48.

121. Kitagawa K, Niikura Y. Caspase-independent mitotic death (CIMD). Cell Cycle. 2008;7(8):1001-5.

122. Gan PP, McCarroll JA, Po'uha ST, Kamath K, Jordan MA, Kavallaris M. Microtubule Dynamics, Mitotic Arrest, and Apoptosis: Drug-Induced Differential Effects of βIII-Tubulin. Mol Cancer Ther. 2010;9(5):1339-48.

123. Wade R. On and Around Microtubules: An Overview. Mol Biotechnol. 2009;43(2):177-91.

124. Jordan MA, Wilson L. Microtubules as a target for anticancer drugs. Nat Rev Cancer. 2004;4(4):253-65.

125. Honore S, Pasquier E, Braguer D. Understanding microtubule dynamics for improved cancer therapy. Cell Mol life Sci. 2005;62(24):3039-56.

126. Amayed P, Pantaloni D, Carlier M-F. The Effect of Stathmin Phosphorylation on Microtubule Assembly Depends on Tubulin Critical Concentration. J Biol Chem. 2002;277(25):22718-24.

127. Beghin A, Galmarini CM, Dumontet C. Tubulin Folding Pathways: Implication in the Regulation of Microtubule Dynamics. Curr Cancer Drug Targets. 2007;7(8):697-703.

128. Verdier-Pinard P, Wang F, Burd B, Angeletti RH, Horwitz SB, Orr GA. Direct analysis of tubulin expression in cancer cell lines by electrospray ionization mass spectrometry. Biochemistry. 2003;42(41):12019-27.

129. Margolis RL, Wilson L. Microtubule treadmilling: what goes around comes around. Bioessays. 1998;20(10):830-6.

130. Pasquier E, Sinnappan S, Munoz MA, Kavallaris M. ENMD-1198, a New Analogue of 2-Methoxyestradiol, Displays Both Antiangiogenic and Vascular-Disrupting Properties. Mol Cancer Ther. 2010;9(5):1408-18.

131. Jordan MA, Kamath K. How Do Microtubule-Targeted Drugs Work? An Overview. Curr Cancer Drug Targets. 2007;7(8):730-42.

132. Uppuluri S, Knipling L, Sackett DL, Wolff J. Localization of the colchicine-binding site of tubulin. Proc Natl Acad Sci U S A. 1993;90(24):11598-602.

133. Stander A, Joubert F, Joubert A. Docking, Synthesis, and in vitro Evaluation of Antimitotic Estrone Analogs. Chem Biol Drug Des. 2011;77(3):173-81.

134. D'Amato RJ, Lin CM, Flynn E, Folkman J, Hamel E. 2-Methoxyestradiol, an endogenous mammalian metabolite, inhibits tubulin polymerization by interacting at the colchicine site. Proc Natl Acad Sci U S A. 1994;91(9):3964-8.

135. Hotchkiss RS, Strasser A, McDunn JE, Swanson PE. Cell Death. NEJM. 2009;361(16):1570-83.

136. Zong WX, Thompson CB. Necrotic death as a cell fate. Genes Dev. 2006;20(1):1-15.

137. Maiuri MC, Zalckvar E, Kimchi A, Kroemer G. Self-eating and self-killing: crosstalk between autophagy and apoptosis. Nat Rev Mol Cell Biol. 2007;8(9):741-52.

138. Eisenberg-Lerner A, Bialik S, Simon HU, Kimchi A. Life and death partners: apoptosis, autophagy and the cross-talk between them. Cell Death Differ. 2009;16(7):966-75.

139. Vakifahmetoglu H, Olsson M, Zhivotovsky B. Death through a tragedy: mitotic catastrophe. Cell Death Differ. 2008;15(7):1153-62.

140. Caruso R, Fedele F, Lucianòò R, Branca G, Parisi C, Paparo D, et al. Mitotic Catastrophe in Malignant Epithelial Tumors: The Pathologist's Viewpoint. Ultrastruct Pathol. 2011;35(2):66-71.

141. Zong W, Lindsten T, Ross A, MacGregor G, Thompson C. BH3-only proteins that bind pro-survival Bcl-2 family members fail to induce apoptosis in the absence of Bax and Bak. Genes Dev. 2001;15:1481-86.

142. Krysko DV, Vanden Berghe T, D'Herde K, Vandenabeele P. Apoptosis and necrosis: detection, discrimination and phagocytosis. Methods. 2008;44(3):205-21.

143. Ziegler U, Groscurth P. Morphological features of cell death. News Physiol Sci. 2004;19:124-8.

144. Kerr JF, Wyllie AH, Currie AR. Apoptosis: a basic biological phenomenon with wide-ranging implications in tissue kinetics. Br J Cancer. 1972;26(4):239-57.

145. Koopman G, Reutelingsperger CP, Kuijten GA, Keehnen RM, Pals ST, van Oers MH. Annexin V for flow cytometric detection of phosphatidylserine expression on B cells undergoing apoptosis. Blood. 1994;84(5):1415-20.

146. Martin SJ, Reutelingsperger CP, McGahon AJ, Rader JA, van Schie RC, LaFace DM, et al. Early redistribution of plasma membrane phosphatidylserine is a general feature of apoptosis regardless of the initiating stimulus: inhibition by overexpression of Bcl-2 and Abl. J Exp Med. 1995;182(5):1545-56.

147. Fadok VA, Voelker DR, Campbell PA, Cohen JJ, Bratton DL, Henson PM. Exposure of phosphatidylserine on the surface of apoptotic lymphocytes triggers specific recognition and removal by macrophages. J Immunol. 1992;148(7):2207-16.

148. Aubry JP, Blaecke A, Lecoanet-Henchoz S, Jeannin P, Herbault N, Caron G, et al. Annexin V used for measuring apoptosis in the early events of cellular cytotoxicity. Cytometry. 1999;37(3):197-204.

149. Andree HA, Reutelingsperger CP, Hauptmann R, Hemker HC, Hermens WT, Willems GM. Binding of vascular anticoagulant alpha (VAC alpha) to planar phospholipid bilayers. J Biol Chem. 1990;265(9):4923-8.

150. Wang J, Lenardo MJ. Roles of caspases in apoptosis, development, and cytokine maturation revealed by homozygous gene deficiencies. J Cell Sci. 2000;113(5):753-7.

151. Yi CH, Yuan J. The Jekyll and Hyde functions of caspases. Dev Cell. 2009;16(1):21-34.

152. McStay GP, Salvesen GS, Green DR. Overlapping cleavage motif selectivity of caspases: implications for analysis of apoptotic pathways. Cell Death Differ. 2007;15(2):322-31.

153. Boatright KM, Renatus M, Scott FL, Sperandio S, Shin H, Pedersen IM, et al. A Unified Model for Apical Caspase Activation. Mol Cell. 2003;11(2):529-41.

154. Kruidering M, Evan GI. Caspase-8 in apoptosis: the beginning of "the end"? IUBMB Life. 2000;50(2):85-90.

155. Ashkenazi A, Dixit VM. Death receptors: signaling and modulation. Science. 1998;281(5381):1305-8.

156. Scott FL, Stec B, Pop C, Dobaczewska MK, Lee JJ, Monosov E, et al. The Fas-FADD death domain complex structure unravels signalling by receptor clustering. Nature. 2009;457(7232):1019-22.

157. Scaffidi C, Medema JP, Krammer PH, Peter ME. FLICE Is Predominantly Expressed as Two Functionally Active Isoforms, Caspase-8/a and Caspase-8/b. J Biol Chem. 1997;272(43):26953-8.

158. Kuida K, Zheng TS, Na S, Kuan C, Yang D, Karasuyama H, et al. Decreased apoptosis in the brain and premature lethality in CPP32-deficient mice. Nature. 1996;384(6607):368-72.

159. Porter AG, Janicke RU. Emerging roles of caspase-3 in apoptosis. Cell Death Differ. 1999;6(2):99-104.

160. Ola M, Nawaz M, Ahsan H. Role of Bcl-2 family proteins and caspases in the regulation of apoptosis. Mol Cell Biochem. 2011;351(1):41-58.

161. Kelly PN, Strasser A. The role of Bcl-2 and its pro-survival relatives in tumourigenesis and cancer therapy. Cell Death Differ. 2011;18(9):1414-24.

162. O'Reilly LA, Print C, Hausmann G, Moriishi K, Cory S, Huang DC, et al. Tissue expression and subcellular localization of the pro-survival molecule Bcl-w. Cell death differ. 2001;8(5):486-94.

163. Holmgreen SP, Huang DC, Adams JM, Cory S. Survival activity of Bcl-2 homologs Bcl-w and A1 only partially correlates with their ability to bind pro-apoptotic family members. Cell Death Differ. 1999;6(6):525-32.

164. Rautureau GJ, Day CL, Hinds MG. The structure of Boo/Diva reveals a divergent Bcl-2 protein. Proteins. 2010;78(9):2181-6.

165. Erlacher M, Michalak EM, Kelly PN, Labi V, Niederegger H, Coultas L, et al. BH3-only proteins Puma and Bim are rate-limiting for γ-radiation and glucocorticoid-induced apoptosis of lymphoid cells in vivo. Blood. 2005;106(13):4131-8.

166. Gong Y, Somwar R, Politi K, Balak M, Chmielecki J, Jiang X, et al. Induction of BIM Is Essential for Apoptosis Triggered by EGFR Kinase Inhibitors in Mutant EGFR-Dependent Lung Adenocarcinomas. PLoS Med. 2007;4(10):1655-68.

167. Willis SN, Fletcher JI, Kaufmann T, van Delft MF, Chen L, Czabotar PE, et al. Apoptosis Initiated When BH3 Ligands Engage Multiple Bcl-2 Homologs, Not Bax or Bak. Science. 2007;315(5813):856-9.

168. Kuwana T, Bouchier-Hayes L, Chipuk JE, Bonzon C, Sullivan BA, Green DR, et al. BH3 Domains of BH3-Only Proteins Differentially Regulate Bax-Mediated Mitochondrial Membrane Permeabilization Both Directly and Indirectly. Molecular cell. 2005;17(4):525-35.

169. Tan Y, Dourdin N, Wu C, De Veyra T, Elce JS, Greer PA. Ubiquitous Calpains Promote Caspase-12 and JNK Activation during Endoplasmic Reticulum Stress-induced Apoptosis. J Biol Chem. 2006;281(23):16016-24.

170. Berube C, Boucher L-M, Ma W, Wakeham A, Salmena L, Hakem R, et al. Apoptosis caused by p53-induced protein with death domain (PIDD) depends on the death adapter protein RAIDD. Proc Natl Acad Sci USA. 2005;102(40):14314-20.

171. Huai J, Jockel L, Schrader K, Borner C. Role of caspases and non-caspase proteases in cell death. F1000 Biol Rep. 2010;2:48.

172. Kurokawa H, Nishio K, Fukumoto H, Tomonari A, Suzuki T, Saijo N. Alteration of caspase-3 (CPP32/Yama/apopain) in wild-type MCF-7, breast cancer cells. Oncol Rep. 1999;6(1):33-7.

173. Wang YF, Jiang CC, Kiejda KA, Gillespie S, Zhang XD, Hersey P. Apoptosis Induction in Human Melanoma Cells by Inhibition of MEK Is Caspase-Independent and Mediated by the Bcl-2 Family Members PUMA, Bim, and Mcl-1. Clin Cancer Res. 2007;13(16):4934-42.

174. Dalby K, Tekedereli I, Lopez-Berestein G, Ozpolat B. Targeting the pro-death and pro-survival functions of autophagy as novel therapeutic strategies in cancer. Autophagy. 2010;6(3):322-9.

175. Lum JJ, DeBerardinis RJ, Thompson CB. Autophagy in metazoans: cell survival in the land of plenty. Nat Rev Mol Cell Biol. 2005;6(6):439-48.

176. Lorin S, Pierron G, Ryan KM, Codogno P, Djavaheri-Mergny M. Evidence for the interplay between JNK and p53-DRAM signalling pathways in the regulation of autophagy. Autophagy. 2010;6(1):153-4.

177. Olzmann JA, Chin L-S. Parkin-mediated K63-linked polyubiquitination: A signal for targeting misfolded proteins to the aggresome-autophagy pathway. Autophagy. 2008;4(1):85-7.

178. Johnston JA, Ward CL, Kopito RR. Aggresomes: a cellular response to misfolded proteins. J Cell Biol. 1998;143(7):1883-98.

179. Sridhar S, Botbol Y, Macian F, Cuervo AM. Autophagy and disease: always two sides to a problem. J Pathol. 2012;226(2):255-73.

180. Xie Z, Klionsky DJ. Autophagosome formation: core machinery and adaptations. Nat Cell Biol. 2007;9(10):1102-9.

181. Kurihara Y, Kanki T, Aoki Y, Hirota Y, Saigusa T, Uchiumi T, et al. Mitophagy plays an essential role in reducing mitochondrial production of reactive oxygen species and mutation of mitochondrial DNA by maintaining mitochondrial quantity and quality in yeast. J Biol Chem. 2012;287(5):3265-72.

182. Sibirny AA. Mechanisms of autophagy and pexophagy in yeasts. Biochemistry. 2011;76(12):1279-90.

183. Tasdemir E, Maiuri MC, Tajeddine N, Criollo A, Vicencio JM, Hickman JA, et al. Cell Cycle-Dependent Induction of Autophagy, Mitophagy and Reticulophagy. Cell Cycle. 2007;6(18):2263-7.

184. Filimonenko M, Isakson P, Finley KD, Anderson M, Jeong H, Melia TJ, et al. The Selective Macroautophagic Degradation of Aggregated Proteins Requires the PI3P-Binding Protein Alfy. Mol Cell. 2010;38(2):265-79.

185. Koga H, Martinez-Vicente M, Arias E, Kaushik S, Sulzer D, Cuervo AM. Constitutive upregulation of chaperone-mediated autophagy in Huntington's disease. J Neurosci. 2011;31(50):18492-505.

186. Raftopoulou M. Autophagy: to die or not to die. Nat Cell Biol. 2005;7(11):1056-.

187. Wang CW, Klionsky DJ. The molecular mechanism of autophagy. Mol Med. 2003;9(3-4):65-76.

188. Levine B, Ranganathan R. Autophagy: Snapshot of the network. Nature. 2010;466(7302):38-40.

189. Levine B, Kroemer G. Autophagy in the Pathogenesis of Disease. Cell. 2008;132(1):27-42.

190. Ravikumar B, Vacher C, Berger Z, Davies JE, Luo S, Oroz LG, et al. Inhibition of mTOR induces autophagy and reduces toxicity of polyglutamine expansions in fly and mouse models of Huntington disease. Nat Genet. 2004;36(6):585-95.

191. Nishimoto S, Nishida E. MAPK signalling: ERK5 versus ERK1/2. EMBO Rep. 2006;7(8):782-6.

192. Kang R, Zeh HJ, Lotze MT, Tang D. The Beclin 1 network regulates autophagy and apoptosis. Cell Death Differ. 2011;18(4):571-80.

193. Behrends C, Gygi SP, Harper JW, Sowa ME. Network organization of the human autophagy system. Nature. 2010;466(7302):68-76.

194. Liang XH, Jackson S, Seaman M, Brown K, Kempkes B, Hibshoosh H, et al. Induction of autophagy and inhibition of tumorigenesis by beclin 1. Nature. 1999;402(6762):672-6.

195. Yue Z, Jin S, Yang C, Levine AJ, Heintz N. Beclin 1, an autophagy gene essential for early embryonic development, is a haploinsufficient tumor suppressor. Proc Natl Acad Sci U S A. 2003;100(25):15077-82.

196. Coppola D, Helm J, Ghayouri M, Malafa MP, Wang H-G. Down-Regulation of Bax-Interacting Factor 1 in Human Pancreatic Ductal Adenocarcinoma. Pancreas. 2011;40(3):433-7.

197. Chen N, Karantza V. Autophagy as a therapeutic target in cancer. Cancer Biol Ther. 2011;11(2):157-68.

198. Maiuri MC, Tasdemir E, Criollo A, Morselli E, Vicencio JM, Carnuccio R, et al. Control of autophagy by oncogenes and tumor suppressor genes. Cell Death Differ. 2009;16(1):87-93.

199. Cheng H-C, Kim SR, Oo TF, Kareva T, Yarygina O, Rzhetskaya M, et al. Akt Suppresses Retrograde Degeneration of Dopaminergic Axons by Inhibition of Macroautophagy. J Neurosci. 2011;31(6):2125-35.

200. Kang R, Tang D, Loze MT, Zeh HJ. Apoptosis to autophagy switch triggered by the MHC class III-encoded receptor for advanced glycation endproducts (RAGE). Autophagy. 2011;7(1):91-3.

201. Kondo Y, Kanzawa T, Sawaya R, Kondo S. The role of autophagy in cancer development and response to therapy. Nat Rev Cancer. 2005;5(9):726-34.

202. Shimizu S, Kanaseki T, Mizushima N, Mizuta T, Arakawa-Kobayashi S, Thompson CB, et al. Role of Bcl-2 family proteins in a non-apoptotic programmed cell death dependent on autophagy genes. Nat Cell Biol. 2004;6(12):1221-8.

203. Akar U, Ozpolat B, Mehta K, Fok J, Kondo Y, Lopez-Berestein G. Tissue transglutaminase inhibits autophagy in pancreatic cancer cells. Mol Cancer Res. 2007;5(3):241-9.

204. Zhou F, Yang Y, Xing D. Bcl-2 and Bcl-xL play important roles in the crosstalk between autophagy and apoptosis. FEBS Journal. 2011;278(3):403-13.

205. Li B-X, Li C-Y, Peng R-Q, Wu X-J, Wang H-Y, Wan D-S, et al. The expression of beclin 1 is associated with favorable prognosis in stage IIIB colon cancers. Autophagy. 2009;5(3):303-6.

206. Liang XH, Yu J, Brown K, Levine B. Beclin 1 Contains a Leucine-rich Nuclear Export Signal That Is Required for Its Autophagy and Tumor Suppressor Function. Cancer Res. 2001;61(8):3443-9.

207. Adi-Harel S, Erlich S, Schmukler E, Cohen-Kedar S, Segev O, Mizrachy L, et al. Beclin 1 self-association is independent of autophagy induction by amino acid deprivation and rapamycin treatment. J Cell Biochem. 2010;110(5):1262-71.

208. Wirawan E, Vande Walle L, Kersse K, Cornelis S, Claerhout S, Vanoverberghe I, et al. Caspase-mediated cleavage of Beclin-1 inactivates Beclin-1-induced autophagy and enhances apoptosis by promoting the release of proapoptotic factors from mitochondria. Cell Death Dis. 2010;1(1):e18.

209. Cherra SJ, Kulich SM, Uechi G, Balasubramani M, Mountzouris J, Day BW, et al. Regulation of the autophagy protein LC3 by phosphorylation. J Cell Biol. 2010;190(4):533-9.

210. Fimia GM, Di Bartolomeo S, Piacentini M, Cecconi F. Unleashing the Ambra1-Beclin 1 complex from dynein chains: Ulk1 sets Ambra1 free to induce autophagy. Autophagy. 2011;7(1):115-7.

211. Pattingre S, Tassa A, Qu X, Garuti R, Liang XH, Mizushima N, et al. Bcl-2 antiapoptotic proteins inhibit Beclin 1-dependent autophagy. Cell. 2005;122(6):927-39.

212. Chang NC, Nguyen M, Germain M, Shore GC. Antagonism of Beclin 1-dependent autophagy by BCL-2 at the endoplasmic reticulum requires NAF-1. EMBO J. 2010;29(3):606-18.

213. Chen C-H, Wang W-J, Kuo J-C, Tsai H-C, Lin J-R, Chang Z-F, et al. Bidirectional signals transduced by DAPK-ERK interaction promote the apoptotic effect of DAPK. EMBO J. 2005;24(2):294-304.

214. Shi C-S, Kehrl JH. TRAF6 and A20 Regulate Lysine 63-Linked Ubiquitination of Beclin-1 to Control TLR4-Induced Autophagy. Sci Signal. 2010;3(123):ra42.

215. Tang D, Kang R, Cheh CW, Livesey KM, Liang X, Schapiro NE, et al. HMGB1 release and redox regulates autophagy and apoptosis in cancer cells. Oncogene. 2010;29(38):5299-310.

216. Skinner M. Autophagy: In the hands of HMGB1. Nat Rev Mol Cell Biol. 2010;11(11):756-7.

217. Djavaheri-Mergny M, Maiuri MC, Kroemer G. Cross talk between apoptosis and autophagy by caspase-mediated cleavage of Beclin 1. Oncogene. 2010;29(12):1717-9.

218. Seol D-W, Li J, Seol M-H, Park S-Y, Talanian RV, Billiar TR. Signaling Events Triggered by Tumor Necrosis Factor-related Apoptosis-inducing Ligand (TRAIL): Caspase-8 Is Required for TRAIL-induced Apoptosis. Cancer Res. 2001;61(3):1138-43.

219. Hou W, Han J, Lu C, Goldstein LA, Rabinowich H. Autophagic degradation of active caspase-8: A crosstalk mechanism between autophagy and apoptosis. Autophagy. 2010;6(7):891-900.

220. Yousefi S, Perozzo R, Schmid I, Ziemiecki A, Schaffner T, Scapozza L, et al. Calpain-mediated cleavage of Atg5 switches autophagy to apoptosis. Nat Cell Biol. 2006;8(10):1124-32.

221. Leber B, Andrews DW. Closing in on the link between apoptosis and autophagy. F1000 Biol Rep. 2010;2:88.

222. Agostinis P, Agrawal DK, Baba M, Baehrecke EH, Bahr BA, Ballabio A, et al. Guidelines for the use and interpretation of assays for monitoring autophagy in higher eukaryotes. Autophagy. 2008;4(2):151-75.

223. Matei D, Schilder J, Sutton G, Perkins S, Breen T, Quon C, et al. Activity of 2 methoxyestradiol (Panzem NCD) in advanced, platinum-resistant ovarian cancer and primary peritoneal carcinomatosis: a Hoosier Oncology Group trial. Gynecol Oncol. 2009;115(1):90-6.

224. Mooberry SL. Mechanism of action of 2-methoxyestradiol: new developments. Drug Resist Updat. 2003;6(6):355-61.

225. Tevaarwerk AJ, Holen KD, Alberti DB, Sidor C, Arnott J, Quon C, et al. Phase I trial of 2-methoxyestradiol NanoCrystal dispersion in advanced solid malignancies. Clin Cancer Res. 2009;15(4):1460-5. Epub 2009/02/21.

226. EntreMed [homepage on the internet]. Rockville: EntreMed; [updated 2011; cited 2011 Sept 30]; Clinical Trials [about 2 screens]. Available from: http://www.entremed.com/clinic/.

227. Maran A, Zhang M, Kennedy AM, Sibonga JD, Rickard DJ, Spelsberg TC, et al. 2-methoxyestradiol induces interferon gene expression and apoptosis in osteosarcoma cells. Bone. 2002;30(2):393-8.

228. Parks M, Tillhon M, Donà F, Prosperi E, Scovassi AI. 2-Methoxyestradiol: New perspectives in colon carcinoma treatment. Mol Cell Endocrinol. 2011;331(1):119-28.

229. Kato S, Sadarangani A, Lange S, Delpiano AM, Vargas M, Brañes J, et al. 2-Methoxyestradiol Mediates Apoptosis Through Caspase-Dependent and Independent Mechanisms in Ovarian Cancer Cells But Not in Normal Counterparts. Reprod Sci. 2008;15(9):878-94.

230. Leese MP, Leblond B, Smith A, Newman SP, Di Fiore A, De Simone G, et al. 2-Substituted Estradiol Bis-sulfamates, Multitargeted Antitumor Agents: Synthesis, In Vitro SAR, Protein Crystallography, and In Vivo Activity†. Journal of Medicinal Chemistry. 2006;49(26):7683-96.

231. Dunn JF, Merriam GR, Eil C, Kono S, Loriaux DL, Nisula BC. Testosterone-estradiol binding globulin binds to 2-methoxyestradiol with greater affinity than to testosterone J Clin Endocrinol Metab. 1980;51(2):404-6.

232. Lakhani NJ, Sparreboom A, Xu X, Veenstra TD, Venitz J, Dahut WL, et al. Characterization of in vitro and in vivo metabolic pathways of the investigational anticancer agent, 2-methoxyestradiol. J Pharm Sci. 2007;96(7):1821-31.

233. Berg D, Sonsalla R, Kuss E. Concentrations of 2-methoxyoestrogens in human serum measured by a heterologous immunoassay with an 125I-labelled ligand. Acta Endocrinol (Copenh). 1983;103(2):282-8.

234. Seegers JC, Aveling ML, Van Aswegen CH, Cross M, Koch F, Joubert WS. The cytotoxic effects of estradiol-17 beta, catecholestradiols and methoxyestradiols on dividing MCF-7 and HeLa cells. J Steroid Biochem. 1989;32(6):797-809.

235. PubChem Compound Database [homepage on the internet]. Rockville Pike: National Center for Biotechnology Information; [updated 2011; cited 2011 Sept 30]; 2-methoxyestradiol - Compound Summary [about 9 screens]. Available from: http://pubchem.ncbi.nlm.nih.gov/summary/summary.cgi?cid=66414#subheading.

236. Mabjeesh NJ, Escuin D, LaVallee TM, Pribluda VS, Swartz GM, Johnson MS, et al. 2ME2 inhibits tumor growth and angiogenesis by disrupting microtubules and dysregulating HIF. Cancer Cell. 2003;3(4):363-75.

237. Semenza GL. Targeting HIF-1 for cancer therapy. Nat Rev Cancer. 2003;3(10):721-32.

238. Kimbro KS, Simons JW. Hypoxia-inducible factor-1 in human breast and prostate cancer. Endocr Relat Cancer. 2006;13(3):739-49.

239. Bardos JI, Ashcroft M. Negative and positive regulation of HIF-1: a complex network. Biochim Biophys Acta. 2005;1755(2):107-20.

240. Kamath K, Okouneva T, Larson G, Panda D, Wilson L, Jordan MA. 2-Methoxyestradiol suppresses microtubule dynamics and arrests mitosis without depolymerizing microtubules. Mol Cancer Ther. 2006;5(9):2225-33.

241. Sweeney C, Liu G, Yiannoutsos C, Kolesar J, Horvath D, Staab MJ, et al. A Phase II Multicenter, Randomized, Double-Blind, Safety Trial Assessing the Pharmacokinetics, Pharmacodynamics, and Efficacy of Oral 2-Methoxyestradiol Capsules in Hormone-Refractory Prostate Cancer. Clin Cancer Res. 2005;11(18):6625-33.

242. Cushman M, He HM, Katzenellenbogen JA, Lin CM, Hamel E. Synthesis, antitubulin and antimitotic activity, and cytotoxicity of analogs of 2-methoxyestradiol, an endogenous mammalian metabolite of estradiol that inhibits tubulin polymerization by binding to the colchicine binding site. J Med Chem. 1995;38(12):2041-9.

243. Rajkumar SV, Richardson PG, Lacy MQ, Dispenzieri A, Greipp PR, Witzig TE, et al. Novel Therapy with 2-Methoxyestradiol for the Treatment of Relapsed and Plateau Phase Multiple Myeloma. Clin Cancer Res. 2007;13(20):6162-7.

244. Tinley TL, Leal RM, Randall-Hlubek DA, Cessac JW, Wilkens LR, Rao PN, et al. Novel 2-Methoxyestradiol Analogues with Antitumor Activity. Cancer Res. 2003;63(7):1538-49.

245. Klauber N, Parangi S, Flynn E, Hamel E, D'Amato RJ. Inhibition of Angiogenesis and Breast Cancer in Mice by the Microtubule Inhibitors 2-Methoxyestradiol and Taxol. Cancer Res. 1997;57(1):81-6.

246. Dubey RK, Jackson EK. Potential vascular actions of 2-methoxyestradiol. Trends Endocrinol Metab. 2009;20(8):374-9.

247. LaVallee TM, Zhan XH, Johnson MS, Herbstritt CJ, Swartz G, Williams MS, et al. 2-methoxyestradiol up-regulates death receptor 5 and induces apoptosis through activation of the extrinsic pathway. Cancer Res. 2003;63(2):468-75.

248. Chauhan D, Li G, Hideshima T, Podar K, Mitsiades C, Mitsiades N, et al. JNK-dependent release of mitochondrial protein, Smac, during apoptosis in multiple myeloma (MM) cells. J Biol Chem. 2003;278(20):17593-6.

249. Huang P, Feng L, Oldham EA, Keating MJ, Plunkett W. Superoxide dismutase as a target for the selective killing of cancer cells. Nature. 2000;407(6802):390-5.

250. Hagen T, D'Amico G, Quintero M, Palacios-Callender M, Hollis V, Lam F, et al. Inhibition of mitochondrial respiration by the anticancer agent 2-methoxyestradiol. Biochem Biophys Res Commun. 2004;322(3):923-9.

251. Carothers AM, Hughes SA, Ortega D, Bertagnolli MM. 2-Methoxyestradiol induces p53-associated apoptosis of colorectal cancer cells. Cancer Lett. 2002;187(1-2):77-86.

252. Kumar AP, Garcia GE, Orsborn J, Levin VA, Slaga TJ. 2-Methoxyestradiol interferes with NF kappa B transcriptional activity in primitive neuroectodermal brain tumors: implications for management. Carcinogenesis. 2003;24(2):209-16.

253. Lottering M-L, Haag M, Seegers JC. Effects of 17β-Estradiol Metabolites on Cell Cycle Events in MCF-7 Cells. Cancer Res. 1992;52(21):5926-32.

254. Lottering ML, de Kock M, Viljoen TC, Grobler CJ, Seegers JC. 17beta-Estradiol metabolites affect some regulators of the MCF-7 cell cycle. Cancer Lett. 1996;110(1-2):181-6.

255. Joubert A, Marais S, Maritz C. Influence of 2-methoxyestradiol on MCF-7 cells: An improved differential interference contrasting technique and Bcl-2 and Bax protein expression levels. Biocell. 2009;33:67-70.

256. Zoubine MN, Weston AP, Johnson DC, Campbell DR, Banerjee SK. 2-methoxyestradiol-induced growth suppression and lethality in estrogen-responsive MCF-7 cells may be mediated by down regulation of p34cdc2 and cyclin B1 expression. Int J Oncol. 1999;15(4):639-46.

257. Lippert C, Seeger H, Mueck AO. The effect of endogenous estradiol metabolites on the proliferation of human breast cancer cells. Life Sci. 2003;72(8):877-83.

258. Liu Z-J, Lee WJ, Zhu BT. Selective Insensitivity of ZR-75-1 Human Breast Cancer Cells to 2-Methoxyestradiol: Evidence for Type II 17β-Hydroxysteroid Dehydrogenase as the Underlying Cause. Cancer Res. 2005;65(13):5802-11.

259. Han G-Z, Liu Z-J, Shimoi K, Zhu BT. Synergism between the Anticancer Actions of 2-Methoxyestradiol and Microtubule-Disrupting Agents in Human Breast Cancer. Cancer Res. 2005;65(2):387-93.

260. Lewis JS, Thomas TJ, Pestell RG, Albanese C, Gallo MA, Thomas T. Differential effects of 16α-hydroxyestrone and 2-methoxyestradiol on cyclin D1 involving the transcription factor ATF-2 in MCF-7 breast cancer cells. J Mol Endocrinol. 2005;34(1):91-105.

261. Kirches E, Warich-Kirches M. 2-Methoxyestradiol as a Potential Cytostatic Drug in Gliomas? Anti-Cancer Agents Med Chem. 2009;9(1):55-65.

262. Lorin S, Borges A, Ribeiro Dos Santos L, Souquère S, Pierron G, Ryan KM, et al. c-Jun NH2-Terminal Kinase Activation Is Essential for DRAM-Dependent Induction of Autophagy and Apoptosis in 2-Methoxyestradiol–Treated Ewing Sarcoma Cells. Cancer Res. 2009;69(17):6924-31.

263. Davoodpour P, Landström M. 2-Methoxyestradiol-induced Apoptosis in Prostate Cancer Cells Requires Smad7. J Biol Chem. 2005;280(15):14773-9.

264. Qadan LR, Perez-Stable CM, Anderson C, D'Ippolito G, Herron A, Howard GA, et al. 2-Methoxyestradiol Induces G2/M Arrest and Apoptosis in Prostate Cancer. Biochem Biophys Res Commun. 2001;285(5):1259-66.

265. Li L, Bu S, Backstrom T, Landstrom M, Ulmsten U, Fu X. Induction of Apoptosis and G2/M Arrest by 2-Methoxyestradiol in Human Cervical Cancer HeLaS3 Cells. Anticancer Research. 2004;24(2B):873-80.

266. Li L, Da J, Landstrom M, Ulmsten U, Fu X. Antiproliferative activity and toxicity of 2-methoxyestradiol in cervical cancer xenograft mice. Int J Gynecol Cancer. 2005;15(2):301-7.

267. Joubert A, Maritz C, Joubert F. Influence of prostaglandin A2 and 2-methoxyestradiol on Bax and Bcl-2 expression levels in cervical carcinoma cells. Biomed Res. 2005;26(2):87-90.

268. Schumacher G, Kataoka M, Roth JA, Mukhopadhyay T. Potent Antitumor Activity of 2-Methoxyestradiol in Human Pancreatic Cancer Cell Lines. Clin Cancer Res. 1999;5(3):493-9.

269. Fotsis T, Zhang Y, Pepper MS, Adlercreutz H, Montesano R, Nawroth PP, et al. The endogenous oestrogen metabolite 2-methoxyoestradiol inhibits angiogenesis and suppresses tumour growth. Nature. 1994;368(6468):237-9.

270. Dobos J, Tímár J, Bocsi J, Burián Z, Nagy K, Barna G, et al. In vitro and in vivo antitumor effect of 2-methoxyestradiol on human melanoma. Int J Cancer. 2004;112(5):771-6.

271. Amorino GP, Freeman ML, Choy H. Enhancement of Radiation Effects In Vitro by the Estrogen Metabolite 2-Methoxyestradiol. Radiat Res. 2000;153(4):384-91.

272. Mukhopadhyay T, Roth JA. Superinduction of wild-type p53 protein after 2-methoxyestradiol treatment of Ad5p53-transduced cells induces tumor cell apoptosis. Oncogene. 1998;17(2):241-6.

273. Matei D, Schilder J, Sutton G, Perkins S, Breen T, Quon C, et al. Activity of 2 methoxyestradiol (Panzem® NCD) in advanced, platinum-resistant ovarian cancer and primary peritoneal carcinomatosis: A Hoosier Oncology Group trial. Gynecol Oncol. 2009;115(1):90-6.

274. Reiser F, Way D, Bernas M, Witte M, Witte C. Inhibition of normal and experimental angiotumor endothelial cell proliferation and cell cycle progression by 2-methoxyestradiol. Proc Soc Exp Biol Med. 1998;219(3):211-6.

275. Joubert A, Maritz C, Joubert F. Bax/Bcl-2 expression levels of 2-methoxyestradiol-exposed esophageal cancer cells. Biomed Res. 2005;26(3):131-4.

276. Lin HL, Liu TY, Wu CW, Chi CW. 2-Methoxyestradiol-induced caspase-3 activation and apoptosis occurs through G(2)/M arrest dependent and independent pathways in gastric carcinoma cells. Cancer. 2001;92(3):500-9.

277. Kumar S, Boehm J, Lee JC. p38 MAP kinases: key signalling molecules as therapeutic targets for inflammatory diseases. Nat Rev Drug Discov. 2003;2(9):717-26.

278. Lutter M, Perkins G, Wang X. The pro-apoptotic Bcl-2 family member tBid localizes to mitochondrial contact sites. BMC Cell Biol. 2001;2(1):22.

279. Chen Y, McMillan-Ward E, Kong J, Israels SJ, Gibson SB. Oxidative stress induces autophagic cell death independent of apoptosis in transformed and cancer cells. Cell Death Differ. 2007;15(1):171-82.

280. Van Zijl C, Lottering ML, Steffens F, Joubert A. In vitro effects of 2-methoxyestradiol on MCF-12A and MCF-7 cell growth, morphology and mitotic spindle formation. Cell Biochem Funct. 2008;26(5):632-42.

281. Newman SP, Ireson CR, Tutill HJ, Day JM, Parsons MFC, Leese MP, et al. The Role of 17β-Hydroxysteroid Dehydrogenases in Modulating the Activity of 2-Methoxyestradiol in Breast Cancer Cells. Cancer Res. 2006;66(1):324-30.

282. Tsuchiya Y, Nakajima M, Yokoi T. Cytochrome P450-mediated metabolism of estrogens and its regulation in human. Cancer Lett. 2005;227(2):115-24.

283. Tevaarwerk AJ, Holen KD, Alberti DB, Sidor C, Arnott J, Quon C, et al. Phase I Trial of 2-Methoxyestradiol NanoCrystal Dispersion in Advanced Solid Malignancies. Clin Cancer Res. 2009;15(4):1460-5.

284. Du B, Li Y, Li X, A Y, Chen C, Zhang Z. Preparation, characterization and in vivo evaluation of 2-methoxyestradiol-loaded liposomes. Int J Pharm. 2010;384(1-2):140-7.

285. Visagie MH, Joubert AM. In vitro effects of 2-methoxyestradiol-bis-sulphamate on reactive oxygen species and possible apoptosis induction in a breast adenocarcinoma cell line. Cancer Cell Int. 2011;11(1):43.

286. Stander XX, Stander BA, Joubert AM. In vitro effects of an in silico-modelled 17β-estradiol derivative in combination with dichloroacetic acid on MCF-7 and MCF-12A cells. Cell Prolif. 2011;44(6):567-81.

287. Visagie MH, Mqoco T, Stander AB, Vieira WA, Lafanechere L, Renaud MP, et al. Novel sulphamoylated 2-methoxyestradiol analogues and their *in vitro* signalling pathways in a human cervical adenocarcinoma cell line. Unpublished data.

288. Mqoco T, Vissagie M, Marais S, Joubert A. *In vitro* influence of novel sulphamoylated 2-methoxyestradiol analogues on signaling pathways in a human cervical adenocarcinoma cell line. Unpublished data.

289. MacCarthy-Morrogh L, Townsend PA, Purohit A, Hejaz HAM, Potter BVL, Reed MJ, et al. Differential Effects of Estrone and Estrone-3-O-Sulfamate Derivatives on Mitotic Arrest, Apoptosis, and Microtubule Assembly in Human Breast Cancer Cells. Cancer Res. 2000;60(19):5441-50.

290. Leese MP, Newman SP, Purohit A, Reed MJ, Potter BV. 2-Alkylsulfanyl estrogen derivatives: synthesis of a novel class of multi-targeted anti-tumour agents. Bioorg Med Chem Lett. 2004;14(12):3135-8.

291. LaVallee TM, Burke PA, Swartz GM, Hamel E, Agoston GE, Shah J, et al. Significant antitumor activity in vivo following treatment with the microtubule agent ENMD-1198. Mol Cancer Ther. 2008;7(6):1472-82.

292. Elger W, Schwarz S, Hedden A, Reddersen G, Schneider B. Sulfamates of various estrogens are prodrugs with increased systemic and reduced hepatic estrogenicity at oral application. J Steroid Biochem Mol Biol. 1995;55(3–4):395-403.

293. Ho YT, Purohit A, Vicker N, Newman SP, Robinson JJ, Leese MP, et al. Inhibition of carbonic anhydrase II by steroidal and non-steroidal sulphamates. Biochem Biophys Res Commun. 2003;305(4):909-14.

294. Sly WS, Hu PY. Human carbonic anhydrases and carbonic anhydrase deficiencies. Annu Rev Biochem. 1995;64:375-401.

295. Pastorekova S, Ratcliffe PJ, Pastorek J. Molecular mechanisms of carbonic anhydrase IX-mediated pH regulation under hypoxia. BJU Int. 2008;101 Suppl 4:8-15.

296. Chiche J, Ilc K, Laferrière J, Trottier E, Dayan F, Mazure NM, et al. Hypoxia-Inducible Carbonic Anhydrase IX and XII Promote Tumor Cell Growth by Counteracting Acidosis through the Regulation of the Intracellular pH. Cancer Res. 2009;69(1):358-68.

297. Stubbs M, McSheehy PM, Griffiths JR, Bashford CL. Causes and consequences of tumour acidity and implications for treatment. Mol Med Today. 2000;6(1):15-9.

298. Leese MP, Leblond B, Smith A, Newman SP, Di Fiore A, De Simone G, et al. 2-substituted estradiol bis-sulfamates, multitargeted antitumor agents: synthesis, in vitro SAR, protein crystallography, and in vivo activity. J Med Chem. 2006;49(26):7683-96.

299. Elger W, Schwarz S, Hedden A, Reddersen G, Schneider B. Sulfamates of various estrogens are prodrugs with increased systemic and reduced hepatic estrogenicity at oral application. J Steroid Biochem Mol Biol. 1995;55(3-4):395-403. Epub 1995/12/01.

300. Vorster C, Joubert A. In vitro effects of 2-methoxyestradiol-bis-sulphamate on cell growth, morphology and cell cycle dynamics in the MCF-7 breast adenocarcinoma cell line. Biocell. 2010;34(2):71-9.

301. Ireson CR, Chander SK, Purohit A, Perera S, Newman SP, Parish D, et al. Pharmacokinetics and efficacy of 2-methoxyoestradiol and 2-methoxyoestradiol-bis-sulphamate in vivo in rodents. Br J Cancer. 2004;90(4):932-7.

302. Newman SP, Leese MP, Purohit A, James DRC, Rennie CE, Potter BVL, et al. Inhibition of in vitro angiogenesis by 2-methoxy- and 2-ethyl-estrogen sulfamates. Int J Cancer. 2004;109(4):533-40.

303. Wood L, Leese MP, Mouzakiti A, Purohit A, Potter BVL, Reed MJ, et al. 2-MeOE2bisMATE induces caspase-dependent apoptosis in CAL51 breast cancer cells and overcomes resistance to TRAIL via cooperative activation of caspases. Apoptosis. 2004;9(3):323-32.

304. Visagie MH, Joubert AM. 2-Methoxyestradiol-bis-sulfamate induces apoptosis and autophagy in a tumorigenic breast epithelial cell line. Mol Cell Biochem. 2011;357(1-2):343-52.

305. American Type Culture Collection (ATCC) [homepage on the internet]. Manassas: ATCC; [updated 2011; cited 2011 Sept 30]; HeLa cell line: ATCC CCL-2™ [about 8 screens]. Available from: http://www.atcc.org/ATCCAdvancedCatalogSearch/ProductDetails/tabid/452/Default.aspx?ATCCNum=CCL-2&Template=cellBiology.

306. Kleeff J, Kornmann M, Sawhney H, Korc M. Actinomycin D induces apoptosis and inhibits growth of pancreatic cancer cells. Int J Cancer. 2000;86(3):399-407.

307. Scarlatti F, Bauvy C, Ventruti A, Sala G, Cluzeaud F, Vandewalle A, et al. Ceramide-mediated Macroautophagy Involves Inhibition of Protein Kinase B and Up-regulation of Beclin 1. J Biol Chem. 2004;279(18):18384-91.

308. Bursch W, Ellinger A, Kienzl H, Torok L, Pandey S, Sikorska M, et al. Active cell death induced by the anti-estrogens tamoxifen and ICI 164 384 in human mammary carcinoma cells (MCF-7) in culture: the role of autophagy. Carcinogenesis. 1996;17(8):1595-607.

309. Foukas LC, Berenjeno IM, Gray A, Khwaja A, Vanhaesebroeck B. Activity of any class IA PI3K isoform can sustain cell proliferation and survival. Proc Natl Acad Sci U S A. 2010;107(25):11381-6.

310. Bhati R, Gökmen-Polar Y, Sledge GW, Fan C, Nakshatri H, Ketelsen D, et al. 2-Methoxyestradiol Inhibits the Anaphase-Promoting Complex and Protein Translation in Human Breast Cancer Cells. Cancer Res. 2007;67(2):702-8.

311. Eagle H, Oyama VI, Levy M, Horton CL, Fleischman R. The growth response of mammalian cells in tissue culture to L-glutamine and L-glutamic acid. J Biol Chem. 1956;218(2):607-16.

312. Eagle H. The minimum vitamin requirements of the L and HeLa cells in tissue culture, the production of specific vitamin deficiencies, and their cure. J Exp Med. 1955;102(5):595-600.

313. Classical media and salts [homepage on the internet]. St. Louis: Sigma-Aldrich; [updated 2011; cited 2011 Dec 20]; DMEM [one screen]. Available from: http://www.sigmaaldrich.com/life-science/cell-culture/classical-media-salts/dmem.html.

314. Advanced imaging laboratory [homepage on the internet]. Victoria: University of Victoria; [updated 2005 Sept 21; cited 2012 Feb 10]; epi-fluorescence with the microscope [about 11 screens]. Available from: http://web.uvic.ca/ail/techniques/epi-fluorescence.html.

315. Brown M, Wittwer C. Flow Cytometry: Principles and Clinical Applications in Hematology. Clin Chem. 2000;46(8):1221-9.

316. Nunez R. DNA measurement and cell cycle analysis by flow cytometry. Curr Issues Mol Biol. 2001;3(3):67-70.

317. Van Cruchten S, Van den Broeck W. Morphological and Biochemical Aspects of Apoptosis, Oncosis and Necrosis. Anat Histol Embryol. 2002;31(4):214-23.

318. Riccardi C, Nicoletti I. Analysis of apoptosis by propidium iodide staining and flow cytometry. Nat Protocols. 2006;1(3):1458-61.

319. Darzynkiewicz Z, Bedner E, Smolewski P. Flow cytometry in analysis of cell cycle and apoptosis. Semin Hematol. 2001;38(2):179-93.

320. Jacoberger JW. Intracellular antigen staining: quantitative immunofluorescence. Methods. 1991;2:207-18.

321. Suzuki T, Fujikura K, Higashiyama T, Takata K. DNA Staining for Fluorescence and Laser Confocal Microscopy. J Histochem Cytochem. 1997;45(1):49-53.

322. Enzo Life Sciences [homepage on the internet]. New York: Enzo Life Sciences; [updated 2011; cited 2011 Dec 21]; ProteoStat® Aggresome detection kit for flow cytometry and fluorescence microscopy [about 2 screens]. Available from: http://www.enzolifesciences.com/ENZ-51035/proteostat-reg-aggresome-detection-kit-for-flow-cytometry-and-fluorescence-microscopy/.

323. Paddock SW, Fellers TJ, Davidson MW. Microscopy U [homepage on the internet]. Melville: Nikon; [updated 2010; cited 2011 Sept 02]; Fundamental Concepts in Confocal Microscopy [about 9 screens]. Available from: http://www.microscopyu.com/articles/confocal/confocalintrobasics.html.

324. Microscopy Resource Centre [homepage on the internet]. Center Valley: Olympus America Inc.; 2010 [updated 2010; cited 2011 30 Sept]; Fundamental Concepts in DIC Microscopy [about 30 screens]. Available from: http://www.olympusmicro.com/primer/techniques/dic/dicintro.html.

325. Danz R, Vogelgsang A, Käthner R. PlasDIC – a useful modification of the differential interference contrast according to Smith/Nomarski in transmitted light arrangement [homepage on the internet]. Göttingen: Photonik; [updated 2004; cited 2012 Feb 10]; Microscopy [about 6 screens]. Available from: http://www.zeiss.com.sg/C12567BE00472A5C/EmbedTitelIntern/Article-PlasDic_Photonic_e/$File/PlasDIC_Photonik_2004March_e.pdf.

326. Seegers JC, Aveling M-L, van Aswegen CH, Cross M, Koch F, Joubert WS. The cytotoxic effects of estradiol-17β, catecholestradiols and methoxyestradiols on dividing MCF-7 and Hela cells. J Steroid Biochem. 1989;32(6):797-809.

327. Kanzawa T, Kondo Y, Ito H, Kondo S, Germano I. Induction of Autophagic Cell Death in Malignant Glioma Cells by Arsenic Trioxide. Cancer Res. 2003;63(9):2103-8.

328. Visagie M, Joubert A. 2-Methoxyestradiol-bis-sulfamate induces apoptosis and autophagy in a tumorigenic breast epithelial cell line. Molecular and Cellular Biochemistry. 2011;357(1):343-52.

329. Aoki H, Takada Y, Kondo S, Sawaya R, Aggarwal BB, Kondo Y. Evidence That Curcumin Suppresses the Growth of Malignant Gliomas in Vitro and in Vivo through Induction of Autophagy: Role of Akt and Extracellular Signal-Regulated Kinase Signaling Pathways. Mol Pharmacol. 2007;72(1):29-39.

330. Miyazaki T, Arai S. Two Distinct Controls of Mitotic Cdk1/Cyclin B1 Activity Requisite for Cell Growth Prior to Cell Division. Cell Cycle. 2007;6(12):1418-24.

331. Boucrot E, Kirchhausen T. Mammalian Cells Change Volume during Mitosis. PLoS ONE. 2008;3(1):e1477.

332. Androic I, Kramer A, Yan R, Rodel F, Gatje R, Kaufmann M, et al. Targeting cyclin B1 inhibits proliferation and sensitizes breast cancer cells to taxol. BMC Cancer. 2008;8(1):391.

333. Claxton NS, Ottenberg GK, Olenych SG, Griffin JD, Davidson MW. Olympus FluoView™ [homepage on the internet]. Center Valley: Olympus Corporation; [updated 2009; cited 2011 Sept 02]; Staining Cells and Tissue Cryosections with Tubulin Primary Antibodies, Phallotoxins, and Synthetic Fluorophores [about 11 screens]. Available from: http://www.olympusfluoview.com/applications/protocols/cellsandtissuestubulin.html.

334. DAPI Nuclear Counterstain [homepage of the internet]. Rockford: Thermo Fisher Scientific Inc.; [updated 2011; cited 2011 Dec 21]; A blue nuclear counterstain for fluorescence microscopy and cellular imaging [about 4 screens]. Available from: http://www.piercenet.com/browse.cfm?fldID=01041204.

335. Mooberry SL. New insights into 2-methoxyestradiol, a promising antiangiogenic and antitumor agent. Curr Opin Oncol. 2003;15(6):425-30.

336. Foster PA, Ho YT, Newman SP, Leese MP, Potter BVL, Reed MJ, et al. STX140 and STX641 Cause Apoptosis via the Intrinsic Mitochondrial Pathway and Down-regulate Survivin and XIAP Expression in Ovarian and Prostate Cancer Cells. Anticancer Res. 2009;29(10):3751-7.

337. Chander SK, Foster PA, Leese MP, Newman SP, Potter BVL, Purohit A, et al. In vivo inhibition of angiogenesis by sulphamoylated derivatives of 2-methoxyoestradiol. Br J Cancer. 2007;96(9):1368-76.

338. Eichenlaub-Ritter U, Winterscheidt U, Vogt E, Shen Y, Tinneberg H-R, Sorensen R. 2-Methoxyestradiol Induces Spindle Aberrations, Chromosome Congression Failure, and Nondisjunction in Mouse Oocytes. Biol Reprod. 2007;76(5):784-93.

339. Ting CM, Lee YM, Wong CKC, Wong AS, Lung HL, Lung ML, et al. 2-Methoxyestradiol induces endoreduplication through the induction of mitochondrial oxidative stress and the activation of MAPK signaling pathways. Biochem Pharmacol. 2010;79(6):825-41.

340. Wang J, Lou P, Lesniewski R, Henkin J. Paclitaxel at ultra low concentrations inhibits angiogenesis without affecting cellular microtubule assembly. Anticancer Drugs. 2003;14(1):13-9.

341. Van Zijl C, Lottering M-L, Steffens F, Joubert A. In vitro effects of 2-methoxyestradiol on MCF-12A and MCF-7 cell growth, morphology and mitotic spindle formation. Cell Biochem Funct. 2008;26(5):632-42.

342. Day JM, Newman SP, Comninos A, Solomon C, Purohit A, Leese MP, et al. The effects of 2-substituted oestrogen sulphamates on the growth of prostate and ovarian cancer cells. J Steroid Biochem Mol Biol. 2003;84(2–3):317-25.

343. Day JM, Foster PA, Tutill HJ, Newman SP, Ho YT, Leese MP, et al. BCRP expression does not result in resistance to STX140 in vivo, despite the increased expression of BCRP in A2780 cells in vitro after long-term STX140 exposure. Br J Cancer. 2009;100(3):476-86.

344. Newman SP, Foster PA, Stengel C, Day JM, Ho YT, Judde J-G, et al. STX140 Is Efficacious In vitro and In vivo in Taxane-Resistant Breast Carcinoma Cells. Clin Cancer Res. 2008;14(2):597-606.

345. Michels J, Johnson PW, Packham G. Mcl-1. Int J Biochem Cell Biol. 2005;37(2):267-71.

346. Craig RW. MCL1 provides a window on the role of the BCL2 family in cell proliferation, differentiation and tumorigenesis. Leukemia. 2002;16(4):444-54.

347. Wertz IE, Kusam S, Lam C, Okamoto T, Sandoval W, Anderson DJ, et al. Sensitivity to antitubulin chemotherapeutics is regulated by MCL1 and FBW7. Nature. 2011;471(7336):110-4.

348. Djavaheri-Mergny M, Wietzerbin J, Besancon F. 2-Methoxyestradiol induces apoptosis in Ewing sarcoma cells through mitochondrial hydrogen peroxide production. Oncogene. 2003;22(17):2558-67.

349. Gao N, Rahmani M, Dent P, Grant S. 2-Methoxyestradiol-induced apoptosis in human leukemia cells proceeds through a reactive oxygen species and Akt-dependent process. Oncogene. 2005;24(23):3797-809.

350. She M-r, Li J-g, Guo K-y, Lin W, Du X, Niu X-q. Requirement of reactive oxygen species generation in apoptosis of leukemia cells induced by 2-methoxyestradiol. Acta Pharmacol Sin. 2007;28(7):1037-44.

351. Harvey SL, Charlet A, Haas W, Gygi SP, Kellogg DR. Cdk1-Dependent Regulation of the Mitotic Inhibitor Wee1. Cell. 2005;122(3):407-20.

352. Attalla H, Westberg JA, Andersson LC, Adlercreutz H, Mäkelä TP. 2-Methoxyestradiol-Induced Phosphorylation of Bcl-2: Uncoupling from JNK/SAPK Activation. Biochem Biophys Res Commun. 1998;247(3):616-9.

353. Kalousek I, Brodska B, Otevrelova P, Roselova P. Actinomycin D upregulates proapoptotic protein Puma and downregulates Bcl-2 mRNA in normal peripheral blood lymphocytes. Anticancer Drugs. 2007;18(7):763-72.

354. Kadowaki M, Razaul Karim M, Carpi A, Miotto G. Nutrient control of macroautophagy in mammalian cells. Mol Aspects Med. 2006;27(5–6):426-43.

355. Cho DH, Jo YK, Hwang JJ, Lee YM, Roh SA, Kim JC. Caspase-mediated cleavage of ATG6/Beclin-1 links apoptosis to autophagy in HeLa cells. Cancer Lett. 2009;274(1):95-100.

356. Luo S, Rubinsztein DC. Apoptosis blocks Beclin 1-dependent autophagosome synthesis: an effect rescued by Bcl-xL. Cell Death Differ. 2010;17(2):268-77.

357. Yousefi S, Perozzo R, Schmid I, Ziemiecki A, Schaffner T, Scapozza L, et al. Calpain-mediated cleavage of Atg5 switches autophagy to apoptosis. Nat Cell Biol. 2006;8(10):1124-32.

358. Betin VMS, Lane JD. Caspase cleavage of Atg4D stimulates GABARAP-L1 processing and triggers mitochondrial targeting and apoptosis. J Cell Sci. 2009;122(14):2554-66.

359. Lee JS, Li Q, Lee JY, Lee SH, Jeong JH, Lee HR, et al. FLIP-mediated autophagy regulation in cell death control. Nat Cell Biol. 2009;11(11):1355-62.

360. Akar U, Chaves-Reyez A, Barria M, Tari A, Sanguino A, Kondo Y, et al. Silencing of Bcl-2 expression by small interfering RNA induces autophagic cell death in MCF-7 breast cancer cells. Autophagy. 2008;4(5):669-79.

361. Krishnamurthy P, Schuetz JD. Role of ABCG2/BCRP in Biology and Medicine. Annu Rev Pharmacol Toxicol. 2006;46(1):381-410.